A UNITED STATES
EPARTMENT OF
COMMERCE
PUBLICATION

NBS SPECIAL PUBLICATION 356

Damage in Laser Materials: 1971

U.S.
DEPARTMENT
OF
COMMERCE

UNITED STATES DEPARTMENT COMMERCE • Maurice H. Stans, *Secretary*
NATIONAL BUREAU OF STANDARDS • Lewis M. Branscomb, *Director*

Damage in Laser Materials: 1971

Proceedings of a Symposium Sponsored by
the American Society for Testing and Materials
and by the National Bureau of Standards
May 19-20, 1971, NBS, Boulder, Colorado

Edited by
Alexander J. Glass
Wayne State University
Detroit, Michigan 48202
and
Arthur H. Guenther
Air Force Weapons Laboratory
Kirtland AFB, New Mexico 87117

U.S. National Bureau of Standards, Special Publication 356

Nat. Bur. Stand. U.S., Spec. Publ. 356, 174 pages (Nov. 1971)
CODEN: XNBSA

Issued November 1971

Forword

These proceedings report in detail the formal papers and discussions presented at the 3rd Annual Symposium on Damage in Laser Materials held at the National Bureau of Standards, Boulder, Colorado on May 19 and 20, 1971. This meeting was jointly sponsored by the National Bureau of Standards and the American Society of Testing and Materials. The major topics covered were Diagnostic Development, Damage Testing and Assessment, Damage Theory, and Physical Characteristics of Optical Media of importance in controlling damage, as well as Damage to Thin Film Coatings and Nonlinear Optical Materials.

The co-chairmen, Dr. Alexander J. Glass of Wayne State University, Detroit, Michigan, and Dr. Arthur H. Guenther of the Air Force Weapons Laboratory, Kirtland AFB, New Mexico, take full responsibility for synopsis of comments following each paper as well as the summary and conclusions of the meeting.

It is suggested that individuals interested in the subject of this meeting obtain publication NMAB-271, "Report of the Committee on the Fundamentals of Damage in Laser Glass" which is available for sale from the National Technical Information Service, Springfield, Virginia 22151, at a cost of $3.00. Proceedings of the 1969 ASTM Symposium were published in December 1969 as "Damage in Laser Glass", ASTM Special Technical Publication No. 469 "Library of Congress Catalog Card No. 74-102757". Proceedings of the 1970 Symposium were published in December 1970 as "Damage in Laser Materials", National Bureau of Standards Special Publication No. 341 at a cost of $1.25, with "Library of Congress Catalog Card Number 73-609162".

It is our intention to convene another symposium next year in Boulder during June to update and document the state of the art on Damage in Laser Materials at that time. This meeting will cover the subject historically presented at these symposia with additional emphasis on thin film damage and surface damage as a function of surface preparation and characteristics, e.g. surface scatter. We shall endeavor to address the problem of the damage of materials and components at 10.6μm, an area of increasing importance. We wish to encourage the reader to contact us on matters pertinent to the intent of these conferences.

A. H. Guenther

Library of Congress Catalog Card Number: 77-181048

Contents

	Page
Foreword ..... A. H. Guenther	iii
Summary and Conclusions ..... A. J. Glass and A. H. Guenther	vi
Introductory Remarks ..... A. J. Glass	1
Keynote Address ..... J. D. Myers	2
Damage by Laser Radiation of Improved Neodymium-Activated Laser Glass, Colored Glasses and Optical Glasses ..... N. Neuroth, R. Hasse and A. Knecht	3
Laser Glass Damage Threshold Studies at Owens-Illinois ..... N. L. Boling and R. W. Beck	15
Investigation of Cumulative Effects in Microscopically Damaged Quartz ..... David F. Edwards, C. Y. She, V. G. Draggoo, T. W. Broberg and G. L. McAllister	24
Plasma Formation Upon Laser Irradiation of Transparent Dielectric Materials Below the Damage Threshold ..... B. E. Henderson, R. R. Getty, G. E. Leroi and D. L. Rousseau	31
Diffusion Effects in High Power Laser Damage ..... Wilbur Franklin	37
Time Evolution of Damage Tracks in Sapphire and Ruby ..... Concetto R. Giuliano	44
Theory of Self-Focusing for Fast Nonlinear Response ..... J. Marburger	51
Electrostrictive Laser Beam Focusing in Glass and Small-Scale Track Formation ..... Edwin L. Kerr	61
The Probability and Dynamics of Damaging Optical Materials with Lasers ..... Michael Bass and Harrison H. Barrett	76
Optically-Induced Physical Damage to $LiNbO_3$, Proustite, and $LiIO_3$ ..... Wm. D. Fountain, L. M. Osterink, and G. A. Massey	91
Catastrophic Surface Damage Produced in $Ba_2NaNb_5O_{15}$ Crystals During Intracavity Frequency Doubling ..... Robert Webb	98
Investigation of Damage in Laser Glass ..... Chiyoe Yamanaka, Takatomo Sasaki, Masanobu Hongyo and Yasuaki Nagao	104
Direct Nondestructive Measurement of Self-Focusing in Laser Glass ..... Brian E. Newnam and L. G. DeShazer	113
Ruby Laser Damage Thresholds in Evaporated Thin Films and Multilayer Coatings ..... A. Francis Turner	119
Investigations Toward Understanding the Physics of Laser Damage to Thin Dielectric Films ..... L. G. DeShazer and J. H. Parks	124

Page

An Investigation of Laser Induced Damage to Four Different Single Purpose Anti-Reflection Coatings on Fused Silica Substrates..... 137
R. Russel Austin and Arthur H. Guenther

Minimizing Susceptibility to Damage in CO_2 Laser Mirrors..... 153
H. E. Bennett

Appendix
Participants..... 163

Damage in Laser Materials
3rd ASTM Symposium
May 19-20, 1971

Abstract

The third ASTM Symposium on Damage in Laser Materials was held at the National Bureau of Standards in Boulder, Colorado, on May 19-20 of this year. This symposium is held as part of the activity of Subcommittee II on Lasers and Laser Materials, of the ASTM. Subcommittee II is charged with the responsibility of formulating standards for laser materials, components, and devices. The chairman of Subcommittee II is John D. Myers, of Owens-Illinois, Inc. Co-chairmen for the damage symposia are Dr. Arthur H. Guenther, of the Air Force Weapons Laboratory, and Professor Alexander J. Glass, Chairman of the Department of Electrical Engineering at Wayne State University.

Approximately 50 attendees at the symposium heard 17 papers on topics relating to laser-induced damage in glass, crystalline materials, nonlinear optical materials, thin film dielectric coatings, and mirrors. Particular attention was given to the processes of plasma formation at dielectric surfaces, and to the role played by self-focusing in bulk damage in solids. The principal conclusions arrived at the Symposium, the content of each of the papers, and recommendations for future investigations are summarized below.

The proceedings of these Symposia represent the major source of information in the field of damage in laser materials. The Symposia themselves, along with the periodic meetings of Subcommittee II, provide a unique forum for the exchange of information regarding laser materials specifications among the manufacturers and users of laser devices, components and systems. The Symposium also serves as a mechanism of information gathering, to enable the Subcommittee to write informed and realistic specifications.

Key Words: Laser damage, laser materials, self-focusing.

Summary & Conclusions

1. Principal Conclusions

It was apparent from the content of the papers presented at this Symposium that considerable progress has been made in understanding the nature of the processes which lead to material damage under intense illumination. It is now unequivocally demonstrated that surface damage is always accompanied by the formation of a luminous plasma, composed mostly of materials ejected from the surface itself. The process whereby this plasma is formed is sensitive to the cleanliness of the surface, and to the history of the surface finish, which may be the same thing. It is indifferent to the composition or absence of background gas at the surface. It seems possible to affect the surface damage threshold, at least in some materials, by immersing the surface in a liquid, or optically contacting it to a surface of different composition. Some features of the surface damage mechanism remain unclear, such as the effects of surface roughness, the possibility of altering the surface damage threshold by chemical treatment or ion implantation, and the physics of the initiation process whereby the plasma is formed. Since surface plasma formation remains the principal limitation to the operation of glass lasers, and since there is evidence that the threshold for surface damage can be increased, perhaps by factors of ten, by various surface treatments, methods of raising the surface damage threshold in laser glass should receive high priority.

The extension of the discussions of the Symposium into the areas of nonlinear optics materials and coated surfaces does not come about from a diminution in interest in damage in laser glass, but instead reflects the increased understanding of the processes whereby glass damage can be avoided. Bulk damage in laser glass resulting from heating platinum inclusions is now a problem of production control, and is well enough understood to be avoided.

Once this source of local damage is removed, the threshold for bulk damage in glass, as in most transparent solids, is the threshold for self-trapping. It is now clear, from the elegant work of John Marburger, of the University of Southern California, and Concetto Giuliano, of the Hughes Research Laboratory, independently confirmed by Michael Bass, of Raytheon, that the damage track observed in a broad range of materials is the fossil record of the moving focus generated by dynamic self-focusing of the incident light. The observed threshold for this process, as shown by Edwin Kerr, of Perkin-Elmer, is sensitive to the beam geometry, and to the duration of the incident pulse. On the basis of Kerr's work, however, one can relate the effective threshold for self-focusing with a given set of operating parameters to the intrinsic threshold for bulk damage in the material.

There is also evidence that the self-trapping process plays a role in surface damage. Even if no bulk damage occurs during a pulse, the light intensity at the exit face of a sample is increased by self-focusing to produce regions of high electron emission, which initiates plasma formation. It is not clear at this time if surface plasma formation takes place only via the self-focusing mechanism, or if the photo-current densities which are produced in an unfocused beam are sufficiently high to lead to plasma initiation.

It was emphasized by Bass that the damage process is intrinsically statistical. Accordingly, one must define the concept of damage threshold in terms of the probability that damage will be observed at a given power level in a certain number of laser shots. Given a model of the damage process, the likelihood of damage for a given material can be stated in terms of the single-shot damage probability, p_1, which is a function of incident intensity. Experimentally, it is observed that the relation for a large class of materials can be written as $p_1 \sim \exp(-K/I^{\frac{1}{2}})$, where K is a constant for a given sample of material, and I is the incident laser intensity.

It is apparent that in any measurement of damage phenomena, it is essential that one be able to measure the local intensity of the incident light. In general, this requires that damage testing be done with a single mode (TEM_{oo}) laser. Evidence is reported in this Symposium indicating that in the presence of multimode illumination, even the mechanisms of damage may be different from that under single mode illumination. There seems to be little chance of interpreting observations of damage in an quantitative fashion under the action of multimode illumination.

Damage studies in nonlinear optics materials are more difficult to interpret than studies in glass and ruby. One reason for this is the lack of homogeneity and reproduceable properties in most crystalline NLO materials commercially available today. Significant variations of scattering loss, UV absorption, and optical quality are seen from sample to sample of the same material. Accordingly, different samples exhibit significantly different damage levels. In addition to the variations in material, there is the added effect that damage in the presence of two or more optical frequencies, in a nonlinear medium, occurs at a power density much lower than the single frequency damage threshold. The reasons for this discrepancy are currently unclear.

The emphasis of the ASTM Damage Symposium is shifting away from laser materials themselves to other components of the laser system. We can look forward to continued interest in damage to thin films and multilayer coatings. There is increasing interest in damage at infrared wavelengths, especially at 10.6 μm, and to reflecting surfaces. The sensitivity of the damage threshold to the way in which the surface is fabricated remains an important topic of interest.

2. Summary of Papers

2.1 Damage in Glass

The first group of presentations at the Symposium were concerned with damage to various laser and optical glasses. While the bulk damage mechanism is rapidly becoming well defined, inprovements in the understanding of surface damage mechanisms are required to achieve higher threshold values. In part, in most situations, surface damage is the limitation in high power system applications. The improvement in our understanding of bulk damage mechanisms is in no small part due to improved diagnostic techniques, the prime area covered in this group of papers. They include results on damage resistance of a recently developed Schott glass, holographic techniques of damage diagnosis, spectroscopic characterizations of the plasma accompanying surface damage, the chemistry relating to the plasma formation, and finally a description of a new direct non-destructive measurement of self-focusing in laser glass.

Dr. Norbert Neuroth of the Schott Company led off the Symposium by reporting damage results on their improved 1% efficiency LG 630 and LG 650 glasses doped to 3% and 5% Nd respectively. The passive loss of these glasses is in the range of 0.15 to 0.2%/cm. He reported, as well, on glasses containing up to 10% Nd, at which level concentration quenching was observed. Evidence of concentration quenching was a reduction in lifetime from 600 μsec to 400 μsec. Damage testing was generally performed at 40 nsec with either a 20 mm or 60 mm f.l. lens. As expected, two types of damage were reported. For the short focal length lens, localized, star-patterned pictures were observed, while with the longer focal length lens, filimentary damage was evident. Surface damage thresholds ranged between 20 and 40 J/cm^2 in a 30 ns pulse duration. Additional comparative tests were performed both on passive and pumped samples.

Of considerable interest were results of tests performed on colored filter glass and undoped optical glass. For the filter glass study, damage exhibited both fracture and melting, and an analytical relation was developed between damage threshold and absorption coefficient. This relation states that the energy at threshold was equal to 185 J/cm^2 divided by $k^{0.74}$ were k is the absorption coefficient in cm^{-1}. A correlation was observed between the surface damage thresholds for different optical glasses and specific glass properties. Observed damage thresholds were correlated with the percentage of glass forming oxides, the specific heat and viscosity-related temperature for softening.

The application of pulsed holography to laser induced damage was the subject of a paper by Dr. Norman Boling and Robert Beck of Owens-Illinois Inc. The study concerned the association of various distinctive fringe positions and fringe motions with acoustic disturbances and plasma characteristics. Once the importance of not employing focused beams for this study was established, characteristic acoustic phenomena associated with longitudinal, shear and rayleigh surface waves were easily identified.

A detailed study of the surface plasma produced concurrent with damage indicated an initial expansion velocity greater than 7×10^5 cm/sec at an ion temperature of greater than 5×10^4 °K, with corresponding electron densities between 10^{18} and 10^{19} e/cc. These holographic results were employed to assess the possible role of electrostriction, Stimulated Brillouin Scattering and plasma produced shock-waves and ionic bombardment of the surface in the damage process.

An important result of work relating to the reduction of inclusion damage was reported as well. Pt inclusions are caused by the presence of oxygen in the melting environment. One can not arbitrarily remove O_2 completely by use of inert atmosphere, for there the Pt crucible is attacked by components of the molten glass, such as Si. Therefore it was deemed that O_2 concentration was critical, and through the application of thermodynamic considerations a buffer of CO and CO_2 was employed as a pumping gas to control the O_2 concentration within narrow limits.

In a paper read by Dr. Arthur Guenther of the Air Force Weapons Laboratory for Prof. Chiyoe Yamanaka and his coworkers at Osaka University, Japan, a rather complete review of that institute's research into passive and active glass damage was presented. Previously reported results were confirmed, such as plasma formation concurrent with damage, a damage threshold at the exit surface lower than that at the entrance surface of optical elements; and improvement in surface damage susceptibility through the use of various chemical treatments. It was found that HF etching raised the damage threshold for Barium Crown glass from 28 J/cm^2 to 40 J/cm^2, for a 10 minute etch in a 10% HF solution. For 25 nsec exposures, bulk damage threshold did not appear to be sensitive to the concentration of platinum inclusions. The damage threshold for glass with platinum inclusions was approximately 12 ± 3 J/cm^2, while for inclusion-free glass, it was reported to be 400 J/cm^2. Considerable attention was paid to the analysis of both integrated and time resolved spectroscopy of both internal and surface plasmas, and the interpretation of these spectra in light of various damage mechanisms.

Dr. George Leroi reported, in review form, research accomplished in the Dept. of Chemistry at Michigan State University, on plasma formation on laser irradiation of dielectric materials. The measured positive and negative particle emission currents were analysed with regard to a proposed phenomenological model. The observed currents were ascribed to laser heating of surface contaminants, with subsequent production of high energy photons, and thermionic emission of electrons and ions. An important result is that these emission currents can be greatly reduced (but not completely eliminated) by careful precleaning and repeated laser irradiation at power levels below the damage threshold. Much smaller emissions have been obtained from "clean" surfaces than were previously considered to be intrinsic to the dielectric materials tested. These included soft glass, pyrex, fused quartz, suprasil quartz, CaF_2, LiF and sapphire.

In a paper related primarily to the onset of bulk damage, Brian Newman and Lawrence DeShazer, of the University of Southern California, discussed the development of a direct but non-destructive test for measuring the onset of self-focusing in laser glass. This was accomplished by comparing the temporal shape of the transmitted on-axis pulse with the input pulse, and constructing a non-linear wave equation. It was shown that if the response of the medium is fast enough, the critical power for self-focusing, P_c and the non-linear refractive index n_2 could be calculated without regard to specific mechanisms. A result for BSC-2 glass under 10 nsec irradiation at 0.6943 μm indicated a value of $P_c = 0.9$ MW, and n_2 of 2×10^{-13} esu, which is similar to results reported by Duguay at the 1970 Symposium on Laser Damage. It was pointed out that a well controlled transverse distribution was required of the irradiating laser to make accurate measurements of the pulse sharpening of the on-axis contour during self-focusing.

2.2 Damage in Crystalline Materials

Experimental studies of both bulk and surface damage in crystalline materials were reported by several of the participants in the Symposium. Materials studied included crystalline quartz, ruby, sapphire, and a variety of nonlinear optical materials. A common feature of all the investigations was the emphasis placed on the difference between damage generated with a single mode (TEM_{oo}) laser and that incurred in the beam of a multimode laser. Since each investigation is carried out under different conditions, no direct, quantitative comparison of the results is possible. The damage threshold numbers quoted were dependent on the experimental conditions.

Professor David Edwards, of Colorado State University has investigated bulk damage in crystalline quartz, using a ruby laser system operating both in the TEM_{oo} mode, and with a spatially multimode output. Significant differences were seen in the threshold and morphology of damage incurred in the multimode beam and the single mode beam. It is difficult to provide a quantitative interpretation of multimode results due to the lack of reproducability of the beam intensity distribution from shot to shot. It was observed, however, that the multimode damage threshold was correlated with the elastic-wave velocity in the medium, with the threshold being highest for that geometry in which the resultant elastic-wave had the highest velocity in the medium. This effect was confirmed by the spatial properties of the bulk damage. When the elastic-wave velocity was isotropic in the plane perpendicular to the incident laser beam, the resultant damage volume was circular in cross-section. When the wave velocity was not isotropic in the transverse plane, however, a cruciform pattern was observed. With a single mode laser, no such spatial dependence was observed. It is proposed that the multimode damage

results from strong coupling to the phonon spectrum of the crystal via the electrostrictive mechanism which is sensitive to gradients in the laser intensity pattern. In single mode damage, the interaction seems to be of a different nature, and may be due either to self-focusing, or to direct interaction with the electrons rather than coupling to the crystal lattice.

Dr. Concetto Giuliano, of the Hughes Research Laboratory, reported the first direct observation in solids of the effect of the moving focal spot caused by self-trapping. Experiments were carried out with a ruby oscillator amplifier system, operated in the TEM_{oo} mode. Bulk damage was observed with a focused beam in sapphire and ruby samples. The light emitted from the luminous plasma formed at the damage site was recorded on an STL streak camera, to give a temporally and spatially resolved record of the locus of the damage. The damage locus was observed to start at the geometrical focus of the beam, and progress towards the laser as the pulse intensity increased, creating a damage track in the sample. The track terminus was reached at or near the peak of the laser pulse. For a temporally modulated pulse, the damage locus was observed to dwell in the medium at each local maximum of the pulse, creating a local damage star. The results of this investigation showed good quantitative agreement with the theoretical model proposed by Marburger, which is described below.

The probabilistic nature of the damage process was emphasized by Dr. Michael Bass, of the Raytheon Research Division. He pointed out that at any level of irradiation, there is a non-zero probability of observing damage. This probability increases monotonically with increased local light intensity. At a given level of irradiation, the probability that damage will occur on the nth pulse is given by a binominal distribution, $p_n = (1-p_1)^{(n-1)} p_1$, where p_1 is the single shot probability of damage. On a model similar to that proposed by Shockley for avalanche breakdown, the single shot damage probability is shown to be proportional to exp (-K/E), where K is a constant determined by the material and experimental conditions; and E is the electric field of the light wave. Experimental evidence was obtained in a large number of crystalline and amorphous materials showing that a plot of log p_1 vs. $\sqrt{I}$ (where I is the local laser intensity), yielded a straight line dependence as predicted on the avalance model. Data are presented for surface damage in these materials observed at the focus of a TEM_{oo}, Nd:YAG laser. Additionally, Dr. Bass presented streak-camera records of bulk damage in lucite acrylic plastic and glass. Evidence is obtained of a moving focal spot due to self-trapping, similar to that presented by Giuliano.

Results were reported by William Fountain, of Sylvania Electric Systems, on bulk and surface damage in three nonlinear optical materials: $LiNbO_3$, $LiIO_3$, and proustite. The beam of a TEM_{oo}, Nd:YAG laser was focused with a long focal-length lens, and each sample was then placed in the diverging portion of the beam, downstream of the focus. By moving the sample towards the focus, the incident power density was increased to the point where damage occured. Proustite exhibited catastrophic damage, ascribed to local heating due to absorption, at an incident power density of a few hundred watts/cm^2 cw, or 10 MW/cm^2 in a 10 nsec pulse. If this absorption is intrinsic in the material, proustite will not be a useful candidate for near-IR applications.

Lithium Iodate showed damage at the entrance surface at about 400 MW/cm^2 in 10 nsec pulses. This damage may have been due to the conditions of the surface polish. When used as an external frequency doubler, $LiIO_3$, exhibited bulk damage at power densities of only 30 MW/cm^2 in the fundamental, and 15 MW/cm^2 at the harmonic. Evidence of chemical decomposition of the material, in the form of free iodine deposits, was found in the damage regions.

In lithium niobate, exit face damage, accompanied by visible plasma, was seen at about 170 MW/cm^2 in 10 nsec pulses. When the crystal was immersed in Dow Corning 200 fluid, a plasma was seen in the fluid at the interface, but no residual damage to the crystal was observed. When the crystal was optically contacted to either quartz or YAG plates, the exit face damage threshold was raised to about 700 MW/cm^2. In a mode-locked YAG laser beam, no damage was seen in $LiNbO_3$ at single pulse energy densities up to 0.32 joules/cm^2. The crystal did show entrance face damage at incident energy densities close to 0.70 joules/cm^2 in the beam of a mode-locked glass laser. Like lithium iodate, lithium niobate showed a much lower damage threshold in the presence of the green harmonic, when used as a frequency doubler.

The damage threshold reduction, in the presence of harmonic generation, was explored in detail by Robert Webb, of Holobeam. In his studies, a crystal of barium sodium niobate was used as a frequency doubling element inside the cavity of a single mode, Nd:YAG laser. It was found that the efficiency of conversion that could be obtained was limited by surface damage to the nonlinear crystal. Damage was seen at power levels of 3 MW/cm^2 at the 1.065 μ fundamental, and 10 KW/cm^2 in the harmonic. The observed damage levels were approximately the same for crystals coated with either thorium fluoride or magnesium fluroide. Two mechanisms were proposed as possible causes of the damage seen in the presence of the harmonic. One was the possible presence of absorption in the material at the sum frequency, i.e. at the third harmonic, coupled by a nonlinear interaction to the two waves present in the medium. The other possible cause discussed was the presence of stimulated Brillouin scattering in the medium leading to amplification of the phonon field. The presence of reduced damage thresholds in the presence of the harmonic emerged from both Webb's and Fountain's papers as a point of significant concern in the design and use of frequency doubling crystals.

2.3 Theoretical Contributions

Obviously, these experimental investigations must be supported by the development of theoretical models for the processes involved. The dynamics of electrostrictive self-focusing, the moving focus picture of self-focusing, and laser-enhanced diffusion phenomena, were each the subject of a theoretical investigation reported at the Symposium.

Edwin Kerr, of Perkin-Elmer, discussed calculations of solutions to the equation of light propagation the presence of electrostrictive self-focusing. The latter was described by a sound equation representing the finite rate at which density changes can occur in the medium. It was found that the threshold for self-focusing increases rapidly over the steady-state value for pulses short compared to the time for acoustical propagation across the focal diameter. For trains of short pulses, such as are produced by mode-locked lasers, cumulative effects are predicted to occur. Above the threshold for trapping, one is interested in the relation between the maximum power density achieved in the medium, and the power incident on the entrance face of the sample. This dependence has been calculated, and computed results are given. Experimental confirmation was obtained by plotting the incident power level required in a beam of given radius to cause damage in a glass sample. The damage threshold for a given sample was then obtained from application of the theoretical relations. Bulk damage thresholds for pulses of 55 nsec duration are reported for Flint Glass (2.5 GW/cm^2), BSC Glass (60 GW/cm^2) and Fused Silica (180 GW/cm^2).

If the incident power density is sufficiently high to cause self-focusing in the sample, the maximum power density at the focus is undetermined since the theoretical results diverge. Dr. Kerr showed that if one includes the effects of gradients in the nonlinear refractive index, which become significant in the vicinity of the focus, this singularity is relieved, and one can obtain predictions for the trapped minimum radius as a function of the incident power. The theory also predicts significant depolarization of the transmitted beam, which has been experimentally confirmed.

Professor John Marburger, of the University of Southern California, presented a brief review of the theory of self-focusing, and then described a dynamical model of the moving focal spot induced in self-focusing media. The essential features of the motion of the focal spot were computed. While the incident light intensity is increasing, one branch of the solution corresponds to a focal spot moving towards the laser. This portion of the process is well accounted for by Marburger's theory, and experimental evidence in support of the theory was presented in Giuliano's paper. A qualitative description was given of the behavior of the other branch of the solution corresponding to a secondary focus downstream of the geometrical focus in the medium. Marburger also described the effects to be expected from the retrograde motion of the primary self-focus on the decaying portion of the laser pulse. The effects of both the prompt and delayed nonlinear response of the medium were discussed.

Professor Wilbur Franklin, of Kent State University, proposed a theory of enhanced ionic diffusion in crystalline solids in the presence of intense electromagnetic fields. Several forms of interaction are possible. If the incident light leads to direct phonon excitation, diffusion processes will be enhanced. If, instead, the effect of illumination is primarily to excite conduction electrons, this can decrease the activation energy associated with the diffusion of defects. Increased local pressure, due to electrostriction, can also decrease the free energy for ion migration. The explicit form of the dependence of the activation energy for defect diffusion on the population of phonon and conduction electron states is exhibited. Professor Franklin also pointed out that ion diffusion can be driven by strong thermal gradients induced by the incident light. Possible consequences include local deviation from stoichiometry, or even the formation of cavities in the medium. These in turn, can act as "free surfaces" for the initiation and propogation of microcracks. Possible mechanisms for photon-phonon interaction include direct absorption, Raman scattering, and electrostriction. As proposed by Robert Hellwarth, of the Hughes Research Laboratory at the 1970 damage symposium, conduction electrons (which couple strongly to the incident light) can interact with the lattice via polaron interactions.

2.4 Thin Films and Mirrors

As a final topic of this year's symposium, laser induced damage to dielectric coatings and mirror surfaces, particularly at 10.6 μm, were discussed. Four different aspects of this problem were discussed. They were; a) the requirement for careful control of the beam intensity distribution of the damage producing laser source; b) a survey of the relative damage resistance of a large number of candidate materials; c) the morphology of damage as determined by both optical and electron microscopic techniques, with an attended correlation to the film systems structural characteristics, and finally; d) a detailed presentation of the physics and engineering practices relating to the reflectivity and absorption of metallic mirrors in the 10.6 μm region of the spectrum.

Although Dr. Francis Turner of Bausch and Lomb was unable to attend the symposium due to ill health, his very complete survey of the relative damage resistance of single laser dielectric films and various multilayer systems, is included in the proceedings. A general observation of the damage threshold for Q-switched ruby laser operation indicates that damage thresholds for multilayer dielectrics fall between

those of their component films. Thresholds were determined by correlation of the damage spot sizes with incident laser power. Extrapolation of spot size to zero radius gives the threshold energy. The obtained tabulation of relative damage thresholds should be of considerable use to manufacturers of thin film coatings.

Professor Lawrence DeShazer and Joel Parks of the University of Southern California stressed the importance of careful control of the intensity distribution of laser sources. Of particular importance is the transverse mode control required, and much of their paper is concerned with the transient transverse behavior of Q-switched lasers. Their intention during the next year is to evaluate monolayer damage in the UV, visible, and IR regions of the spectrum by employing N_2, ruby and Nd^{+3} lasers. Their program will study damage of films on crystalline substrates by scanning electron microscopy, electron diffraction, determination of chemical changes produced in films, and by attempting correlation with transmission and reflectivity measurements.

R. Russell Austin, of Perkin-Elmer, and Dr. Arthur Guenther, of the Air Force Weapons Laboratory, undertook a determination of the damage resistance of four typical anti-reflection coatings. It was attempted to correlate observed damage thresholds with the residual stress developed in single-layer and multilayer coatings, all of which had been deposited on fused quartz substrates using electron-beam heating. Coatings evaluated included quarter-wave (λo = 1.06 μ) layers of MgO-MgF_2, MgF_2-S_1O_2, MgF_2-ThF_4-MgF_2, and MgF_2. A great deal of insight into the morphology of damage was obtained from examination by optical and electron microscopy. It was important to note that there are many more types of laser-induced damage to thin films than are observed in optical substrates or elements. Values of single shot damage, always accompanied by visible plasma formation, ranged between 1 and 2 GW/cm^2 for 30 ns exposures on both entrance and exit surfaces. Numerous suggestions for the development of damage resistance coatings, as well as experimental precautions, were made. In addition, research efforts were proposed to afford an insight into the physics of laser-induced damage to thin film coatings.

The question of minimizing the susceptibility to damage of CO_2 laser mirrors was the topic of a paper by Harold E. Bennett of the Naval Weapons Center. The absorption of mirror coatings is of major concern in CW laser operation and becomes even more critical in high-power, pulsed operation. Reflecting films exhibiting very low absorption can be made employing multilayer dielectric coatings in the visible and near infrared spectral region. At longer wavelengths, however, due to the thickness required and lack of suitable materials for multilayer films, it is advantageous to use evaporated metal films. In this paper, the effects of evaporation conditions, surface finish, overcoating of the surface, tarnish, and anomalous skin effect on the achievable reflectivity and absorption of metal surfaces were discussed. It is concluded, that at 10.6 μm, a properly prepared, un-overcoated silver or gold surfaced mirror may be the best choice for high-power laser applications.

3. Recommendations

Great progress has been made in the development of damage-resistant laser material as well as in developing an understanding of damage mechanisms and increased sophistication in the analysis of damage. By improved manufacturing and fabrication procedures, metallic inclusions have been eliminated as a source of bulk damage in active laser material. At present, the threshold for bulk damage is determined by the threshold for self-focusing. Although it may be possible to affect the threshold for self-focusing by changing the formulation of the material, in particular in the case of laser glass, it seems unlikely that any large increase in the self-focusing threshold will be obtained. As a result the tendency has been to avoid self-focusing by the use of segmented configurations such as slab or disc lasers, particularly as amplifier stages in high powered glass laser systems. Consequently, the single most important limit to high power glass laser performance at the present time is that imposed by the threshold for surface damage. This is an area in which considerable improvements are required in order to realize the full potential of solid state laser systems.

In addition to improving the performance of glass laser systems, research in this area can also have a profound impact on the durability of the other optical elements required in the utilization of high powered laser systems. It is strongly recommended that work be pursued in the area of surface physics and chemistry to develop new methods of increasing the damage threshold of optical surfaces. In any studies of surface damage it is essential that careful attention be paid to surface cleanliness and to obtaining a detailed characterization of the surface finish. Much of the work carried out to date on damage in optical materials has been conducted using pulses of a 30 to 50 nanosecond duration. Still lacking is any systematic investigation of damage of optical materials in the picosecond regime. There is evidence that the dominant damage mechanisms will indeed be different for pulses of picosecond duration. Once a thorough understanding has been obtained of damage in the picosecond regime, one could then attempt the development of a complete time-dependent theory of laser induced damage particularly as it relates to the limits imposed by self-focusing.

In the study of the damage resistance of nonlinear optical materials, we have barely scratched the surface. It is recommended that damage characteristics of nonlinear optical materials be vigorously pursued. Both bulk damage and surface damage are of importance in these materials. As is the case in the study of laser materials, it is important that well controlled sources of illumination be employed, and that the nonlinear optical materials under test be carefully prepared and well characterized. The

influence of the simultaneous presence of multiple wavelengths on the damage threshold in nonlinear optical materials warrants special investigation. However, there is no question at this time that the greatest improvement in the damage resistance of nonlinear optical materials can be obtained through an improvement in the quality and reproduceability of these materials. At present it is not possible to obtain absolute measurements for damage thresholds in nonlinear optical materials due to the variation in the materials themselves.

Very little work has been carried out to date on the study of damage to thin film dielectric coatings. However, as the damage resistance of laser materials is improved, it is obvious that the damage resistance of dielectric doatings must be increased accordingly. The characterization of damage to multi-layered dielectric coatings is made more difficult by the presence of several distinct types of damage failure. A number of suggestions for improvement in the damage resistance of thin films have come forward in the course of this symposium. These suggestions should be investigated. It has also been pointed out that the damage threshold in the case of dielectric coatings requires special definition, since the physical disruption of the coating itself may not be disastrous, but rather that failure might result from concurrent effects, such as a degradation in the surface reflectivity or in the coating's environmental durability. It is recommended further that a systematic study be carried out of the damage resistance of coatings deposited by several different techniques, and that specialized coatings such as inhomogeneous or periodic coatings also be investigated. Although these coatings are somewhat difficult to fabricate and may prove somewhat expensive to manufacture, their use may also lead to significant improvements in the damage resistance of coated optical elements. With the advent of high powered lasers operating in the infrared region of the spectrum, it is essential that the damage symposium now direct its attention to the problems of damage at long wavelengths. Of particular importance here are reflecting elements, which have received little attention by the symposium up to now. Since in many cases we are considering metallic surfaces rather than dielectrics, a new variety of physical mechanisms must be understood in connection with the damage process.

4. Acknowledgment

We would like to acknowledge the invaluable assistance of Dr. Harold Boyne and Mrs. Pauline Smith of the National Bureau of Standards in Boulder, Colorado for their interest, support, and untiring efforts in the operation of this symposium and in the preparation and publication of the proceedings. The continued success of the damage symposium would not have been possible without their support.

5. Bibliography

1) "Damage in Laser Glass", A. J. Glass and A. H. Guenther, Editors, ASTM Special Technical Publication 469, ASTM, Philadelphia, Pa. (1969).

2) "Damage in Laser Materials", A. J. Glass and A. H. Guenther, Editors, NBS Special Publication 341, U. S. Government Printing Office, Washington, D. C. (1970).

3) "Fundamentals of Damage in Laser Glass", N. Bloembergen, National Materials Advisory Board Publication NMAB-271, National Academy of Sciences, Washington, D. C. (1970).

A. J. Glass
A. H. Guenther

Introductory Remarks

Alexander J. Glass

Wayne State University
Detroit, Mich. 48202

It is a distinct pleasure to welcome you once again to the A.S.T.M. Symposium on Damage in Laser Materials. This year the scope of our discussion has been broadened somewhat, to include not only glass and crystalline laser hosts, but also nonlinear optical materials, and coatings. This is true in part because the advances made in recent years in glass damage levels have made it necessary to examine the other components of high power laser systems in terms of their resistance to damage under intense illumination. Like the Deacon in Oliver Wendell Holmes poem, the "Wonderful One-Hoss Shay", we work to perfect a system so evenly balanced that all components will fail simultaneously, with no one weakest link in the chain.

There have been many advances in laser technology in the three years that this Symposium has been meeting. I think that it is still true, today, however, that Nd-doped glass remains the major material for the construction of high energy, high peak power, low repetition rate systems. The glassy state provides a unique combination of optical, physical and spectral properties which render it particularly suited to the storage and sudden release of large amounts of energy. As system designs improve, and efficiencies rise, we shall see larger and larger systems. In particular, due to the growing interest in glass lasers as sources for plasma heating, the ability of glass to withstand damage is continually being challenged. Higher damage levels yield more energetic and more efficient systems, and consequently, higher plasma temperatures and larger heated volumes. We can expect this cycle to continue, as long as interest in laser-produced plasmas persists.

In the papers presented in this symposium, we are mainly concerned with surface damage, both in glass and in nonlinear optics materials, and self-trapping. The problem of inclusions, which played so large a role in our previous discussions, has been brought under control, and now no longer limits the damage level of laser glass. That fact alone is a substantial mark of progress. We shall hear, today and tomorrow, fairly detailed theoretical descriptions of the trapping process, and of the processes of plasma formation at dielectric surfaces. We shall see elegant experimental data, which should stimulate further refinements of theory. The understanding of these damage processes is growing less empirical and more analytical year by year, as the record of these symposia will testify. The final session of this year's Symposium will be devoted to damage in dielectric coatings. Dr. Guenther has borne the burden of organizing this session, for which we are indebted to him. Optical coatings were not unknown in the pre-laser era of optics, but it is only since laser usage that coatings have been required to withstand gigawatt flux levels, in addition to meeting all the usual specifications of durability, uniformity, and spectral selectivity. The inclusion of coatings in this year's discussion stems from the fact that our parent body, Subcommittee II on Laser Standards, is charged with developing standards for laser materials, components, and for systems, and must eventually face the problem of what is a reasonable damage specification for a coated component.

We are once again indebted to the National Bureau of Standards, and especially to Mrs. Pauline Smith, and Dr. Harold Boyne, for their generous aid in the organization of this Symposium, their hospitality in accommodating us here, and their patience and persistence in helping us edit and prepare the proceedings of this Symposium.

Keynote Address

John D. Myers
Chairman Subcommittee II, Lasers, ASTM

The American Society for Testing and Materials is again sponsoring the Symposium on Damage in Laser Materials. As you have no doubt noticed, we have expanded our topics of interest somewhat to include damage in optical coatings and components. It seems that no sooner do we begin to understand what is happening to the laser, than the rest of the system demands attention too.

In my remarks last year, I devoted some time to the subject of "incomplete communication" with regards to damage threshold claims and tried to illustrate some of the embarrassment and frustrations which result. This year I would like to make some comments on another pitfall---misinterpretation of evidence.

I'm sure we have all been party to disputes wherein the laser systems engineer blamed the degraded performance of his system on poor coating and inferior material, while at the same time, his counterpart, who supplied him with the coatings and materials is complaining about the engineer who designs hot spots and focusing reflections into his systems.

Obviously, one or perhaps both have misinterpreted the evidence. As is usually the case, the misinterpretations are influenced by and tend to strengthen attractive or prevailing notions of what is going on, inaccurate or incomplete as they might be. To illustrate this malady without alluding to the laser industry, consider the case of the two women physicists on vacation in Scotland. It seems that they were strolling through the woods one afternoon when they came upon a Scotsman wearing kilts, asleep under a tree. The women gazed at the Scot for a while, wondering about that age-old question, "What does a Scot wear under his kilt?" Finally, their scientific curiosity got the best of them and they quietly, so as not to perturb the system, lifted the kilt and observed...nothing! Scotsmen don't wear anything under their kilts. Amused at their discovery and wishing to leave some evidence of their bold investigation, one of the women tied a blue ribbon around the item of interest. Then they quietly left the scene. Some time later, the Scot awoke and sensing that something was different, lifted the kilt and spied the blue ribbon. Somewhat startled, he said, "Hoot, Mon...I don't know where you've been or what you've been doing...but I'm glad to see you've taken first prize!"

Obviously, a misinterpretation of the facts.

Preconceived ideas regarding what has or has not happened are a constant source of misleading information. Within ASTM and the standards which we generate, we attempt to prevent misinterpretation of evidence by specifying clearly those constraints and areas of relevance wherein the specific tests are applicable. We include, of course, such factors as where it has been and what it has been doing.

On behalf of ASTM - WELCOME - to The Third Laser Damage Symposium.

Damage by Laser Radiation of Improved Neodymium-Activated Laser Glass, Colored Glasses and Optical Glasses

N. Neuroth, R. Hasse and A. Knecht
JENAer Glaswerk Schott & Gen., Mainz, Western Germany

The optical loss of Nd-activated laser glass (absorption 0.15%/cm at 1060 nm) has been reduced resulting in a substantially increased operating efficiency. Recent materials have given induced emission efficiencies approximately triple the results obtained with previously produced glasses. The damage (surface) threshold is reported to be 1.3×10^9 watts/cm^2 for active (lasing) operation. When irradiated passively (from external source) our measurements have shown the damage (bulk) limit to be 2.5×10^9 watts/cm^2. Metallic inclusions are eliminated by the melting process, which does not employ platinum.

Since optical or colored glasses are often used in laser applications, studies have been made of damage processes and limits of these materials also. A number of different glass types were irradiated with 0.7 millisecond laser pulses, and the energy level at which surface damage begins was determined (preliminary data). Among the colored glasses, the damage threshold is primarily a function of the material absorption at the wavelength of the laser beam.

Key Words: Colored glass, damage threshold, laser damage effects, laser efficiency, neodymium glass, optical glass, solid state lasers.

1. Improved Laser Glass

We have succeeded in reducing the optical losses in glass, within the wavelength range around 1060 nanometers, and thus in improving the laser efficiency. Previously, in a glass containing 3% Nd_2O_3, the loss at 1060 nanometers was measured to be approximately 0.5% per cm whereas it is now 0.15%, approximately 1/3 as earlier. In a glass containing 5% Nd_2O_3, the loss was reduced from 0.7% to 0.2% per cm. This results, naturally, in an increase in the laser effect, which is shown in figure 1 where the emitted energy of a rod of length 170 mm and thickness 12 mm: made from the old glass (LG 56) and one made from the new glass (LG 630), is plotted under identical stimulation conditions. The output energy of the LG 630 rod is about three times as high as that of the LG 56 rod with identical input.

Table 1 summarizes a few key properties. The fluorescence life time for Nd_2O_3 contents of 3% and 5% is above 600 microseconds. In case thin rods or activated light-conducting fibers are to be made, the Nd_2O_3 concentration can be increased up to 10% without an overly strong concentration quenching,

Table 1. Properties of improved laser glass

Glass type	LG 630	LG 650
Nd_2O_3 content %	3	5
aosorption at 1o6o nm (%/cm)	o,15	o,2
fluorescence life time (usec)	64o	65o
optical homogeneity	$\pm$ 2·1o^{-6}	$\pm$ 2·1o^{-6}
temperature coefficient of refractive index n at 1o6o nm ($^oC^{-1}$)	-2,2·1o^{-6}	-1,9·1o^{-6}
thermal expansion α ($^oC^{-1}$)	97	95
$(\frac{dn}{dT} - (n-1)\alpha)\cdot(^oC^{-1})$	-2,8·1o^{-6}	-3,o·1o^{-6}
stress optical constant at 535 nm $(\frac{nm/cm}{kp/cm^2})$	2,8o	

i.e., substantial reduction of fluorescence lifetime. A 10% Nd_2O_3 doping results in a fluorescence decay time of approximately 400 microseconds, using the new "600 series" glass host. The optical homogeneity has been maintained at the previous high levels, i.e. over some 10 cm the maximum variation of the refractive index is $\pm 2 \times 10^{-6}$. Furthermore, the temperature coefficient is negative, so that even with extremely heavy pumping there is only a small deviation of the beam wave front in passing through the rod. The divergence of the laser beam output from a rod of LG 650 glass, 170 mm length and 8 mm diameter, operating at a radiant energy of 2 joules, is approximately 2.5 mrad and, at a radiant energy of 16 joules, 2.8 mrad.

Figures 2 and 3 show the laser efficiency as a function of the reflectivity of the output mirror for a rod 170 mm in length and 12 mm diameter (fig. 2), and for a rod 76 mm in length and 8 mm diameter (fig. 3). These rods have been stimulated, in both cases, with a xenon flash lamp (equal in length to the rod) in an elliptical aluminum reflector (large axis 50 mm). Even in such a conventional type device an efficiency of 1% was attained with a 76 mm long rod, when using Nd_2O_3 concentration of 5%.

Table 2 summarizes results of tests carried out on an 8 mm diameter, water cooled rod operating in rapid impulse sequence. The efficiency is 1/3 to 1/4 percent. With a repetition rate of 3 pulses per second, an energy of 2 joules/pulse is possible.

Table 2. Radiation energy at high pulse frequency. Rod: LG 630 glass, 8 mm diameter, 170 mm length, water-cooled. Lamp: FX 65, water-cooled distance from laser rod approximately 20 mm. Reflector: Selective reflecting Duran 50 (cold-light-mirror): Reflectance of output mirror 72%.

Pulse frequency (p.p.s.)	Energy per single pulse (Joule)	Pulse duration (ms)	Mean output power (Watt)	Pumping energy per pulse (Joule)
1,6	5	1,0	8	1400
1,6	2,5	0,65	4	880
1,6	1,5	0,60	2,4	650
3,2	2,6	0,7	8,3	1000
3,2	1,2	0,6	3,8	600
3,2	0,5	0,4	1,6	450
6,3	0,05	0,3	0,3	320

2. Damage Threshold of the Laser Glasses

Figure 4 shows the device used for measuring the damage threshold of our glasses. A rod of LG 650 glass, 76 mm in length by 8 mm diameter, is pumped in an elliptical reflector by means of a xenon flash lamp. The resonator mirrors consist of a roof prism and a resonant reflector, being rotated at a speed of 16,000 r.p.m. The distance between prism and face plates is 53 cm. The half band width of the pulse is normally 40 nanoseconds. A glass plate which laterally reflects approximately 8% of the laser beam intensity is inserted in order to monitor the pulse duration and half band width. The beam intensity is varied with neutral density filters. To focus the beam, we use two lenses of different focal lengths as the beam spot diameter, measured in the focal plane, has been found to be particularly critical. We have determined this value by measuring the optical breakdown in air. In [1] it is stated that this breakdown occurs at a power density of 24×10^9 W/cm^2 (pulse duration: 40 ns). The intensity of the beam diverging beyond the focal point is measured versus increasing energy. So long as no breakdown in air occurs, the same energy is measured as before focusing. When breakdown in air occurs, however, the energy of the beam diverging from the focal point is lower. We have learned that the energy density of the beam differs slightly for rods of identical size. (The values in Table 3, marked by an asterisk, are less certain because the rod was damaged before the determination of the spot size.) Using the shorter (20 mm) focal length lens, lower damage thresholds are obtained than with the 60 mm f.l. lens. The character of the destruction within the glass is also different (fig. 5). In the samples damaged with the short focal length lens, the cracks are star-shaped, originating from a point. However, in the samples damaged with the 60 mm focal length lens the cracks occur along the beam direction. To clairfy this phenomenon, further tests must be made.

Table 3. Damage threshold of SCHOTT laser glasses.

Glass Type	Melt No.	Passiv SCHOTT f = 22 mm		40 ns Pulse f = 60 mm		T.H. Munich f = 150 mm		Pulse Length	Activ CGE 30 ns Pulse	
		(J/cm^2)	(GW/cm^2)	(J/cm^2)	(GW/cm^2)	(J/cm^2)	(GW/cm^2)	(ns)	(J/cm^2)	(GW/cm^2)
Old Types:										
LG 55	14829					41	2,6	16	30	1,0
LGN 55	15066					40	2,7	15		
	16177	73(*)	1,8(*)	106	2,6					
LG 56	14990					51	3,4	15	40	1,3
	15301	50(*)	1,2(*)	90	2,2	55	3,7	15	40	1,3
LG 57	16058					50	3,6	14	30	1,0
	16145	67(*)	1,7(*)	94	2,3					
Improved Types:										
LG 630	16091	67	1,7	102	2,5	49	2,9	17	20	0,7
	16161	47	1,2	124	3,1	42	3,0	14	40	1,3

In Table 2 the passive damage threshold is listed according to our measurements with pulses of 40 nanoseconds, and the results obtained at the Technische Hochschule, Munchen (Prof. W. Kaiser and Dr. H. Puell) using pulses of 15 nanoseconds, as well as the data supplied by the Compagnie Generale D'Electricite, Marcoussis, (Mr. J. Davit) on the active damage threshold. This is the energy or power density which can be produced with a rod from the glass melt involved, without any damage occurring. At higher energies surface damage may occur. The glass rods were of lengths from 300 to 700 mm. The samples for measuring the passive destruction were of the following dimensions: 20 x 20 x 20 mm and 20 x 20 x 30 mm. The lowest energy or power density at which a damage can be noticed with the naked eye is stated. The focal length of the focusing lens used at the Technische Hochschule, Munchen was 150 mm. There, also, the spot size of the beam in the focal plane was determined by breakdown in air.

The results of our measurement with a focal length of 60 mm are in satisfactory accordance with the results of the measurements made at the Technische Hochschule,Munchen taking into account the different pulse duration. The ratio between active (surface) and passive (interior) damage threshold (measurements by CGE vs. measurements by Schott and by Technische Hochschule, Munchen) appears to be between 1 : 2 and 1 : 3. The improved glasses show the same damage threshold as the glasses from earlier productions.

3. Surface Damage of Colored Glasses

Colored glasses are used in laser technology in many ways. For example: a) The radiation of the flash lamp is filtered, so that only the spectral range is transmitted which is useful in stimulating the laser material. b) The stimulating radiation is filtered off from the laser radiation. c) Filter glasses are used for eye protection, i.e. the filter itself must absorb the laser radiation, while transmitting in other areas of the visible spectrum (where there is no laser energy).

It is interesting to know the damage threshold of these glasses. For this test we have applied no giant pulses but only pulses with a duration of approximately 0.7 milliseconds. These pulses were generated with a 170 mm long Nd-glass rod of diameter 12 mm and the radiation was directed at the surface of a sample of 40 x 20 x 5 mm by means of a lens with focal length 22 mm. The beam spot size at the focal point of the lens was measured in this case as follows: The light diverging from the focal point was focused on a photocell by means of a large aperture convex lens. Between the focal point of the first lens and the second focusing lens an iris was placed at varying distances from the focal point. Laser pulses of identical intensity were generated, and the aperture of the iris diaphragm was reduced until the photocell indicated 50% of the intensity of the unlimited beam. This method yielded, to a precision of 20%, the same beam spot size at the focal point as the method, described above, of measuring the air breakdown with giant pulses. With lenses of 20 mm focal length, the image defects are so large that conventional evaluation of the beam cross section in the focal point from the divergence of the laser beam is not possible.

For practical considerations, surface destruction was measured first--as it occurs normally at a lower energy than the internal (bulk) destruction which is to be measured and reported later. In most

450-417 O-71—2

cases the surface damage site shows molten residue (fig. 6). In some glass types, cracks or chips are observed extending vertically from the damage spot. In figure 7 the damage threshold is plotted as a function of the absorption coefficient for the laser wavelength (1060 nm). The higher the absorption, the lower the damage threshold. When you attempt to approximate the correlation by a straight line in the double logarithmic scale, the "best fit" straight line is found to be given by the following formula:

$$E_{thr} = \frac{185}{k^{0.74}}$$

E_{thr} = threshold energy in joule/cm^2

k = absorption constant in cm^{-1} (according to the relation $K = \frac{1}{d} \ln \frac{1}{Ti}$,

where means d = sample thickness and Ti = internal transmission).

This empirical formula is valid for k-values in the region 10^{-2} to 50. The measured deviations from this approximating function are fairly large. This is due to the different chemical composition of the various glass types considered and the formula is offered only as a practical "guide". This representation is also suited to estimating the order of magnitude of the damage threshold in the case of laser beams having different wave lengths, provided the absorption of the colored glass at the wave length in question is used. In cases where the absorption coefficient is smaller than 0.01 cm^{-1}, no statement can be made because properties other than the absorption are then more important in predicting the destruction process. Also, this can be the case where short laser pulses (nanoseconds, picoseconds) are involved.

4. Surface Damage of Optical Glasses

The laser technology offers many applications for optical glass: in the laser as a resonator mirror or as a totally reflecting prism, or for beam focusing or beam expansion. In these applications, it is interesting to know the energy density to which our glasses can be used without being damaged.

Here, also, we have investigated the destruction of the surface, because it occurs at a lower energy than the internal damage. The threshold value of the surface damage is, however, a function not only of the glass type, but also of the surface finish. On all samples (40 x 20 x 5 mm) a high quality "pitch polish" finish was obtained in order to match the practical conditions in an optical apparatus. In colored glasses there is a dependence on volume absorption. However optical glasses show practically no bulk absorption, and this process is therefore not of major importance in the damage mechanism. However, small absorbing particles (undissolved melting residues, small crystals, or dissolved crucible materials--in praticular, platinum) may be present in the glass. Such absorption centers cause heavy localized heating which generates stresses exceeding the ultimate stress limit of the material. Thus, the damage threshold will be a function of the concentration of such localized centers, i.e. of the purity or microhomogeneity of the glass or the surface. According to [2], particles smaller than 0.1 micron are of no significance in irradiation with laser pulses having a duration of 30 nanoseconds or more, since the heat dissipation into the environment takes place so fast that no major thermal stresses can build up. This would naturally apply to the relatively long pulses such as we have used here and only those centers of 1 micron and larger diameter are to be considered critical. The second relevant factor is the internal strength of the glass against mechanical pressure and tension. The phenomena of ionization and electrostriction, which are essential for nanosecond pulses, are of no significance for the relatively long pulses (0.7 msec.) applied here.

Table 4 is a listing of the lowest energies at which damage could be detected with the naked eye for the various materials. The differences between the various glass types cannot be explained in detail at this time. Roughly speaking, crown glass types seem to be more durable than flint glasses. Exceptions are the types Sk, SSK, LaK, whose behavior differs very much according to type number, or whose damage threshold is only very low. Among flint glasses, there are few types with high damage threshold, such as KF, KzF, KzFS, TiF.

In very many of these glasses, the damage site on the glass surface shows molten residue similar to those in the colored glasses, in contrast to the internal failures observed after descruction by giant pulses.

Table 4 Damage threshold of SCHOTT optical glasses. Min. energy density causing visible damage.

Glasstype	Damage Threshold kJ/cm^2	Glasstype	Damage Threshold kJ/cm^2
FK 1	>16	SK 2	15,2
FK 1	>16	SK 3	8,2
FK 3	16,9	SK 4	9,8
FK 5	>16	SK 5	6,6
FK 6	>16	SK 6	5,3
FK 50	16,9	SK 7	12,3
FK 51	16,9	SK 8	6,8
		SK 9	8,4
PK 1	>16	SK 10	12,9
PK 2	>16	SK 11	12,8
PK 3	15,3	SK 11	16,8
PK 50	>16	SK 12	12,8
		SK 13	9,6
PSK 2	>16	SK 14	16,0
PSK 3	>16	SK 15	11,6
PSK 50	>16	SK 16	>16
PSK 51	>16	SK N 18	>16
PSK 52	16,1	SK 19	6,2
PSK 53	16,1	SK 20	12,8
		SK 51	10,0
BK 1	>16	SK 52	7,8
BK 3	>16		
BK 4	>16	KF 1	15,5
BK 4	13,3	KF 2	14,2
BK 5	>16	KF 3	>16
BK 6	>16	KF 6	>16
BK 7	>16	KF 8	5,6
BK 8	>16	KF 9	13,8
BK 10	>16		
BK 50	16,7	BaLF 1	3,3
UBK 7	>16	BaLF 2	6,0
		BaLF 3	5,0
Ba LK 1	15,1	BaLF 4	7,8
Ba LK 3	>16	BaLF 5	4,7
Ba LK 3	>16	BaLF 6	4,3
		BaLF 7	5,0
K 3	>16	BaLF 8	6,8
K 4	>16	BaLF 50	7,6
K 5	>16	BaLF 51	12,4
K 7	>16		
K 10	>16	SSK 1	6,7
K 11	>16	SSK 2	2,1
K 50	>16	SSK 3	1,6
UK 50	>16	SSK 4	4,1
		SSK N 5	2,9
ZK 1	14,6	SSK N 8	7,8
ZK 2	>16	SSK N 18	7,0
ZK 5	15,9	SSK 50	3,4
ZK N7	>16	SSK 51	6,5
ZK 8	>16		
		LaK 3	3,6
BaK 1	16,1	LaK N 6	12,9
BaK 2	15,8	LaK N 7	16,0
BaK 3	15,6	LaK 8	>16
BaK 4	>16	LaK N 9	4,4
BaK 5	14,3	LaK 10	12,0
BaK 6	16,3	LaK 11	15,9
BaK 50	8,1	LaK N 12	< 0,2
		LaK N 13	4,4
SK 1	5,2	LaK N 14	5,9
SK 1	15,4	LaK 16	16,0

Table 4, continued

Glasstype	Damage Threshold kJ/cm^2	Glasstype	Damage Threshold kJ/cm^2
LaK N 16	7,2	BaSF 12	3,0
LaK 17	2,0	BaSF 13	1,8
LaK N 18	10,0	BaSF 14	5,0
LaK N 19	7,6	BaSF 15	2,8
LaK 21	> 16	BaSF 50	0,7
LaK 22	4,0	BaSF 51	4,3
LaK 23	6,2	BaSF 52	< 0,2
LaK 24	12,8	BaSF 53	2,7
LaK 25	4,8	BaSF 54	0,8
		BaSF 55	2,4
LLF 1	4,5	BaSF 55	2,6
LLF 2	8,6	BaSF 56	1,8
LLF 3	3,5		
LLF 4	4,2	LaF N 2	4,1
LLF 6	5,5	LaF N 3	10,3
LLF 7	4,0	LaF N 7	1,0
		LaF N 8	5,6
BaF 1	2,6	LaF 9	1,0
BaF 2	6,9	LaF N 11	0,9
BaF 3	7,0	LaF 12	3,2
BaF 4	5,2	LaF 13	2,5
BaF 5	5,6	LaF 20	5,5
BaF 6	6,2	LaF 21	2,0
BaF 7	6,6	LaF 22	< 0,2
BaF 8	4,3	LaF 23	11,9
BaF 9	3,6	LaF 24	11,6
BaF N 10	8,4	LaF 25	7,3
BaF N 11	6,2		
BaF 12	3,7	LaSF 1	8,8
BaF 13	1,5	LaSF N 3	5,1
BaF 50	1,2	LaSF 5	0,8
BaF 51	1,3	LaSF 6	1,1
BaF 52	1,6	LaSF 7	2,0
		LaSF 8	3,7
LF 1	6,5	LaSF 9	1,8
LF 2	4,1	LaSF 11	9,4
LF 3	3,9	LaSF 12	1,0
LF 4	4,2	LaSF 13	3,2
LF 5	5,0		
LF 6	8,2	SF 1	0,9
LF 7	9,4	SF 1	1,0
LF 8	5,7	SF 2	3,4
		SF 3	< 0,2
F 1	3,7	SF 4	< 0,2
F 2	2,8	SF 5	1,5
F 3	1,5	SF 5	1,0
F 4	2,5	SF 6	0,5
F 5	4,0	SF 7	1,0
F 6	2,9	SF 7	2,2
F 7	3,5	SF 8	1,5
F 7	4,2	SF 9	1,8
F 8	3,4	SF 10	0,7
F 9	3,4	SF 11	0,2
F 10	1,7	SF 12	1,2
F 11	1,2	SF 13	1,1
F 13	3,6	SF 14	0,8
F 14	1,3	SF 15	< 0,2
F 15	3,5	SF 16	1,1
		SF 17	1,6
BaSF 1	1,7	SF 18	0,4
BaSF 1	3,6	SF 19	0,8
BaSF 2	1,9	SF 50	4,6
BaSF 3	3,0	SF 51	1,4
BaSF 5	2,7	SF 52	1,3
BaSF 6	2,4	SF 53	0,7
BaSF 10	5,6	SF 54	0,4

Table 4, continued.

Glasstype	Damage Threshold kJ/cm^2	Glasstype	Damage Threshold kJ/cm^2
SF 55	< 0,2	Kz F 1	>16
SF 56	0,3	Kz F 2	>16
SF 57	< 0,2	Kz F 4	>16
SF 58	< 0,2	Kz F 5	>16
SF 59	0,2	Kz F 6	>16
SF 61	0,4		
		Kz FS 1	>16
Ti K 1	> 16	Kz FS 2	>16
		Kz FS N 4	2,1
Ti F 1	11,6	KzFS 5	13,8
Ti F 2	16,8	Kz FS 6	15,8
Ti F 3	>16	Kz FS 7	16
Ti F 4	1,1		
Ti F 5	1,8		
Ti F 6	4,8		

We have investigated which properties are essential for the resistance of the glasses to laser beam pulses. A certain correlation exists between the portion (percent by volume) of the glass-forming oxides and the damage threshold, as has already been mentioned in [3] (fig. 8). Normally, the content of glass-forming agents is higher in crown glasses than in flint glasses. Furthermore, there is a correlation between the damage threshold and the specific heat (fig.9) and also between the product of the specific heat and the temperature at which the viscosity of the glass is 10^4 poises (fig.10).

The same order of magnitude of the damage threshold in laser beam pulses of a duration of 1 ms has been found in [4] and [5]. Most bibliographic references concern the destruction by bombardment with pulses of nanoseconds and shorter where, primarily, processes other than thermal stresses are essential. The values stated are provisional and not guaranteed for general production, since--in most cases--only one melt of each glass type has been analyzed and, as yet, the variations between several melts are undetermined. We recommend one should remain considerably below the value of the damage threshold reported, if possible, due to these uncertainties.

References

[1] Akhmanov, S.A., Kovrigin, A.I., Strukov, M.M., Khokhlov, R.V., Frequency dependence of the threshold of optical breakdown in air, JETP-Letters 1, (1965), 25-29.

[2] Hopper, R.W., Uhlmann, D.R., Mechanism of inclusion damage in laser glass, J. Appl. Phys. 41, (1970) 4023-4037.

[3] Greco, E.J., and Martinelli, J.A., Compositional dependency of laser-induced damage in glass, J. American Ceramic Society, 50, (1967) 270.

[4] Martinelli, J., Laser-induced damage thresholds for various glasses, J. Appl. Phys. 37, (1966), 1939-1940.

[5] Gangardt, M.G., Grasyuk, A.Z., and Zubarev, I.G., Mechanism for glass destruction by the radiation from ruby and neodymium lasers (free-generation mode), Sov. Phys. - Solid State, 11, (1970), 2397-2401.

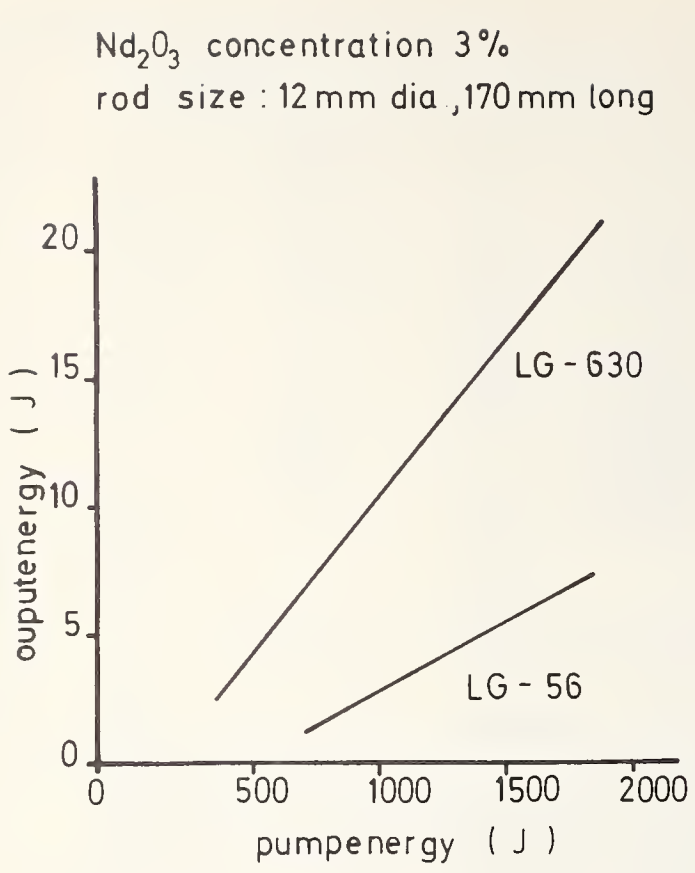

Fig. 1 Output energy versus pump energy of improved SCHOTT laser glass LG 630 in comparison to the glass LG 56 of former production (in both types 3% Nd_2O_3)

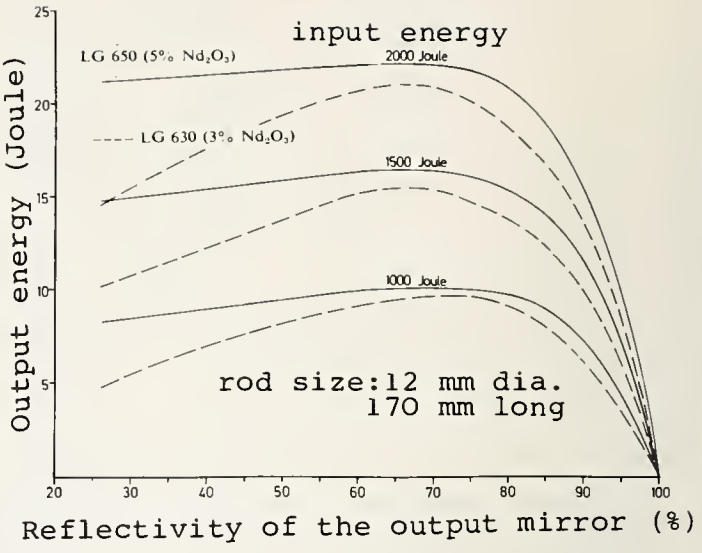

Fig. 2 Output energy versus reflectivity of the output mirror

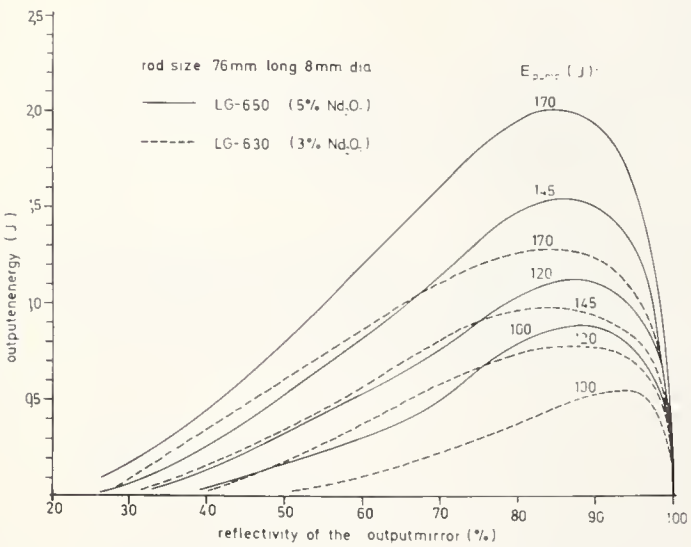

Fig. 3 Output energy versus reflectivity of the output mirror

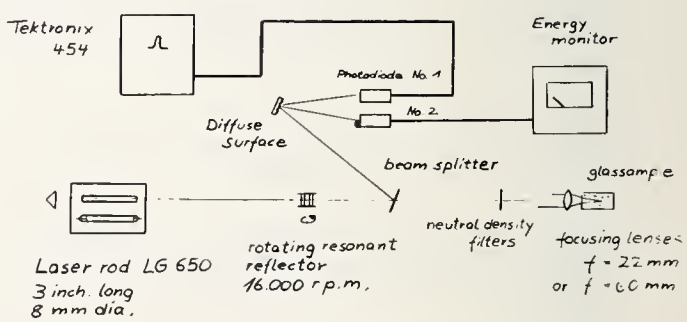

Fig. 4 Experimental set-up used to measure the damage threshold (giant pulses)

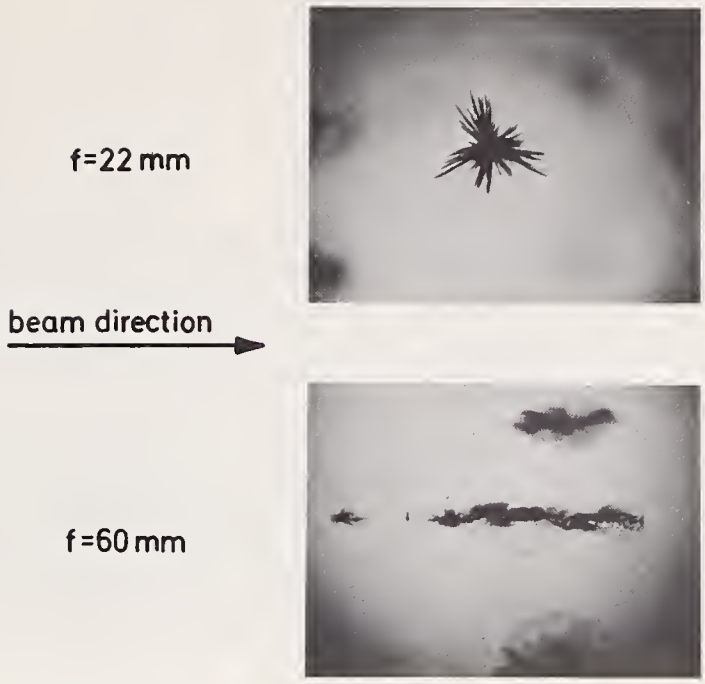

Fig. 5 Internal damage caused by focused laser beam (f = focal length)

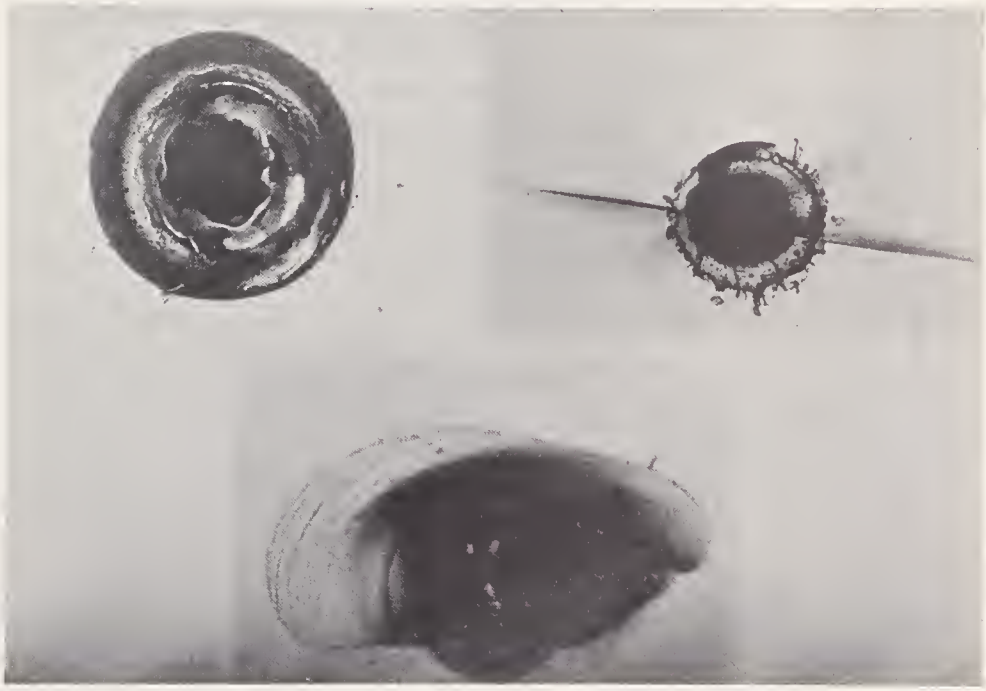

Fig. 6 Surface damage of SCHOTT optical color glasses

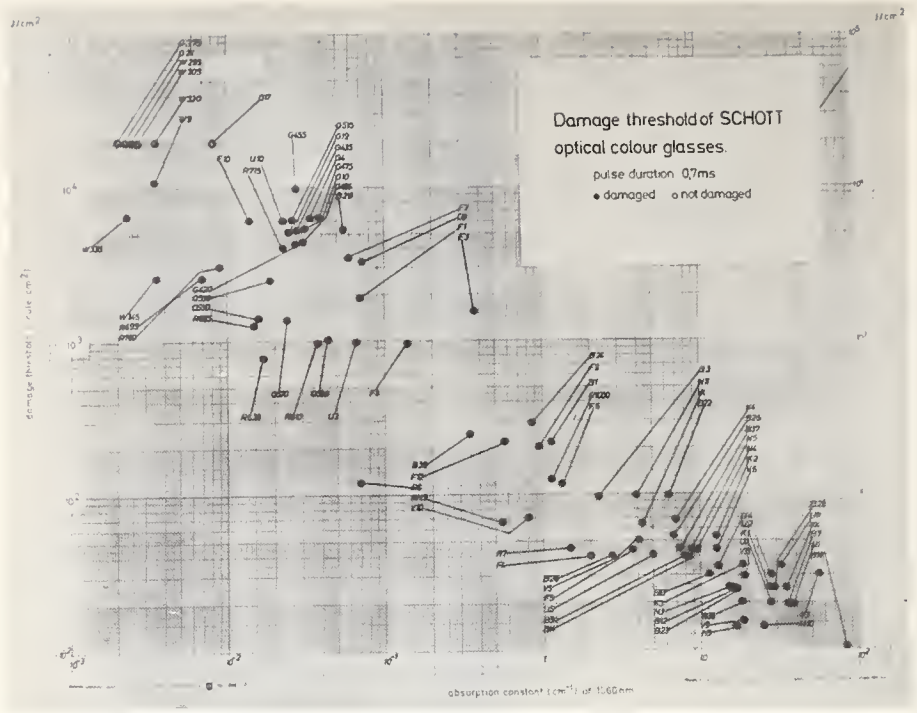

Fig. 7 Surface damage threshold of SCHOTT optical color glasses versus glass absorption

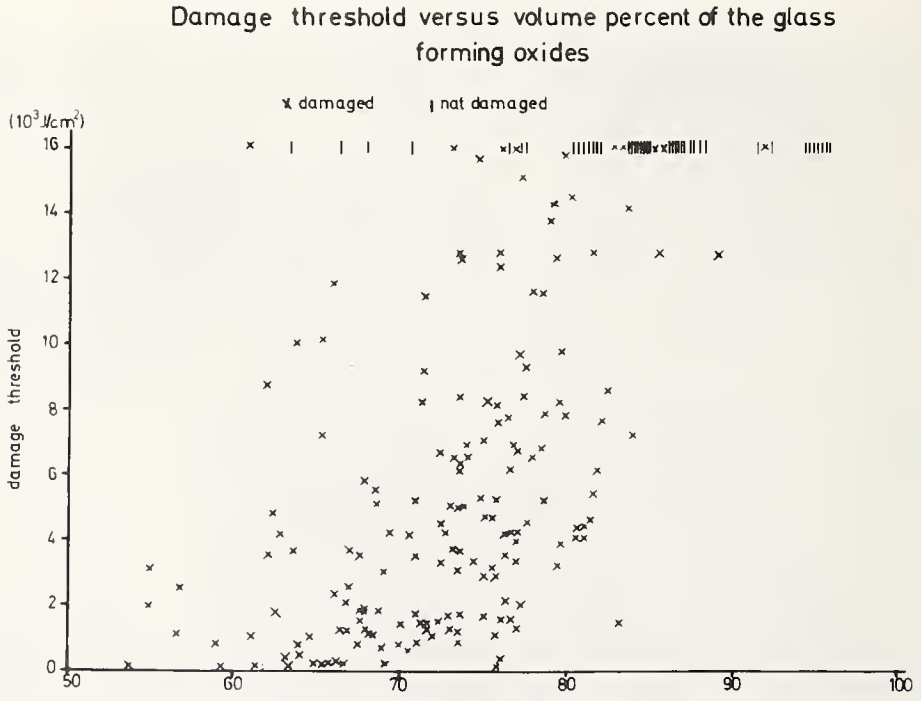

Fig. 8 Correlation of damage threshold and volume per cent of glass forming oxides

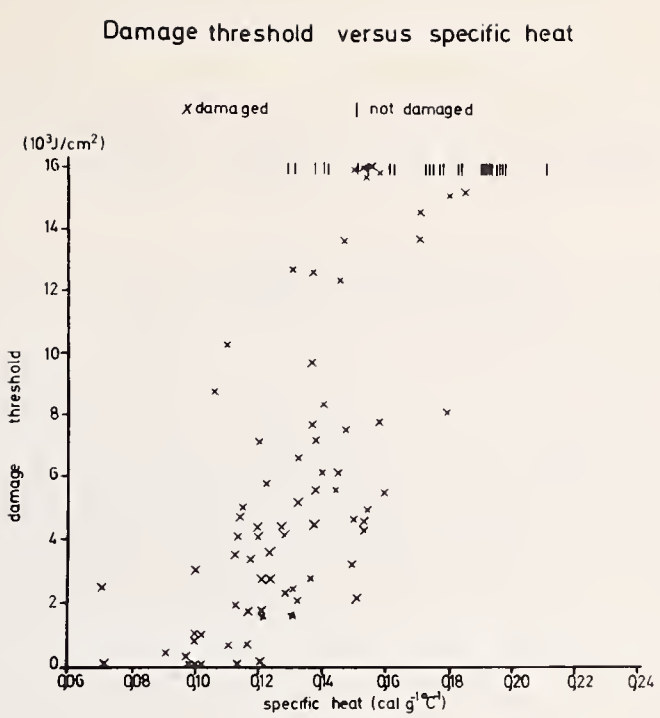

Fig. 9 Correlation of damage threshold and specific heat

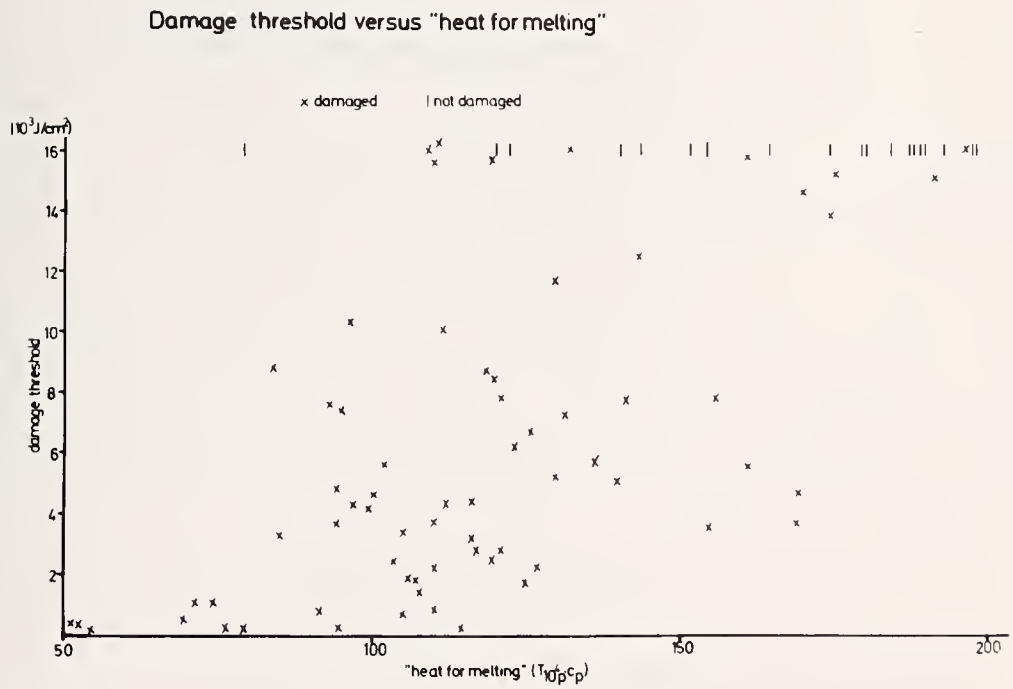

Fig. 10 Corrleation of damage threshold and "heat for melting"

COMMENTS ON PAPER BY NORBERT NEUROTH

In response to questions from the floor, a number of points of experimental procedure in connection with this investigation were clarified. It was established that the pumped samples were protected from the ultraviolet radiation of the flash lamp by enclosing the sample in a supremax tube. During damage testing which was carried out on a single shot basis, air cooling was employed; while water cooling was employed during rapid pulse sequences. The output of the test laser was not subject to transverse mode control. In the tests the full output of the laser was used. Two methods were used to measure the peak power density in the laser output. One was the observation of the threshold for the formation of an air spark at the focal point of a lens. The other was a technique whereby an iris was placed in the beam of the laser and the aperture diameter at which half of the total energy was transmitted was determined. From this measurement the peak power density could be estimated from the measurement of total energy and pulse duration. The two methods agreed to within 30%. The definition employed for damage threshold was the following: the damage threshold was defined as the lowest power density at which visible damage of the sample was observed with the unaided eye. Some spread in the results was observed. A much greater variation in the observed damage threshold was seen in filter glasses than in laser glass. This was attributed to the much higher degree of reproducibility required in melting laser glass. For a given sample of laser glass the observed damage threshold was seen to depend on focal length of the lens employed in the test and for a given focal length and given sample, damage thresholds were observed to be reproducible to within about 35%. The difference in the damage threshold observed in active tests and passive tests was attributed in part to thermal stresses induced by the pump light in the active measurements, and in part to the self-focusing of the incident laser beam in pumped samples, which in turn raised the local power density. The lower extinction coefficient quoted for the new Schott laser glasses was attributed primarily to a reduction in the iron content of the glass but also, possibly, to a decrease in scattering losses. Two results for damage with picosecond pulses were quoted by the speaker. Jean Davit at C.G.E. has reported a damage threshold in a picosecond regime of 20 joules per square centimeter for filamentary damage. This result was somewhat dependent on sample size and was reported in the Proceedings of the 1970 Symposium on Damage in Laser Materials. Recently, damage well above threshold has been observed at the Max Planck Institute in Munich at power levels of 50 gigawatts per square centimeter in 10 picosecond pulses.

Laser Glass Damage Threshold Studies At Owens-Illinois

N. L. Boling and R. W. Beck

Owens-Illinois Inc.
1700 N. Westwood Ave.
Toledo, Ohio

Owens-Illinois is continuing its efforts toward an understanding of damage induced in laser glass materials exposed to high intensity laser pulses. While previous efforts have been directed toward a characterization of the magnitudes of the threshold damage due to particulate inclusions, surface interactions, and self-focusing, current work concerns itself primarily with an investigation of the mechanisms responsible for surface damage. To this end, a high intensity, TEM_{oo} mode, neodymium glass, oscillator-amplifier system is used to induce surface damage in damples of laser glass, while a TEM_{oo} mode ruby laser is used to record high speed holograms of the damage interactions. This technique not only allows an investigation of the plasma produced at the sample surface but also detects the creation of shock waves within the sample. With various time delays between the damaging and the recording laser pulses it is possible to evaluate the temporal development of both the plasma and the shock wave. By using multiple exposure techniques further information is obtained from the recorded refractive index variations.

A brief discussion of the glass and ruby lasers as well as the holographic technique will be presented with primary emphasis placed upon the interpretation of the recorded plasmas and shock waves and their significance to laser glass surface damage.

Key Words: Holography, inclusion damage, plasma and shock waves, and self-focusing surface damage.

1. Introduction

The continuing effort at Owens-Illinois to further increase the damage threshold of laser glass has been divided into two areas, inclusion damage and surface damage. The problem of inclusion damage, having previously been characterized in this and other laboratories, is being approached at the glass melting stage, the goal being to completely eliminate all damaging inclusions from the finished laser glass. Surface damage is being studied from two complementary aspects, investigations of mechanisms responsible for surface damage and studies of the efficacy of various treatments of the glass which might increase the damage threshold. The problem of self trapping or bulk damage is under investigation only to the extent that it is related to surface damage and/or the experimental technique used for studying surface damage lends itself to this end. High speed holography is the technique employed to study damage. The holograms obtained yield information about acoustic disturbances in the glass and plasmas on the surface immediately after the passage of a damaging pulse through a glass sample.

The laser employed for inducing damage is a high power, Q-switched, glass laser. It is currently undergoing modification to yield an output in the TEM_{oo} mode.

2. Inclusion Studies

Several types of inclusions have been hypothesized to cause damage to laser glass but the most likely suspect in glass melted in platinum crucibles is platinum inclusions. Consequently, in attempting to prevent the occurrence of inclusions it is proper to address the question of possible mechanisms by which platinum can enter the glass during the melting process. Many such mechanisms have been suggested but the most probable culprit is oxygen in the melting environment. Obviously, then, the thing to do is to eliminate oxygen from the melting environment. However, this can be done only to a degree with glass melted in a platinum crucible. When the partial pressure of oxygen is lowered too

far, the platinum of the crucible is attacked by components of the glass, silicon being the first to react with platinum as the oxygen partial pressure is lowered. The trick is to lower the oxygen content far enough to prevent formation of platinum inclusions in the glass but not so far as to cause crucible attack.

During the past year we have theoretically examined the thermodynamics of the melting of laser glass in a platinum crucible under a reduced partial pressure of oxygen. These studies have indicated that it is indeed possible to strike the happy medium between introduction of platinum into the glass and crucible attack. The desired partial pressure of oxygen can be attained and maintained through the use of $CO\text{-}CO_2$ as a purging gas during melting. This acts as a buffer which controls the amount of oxygen within relatively narrow limits.

In the near future, melts will be made utilizing $CO\text{-}CO_2$ as a means of oxygen control. The glass from these melts will be analyzed for platinum and damage tested by a high power laser beam.

3. TEM_{oo} Mode Laser

In the past many studies of surface and self trapping damage have been conducted by various groups. Some of these groups have used low energy output lasers operating in the TEM_{oo} mode. The laser beam is focused in order to obtain the power densities required to cause damage. Other investigators have used high energy output lasers operating multimode. Several objections can be raised to either of these procedures. The validity of these objections is suggested by the fact that wide discrepancies exist among reported damage thresholds.

Because of these various objections raised to focused or multimodal systems we have decided to modify the glass laser system which we have been using for damage studies at Owens-Illinois. Until recently this oscillator-amplifier system was operated multimode and was capable of delivering more than 100 joules in a 40 ns pulse. The modification, which is still in process, will result in a system which operates in the TEM_{oo} mode with an output of 40-50 joules in 30-50 nanoseconds. The oscillator and two amplifiers of this system have been assembled. A diagram of the oscillator is shown in Figure 1. The Brewster-Brewster rod is of 3/4" diameter x 12" length, with 9" pumped by two close wrapped helical flashlamps. The energy to each lamp is nominally 3500 joules. The TEM_{oo} mode is achieved through the use of a 2.0 mm aperture in the cavity. The output of the oscillator is approximately 250 mj.

A plano-plano mirror configuration is utilized in the oscillator, although it is expected that improved operation could be obtained with a plano-concave arrangement. The lack of difficulty in obtaining the TEM_{oo} mode and the fact that we were anxious to proceed with other work caused us to forego experimenting with curved mirrors. We plan to do this soon.

Figure 2 shows the oscillator-amplifier system as completed up to the present time. The two amplifiers are similar in construction to the oscillator lamp and rod configuration described above. One more similar amplifier will be added soon. The output of the system in its present form is about 8 joules in a 5.5 mm diameter beam. The divergence of the beam from the 5.5 mm aperture varies from 140 microradians to 230 microradians depending on the energy output.

Although the system is not complete and further modifications even of the oscillator and two amplifiers described will probably be made, some comments concerning some of the problems encountered in constructing the system are perhaps in order.

In the first attempt to obtain the TEM_{oo} mode no particular emphasis was placed on the quality of the oscillator rod used. With the same configuration as that shown in Figure 1 and a rod with one wave full aperture stress in it, we were unable to obtain any single spatial mode, even with an aperture as small as 0.5 mm diameter. Replacement of this rod with a carefully selected rod exhibiting less than 1/5 wave full aperture optical distortion resulted in easy attainment of the TEM_{oo} mode, even with an aperture as large as 3.5 mm.

Another point of interest is the effect of an inclusion in an amplifier rod. When the rod of the first amplifier was utilized in the previous multimode system, an inclusion present in the rod did not manifest itself in any apparent way in the output beam. However, when the TEM_{oo} mode beam was amplified by this rod the presence of the inclusion became very apparent in the near field burn pattern. Figure 3 shows this burn pattern. The relatively large hole probably stems from the heating of the inclusion by the laser pulse, and the fact that it shows up in single mode operation while it does not in multimode operation can be attributed to the spatial coherence across the entire single mode beam.

The use of apertures in the system has been found necessary in order to obtain a "clean" output. However, the positioning of these apertures is critical. The slightest misalignment results in the loss of the circular symmetry in the output beam.

Finally, it should be mentioned that the system described here is the result of a modification of an already existing system. The system would be different in several respects if it had been designed from scratch.

4. Surface Damage Studies

4.1. Damage Mechanisms

Several investigators have hypothesized various mechanisms to be responsible for surface damage of glass subjected to a high power laser pulse. Some of these are as follows:

(1) The electrostrictive interaction between the laser beam and the glass causes a radial constriction of the glass. The Poisson effect resulting from the squeeze causes a compression wave to be propagated along the laser beam. When this compression reaches the surface the unloading effect causes rupture of the surface.

(2) Stimulated Brilloiun scattering initiates and amplifies an acoustic wave which propagates along the forward direction of the beam. This wave ruptures the surface upon incidence.

(3) The surface plasma, which invariably accompanies surface damage and which forms in the first few nanoseconds of the laser pulse, rapidly expands upon partial absorption of the tail end of the pulse. This expansion creates a shock wave which damages the surface. The plasma originally stems from desorption of impurities from the surface.

(4) The surface plasma of (3) bombards the surface with thermally energetic ions. This results in thermal erosion of the surface.

Self trapping could play a role in any of these mechanisms. It would be particularly effective in cases (1) and (2) where the magnitude of the internal acoustic disturbances would be much greater in a trapped portion of the beam.

4.2. Holographic Studies of Damage

We have been using high speed holography to investigate the mechanisms responsible for damage. Figure 4 is a diagram of the essentials of the experimental arrangement. A 40 ns damaging pulse from the glass laser is passed through a one inch cube of ED-2 laser glass. (Some of the samples in this paper were 3/4" on one side.) The damaging beam was passed through a lens prior to incidence on the sample. This was either a 10 or 25 cm focal length lens. In the 10 cm case the surface to be studied was placed near the focal point, this inspite of the objections alluded to above. The reason for this was that only one amplifier was in the glass laser system at the time and such operation was necessary to easily achieve damaging power densities. When the 25 cm lens was used the focal point was several cm from the exit surface of the sample.

At a selected time after the damage pulse, a hologram is made of the sample through the use of a ruby laser which emits a TEM_{oo} pulse of 20 ns duration. The time interval between the damage pulse and the hologram pulse can be varied from 0 to several microseconds. Up to 500 ns the interval can be controlled to within 10 ns.

Two types of holograms are made with this apparatus, single exposure and double exposure. The single exposure, in which the ruby laser is fired only once, results in a shadowgram superimposed on the hologram of the sample. The shadowgram shows regions in which the optical density changes rapidly in space. The double exposure technique, which is of course quite well known, requires that a hologram first be made of the sample without the damaging pulse. Next, the sample is subjected to the damaging pulse and another hologram is made after the selected time interval. The result is a hologram of the sample with fringes due to the difference in its state between the two holograms. A shadowgram is also present in the resulting hologram.

Figure 5 is a photo of the virtual image of a hologram made by a single exposure. The damaging beam was passed through a 10 cm lens focused just beyond the exit surface. (The exit face is in the right hand side of the photo in this and all other photos in this paper.) The delay, that is the time between the damaging pulse and the ruby pulse, is 190 ns. The damage to this sample took the form of a small pit, which is characteristic of exit damage. Two acoustic waves can be seen clearly in the photo. Note that the origin of these waves is obviously the damage site in the surface and that no other disturbances are seen inside the sample.

The plasma associated with the damage can be clearly seen in the photo. A salient feature of this plasma is that part of it is opaque to the ruby laser used to make the hologram. This can be interpreted to mean that the electron density in the opaque region is large enough to render the plasma frequency greater than the ruby laser frequency. Simple calculations show that the cutoff density for light of the rub wavelength is approximately 2×10^{21} electrons/cm^3. Although this interpretation of the opaqueness is in keeping with the results of other investigators[1,2] who have observed that a large part of the damaging pulse is absorbed by the plasma, some of the double exposure holograms we have taken cast doubt on it. Another possible interpretation is that the opaque area is due to the glass expelled from the damage site.

The conditions described for Figure 5 also apply to Figure 6 except the delay is 1400 ns. Again two waves are clearly seen moving away from the damage site.

Interesting features of Figures 5 and 6 are the shape of the plasma and the pear shaped shadow visible just in front of the opaque region. Figure 7, which was taken from a double exposure hologram, and consequently exhibits the fringes characteristic of such a hologram, shows this pear form even more clearly. That this particular shape is not solely the result of the interaction of the laser beam with the surface is evidenced by Figure 8 which shows a double exposure of the air spark formed at the focal point of the 10 cm lens. The characteristic shape of the plasma in Figures 5-7 is obviously due to two air breakdown points near the focal point of the 10 cm lens.

This, incidentally, points up the danger of using a focused beam to study damage. One can easily imagine that results of damage threshold measurements could be affected by a damaging beam of this sort.

Returning to Figure 7, in which the delay is 1500 ns, note again the opaque region. A troublesome aspect of this is the failure of the fringes to grow more dense as the opaque area is approached. Calculations indicate that one fringe in this plasma corresponds to an electron density change of about 3×10^{18} electrons/cm^3. Thus a plasma frequency greater than the frequency of ruby light should yield a great number offringes. Also troublesome is the idea that the plasma is dense enough to be opaque at such a long time after the damaging pulse.

In Figures 5-7 two distinct acoustic waves can be seen propagating away from the damage site. In Figure 6 the first wave has reached the surface of the sample and been reflected as two waves, the first (leading) a longitudinal wave and the second a transverse wave. This is also the relation between the two waves propagating away from the damage site. Taking the measured values of the bulk modulus, the shear modulus, and the density of ED-2, the glass used in these experiments, the speeds of a longitudinal wave and shear wave are calculated to be 6.5×10^5 cm/sec and 3.8×10^5 cm/sec respectively. The ratio of these is 1.7. Measurements of the distances traveled by the two waves on several different holograms taken with various time delays consistently yield a ratio of 1.8.

In Figure 7 a distinct "kink" can be seen where the transverse wave meets the surface of the sample. This is probably due to a Rayliegh surface wave propagating along the surface away from the damage site. The speed of such a wave in a material is 0.9 times the speed of a transverse wave, so the relative distances from the damage site of the transverse wave and the "kink" in Figure 7 are about right to support such an interpretation.

Figure 9 is a single exposure taken with a delay of 190 ns. The 10 cm lens is focused inside the sample and self tracking damage can be seen. Surrounding the track is a cylindrical acoustic wave. Close examination shows that this cylinder is an envelope of a series of waves propagating away from the damage track. Figure 10 shows this even more clearly. Waves can be seen propagating in both directions; e.e., toward the exit and entrance faces.

Another interesting feature of Figure 10 is the appearanceof an acoustic wave at the entrance face. In fact, the purpose of this particular shot, in which several joules were focused on the entrance surface with the 10 cm lens, was to attempt to create an acoustic wave at the entrance surface. A small amount of pitting at the entrance was observed but the major damage was internal and on the exit face. Figure 11, which is a photo of the damage shot taken with an open shuttered camera, indicates how much more extensive the exit and internal damage are than the entrance damage. Damage tracks from previous shots are also seen in the photo. Note that the exit plasma is about as large as the entrance plasma even though the lens was focused at the entrance.

Figures 12-16 are all photos of double exposure holograms. The damaging beam was passed through a 25 cm lens whose focal point was several cm beyond the exit surface. The energy density is about the same for every photo - approximately 100 j/cm^2 at the exit face. Delay times, corresponding to the numerical order of the Figures, are 270 ns, 580 ns, 880 ns, 1600 ns, and 1900 ns. In the longer delay photos reflections from the surface are seen.

From this series of photos the rate of expansion of the plasma can be obtained. This expansion rate, which is the speed of sound in the plasma, depends upon the ion temperature of the plasma and is given by[3]

$$V_T = [\gamma(\gamma - 1)\, e]^{1/2}, \tag{1}$$

where e is the internal energy per gram of the plasma and γ is the effective adiabatic exponent.

The internal energy for air has been calculated[3] to be

$$e \simeq 2.7 \times 10^5\, T^{3/2}\, (\rho/\rho_o)^{0.12} \text{ erg/gm}, \tag{2}$$

where ρ/ρ_o is the density of air referred to standard conditions.

Using this as a rough approximation of the internal energy of the surface plasmas in these photos we obtain, with $\gamma = 1.2$,

$$T_i \simeq 5.4 \times 10^{-4}\, V_T^{4/3} \tag{3}$$

Table 1 lists the average transverse (to the direction of the laser beam) velocities $\langle V_T \rangle$ obtained by measuring the expansion of the plasma between two times t_1 and t_2.

That is

$$\langle V_T \rangle = \frac{r_2 - r_1}{t_2 - t_1}, \tag{4}$$

where r_2 is the radius of the plasma at time t_2 and r_1 the radius at t_1. The listed values of T_i are obtained from (3).

Table 1. Plasma expansion velocities and ion temperatures.

t_1(ns)	t_2(ns)	$\langle V_T \rangle$ cm/sec	T_i °K
0	270	7.4×10^5	3×10^4
270	580	2.6×10^5	9×10^3
580	880	2.3×10^5	8×10^3
880	1600	1.5×10^5	4×10^3
1600	1900	1.4×10^5	4×10^3

The ion temperature T_i of 3.6×10^4°K obtained from the average expansion velocity between 0 (the peak of the damaging pulse) and 270 ns is probably appreciably lower than T_i in the inchoative plasma near the end of the damaging pulse. Studies of ion temperatures in air sparks[2] indicate that T_i drops sharply in the first few tens of nanoseconds after the pulse.

4.3. Discussion

Although much analysis remains to be done and more extensive and well characterized experiments using the holographic technique presented in this paper need to be performed, some rough conclusions can be tentatively reached.

In none of the holograms taken thus far has any acoustic disturbance been detected moving toward the exit surface, except when there is gross internal damage of the sample. Acoustic disturbances are usually not seen at the entrance surface. Based upon the information presented in this paper and other holograms not presented herein, electron densities in the exit and entrance plasmas are generally between 10^{18} and 10^{19} electrons/cm^3, and perhaps much higher in the exit plasma in some cases. A typical expansion velocity of the exit plasma in its incipient stage is greater than 7×10^5 cm/sec. The ion temperature in the exit plasma is probably initially greater than 5×10^4°K.

In general, any hypothesis that purports to explain the surface damage phenomena must take into account the great difference between the entrance and exit damage thresholds. Most of the proposed mechanisms do this. The stimulated Brillouin acoustic wave travels toward the exit surface. In the plasma shock and thermal erosion hypotheses the well known tendency of the plasma to grow into the laser beam accounts for entrance and exit differences.

There appears to be another difference between exit and entrance damage and that is that the exit plasma is at least as dense and hot as the entrance plasma and usually appreciably larger, at least after the damage threshold has been reached. (It is reported[4] that the entrance plasma appears before the exit plasma as the energy density is increased toward the damage threshold.)

A phenomenological model which accounts for both the larger exit plasma and the higher entrance damage threshold is the following: At the exit surface a plasma is initially formed by desorption of impurities by the leading edge of the laser pulse. This might be enhanced by self trapping in the material. This plasma remains in close contact with the surface due to its' propensity to grow into the laser beam. UV radiation from the plasma raises electrons in the surface to the conduction band and this leads to increased absorption of the still incident laser pulse, and, consequently, to an increased rate of plasma growth. The characteristic pit is due to either thermal spallation or a combination of thermal effects and the shock from the expanding plasma acting upon the already thermally weakened surface.

The effectiveness of the shock in producing damage is enhanced by the acoustic impedance match between the surface and the plasma in close contact with it. (The velocity of sound in the plasma is not far removed from that of the shock wave in the glass.) The entrance surface damage threshold is higher and the plasma smaller because the plasma grows away from the surface. Consequently, the entrance is not as effectively subjected to either radiation or shock from the plasma. Any damage to the entrance surface is thermal in origin.

5. Plans For Future Work

Future work on surface damage will have several facets. Some of these are as follows:

(1) Finish assembling the high power glass laser to obtain the proposed characteristics presented in the first part of this paper.

(2) Further study the holographic technique used in an attempt to improve the quality of the holograms obtained.

(3) Further analyze the data already obtained.

(4) Continue to explore methods of surface treatment which might be efficacious in raising the surface damage threshold.

(5) Further modify the damage test glass laser to emit pulses in the nanosecond regime. We feel that this will eventually be necessary in order to completely study the phenomenon of surface damage. In fact, it will be desirable to be able to operate in the picosecond regime eventually, although we anticipate difficulty in attaining the TEM_{oo} mode in this case.

6. Acknowledgment

This work was sponsored by the Advanced Research Projects Agency of DOD.

7. References

(1) M. P. Lisitsa and I. V. Fekeshgazi, Ukrainian Physical Journal, 12, No. 10 p 1701 (1967).

(2) H. DuPont, A. Donzel, and J. Ernest, Applied Physics Letters, 11, No. 9, p 271 (1967).

(3) I. I. Komissarova, G. V. Ostrovskaya, and L. L. Shapiro, Journal Technical Physics, 40, No. 5, p 1072, (1970).

(4) I. A. Fersman and I. D. Khazov, Journal Technical Physics, 40, No. 5, p 1081 (1970).

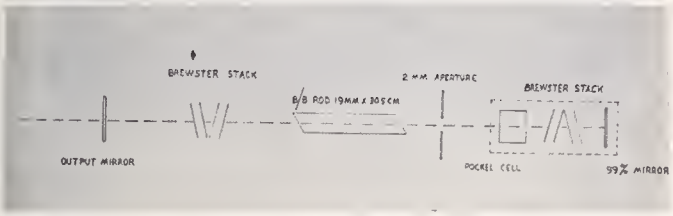

Fig. 1 Oscillator Section of Glass Laser

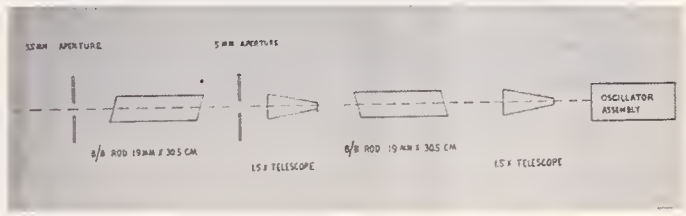

Fig. 2 Oscillator and Amplifiers of Glass Laser

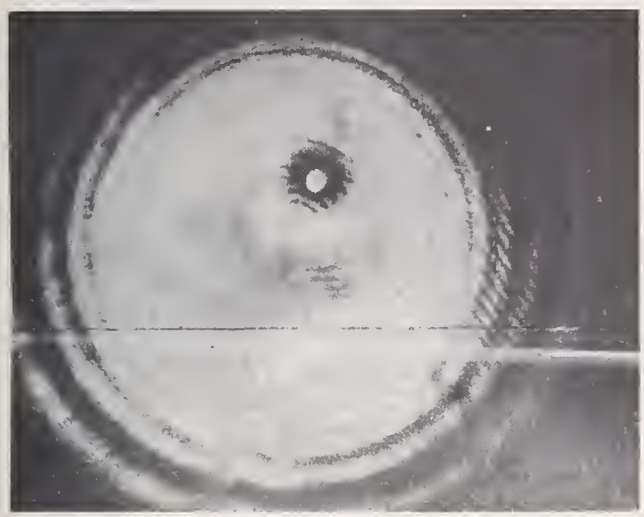

Fig. 3 Near Field Burn Pattern after Amplifier with an Inclusion

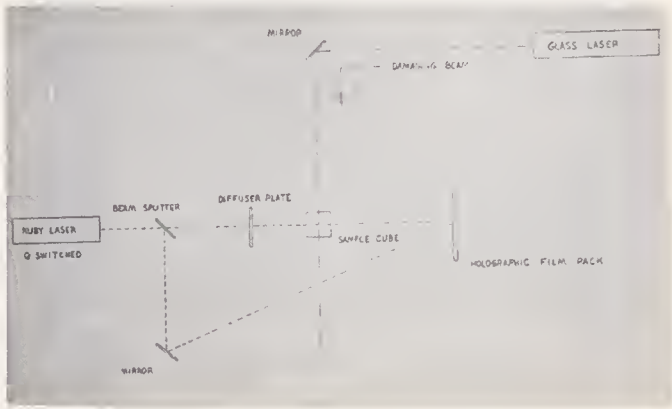

Fig. 4 Holographic Setup

Fig. 5 Single Exposure, 190 ns Delay

Fig. 6 Single Exposure, 1400 ns Delay

450-417 O-71—3

Fig. 7 Double Exposure, 1500 ns Delay

Fig. 8 Air Breakdown at Focus of 10 cm lens

Fig. 9 Damage Track, Single Exposure, 190 ns Delay

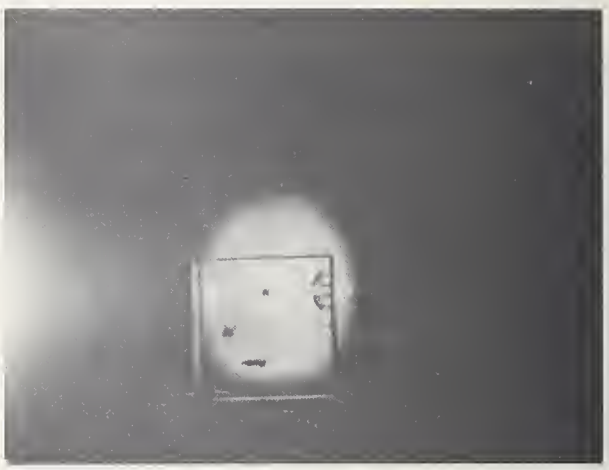

Fig. 10 10 cm lens Focused on Entrance Surface Gross Internal Damage as Acoustic is Wave Visible at the Entrance

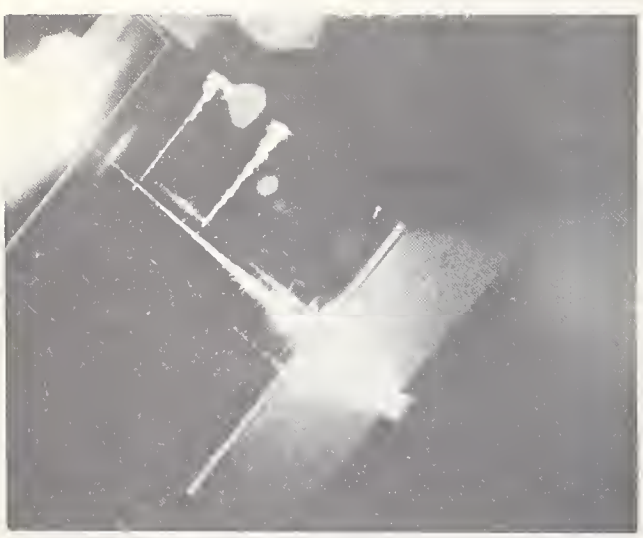

Fig. 11 Photo of Damage Caused by Focusing on Entrance Surface

Fig. 12 Double Exposure Delay 270 ns

Fig. 13 Double Exposure Delay 580 ns

Fig. 14 Double Exposure Delay 880 ns

Fig. 15 Double Exposure Delay 1600 ns

Fig. 16 Double Exposure Delay 1900 ns

COMMENTS ON PAPER BY NORMAN BOLING

The speaker commented on the preliminary nature of this paper. There is a great deal of information contained in the holographic records, not all of which has been extracted. The method itself, however, shows great promise as a means of determining the dynamics of laser damage. It was pointed out in the discussion that laser induced damage effects of this type are strongly geometry dependent and that it would be useful to examine both the cases of damage in a focused beam and in an unfocused beam. In some of the pictures presented there was evidence of four acoustical waves. These were identified as a longitudinal wave, a shear wave, a surface wave, and a fourth wave of undetermined origin. It was suggested that this fourth wave might arise from a shock wave generated outside the surface of the damaged material by spark formation in the air, which then impacted at a later time on the material surface. There was considerable discussion, as usual, on the means by which the spatial character of the laser beam was evaluated. The evidence of single mode behavior was first the size and homogeneity of the burn pattern observed in the near field and secondly, the appearance of strong interference rings over the entire aperture when small inclusions were present in the amplifier rod. This latter effect was proposed as evidence that whatever the intensity profile of the beam might be, it was indeed coherent over the entire aperture. The maximum energy density reported in the laser beam operating in the lowest order mode was approximately 40 joules per square centimeter over an aperture of 5 millimeters diamter.

Investigation of Cumulative Effects in Microscopically Damaged Quartz*

David F. Edwards,[1] C. Y. She,[2] V. G. Draggoo,[2]
T. W. Broberg,[2] and G. L. McAllister[3]

Quantum Electronics Laboratory
Colorado State University
Fort Collins, Colorado 80521

Measurements have been made of the change in the forward scattering component relative to the incident radiation of the multimode laser. The results are inconclusive but evidence is observed of the effects of microscopic damage and the evolution of microscopic into catastrophic damage in crystalline quartz. The catastrophic damage threshold is shown to be dependent on the propagation and polarization directions for the multimode laser. No dependence was observed for the TEM_{oo} laser. A phenomenological model is developed that consistently describes the experimental observations.

Key Words: Catastrophic damage, damage threshold, directional dependence, mechanism, microscopic damage, multimode laser, quartz, TEM_{oo} laser.

1. Introduction

Microscopic damage in transparent solids can take the form of defects created by the intense radiation of a Q-switched laser pulse [1][4]. The presence of microscopic defects, normally invisible to low power optical inspection, can be verified by special diagnostic methods. Microscopic damage in a laser system component can cause a change in the beam quality seriously affecting the system's operation. By comparison, laser produced catastrophic or macroscopic damage in a transparent solid results in "bubbles", pits, or cracks easily visible to the unaided eye. Catastrophic damage in a laser system component such as the laser rod, window or lens can cause the termination of laser operation.

The objectives of the research program being described here have been the following: to develop diagnostic methods to detect microscopic damage, to make an investigation of the criteria governing the onset of laser produced damage and of the damage mechanisms, and to study the evolution of microscopic into macroscopic damage in transparent solids.

For our investigations the transparent solid that received the most attention was crystalline quartz. The reason quartz was selected is that it is crystalline, photochemically inactive, and first-order Raman active. Chemically, quartz has properties similar to those of the laser glasses. The hydrothermally grown quartz crystals that were used were relatively free of intrinsic defects and inclusions. Also the crystals are inexpensive and an appreciable library of data exists on the material.

---

* This work was sponsored in part by a contract with the Air Force Cambridge Research Laboratories, Office of Aerospace Research, USAF.

[1] Electrical Engineering and Physics Departments.

[2] Physics Department.

[3] Electrical Engineering Department.

[4] Figures in brackets indicate the literature references at the end of this paper.

2. Experimental Procedure

The damage was produced in the quartz samples by either of two ruby laser systems. The first laser was constructed such that the output beam was restricted to a single longitudinal mode and the single lowest order transverse mode. This output pattern was verified by detailed probing of the near- and far - laser fields [2]. This laser is called the TEM_{oo} laser. The output of the second laser was confined to a single longitudinal mode but no restrictions were placed on the transverse mode pattern, and as a result several transverse modes oscillate simultaneously giving an irregular beam profile. This laser is called the multimode laser. Shown in Fig. 1 are isodensity contour plots of the beam profiles for these two lasers. These contours were made by photographing each beam in the focal plane of a lens using fine grain Kodak type 649-0 film. The laser beam was first attenuated to prevent saturation and possible destruction of the photographic emulsion [3]. Each contour line in the figure defines an area of equal energy in the beam profile. The smooth and approximately Gaussian distribution of the isodensity contour lines for the TEM_{oo} laser output can be seen from Fig. 1a where the time integrated beam diameter is about 50μ. In Fig. 1b are shown the isodensity contour lines for the output of the multimode laser. The time integrated beam diameter is measured to be 275μ. From the contour lines regions of irregular energy distribution are apparent in the beam. These regions, sometimes called "hot spots," vary from pulse to pulse and vary with time for any given pulse. This variation during a given pulse has been analyzed experimentally and theoretically by McAllister et al. [2] who find that transient effects of gain saturation can lead to non-Gaussian output intensity profiles, "hot spots," and irregular time behavior. The isodensity contours of Fig. 1 show the time integrated energy output for the two lasers. It has been shown [3] that the irregular energy distribution illustrated in Fig. 1b can be enhanced using beam attenuators such as Corning glass filters that have nonlinear absorption properties under intense laser radiation.

The light scattering properties of transparent solids have a sensitive dependence on the density and distribution of microscopic defects [4] and thus two light scattering methods were developed for investigating the laser induced microscopic damage. The first method is that of quantitative Raman spectroscopy and the second is the observation of the change in forward scattering intensity caused by laser produced microscopic defects. Shown in Fig. 2 is a schematic representation of the Raman scattering process. The excitation radiation of frequency ω_i interacts with the electrons of the solid represented by the interaction Hamiltonian H_{ER}. This energy absorbed by the electrons from the optical field is deposited immediately into the lattice. A phonon of frequency ω is created by the electron-lattice interaction, H_{EL}, and later a photon of frequency ω_s is scattered from the solid by the interaction H_{ER}. The radiation of frequency ω_s is the Raman scattered radiation. Including dissipative effects, the Raman scattered radiation, centered at ω_s, will have a finite linewidth, $\Delta\omega$, dependent on the details of the losses. Laser produced microscopic damage might be a mechanism for altering these losses and thus might produce a change in linewidth. Quantitative Raman spectroscopy is the investigation of the linewidth and intensity of the Raman scattered spectral line in addition to the line position. Examples have been given before [5] of the effects of laser microscopic damage on the quantitative Raman spectra in quartz and will not be repeated here. The application of forward light scattering as a diagnostic method for laser produced damage will be described.

A schematic of the forward scattering experiment is shown in Fig. 3. The Q-switched ruby laser is focused into the sample as shown. A fraction of the incident intensity is deflected by the beam splitter P_2 to the MgO scattering plate and from there to the photodiode. The incident beam pulse shape is registered on the Tektronix 519 oscilloscope. Part of the laser pulse transmitted through the sample is recollimated, sent along a delay path and also is scattered by the MgO plate onto the same photodiode. By selecting the proper delay path both the incident and forward scattered laser beams can be recorded on the same oscilloscope trace. Examples of four such traces are shown in Fig. 4 for the multimode laser with no sample in position. The objective of this forward scattering experiemnt is to record the incident and transmitted pulse shapes for a series of laser pulses, each below the catastrophic damage threshold and each in the same sample volume. If microscopic defects are produced, one would expect decreased forward scattering in proportion to the number of defect centers produced, assuming complicating effects such as self-trapping and multimode laser fluctuations were not present. For this experiment the data of interest are the incident and scattered energies which correspond to the areas under the oscilloscope traces in addition to the peak power values. Shown in Fig. 5 are the preliminary results of the forward scattering intensity normalized to the multimode laser intensity used as the radiation source. P(xy) in the figure indicates that the incident laser propagated in the x-crystallographic direction and was polarized along the y-direction. Each laser pulse was about 80% of the macroscopic damage threshold value. For each plot catastrophic damage, either internal or surface or both, was produced by the next laser pulse and thus terminating the measurement. Because of the poor reproducibility of the multimode laser the error bars shown in Fig. 5 are large and represent the standard deviation for the pulses shown in Fig. 4. With the exception of the second measurement, the ratio, E_s/E_o, tends to change for successive laser pulses; some ratios increase and some decrease. The fluctuations in the third plot can perhaps be explained by the poor reproducibility of the multimode laser. While no conclusions can be drawn regarding these plots some indication is shown of the cumulative effects of laser radiation. The forward scattering experiments are being continued using the TEM_{oo} laser to reduce the spread in the data points and improve the reliability of the results.

A second photodiode with an electrical delay line can be inserted into the transmitted beam of Fig. 3 in place of the single photodiode and the optical delay scheme. For some experiments one type of delay is more convenient than the others.

3. Results

In the process of performing the forward scattering experiments, careful measurements were made of the catastrophic damage threshold values and their dependence on propagation and polarization directions of the laser radiation inside the crystal. The results are shown in Fig. 6 for the catastrophic internal damage for the multimode and TEM_{oo} lasers. The notation is the same as before. P(xy) is the peak power density for laser radiation propagating in the x-direction and polarized in the y-direction. This experiment indicates that for the multimode laser the damage threshold value has a pronounced dependence on both the propagation and polarization directions, but this is not the case for the TEM_{oo} laser.

These damage threshold values were estimated from the statistical distributions of data points. For a given propagation and polarization direction the peak power density for each pulse was recorded as to whether catastrophic damage was produced. A new sample volume was used for each pulse. The $+5GW/cm^2$ values correspond to the damage threshold power density above which 80% of the laser pulses produced catastrophic damage. Below the $-5GW/cm^2$ values 80% of the laser pulses did not produce catastrophic damage. The damage threshold peak power density is the median of these two values. For the z-propagation direction experiments about 75 data points were used. About 30 data points were used for the x- and y-propagation direction measurements. The damage threshold value for the TEM_{oo} laser, $P(ij) = 28 \pm 5GW/cm^2$ falls within the range of values quoted by Olness [6] ($13\text{-}30GW/cm^2$) but is greater than the values given by Bass [7] ($1.2\text{-}6.4GW/cm^2$). These differences in threshold value for crystalline quartz cannot be explained based on the data available. The threshold value P(ij) quoted in Fig. 6 was obtained from the following measurements. The laser peak power was measured using an ITT FW114 photodiode that had previously been calibrated at the National Bureau of Standards. The beam cross section at the focal plane of the lens was measured by photographing the attenuated beam after it was focused onto Kodak type 649-0 film (Fig. 1a) or Polariod type film. The beam diameter was taken at the 1/e point of the beam profile.

The peak power density values listed in Fig. 6 for the multimode laser should only be considered as relative and not compared with $P(ij) = 28 \pm 5GW/cm^2$ for the TEM_{oo} laser. For the multimode laser the peak power density values have been averaged over space and time because of the complex nature of the multimode laser. From Fig. 1b the energy output is distributed unevenly and unpredictably over several "hot spots". The cross-sectional area at the focal plane of the multimode laser was measured using photographic methods which means time integration. In general the temporal dependence of the multimode laser pulse is not smooth as shown in Fig. 4 but instead is irregular in time as shown by McAllister et al. [2]. These irregular temporal spikes have a rise time of 0.1 nsec or less and a width of 0.5 nsec or less. To compare the threshold values of the multimode laser with that of the TEM_{oo} laser the following rough estimate must be made. The multimode laser peak values of Fig. 6 should be reduced in proportion to the area of the "hot spots" to the total cross section area of the beam as shown in Fig. 1b and increased by about 10 to approximate for the irregular spikes. This ratio is roughly 1/50 to 1/100 making the TEM_{oo} threshold value greater than any of the multimode threshold values.

Shown in Fig. 7 are the ratios of the propagation velocities of elastic waves in crystalline quartz and the ratios of the multimode laser damage threshold values. The velocity values were calculated using published elastic data. Comparing these data with the corresponding multimode laser damage threshold values of Fig. 6, one can see that the damage threshold values have a definite velocity dependence.

Surface damage using the multimode laser was found to have a propagation direction dependence but laser polarization direction had no effect on the threshold value. The x-propagation direction values were less than the z-propagation direction values. Insufficient data is available for the surface damage produced by the TEM_{oo} laser.

The internal damage produced by the two lasers had a characteristic pattern depending on the laser propagation direction within the crystal. For an x- or y-propagation direction the damage region was in the form of two planes at 80° to one another as shown in Fig. 8a. The vertex of the two intersecting planes lies along the propagation direction and the z-crystallographic direction is vertical. For propagation in the z-direction the cross section of the damage pattern is approximately circular as shown in Fig. 8b. The x-, y-, and z-direction damage patterns are consistent with the normal mode (stress waves) patterns of the acoustic phonons in quartz. The fracture produced by the TEM_{oo} laser is about 1/10 the size of that produced by the multimode laser, but is similar in shape. Viewing the x- and y-direction damage sites from the side in quasi-monochromatic light, interference fringes are visible for each fracture plane indicating a separation of the two surfaces. For quartz this would indicate an internal pressure in excess of about 3 kbars was produced during the laser pulse. The velocity dependence shown in Fig. 7 indicates that the cracks are probably produced by longitudinal hypersonic waves initiated by an electrostrictive interaction of the incident laser field and the lattice. For our experiments no evidence of damage tracks due to self-focusing was found for any of the damage sites produced by either laser.

4. Summary

In summary, the forward scattering experiments using the multimode laser are inconclusive but evidence is observed of the effects of the microscopic damage and the evolution of microscopic into catastrophic damage in crystalline quartz. These measurements are continuing using the TEM_{oo} laser to improve the reliability of the data.

At the present time no conclusion can be drawn as to the damage mechanism but new definitive data has been discovered and a phenomenological understanding of the damage mechanism has been developed. The directional dependence of the damage threshold values can be explained on the basis of the motion of the ions under the action of the incident laser pulse. As the amplitude of the ionic motion increases, a threshold value will be reached where the ionic bonds are broken resulting in the observed catastrophic damage shown in Fig. 8. This increase in the amplitude of the ionic vibrations in the crystal can be regarded as the amplification of the acoustic phonon oscillations which depend on crystallographic direction and do not depend on the type of laser pulse incident on the crystal (i.e., multimode or TEM_{oo} laser) as shown in Fig. 8. The incident radiation interacts primarily with the electron and the electrons in turn interact with the lattice as shown in Fig. 2. Under some cases the laser radiation can also interact directly with the lattice (for example, electrostriction). For the TEM_{oo} laser pulse the temporal and spatial profiles across the beam are smooth. For this type of pulse the interaction with an insulating crystal such as quartz will be primarily with the electrons and thus the damage threshold value would be independent of the directions of propagation and polarization. The strong spatial and temporal gradients present in the power density profile of the multimode laser can modulate the ionic motion causing acoustic phonons with the same wave vectors and frequencies to absorb energy directly from the incident laser field. The damage threshold values due to this mechanism would be dependent on the propagation and polarization directions of the laser. The experiments reported here consistently support this chain of events suggested by this phenomenological model.

References

[1] Bottger, H., "Multiphonon Absorption in Crystals with Point Defects within a Strong Radiation Field," Physica Status Solidi 28, 611 (1968).

[2] McAllister, G. L., Mann, M. M. and DeShazer, L., "Transverse-Mode Distortions in Giant-Pulse Laser Oscillators," IEEE J. of Quantum Electronics, Vol. QE-6, 1970, p. 44.

[3] Draggoo, V. G., She, C. Y. and Edwards, D. F., "Properties of Laser-Beam Attenuators," (submitted for publication).

[4] Vand, V., Vedam, K. and Stein, R., "The Laser as a Light Source for Ultramicroscopy and Light Scattering by Imperfections in Crystals," J. Appl. Phys. 37, 2551 (1966).

[5] Edwards, D. F., Harker, Y. D., Masso, J. D. and She, C. Y., "Diagnostics and Evidence of Pre-catastrophic Damage in Transparent Solids," ASTM STP469, 1969, p. 128; Edwards, D. F., C. Y. She, J. D. Masso, Y. D. Harker and H. C. Schade, "Raman Scattering in Microscopically Damaged Quartz," NBS Special Publications, 341, 1970, p. 97.

[6] Olness, D., "Laser-Induced Breakdown in Transparent Dielectrics," J. Appl. Phys. 39, 6 (1968).

[7] Bass, M., private communication.

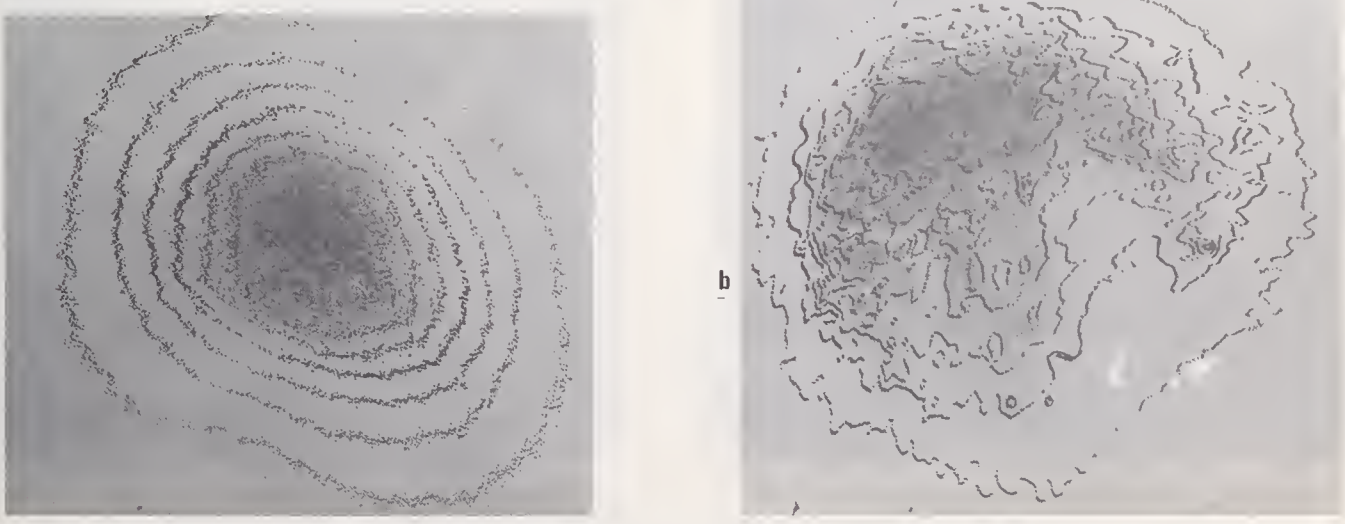

a b

Fig. 1: (a) Isodensity contour plot of the TEM_{oo} laser output. (b) Isodensity contour plot of the multimode laser output.

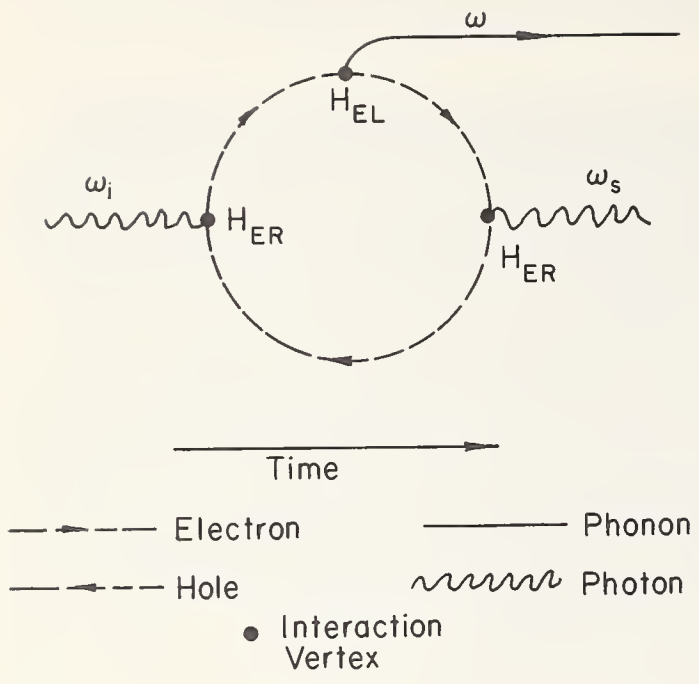

Fig. 2 Schematic representation of the Raman scattering process.

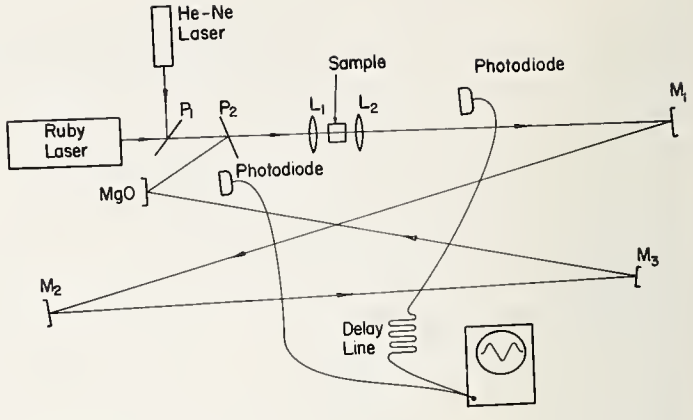

Fig. 3 Schematic of the forward scattering experiment.

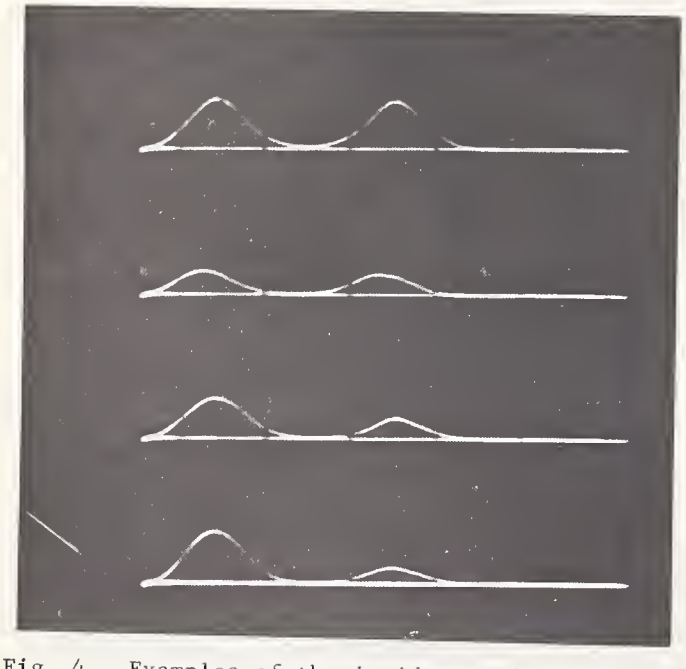

Fig. 4 Examples of the incident and forward scattered pulses for the multimode laser.

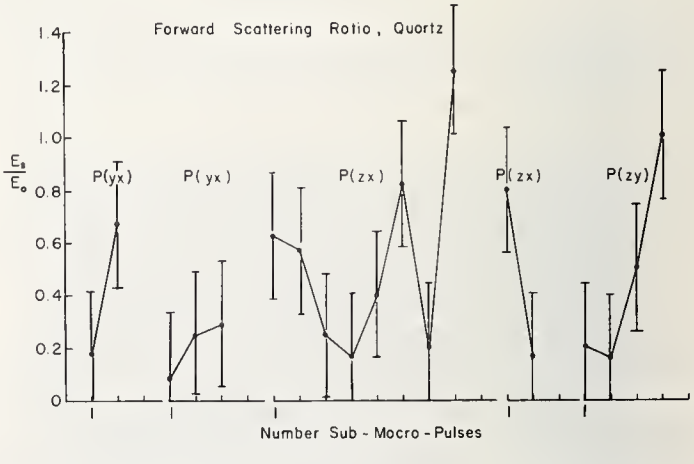

Fig. 5 Preliminary results of the forward scattering intensity normalized to the incident intensity as a function of the number of multimode laser pulses and for different propagation and polarization directions.

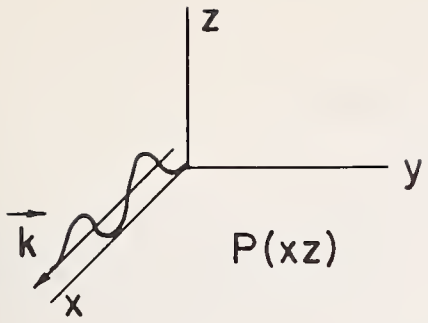

Multimode Laser

$P(xy) = 34 \pm 5$ GW/cm²

$P(xz) = 130 \pm 5$

$P(yx) = 63 \pm 5$

$P(yz) = 47 \pm 5$

$P(zx) = 80 \pm 5$

$P(zy) = 80 \pm 5$

Tem_{oo} Laser

$P(ij) = 28 \pm 5$ GW/cm²

$i, j = x, y, z$

Fig. 6: Catastrophic damage threshold values for the multimode and TEM_{oo} laser.

	v (zx)	v (yx)	v (yz)
v (zy)	1.0	0.83	0.80

	P(zx)	P (yx)	P (yz)
P (zy)	1.0	0.84	0.76

Fig. 7: Hypersonic wave propagation velocity ratios for different propagation and polarization directions in crystalline quartz.

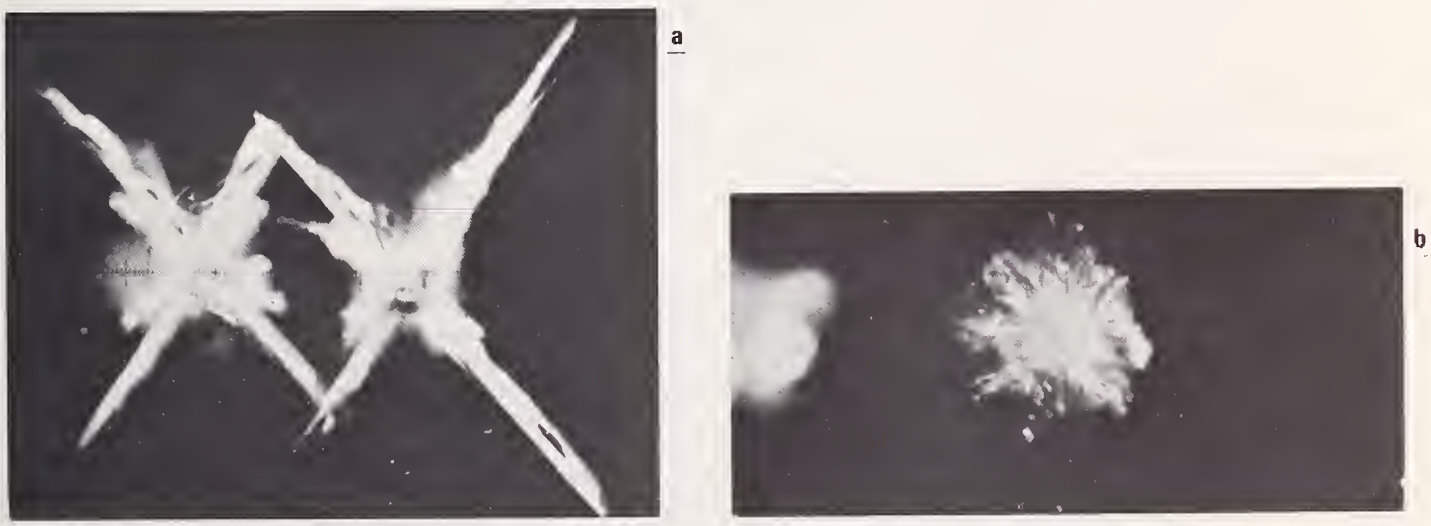

Fig. 8: Typical internal damage site in crystalline quartz for either the multimode of TEM_{oo} laser. (a) Incident laser propagation direction along either the x- or y-crystallographic direction. The z-crystallographic direction is vertical. (b) Incident laser along the z-crystallographic direction.

COMMENTS ON PAPER BY DAVID EDWARDS

Although there were certain unexplained and puzzling features in the data presented, in particular the reduction of the observed scattering as the number of damaged shots increased, certain regularities were observed. The power density required to produce damage was seen to be directly proportional to the velocity of the elastic wave in the medium, and spatial asymmetries of the damage pattern were seen to be well correlated with the directional dependence of the elastic properties of the medium. Thus, in the case in which the velocity of propagation of an elastic wave in the direction perpendicular to the direction of the incident light was spatially uniform, circular damage patterns were obtained; while in those cases when the beam was incident from such a direction that the acoustic velocity varied in direction, damage stars were seen which seem to be oriented with regard to the crystallographic axis of the medium. An exhaustive study of the directional dependence of the damage phenomenon still remains to be carried out.

Plasma Formation Upon Laser Irradiation of Transparent Dielectric Materials Below the Damage Threshold

B. E. Henderson, R. R. Getty and G. E. Leroi

Department of Chemistry
Michigan State University[1]
East Lansing, Michigan 48823

and

D. L. Rousseau

Bell Telephone Laboratories, Inc.
Murray Hill, New Jersey 07974

The interaction of high power laser (ruby or neodymium-glass) radiation with ostensibly transparent materials has been the object of increasing research in recent years. Even at power levels below the threshold for either surface or internal damage, the emission of both positive and negative ions and of high energy radiation has been detected. Both linear and non-linear absorption mechanisms have been proposed, and plasma initiation has been attributed to such factors as surface contaminants, surface defects, internal impurities, and free carrier absorption. In this paper, the experimental procedures, results, and interpretations of several of these investigations will be reviewed. Although the residual ion emission can be greatly reduced by careful pre-cleaning and handling procedures, it can not be eliminated entirely; the ramifications of this conclusion must be considered in the analysis of experiments in which damage is observed.

Key words: Charged-particle emission, damage thresholds, dielectric materials, interaction mechanisms, laser irradiation, plasma formation, review, surface contamination.

1. Introduction

Our interest in laser interaction with transparent materials was generated during early experiments (in the mid-1960's) aimed at using high-power laser radiation as a photochemical light source. Indeed, we were successful in initiating chemical reactions using ruby laser radiation which were quite different from the results obtained using conventional visible light sources. In the course of seeking a mechanism to account for these novel results, we looked into the possibility of laser-induced ionization. It was soon apparent that ion currents were produced in our reaction cells, almost simultaneously with the laser pulse. However, when the sample was removed a similar effect was obtained from the evacuated cell! Thus, prior to continuing the pursuit of our initial goals, a study of the charged particle emission from transparent dielectrics was undertaken [1][2] with the object of controlling the laser-induced ionization.

There has been a tremendous amount of research on the interaction of high-power laser light with opaque materials, and as attested by this 3rd Conference on Laser Damage in Glasses, a great deal of work, both experimental and theoretical in nature, has also been carried out on solids which are normally considered to be "transparent" at a given laser frequency. However, this work has dealt almost exclusively with internal and/or surface damage caused by the laser pulses. It is often reported that such damage is accompanied by a spark, even in vacuum, and there has been a good deal of speculation regarding the origin of the emitted light and the plasma. Our own work has been concerned with the ionization which takes place below the threshold for physical damage,

[1]The work at Michigan State University was supported in part by the U. S. Office of Naval Research.

[2]Numbers in brackets indicate literature references listed at the end of this paper.

which has been calculated and observed to be greater than 10^9 watts/cm^2; our power levels were normally maintained below 5 x 10^7 watts/cm^2.

2. Review

Before describing the experiments undertaken in our laboratory, we wish to summarize other pertinent investigations reported in the literature. The basic references to laser interaction with transparent dielectrics are concerned primarily with damage; these include the reports of the first two Boulder Conferences [2,3], and the summary prepared by the National Materials Advisory Board [4]; however, some of the perceptions and mechanisms described therein are related to the processes occurring below the threshold for physical damage. Another useful compendium is the detailed bibliography entitled "Soviet Research in Laser-Induced Plasma and Gas Breakdown", which covers the 1964-67 period [5]. Historically, it is interesting to note that the Voronov-Delone group at the Lebedev Institute found that the thresholds for breakdown in various noble gases were higher than those reported by earlier investigators. They showed that a plasma could be formed at the surface of the focusing lens and at the cell walls which would lead to initiation of gas breakdown below the intrinsic ionization level [6]. This is now a generally accepted concept [4,7]. Other observations of ions formed at surfaces below the damage threshold have been reported by Muray [8], Hall [9], and Veduta and Sviridenkov [10]. Large increases in the photoconductivity of silicate glasses [11], of ruby [12], and of NaCℓ and $Aℓ_2O_3$ single crystals [13] have also been measured when samples were irradiated with ruby light at powers below the threshold for surface damage. The large concentration of electrons in the conduction band is thought to arise by multiphoton excitation; subsequent interaction with the laser beam, leading to electron cascade ionization, is proposed as the mechanism for plasma formation and eventual damage. This damage theory has also been suggested by several other groups [14-20]. Cascade ionization has also been postulated as a mechanism leading to breakdown of gases, although it is not clear how the "priming" electrons arise. One possibility is the presence of microscopic dust particles or an extremely small amount of absorbing impurity [21].

An excellent review of laser-induced breakdown and damage in silicate glasses is given by Sharma and Rieckhoff [20]. Although some work indicated that the damage threshold for a variety of glasses is dependent on linear absorption of the laser beam (either ruby or neodymium) [22], power-dependence experiments demonstrated that multiphoton processes are occurring [11]. The emission of light invariably accompanies internal or surface damage in glasses. Early experiments on a variety of substrates [23] indicated that the emission was characteristic of the target material, rather than the environment of the sample, and this conclusion has been generally supported by later work [4, 16, 19], although it has been suggested that adsorbed gases may play an important role [24].

Several investigators have studied the dependence of the damage threshold on the chemical nature of the material or on the pre-treatment of the substrate surface. The results are somewhat at variance. Swain's experiments [24] indicate that chemical etching of a polished laser glass surface raises the damage threshold more than the same treatment applied to an unpolished surface. However, Winogradoff, et al. [25] found no striking changes in the damage thresholds for silica glass upon repolishing; somewhat surprisingly, samples with higher water content showed higher thresholds than low water content silica. Giuliano and Hess [26] observed no substantial difference in surface damage of ruby with different methods of surface cleaning. On the other hand, Davit [27] found that the threshold for surface damage of neodymium glass could be raised by treatment with dimethylchlorosilane, or with a solution of sulfuric and hydrofluoric acids; however, the improvement was maintained for only a few minutes. An experiment somewhat similar to those performed in our laboratory has been reported by Lubin [28]. High intensity laser radiation was focused on the inside wall of an evacuated glass chamber. Sensitive electrodes measured the initial plasma density, which was found to be approximately 10^{17} ions/cm^3 (equivalent to about 1 Torr pressure). However, the damage threshold continually rose with repeated lasing, which was taken as support for the contention that easily vaporizable material was being cleaned from the irradiated glass surfaces.

3. Laboratory Investigations

As indicated earlier, our experiments involved the measurement of ion currents emanating from various transparent dielectric materials upon laser irradiation at power levels below the threshold for visible damage [29]. The light source was a 7"-long, 5/8"-diameter ruby pumped by linear flashlamps in a double elliptical configuration. Experiments were performed using both normal burst and Q-switched pulses, the latter being obtained by placing either a Kerr cell or bleachable dye in the cavity. A general schematic of the experimental system is shown in Fig. 1. A small portion of the laser pulse was monitored and displayed on one beam of a Tektronix 555 oscilloscope; using biased electrodes, either the positive or negative ion signal generated within the evacuated experimental cell was displayed on the second beam.

Cells of many varied geometries and electrode configurations were used. Initially they were all glass, similar to those employed in our photochemical experiments. However, spurious effects due to the build-up of static charge on the cell body were observed, and later experiments were conducted using cells similar to that shown in Fig. 2. The dielectric materials normally served as the external windows on the brass cell, being held on by O-rings which facilitated interchange. The additional O-ring flange at the top allowed one of the electrodes to be removed and replaced by a dielectric material, in which case the cell body served as the second electrode. The various Pyrex-to-Kovar seals were employed to eliminate ground loops, and except during experiments to test quenching, the pressure in the cell was maintained below 10^{-5} Torr. The incident laser beam was unfocused (collimated) in both the normal mode and Q-switched experiments.

We believed at the start that the amount of ionization would be a strong function of the window material, and set out to find a transparent window which would give minimal induced emission. Among the materials tried were soft glass, Pyrex, fused quartz, Supracil quartz, LiF, CaF_2, and sapphire. We were surprised (and dismayed) to find that strong ion signals were observed from all of these windows when unfocused, normal burst or Q-switched radiation was used. Since the variation between different samples of the same material, or indeed the same window when mounted on different occasions, was as large as the variation between materials, further experiments were conducted on Pyrex samples.

The normal-burst output of our ruby is a 100 joule pulse with a half-width of approximately 500 microseconds; i.e., 200 kWatts (10^5 watts/cm^2). The ion signal observed upon repeated normal-burst lasing always diminished sharply with the first few shots, and then leveled off at a limiting value about two orders of magnitude below the initial level. This behavior is shown in Fig. 3, and was generally observed whether the early ion currents were relatively large or small. The lowest value of the signal, measured about 5 cm away from the window, obtained after rigorous precleaning with distilled water and spectroquality acetone, was $\sim 10^5$ charged particles per pulse. It is interesting to note that continued lasing at these power levels did not appear to lower the damage threshold; i.e., visible damage was not observed even after several hundred shots.

It has been suggested that adsorbed gases may play a major role in determining the threshold for surface damage, and of course we wondered whether the ions being observed were from adsorbed material. It would be best to test this idea using a mass spectrometer, but we were not set up for such experiments. A more qualitative, but quite exhaustive, test was made as follows: A cell cleaned to constant emission as described above, was filled in turn with air, oxygen, and vapors of water, acetone, and benzene for between an hour and over one day prior to re-evacuation below 10^{-5} Torr. In each case only a slight increase above the limiting ion signal was observed upon laser irradiation; the resulting signal did not approach the initial value prior to laser cleaning. If the pressure in the cell was allowed to rise above $\sim$50 microns, the ion signals were completely quenched.

Experiments were performed in which dust was intentionally allowed to accumulate on the windows prior to their being placed on the cell. The initial signals were then at least an order of magnitude larger than those from "clean" windows, occasionally as large as 10^{10} charged particles/pulse. Again the signal decreased about 2 orders of magnitude upon repeated lasing, and a film appeared to have been baked onto the surface in spots. This film could be readily removed by washing with soap and water.

The magnitude of the ion signal was fairly independent of the method by which the Pyrex windows were cleaned prior to being mounted on the experimental cell. In addition to the distilled water-spectroquality acetone treatment mentioned above, various other ultrapure organic solvents were used, without observable improvement. Films of collodion were allowed to dry on the windows and then peeled off; again, there was little change in the current accompanying laser irradiation. Application of alcoholic KOH followed by careful washing with distilled water, or use of the cleaning procedure recommended to prepare glass surfaces for silvering [in order: benzene, alcohol, nitric acid, distilled water, alcoholic KOH, final distilled water rinse] also had little effect.

Improved time resolution of our ion currents was obtained using Q-switched ruby laser pulses, although the results were qualitatively similar to those of the normal-burst experiments. The Q-switched peak power was on the order of 100 MW and the pulse half-width was about 30 nsec. Thus the power per unit area, $\sim 5 \times 10^7$ watts/cm^2, remained well below the range normally reported for the damage threshold of glass. Two rather distinct negative particle signals were resolved, as depicted in Figs. 4A and 4B. The early signal appears about 40 nsec after the laser pulse, whereas the much larger second negative peak is delayed by about 4 μsec. A single positive ion signal is observed (Fig. 4C), delayed by about 5μsec from the laser pulse. Although there was some variation in the delay time from shot-to-shot, the positive peak was always detected somewhat later than the corresponding negative peak, and it always exhibited significant tailing. Its intensity ranged from 10% to 100% of the late negative peak.

The dependences of the intensities of the resolved current pulses on the laser power were measured over the somewhat limited range available to us. The early negative signal was affected less than the delayed positive and negative peaks, which had similar power dependences. Approximate slopes of log-log plots of the early and late negative pulses, determined by least-squares analysis, were 2.5 and 8, respectively. The large difference suggests that two different processes are responsible for the observed signals. [In their somewhat related experiments on laser-induced photoconductivity below the damage threshold, Sharma and Rieckhoff [11] measured the variation of total charge collected as a function of the incident Q-switched rubv laser photon flux, and obtained power dependences of 3.5 ± 1 for glass and quartz.] If one assumes that the delayed peaks are due to thermionic emission, the power dependence would be consistent with a plasma temperature of approximately 10^4 °K [29,30]. This is similar to the plasma temperatures reported for laser irradiation of opaque solids [31,32], but lower than temperatures of around 10^6 °K found to accompany the generation of plasmas in gases [33].

4. Conclusions

These observations can be qualitatively explained by a mechanism similar to that proposed for opaque materials [31,34]. The following phenomenological model has been proposed [29]. The "intrinsic" threshold for plasma formation upon laser irradiation of transparent dielectric materials is most probably fairly high. However, it is virtually impossible to remove surface contaminants and impurities, and at much lower power densities these adsorbed materials will absorb the incident laser radiation, forming a plasma of ions, electrons and neutrals. In addition, most surfaces have many microscopic imperfections which can contribute to linear absorption [35], as will carriers from shallow traps. The plasma temperature continues to rise due to shock-wave heating and further absorption of the laser light, and the expanding plasma radiates high energy light, including x-rays and vacuum-ultraviolet photons. This radiation causes the ejection of photoelectrons from the cell body, which are detected as the "early" negative pulse, arriving at the anode without interacting with the neutral plasma itself. (An "early" positive peak is sometimes resolved in studies of laser irradiation of metals [31,34], also; it is attributed to the "reverse photoelectric effect", whereby a positive signal results from the photoemission of electrons from the cathode. Because of the cell geometry and small cathode area, no early positive peak was observed in our experiments.) The later ion currents are detected when the expanding plasma breaks up, and its constituent charged species are collected at the appropriate electrode. The late negative pulse is due mainly to electrons from the plasma, delayed by space charge effects. The greater delay of the positive signal is consistent with heavier charged particles, and the observed tailing indicates a distribution of ion masses.

It is not clear whether the residual plasma after repeated laser "cleaning" is due to particulate matter remaining on the dielectric surface, or is indeed characteristic of the material itself. The mechanism for intrinsic plasma formation below the damage threshold should be the same as invoked for surface or bulk damage: initial multiphoton ionization followed by electron multiplication. However, we wish to interject a note of caution. Laboratory air is notoriously unclean, and samples are rarely handled with scrupulous care. Smoke, dust, fingerprints, and the like, will interact strongly with high-power laser radiation. Before undertaking elaborate experiments in the quest to understand and control damage in laser materials, one must be sure that non-volatile impurities and particulate contaminants have been minimized.

5. References

[1] D. L. Rousseau, Ph.D. Thesis, Princeton University (1967).

[2] "Damage in Laser Glass", ASTM Special Technical Publication No. 469 (1969).

[3] "Damage in Laser Materials", NBS Special Publication No. 341 (1970).

[4] "Fundamentals of Damage in Laser Glass", NMAB-271 (1970).

[5] Y. Ksander, ATD Report 68-1-3-1, Library of Congress (1968).

[6] G. S. Voronov and N. B. Delone, JETP Letters 1, 66(1965).

[7] F. Kaczmarek, Acta Phys. Polonica 32, 1003 (1967).

[8] J. J. Muray, Dielectrics 221 (February, 1964).

[9] J. L. Hall, et al., Phys. Rev. Letters 14, 1013 (1965); IEEE J. Quantum Electronics QE-2, 361 (1966).

[10] A. P. Veduta and E. A. Sviridenkov, Zh. Priklad. Spektrosk. 6, 256 (1967).

[11] B. S. Sharma and K. E. Rieckhoff, Can. J. Phys. 45, 3781 (1967).

[12] T. P. Belikova and E. A. Sviridenkov, JETP Letters 3, 257 (1966).

[13] V. S. Dneprovskii, D. N. Klyshko, and A. N. Penin, JETP Letters 3, 251 (1966).

[14] J. P. Budin and J. Raffy, Appl. Phys. Letters 9, 291 (1966).

[15] A. Wasserman, ibid. 10, 132 (1967).

[16] H. Dupont, A. Donzel, and J. Ernest, ibid. 11, 271 (1967).

[17] E. A. Sviridenkov, Soviet Physics-Solid State 9, 1917 (1968).

[18] G. M. Zverev, T. N. Mikhailova, V. A. Pashkov, and N. M. Solov'eva, Soviet Physics-JETP 26, 1053 (1968).

[19] T. P. Belikova, A. N. Savchenko, and E. A. Sviridenkov, ibid. 27, 19 (1968).

[20] B. S. Sharma and K. E. Rieckhoff, Can. J. Phys. 48, 1178 (1970).

[21] Y. B. Zel'dovich and Y. P. Raizer, Soviet Physics-JETP 20, 772 (1965).

[22] R. A. Miller and N. F. Borrelli, Appl. Optics 6, 164 (1967).

[23] C. R. Giuliano, Appl. Phys. Letters 5, 137 (1964).

[24] J. E. Swain, in reference 2.

[25] N. N. Winogradoff, A. H. Neill, Jr., J. Mitchell, W. Haller, G. Cleek, and R. Waxler, NBS Technical Note 531 (1970), Section 4.4.2.1.

[26] C. R. Giuliano and L. D. Hess, in reference 3.

[27] J. Davit, J. Appl. Phys. 39, 6052 (1968).

[28] M. Lubin, unpublished work. Quoted in reference 4.

[29] D. L. Rousseau, G. E. Leroi, and W. E. Falconer, J. Appl. Phys. 39, 3328 (1968).

[30] C. Kittel "Introduction to Solid State Physics" (John Wiley & Sons, Inc., New York, 1966).

[31] C. DeMichelis, IEEE J.Quantum Electronics QE-6, 630 (1970).

[32] "Laser Interaction and Related Plasma Phenomena", H. J. Schwarz and H. Hora, Eds. (Plenum Press, New York, 1971).

[33] See, for example, ref. [5] pp. 2, 5, 6, and 25; ref.[32], p. 259.

[34] D. Lichtman and J. F. Ready, Phys. Rev. Letters 10, 342 (1963); Appl. Phys. Letters 3, 210 (1963).

[35] Y. K. Danileiko, A. A. Manenkov, A. M. Prokhorov, and V. Y. Khaimov-Mal'kov, Soviet Physics-JETP 31, 18 (1970).

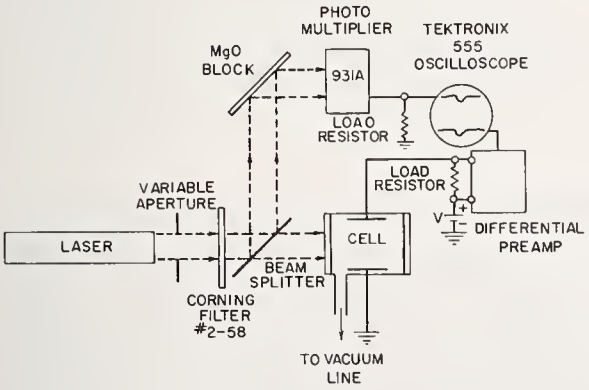

Fig. 1 Schematic diagram of experimental system used in the detection of ion currents emanating from transparent dielectric windows.

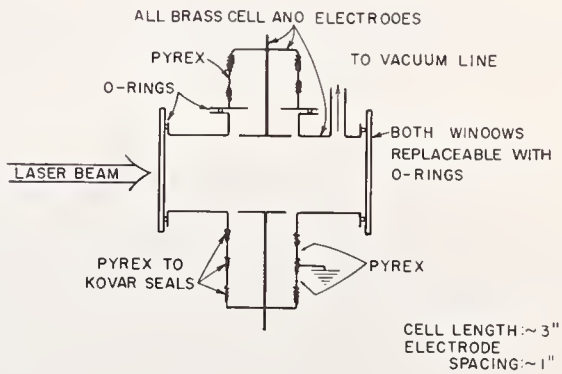

Fig. 2 Vacuum cell used to investigate plasma emission from dielectric windows.

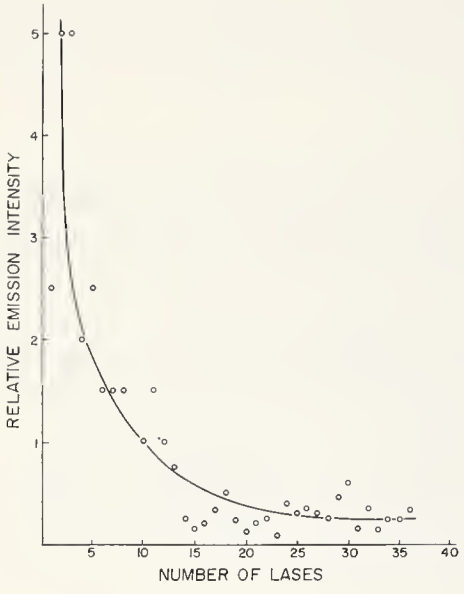

Fig. 3 Typical dependence of the magnitude of of the ion signal on the number of normal-burst laser pulses.

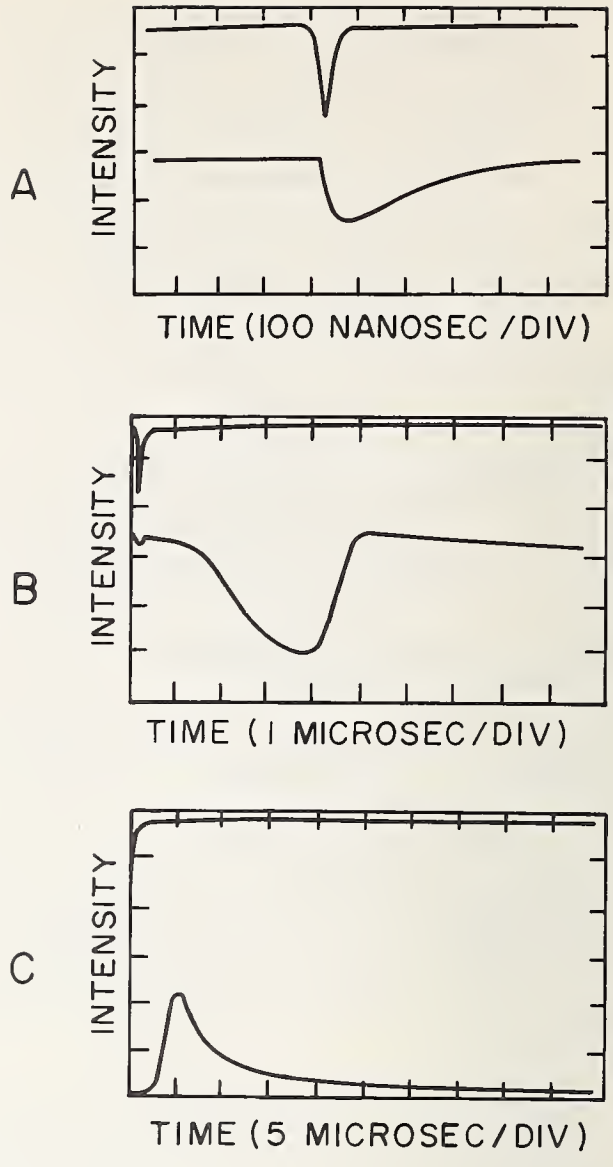

Fig. 4 Current pulses produced by Q-switched ruby laser radiation of Pyrex windows. The upper trace in each case shows the time dependence of the laser pulse. A - The early electron signal; time constant ~ 20 nsec. B - The complete negative particle signal showing both early and late peaks; time constant ~ 50 nsec. C - The positive ion signal; time constant ~ 50 nsec.

COMMENTS ON PAPER BY GEORGE LEROI

The discussion centered on the question of the dependence of the observed ion electron emission on the techniques employed to clean the windows of the test cell. It was reported that the cleaning technique which yielded the lowest emission was the repeated use of multiply distilled water followed finally by a cleaning with spectral acetone. Further reduction was effected by baking and then repeatedly irradiating the evacuated cell with laser pulses. Higher levels of ion and electron emission were observed when other cleaning techniques were used, such as washing with various acids. The speaker mentioned that this last result was apparently at variance with the results reported by Swain at the 1969 ASTM Symposium on Laser Damage.

Diffusion Effects in High Power Laser Damage

Wilbur Franklin

Physics Department
Kent State University
Kent, Ohio 44242

The theory of diffusion in laser solids in the presence of high optical power densities is presented. It is shown that a small number of laser-excited phonons, n_e, having the proper wavevector for diffusion, can affect the diffusivity significantly. The effects of a thermal gradient and of pressure are evaluated quantitatively under certain conditions. In addition, since the activation energy for defect migration can be substantially reduced upon excitation of the localized ground state electron, diffusion effects are shown to be possible under typical laser damage conditions.

Key Words: Atomic migration, damage threshold, diffusion, laser damage, nonlinear optics, thermal diffusion.

1. Introduction

Theoretical work is presented here relating the photon-phonon conversion, which preceeds laser damage, to atomic and ionic migration. The conversion of photons of $\leq 10^9$ W/cm^2 power density to excited electrons and phonons is shown to affect diffusion by various mechanisms which include thermal diffusion in a phonon number gradient, ∇n, excitation of both localized electron and phonon states at defects, Raman scattering which may or may not be stimulated, etc. The externally imposed fields--caused by the laser's intensity--which provide the driving force for migration are gradients in temperature, ∇T, stress, $\nabla \sigma$, and charge, ∇q. It is shown that in ruby, sapphire and laser glasses, all of which are compounds containing slowly diffusing oxygen and fast diffusing metal ions, that partial separation of the ions is possible. This leads to local deviations from stoichiometry and, perhaps, changes of state, which result in turn in changes of index of refraction. In addition, significant diffusion in the very high temperatures ($\approx 10^4$ °K) possible at inclusions of specific type and size [1],[1] is shown to be possible.

Internal or bulk damage such as damage tracks or bubbles is considered here. The observations of internal damage which have not yet been adequately explained include the effects on Raman scattering due to "microscopic" damage [2] preceeding visually observable damage and the structure and mechanism of formation of the visually observable bubbles.

Some initial theoretical work has been done on the related topic of laser-stimulated diffusion [3], [4]--a process which involves enhanced diffusion caused by ∇n, which results, in turn, from one of the photon-phonon conversion processes. For pulse times of $\geq 10^{-8}$ sec the electrostriction focusing mechanism developed by Kerr [5] is assumed. For short pulse times, the electronic Kerr effect or the polaron mechanism proposed by Hellwarth [6] is assumed. In the following sections the effects of laser-excited phonons and of stress on the migration process are analysed. Thermal diffusion is then developed followed by a discussion of the mechanisms of photon-phonon conversion. The discussion includes a description of a proposed process for the formation of visually observable bubbles which is preceeded by substantial defect formation.

---

[1] Figures in brackets indicate the literature references at the end of this paper.

450-417 O-71—4

2. Basic Considerations of the Diffusion Event

2.1 Diffusivity and Activation Energy

The diffusion jump time is solids [7] is typically 2-3 X 10^{-13} sec which is 10^5 times faster than the typical ruby pulse time of 3 X 10^{-8} sec and 10^2 times slower than the period of ruby light. The atom's lifetime at a lattice site (or quasi-stationary site in glass) is $>>10^{-13}$ sec and is exponentially dependent on 1/T. For the electric field of an externally or self-focused ruby beam to affect diffusion sufficiently to cause visibly observable effects in laser glass, ruby or sapphire in times of $\leq 3 \times 10^{-8}$ sec (the pulse time usually assumed here) the local temperature and one or more of ∇T, $\nabla\sigma$ or ∇q must be sufficiently high. In addition, a localized reduction of force constants can occur at excited defect centers with a consequent decrease in activation energy for migration, ΔE_m.

Consider the diffusivity tensor, D_{ij}, in a sample exposed to an external light source which excites phonons of wavevector $\vec{k}_e$ and number density n_e in the sample. Thermal phonons of wavevector $\vec{k}_s$ and number density n_s also exist but we assume that $n_s << n_e$ at room temperature. We distinguish the laser-stimulated phonons from the thermally excited band phonons since their wavevector and branch, or localized mode structure, may differ considerably from those of the thermal phonons. With externally excited phonons the diffusivity at a position x in the sample is given by

$$D_{ij}(x) = D_{ij}^{o}\, e^{-\Delta E/kT_{eff}} \tag{1}$$

where T_{eff} is an effective local temperature including both Σn_s and n_e. The activation energy, in the quasi-harmonic approximation, is given by

$$\Delta E = \frac{1}{2} \sum \Phi_{ij}\begin{pmatrix} \ell\ell' \\ \kappa\kappa' \end{pmatrix} u_{ic}\begin{pmatrix} \ell \\ \kappa \end{pmatrix} u_{jc}\begin{pmatrix} \ell' \\ \kappa' \end{pmatrix} \tag{2}$$

where Φ_{ij} is a component of the two-body force constant tensor relating the i component of the critical displacement of atom κ in the ℓth unit cell to the j component of the displacement of the $\kappa'\ell'$ atom. Eq (2) represents the minimum static displacement energy for an N-body system containing an atom or ion in its saddle-point-configuration (activated state). It is important to note in defect systems that optically excited electron states can decrease Φ and, hence, ΔE substantially. For example, Lüty [8] found that ΔE for the reorientation migration of certain F_A centers in KCl decreased by a factor of about 15 when the localized electron was in the excited state. For the F center in KCl, ΔE in the excited state was found to be 0.2 that in the ground state.

2.2 Effects of Pressure

Another factor which can alter migration significantly in certain systems is stress. Considering the special case of pressure for simplicity, an additional factor given by

$$\frac{\tilde{\nu}_o}{\tilde{\nu}}\, e^{-PV^m/kT} \tag{3}$$

is multiplied times the right-hand-side of eq (1) [9]. In eq (3) $\tilde{\nu}_o$ and $\tilde{\nu}$ are the product average frequency of the system with no pressure and with pressure, respectively. If, for example, P = 5 X 10^5 psi then, for an activation volume for migration of 10^{-23} cm^3, PV^m = 0.2 eV. The free energy for migration is then G = ΔE - PV^m = ΔE - 0.2 eV.

2.3 Diffusion in Al_2O_3

Self diffusion in Al_2O_3 has been studied experimentally [10] with the result (See Fig 1) for aluminum diffusion in polycrystalline samples given by

$$D(Al) = 28\, e^{-4.96/kT} \tag{4}$$

where ΔE = 4.96 eV and D_o = 28 cm^2/sec. ΔE for oxygen diffusion was similar to that for Al but D_o was about a factor of 10 less. The diffusivities of metallic ions and of essentially covalently bonded oxygen in glass follow a pattern similar to that in Al_2O_3. However, the requisite diffusivity data for laser glasses presently in use was unavailable for calculation. Hence, ruby and sapphire are considered quantitatively here since the diffusivity data for Al_2O_3 was available.

3. Effects of n_e on Diffusion

Consider a lattice with defects such that the 3N degrees of freedom represented by $\Sigma\vec{k},j$ in a perfect lattice are replaced by Σs in the defect lattice. Our interest lies in the effects of n_e on the atomic or ionic migration process. Maradudin [11] has derived the components of the equal-time correlation function, $\langle u_i(\ell\kappa)u_j(\ell'\kappa')\rangle$, in terms of the Green's function for the defect lattice U_{ij} and we can write it for our purposes utilizing an effective temperature

$$\langle u_i\binom{\ell}{\kappa} u_j\binom{\ell'}{\kappa'}\rangle_{tot} = -kT_{eff}\sum_m U_{ij}\left(\begin{matrix}\ell\ell'\\ \kappa\kappa'\end{matrix} - \Omega_m^2\right) \tag{5}$$

where the total correlation function includes n_e as well as thermal phonons. In eq (5) $\Omega_m = 2\pi nkT/h$ and $u_i(\ell\kappa)$ is the ith component of the displacement of the atom κ in the ℓth unit cell. Another way of writing the displacement correlation function utilizes the usual transformation operator which yields a result for the defect lattice, including n_e externally excited phonons of state e, which is given by

$$\langle u_i\binom{\ell}{\kappa} u_j\binom{\ell'}{\kappa'}\rangle_{tot} = \frac{\hbar}{2(m_{\ell\kappa}m_{\ell'\kappa'})^{1/2}}\sum_s \frac{B_i^{(s)}(\ell\kappa)B_j(\ell'\kappa')}{\omega_s}\left[2(n_s+n_e)+1\right] \tag{6}$$

where $m_{\ell\kappa}$ is the mass of the κ atom in the ℓ unit cell and $B_i^{(s)}$ is the ith component of the eigenvector in the defect lattice. If the Green's function in eq (5) is expanded in terms of eigenvalues and eigenvectors then eqs (5) and (6) can be utilized to obtain

$$\Delta E/kT_{eff} = \frac{\sum_j \omega_j^2 \sum m_{\ell\kappa} u_{ic}^2(\ell\kappa) \sum_s \sum_m \omega_s/(\omega_s^2+\Omega_m^2)}{\sum_s \hbar\left[2(n_s+n_e)+1\right]} \tag{7}$$

In eq (7) we have used the diagonalized form of the activation energy (See eq 2) in which the eigenvalues for the system at its saddle point have been utilized. The important thing to note about eq (7) is its inverse dependence on n_e. It is apparent that n_e reduces $\Delta E/kT$ and, since n_s is a small number for solids in the diffusion range, n_e does not, in many cases, have to be very large to produce significant effects on atomic migration. For example, for usual solid-state diffusion temperatures thermal phonons at the Debye frequency have $n_s \approx$ 2-4 phonons, or so.

Anharmonic effects on the equal-time correlation function have been calculated [4]. They become significant for large n. For example, in KCl, for $n_e >> n_s$, anharmonic effects are about 10% when $n_e \approx 2.5$. Consequently, for large laser-excited n_e, the effects of anharmonicity cannot be neglected since the effective local temperature is raised to the point where phonon interactions become significant.

4. Thermal Diffusion

The driving force provided by a phonon gradient gives rise to a flux which must be included with the flux due to a concentration gradient. The ith component of the diffusion flux in both gradients is given by

$$J_i = -D_{ij}\left(\frac{Q^*N}{RT^2}\frac{dT}{dx_j} + \frac{dc}{dx_j}\right) \tag{8}$$

where N is the number density of the migrating species. Q^* is the heat of transport which is given by $Q^* = KE_m + E_f$ in which K is a constant and E_m and E_f are the energies of migration and formation, respectively, of a defect. In a homogeneous laser material without inclusions $\nabla c = 0$ and the driving force is proportional to ∇T, which results from photon absorption. Then the thermal flux at a position x is

$$J_i^{(Th)}(x) = -D_{ij} \frac{Q^* N}{R T^2(x)} \frac{dT(x)}{dx_j} \tag{9}$$

where T(x) is the local temperature at x.

Realistic values of Q* for both positive and negative ions are difficult to obtain either theoretically or from estimates of data which is known for glass and Al_2O_3. In addition, D is not known to the author for the ions in the laser glasses being used. Nor is D known for both aluminum and oxygen diffusion in single crystal Al_2O_3 in the temperature range of interest. Hence, some rather gross approximations will be made here using values which seem representative in the light of known data for these and other materials. Letting N = 2 X 10^{22}/cc, Q_+^* = 50 Kcal/mole and Q_-^* = 100 Kcal/mole then

$$J_+^{(Th)} = -5 \times 10^{26} \frac{D_+}{T^2} \frac{dT}{dx} \tag{10a}$$

$$J_-^{(Th)} = -10^{27} \frac{D_-}{T^2} \frac{dT}{dx} \tag{10b}$$

for the fluxes of positive and negative ions, respectively. As an example, consider $J_+^{(th)}$ in glass exposed to $\geq 10^9$ W/cm^2 at a position adjacent to an inclusion of optimum size for maximum absorption. It has been shown that $\nabla T = 10^8$ to 5 X 10^9 °K/cm occur in these systems.[1] Then, if D for metallic ions in glass is similar to that for Al in Al_2O_3 (See Fig 1) we get $J_+^{(th)} \approx 5 \times 10^{25}$ and 5 X 10^{24} atoms/cm^2-sec at T = 10^4 and 8000°K, respectively, assuming that $\nabla T = 10^8$ °K/cm.

The possible growth of cavities or of hollow shells in Al_2O_3 by counter or differential ionic currents in thermal diffusion is an interesting possibility to investigate. A flux of W atoms across area A in a pulse time T is given by J = W/AT = NV/AT where N is the atomic number density and V the volume. Equating this flux with eq (9) for the growth of a spherical cavity, we get the radius

$$r = \frac{3 T D Q^*}{R T^2} \frac{dT}{dx}. \tag{11}$$

For the flux of 5 X 10^{25} atoms/cm^2-sec derived above for T = 10^4 °K a spherical cavity of radius $2\frac{1}{4}\mu$ is obtained from eq (11). As a second example, consider the growth of a spherical shell under conditions of lower T and ∇T. Assuming that T = 6800°K, ∇T = 5 X 10^7 °K/cm and Q* = 50 Kcal/mole, then, if the outer radius of the shell is 10μ the shell will be 0.1μ thick. This calculation assumes that the fluxes of both the positive and negative ions are equal and opposite. These examples are meant merely to be illustrative since the exact conditions of internal breakdown and some of the material constants are unknown. However, if fluxes large enough to produce cavities are possible then the preceeding events of deviation from stoichiometry in crystals and changes of state are even more probable. In any case the resulting change in index of refraction at the spherical bubble or shell should be sufficient to result in a visually observable bubble. Figs 2a and b portray two possible cases of diffusion in ∇T. In Fig 2a, there are counter currents of positive and negative ions since Q_+^* and Q_-^* have opposite signs. In Fig 2b the signs of Q* are the same but the magnitudes differ.

5. Modes of Photon-Phonon Conversion

The mechanisms of photon-phonon conversion in crystals which give rise to stimulated diffusion either directly or eventually via some phonon decay scheme include IR absorption, optical absorption at defects and Raman scattering both in the pure material and at defects. Excitation of the IR lattice frequency, ω_o, at the power density required to affect the diffusion process can be accomplished using a high power IR laser or the difference frequency of two pulsed optical lasers. Schawlow [12] has pointed out that chemical reaction kinetics, which is similar to diffusion in many ways, should be affected by a process which is similar to that proposed for diffusion [4]. In the IR absorption mechanism, the excited IR frequency decays, as shown in Fig 3, to longitudinal and transverse acoustic modes having $\vec{k}$ large enough (λ short enough) to affect the migration process before decaying into the set of band modes of the lattice spectrum. In this manner, directional control of the migration process be-

comes feasible because of the direction of ∇n_e in eq (8).

In the process involving optical absorption at defect centers, two types of effect on the migration event are possible. First, the local force constants may be decreased substantially, as pointed out above, because of excitation of the ground state electrons in the defect centers. Second, the indirect decay processes of the excited electron, such as that portrayed in Fig 4, create phonons which may be of the proper λ to increase the migration probability significantly.

The third mechanism mentioned for external laser-stimulated effects on the diffusion process is that of Raman scattering at a molecular frequency, ω_v. The nuclear displacement at a space-time point (z,t), excited by the laser and Stokes fields, $\vec{E}_\ell$ and $\vec{E}_s$, respectively, is given in dyadic form by

$$\vec{u}(z,t) = \frac{\epsilon_o}{\omega_v \gamma} \vec{E}_{\ell o} \cdot \left(\frac{\partial \overleftrightarrow{\alpha}}{\partial \vec{u}}\right)_o \cdot \vec{E}_{so}^{\,*} \sin[\omega_v t - (k_\ell - k_s)z - \phi_o] \qquad (12)$$

where γ is the damping constant, $\overleftrightarrow{\alpha}$ the polarizability and ϕ_o the phase angle. A numerical estimate of (12) with a power density of 3×10^8 W/cm^2 for both $\vec{E}_{\ell o}$ and $\vec{E}_{so}$ (assuming efficient SRS or using two lasers at a difference frequency of ω_v) has been given by Garmire, Pandarese and Townes [13] as 5×10^{-4} bond lengths. Following this estimate, focused power densities of $\approx 3 \times 10^{11}$ W/cm^2 give u $\approx$ half the bond length, which is equal to or greater than that required for diffusion with no other forces of any kind taken into account. If ω_v is the localized frequency of an ion adjacent to a vacancy, for instance, then Raman type excitation of a migration event in a directional manner (as indicated by the vector nature of eq 12) appear to be possible at power levels $< 10^{11}$ W/cm^2 when one or more of the other effects mentioned above is included.

The exact nature of photon-phonon conversion in laser material damage and the subsequent phonon decay scheme is a complex process. Since the ruby frequency lies above any lattice or usual localized mode frequency, the absorption is via electronic excitations. Hellwarth [6] has shown, in his polaron theory, that the electron-phonon collision time in sapphire at room temperature is $10^{-14.4}$ to $10^{-13.4}$ sec and that phonon scattering of the electron predominates over that of plasmons, neutral impurities, electrons, etc. In addition to the absorption by free electrons considered in that theory, optical absorption at defect centers should be included with the subsequent localized creation of phonons in a process such as that shown in Fig 4. It is interesting to speculate that, with an optically absorbing defect, the localized phonon cloud induced by the excited electron could lead to defect migration at the absorbing center. Subsequent to the initial absorption, the localized optical modes created during the defect's migration event, because of the strain and asymmetry introduced along the migration path, could lead to further absorption. A self-propagating process might then occur. If counter or differential diffusion of different species of ion also occurs, the resulting deviation from stoichiometry leads to higher diffusivities. In certain systems, deviation from stoichiometry is known to raise the diffusivity by a factor of 10^2-10^3 or more.

6. Discussion

Most of the theory presented here applies to crystalline solids and the numerical calculations done were primarily for Al_2O_3 since some of the requisite data was available for that material. It is shown that, under the conditions giving rise to breakdown of laser materials in high optical power densities, significant atomic or ionic diffusion can occur in the time of a single pulse. Adding in the effects of residual fields on migration after the pulse has ended makes the processes even more probable.

An additional factor not considered above is the production of dislocation or Griffith crack sources by vacancy conglomerates or precipitates. These would be generated quite easily in comparison to the growth of large bubbles or precipitates since they are so small. The condensation of vacancies into prismatic dislocation loops which can act, in turn, as sources for other dislocations is well known. This type of source might then give rise to plastic strain in crystals in the stress field produced by the beam. In glasses, Griffith fracture usually begins at a free surface and vacancy conglomerates inside the sample could provide that surface.

An attempt has been made here to show, with the meager data available, that diffusion may play a significant role in the production of internal damage. In addition, the "microscopic" damage preceeding optical breakdown may result in whole or in part from migration processes. Further experimental work is needed to ascertain with certainty the temperature and thermal gradients at breakdown. In addition, diffusivities and heats of transport for the ions in the substance are needed.

7. Acknowledgements

Discussions with A. J. Glass, C. R. Guiliano, D. F. Edwards, and N. Boling have been helpful in acquainting the author with the problems in the field of laser breakdown. Financial support for the work was provided by the National Science Foundation.

8. References

[1] Hopper, R.W., Lee, C. and Uhlmann, D.R., "The Inclusion Problem in Laser Glass", in Damage in Laser Materials, NBS Special Bulletin 341 (1970) p. 55.

[2] Edwards, D.F., She, C.Y. and Masso, J.D., "Raman Scattering in Microscopically Damaged Quartz", in Damage in Laser Materials, NBS Special Bulletin 341 (1970) p. 97.

[3] Sengupta, P. and Franklin, W., "Photon-Phonon Conversion Effects on Atomic Migration", Bull. Am. Phys. Soc. 16, 396 (1971).

[4] Franklin, W. and Sengupta, P., "Laser-Stimulated Atomic Migration", to be published.

[5] Kerr, E.L. "Laser Beam Self-Focusing and Glass Damage Caused by Electrostrictively Driven Acoustic Waves", to be published.

[6] Hellwarth, R.W., "Role of Photo-Electrons in Optical Damage", in Damage in Laser Materials, NBS Special Bulletin 341 (1970) p. 67.

[7] Franklin, W., "Phonon Theory of Solid-State Diffusion Including Anharmonic Effects", Phys. Rev. 180, 682 (1969).

[8] Lüty, F., "F_A Centers in Alkali Halide Crystals", in Physics of Color Centers, edited by W.B. Fowler, Academic Press, New York (1968) p. 182.

[9] Girifalco, L.A. and Welch, D.O., Point Defects and Diffusion in Strained Metals, Gordon and Breach, New York (1967) p. 33.

[10] Paladino, A.E. and Kingery, W.D., "Aluminum Ion Diffusion in Aluminum Oxide", J. Chem. Phys. 37, 957 (1962).

[11] Maradudin, A.A., "Some Effects of Point Defects on the Vibration of Crystal Lattices", Repts. Prog. Phys., 28, 331 (1965).

[12] Schawlow, A., Private Communication.

[13] Garmire, E., Pandarese, F., and Townes, C.H., "Coherently Driven Molecular Vibrations and Light Modulation",Phys. Rev. Lett., 11, p. 160, (1963).

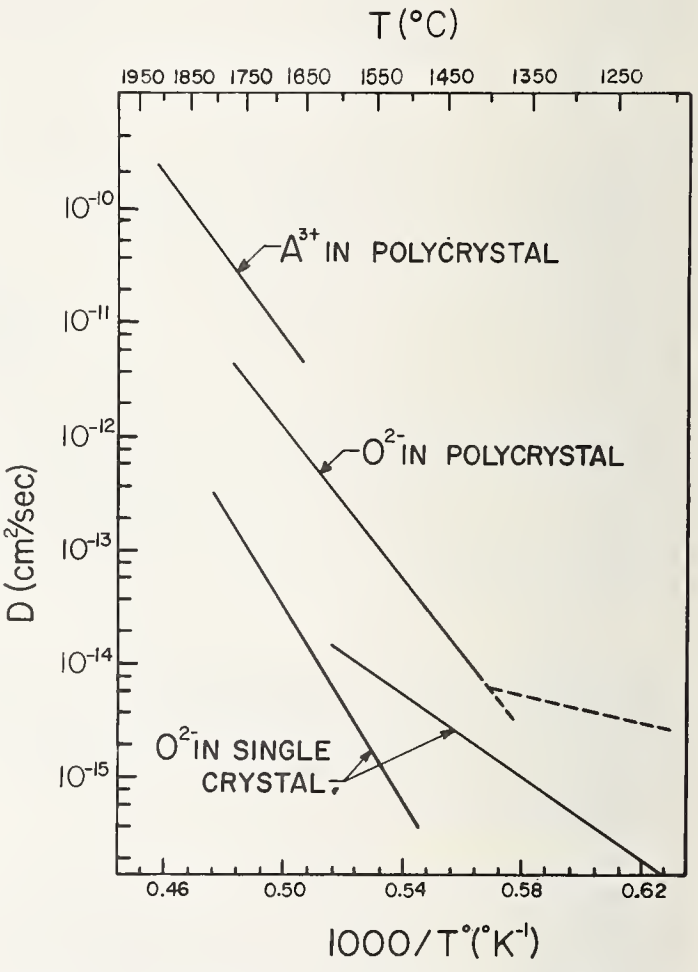

Fig. 1 Diffusion of aluminum and oxygen ions in single and polycrystalline Al_2O_3. Taken from Reference 10.

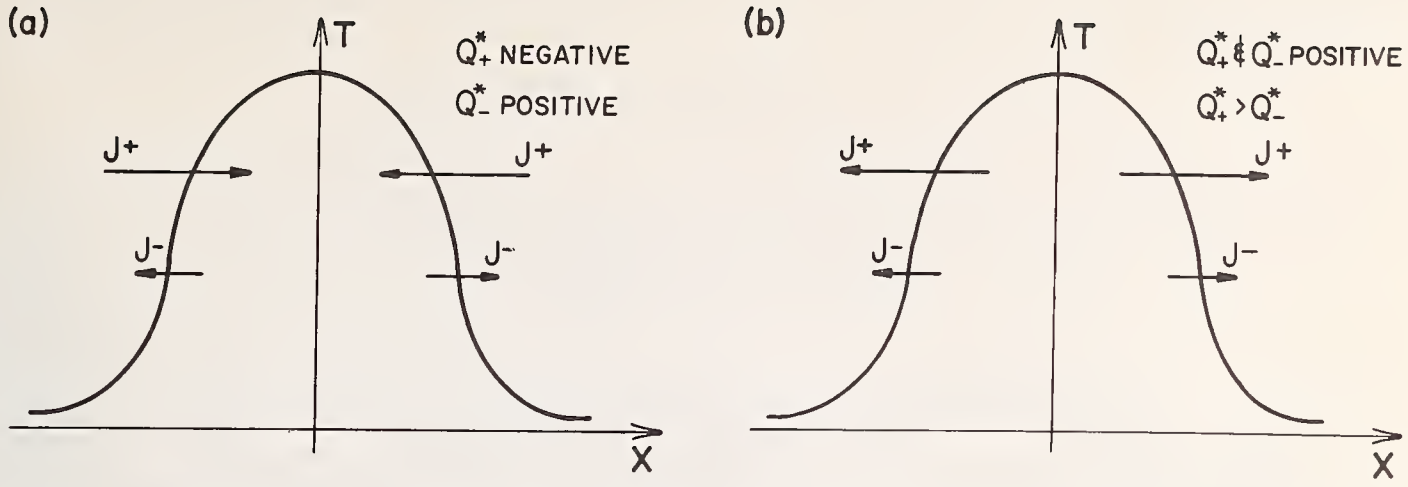

Fig. 2 Schematic diagrams of positive and negative ion fluxes, J_+ and J_-, respectively, in a temperature gradient for + X (a) J_+ is negative and J_- is positive; (b) both J_+ and J_- are positive.

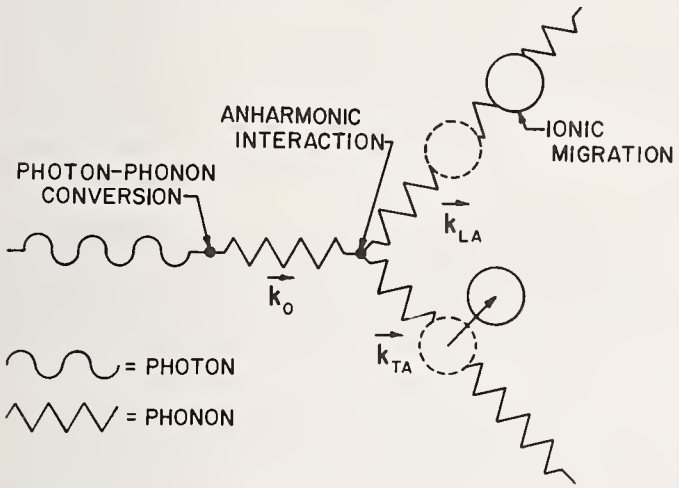

Fig. 3 Diagram depicting IR absorption at a crystal surface followed by anharmonic decay of the optical mode, ω_o, to longitudinal and transverse acoustic modes, ω_{LA} and ω_{TA}, respectively. Ionic displacement in the acoustic phonon field occurs, as portrayed schematically, if the phonon wavevectors are short enough.

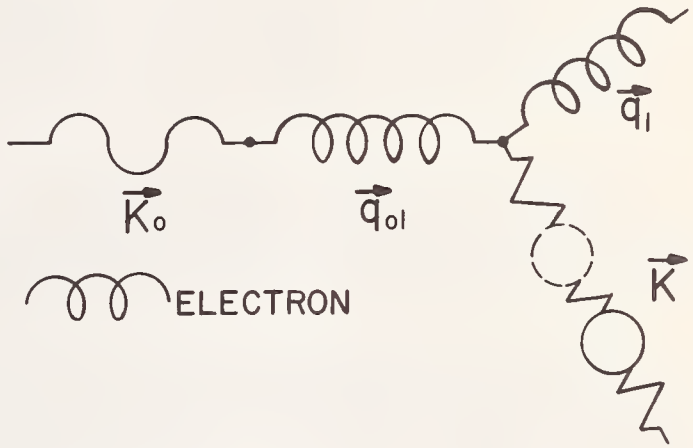

Fig 4 Optical absorption by a localized electron of wavevector $\vec{q}_{o\ell}$ followed by emission of another localized electron and a phonon which aids in the migration of the atom, as indicated. Actually, the phonon cloud about the electron contains many phonons and, in addition, the energy of many phonons is required to affect the migration of the atom.

COMMENTS ON PAPER BY WILBUR FRANKLIN

The speaker commented that at this point in the development of the theory there is no obvious method of distinguishing this mechanism from other competing mechanisms of laser damage. The point was raised, in discussion, that since this mechanism is a diffusion process, one would expect a different dependence of the scale of the damage volume on pulse duration than would be expected from other transport processes. It was proposed that due to the enhanced diffusion of vacancies, a group of vacancies could agglomerate, and act as an internal surface, from which microcracks could propagate. In crystalline materials, dislocation loops could condense, giving rise to plastic strain, even if the crystal was initially free of dislocations.

Time Evolution of Damage Tracks in Sapphire and Ruby*

Concetto R. Giuliano

Hughes Research Laboratories
Malibu, California 90265

A fast streaking camera has been employed to observe the time-evolution of bulk damage filaments in sapphire and ruby on a nanosecond time scale. Externally focused light from a mode controlled ruby laser and amplifier was used to induce damage in the samples studied. Either side-scattered light at 6943 Å or blue-green light from the self-luminous damage sites was detected by the streaking camera. It was found that damage first occurs at or near the natural focus of the lens, and that the damage track grows in an upstream direction toward the laser. The damage filament is formed during the rising portion of the incident laser pulse, reaching its full length at the peak of the pulse. The relationship between the location of the damage at a given instant and the corresponding instantaneous laser power will be discussed in the context of a possible self-focusing mechanism.

Key Words: Bulk damage, filamentary damage, dynamics, moving focus, sapphire, self-focusing, streak photography.

1. Introduction

The causes of laser induced damage can be divided into three separate steps. First, the initiating step, in which the intensity is built up in the medium by a mechanism such as self-focusing. Second, the medium responds to these high intensities by undergoing any of a number of nonlinear processes such as multiphoton absorption and/or phonon generation. Third, the local power dissipation is high enough to exceed the elastic limits of the material, causing catastrophic breakdown.

Much indirect evidence has existed for supporting self-focusing as the initiating mechanism for laser-induced bulk damage. [1,2].*[1] However, different interpretations for the phenomenon have been postulated such as self-trapped filaments of light, repetitive focusing, and moving foci. We have observed the time-development of damage tracks in sapphire and ruby and found that it is most logically explained in terms of a moving focus. This is the first direct observation in support of a moving focus in solids.

We will concern ourselves here with the phenomenon of bulk damage in sapphire, although much of the discussion applies in general for most transparent dielectrics in which filamentary damage is observed. The damage is characterized by a long track, as shown in Fig. 1. Here we see a typical damage track formed by a single pulse from a laser operating in a single longitudinal and transverse mode. The damage filament is characterized by a "head" at the part of the track nearest the sample entrance and a tapering "tail," the end of which occurs at or very near the focal plane of the lens used to focus the laser light in the material. The track often, but not always, displays a region of relatively dense damage at or near the tip of the tail, usually in the form of a crack or "damage star." As we examine the regions of the damage track upstream from the tail (Fig. 1 (b)), we begin to see some subsidiary fracturing alongside the damage filament. This fracturing is randomly located and becomes increasingly dense toward the head of the track where the extent of subsidiary fracturing is maximum (Fig. 1 (c)). If the incident light pulse is not temporally smooth the damage track shows the same filamentary behavior, but in addition, there are occasional regions of more dense damage along the track. An example of this is shown in Fig. 2, where we see a track formed by a pulse in which the laser was oscillating in two longitudinal modes. If the depth of modulation of the incident pulse is large, the filamentary character of the damage track may not be present. Instead, one may see only a series of fractured regions spaced along the light path with gaps of undamaged material between them. We also notice the

*This work was supported by the Advanced Research Projects Agency under ARPA Order 1434 with Air Force Cambridge Research Laboratories.

[1] Numerals in square brackets indicate literature references appearing at the end of this paper.

general feature that the damage filament itself is narrower at the tail of the track (~ 2 to 5 μm) and and broader at the head (several tens of microns). We will later explain these qualitative features of bulk damage in the light of our recent observation of the time-evolution of these damage tracks.

2. Experimental

The experimental setup is shown in Fig. 3. The oscillator employs a 4 inch long x 1/4 inch diameter ruby pumped by two linear lamps in a double elliptical pump cavity. The ruby crystal is water-cooled by a closed-cycle refrigeration system maintained at $0^{\circ}C$. The high reflectivity mirror is coated with a 99+% reflectivity high field damage coating from Perkin Elmer Corporation. Q-switching is accomplished with a solution of cryptocyanine in methanol in a 1 mm path length cell whose transmission is 30% at 6943 Å.

The temperature controlled ($34^{\circ}C$) resonant reflector that was designed to optimize longitudinal mode control consists of two quartz etalons and a quartz spacer, whose combined effect is to enhance cavity modes separated by 2 cm^{-1} and to discriminate against intermediate modes.

Portions of the laser beam are split off in various ways (see Fig. 3), so that the power output, near-and far-field patterns, and Fabry-Perot patterns can be monitored for each shot. This is accomplished in the following way. Light reflecting from wedged beamsplitter W_1 gives two diverging beams; one of them hits the magnesium oxide diffuser, where the scattered light is monitored by a biplanar photodiode used as our power monitor. The second beam from W_1 hits ground-glass screen G, where it is photographed through lens L and the 1 m focal length camera focused at infinity. This gives a magnified (~5x) near-field picture. Another portion of the light is removed by beamsplitter B_1 and hits mirror M_2, which can be placed in or out of position depending on the use of the alignment laser. From M_2 the light either goes to the Fabry-Perot interferometer or can be partially reflected from wedged beamsplitter W_2, where it results in a pair of far-field patterns. A 0.6 neutral density filter is placed near the focal plane of the camera so that the far-field pattern and the Fabry-Perot pattern can be seen at two different exposures. The two Glan prisms are used as a variable attenuator after the amplifier. Beamsplitter B_2 samples the light to photodiode No. 2, which monitors the power incident upon the focusing lens, which was designed for minimum spherical aberration (Special Optics). Photodiode No. 3 monitors the light after the sample. The signals from the two detectors are integrated and displayed on a dual-beam oscilloscope.

The water cooled amplifier ruby is 6 inches long x 0.5 inches diameter, with one end wedged relative to the other by about 0.5°. The input end of the amplifier rod is antireflection coated to minimize the chances of oscillation within the amplifier itself. The ruby rod is closely coupled to a helical flashlamp, which is pumped with a power supply capable of delivering 8 kJ in a 3 msec pulse. The power supply employs a pulse shaping network of 20 sections, each section pumping for 150 μsec. The maximum gain obtained with the amplifier is about 10 dB.

In all experiments described in this paper, the amplifier flashlamp pumping was held constant, and the amount of light incident on the sample was varied by rotating the first of the two Glan prisms. We found that our amplifier acts as a weak negative lens whose focal length depends on optical pumping [3]. Thus we fixed the amplifier pumping to minimize the shot-to-shot variations in the beam characteristics. Typical output from the oscillator plus amplifier is about 150 mJ in pulses which can range from about 15 to 30 nsec. The far-field beam profile was measured to be gaussian down to 8% of the peak using a modified multiple-lens camera technique [4].

The streak camera experimental setup is shown in Fig. 4. We used an STL image converter camera operating in the streaking mode to photograph the self-luminous damage tracks during their formation. The camera was triggered either by the sync pulse from the Pockels cell, when it was used as the Q-switch, or from the laser light itself, when the cryptocyanine Q-switch was employed. For all the experiments described, the light was focused inside the sample using a lens (f = 19 cm) which was designed for minimum spherical aberration. In the latter experiments a portion of the incident light was split off and allowed to enter the camera directly to give a marker streak which gives the relation between the time of formation of a particular point on the damage track and the peak of the incident pulse. In the experiments described here, a Corning 4-94 filter was placed in front of the camera lens. This served to block the laser light which was scattered from the damage sites while passing the self-luminous light in the blue-green part of the spectrum. When the scattered light at 6943 Å is allowed to enter the camera, essentially the same behavior is observed when it is blocked. However, scattered laser light from previously formed damage tracks in the sample constitutes an inconvenient background which interferes with the observation of the track of interest. After each streak photograph was taken, the position of the head and tail of the damage track was determined by examining the crystal using a measuring microscope. These measurements were found to be consistent with the location and extent of the damage inferred from the streak photos.

3. Results of Streak Measurements

Typical streak photographs of the damage in sapphire are shown in Figs. 5 and 6. In Fig. 5 we see the time development of the damage track when an unmodulated pulse is incident on the sample. In Fig. 6 we see the streak photo for a modulated input pulse. (The 750 MHz modulation occurs when the Pockels cell Q-switch is used.) The essential features of these results to be noted are the following.

1. The track first appears at or very near the location of the beam waist.*

2. The track grows in the upstream direction moving toward the sample entrance.

3. The track reaches its maximum length when the incident pulse reaches its peak.

The qualitative behavior of the time evolution of these damage tracks can be described in terms of moving self-focus as follows. At a certain critical power P_c, a self-focus first appears at the beam waist where the damage first occurs. As the power increases the distance z_f required to form a self-focus decreases, and the damage track grows in the upstream direction. The minimum z_f corresponds to the maximum power, thus the head of the track will occur at the peak of the incident pulse. The rate of growth of the track depends on the temporal shape of the laser pulse. The self-focused spot sweeps through the downstream part of the track more quickly than the upstream part, hence the extent of damage is greater at the head than at the tail.

When the incident pulse is modulated, we expect to see local regions of heavy damage associated with the passage of local maxima on the leading edge of the pulse. Each consecutive peak has slightly more power than the preceding one, and therefore causes a self-focus which dwells at slightly smaller z. A glance at the damage track formed from a modulated pulse (Fig. 6) shows the spacing between the heavily damaged regions to decrease toward the head of the track, as one might expect from the above qualitative explanation. Thus, what might appear to be evidence for multiple or repeated focusing could be simply an artifact of temporal spiking on the input pulse, which causes a single focus to pause occasionally as it sweeps upstream.

Streak photographs of damage tracks in ruby show the same qualitative behavior as that seen in sapphire, but the comparison with the self-focusing theory below was not carried out. The general features of damage in ruby are not the same as those in sapphire, and the location and lengths of damage tracks are not as reproducible. One may attribute this to the absorption in ruby at 6943 Å, but the differences have not been investigated in detail (see ref. [3]).

The reduction of data taken from streak and oscilloscope photographs was accomplished by tracing the photographs onto graph paper at a convenient magnification using an opaque projector and picking off values of instantaneous power and damage location at specific times. The two time scales were synchronized by locating the center (most intense region) of the marker streak and allowing this to coincide with the peak of the incident laser pulse. The center of the marker streak was determined "by eye" and was found to be reproducibly locatable to within about 1 nsec (1 mm on the streak photographs). Thus, we obtain values of distance of a particular point on the damage track from the entrance surface z_f and the corresponding instantaneous laser power. An example of the traces is shown in Fig. 7.

4. Comparison of Experiment with Theory

We will now attempt to correlate the above experimental results with the self-focusing theory of Marburger and coworkers [5,6]. Many of the details of this theory are presented in a following paper [7], and we will only dwell on the results as applicable to our experimental results.

The abofe referenced theory assumes that the induced refractive index in the medium δn responds instantly to local changes in the optical intensity. The following equation is obtained from numerical solutions of the nonlinear wave equation (for $P > P_c$).

$$\left((P/P_c)^{1/2} - 0.858\right)^2 = 0.0202 + 0.136\,[ka_o^2/z_f(\infty)]^2 \qquad (1)$$

and

$$z_f^{-1}(\infty) = z_f^{-1}(R) + R^{-1} \quad . \qquad (2)$$

Here, for an incident gaussian equiphase beam, a_o is the e^{-1} radius of the intensity profile at the sample entrance, k is the wave vector in the medium, ^oR is the distance from the crystal entrance to the low intensity beam waist, $z_f(R)$ is the distance from the sample entrance to the self-focus when the incident beam has phase curvature R ($R < 0$ for a converging beam); P and P_c are the incident power and

*In many of the photographs the intensity of the light from the tail of the track is too weak to record. However, subsequent examination of the tracks show that the location of tail is very reproducible from shot to shot.

the critical power for self-focusing, respectively. The theory predicts that two self-foci are formed; they coincide at the low intensity beam focus at $P = P_c$ and at higher power they separate, one moving downstream at the speed of light and the other moving upstream at a rate which depends on the temporal shape of the input pulse. We will deal here with a comparison of the theory and experiment for the backward moving self-focus.

Equation 1 is a hyperbola whose asymptote is

$$(P/P_c)^{1/2} = 0.858 + 0.369\ ka_o^2 \left(\frac{1}{R} + \frac{1}{z_f(R)} \right) . \qquad (3)$$

Thus, for powers greater than about $2P_c$ at plot of $P^{1/2}$ versus z_f^{-1} should give a straight line. Figure 8 shows that this is nearly so.[c] Here we present data taken from a number of streak camera measurements for different peak powers and at two different pulse widths τ.

The evident curvature of the plots in Fig. 8 and their dependence on peak power and pulse duration can be explained by including the slow response of the index change δn which was ignored in the above analysis.

Of the various possible mechanisms for δn, those arising from nonlinearity of electronic response [8] and libration [9] are essentially instantaneous. The largest noninstantaneous mechanism for δn is electrostriction, which leads to an effective nonlinear index of refraction n_2, which decreases as the dimensionless quantity $x = a/u\tau$ increases [10]. Here, a is the spatial beam radius, τ the effective pulse width, and u is the longitudinal sound velocity in the medium. Thus, there is a characteristic time a/u for the electrostrictive nonlinearity to develop, and hence the critical power required to obtain a self-focus will depend on beam size and pulse duration.

The index change leading to a self-focus at a particular distance z_f can only be induced by that portion of the pulse which has passed z_f before the self-focus is formed. Thus, the effective τ should be considered a decreasing function of z_f when considering points along an evolving damage track formed on the leading edge of the pulse. For a converging beam, the beam width a increases with decreasing z. Thus, it becomes increasingly difficult for electrostrictive self-focusing to occur as z_f decreases for a given input pulse; a self-focus formed upstream from the low intensity beam waist cannot take advantage of the small beam radius at the natural focus.

We can crudely account for the effect of electrostriction by replacing P_c^{-1} in (1) by $P_{c1}^{-1} + [P_{c2} f(x)]^{-1}$, where f is an increasing function of x, P_{c1} is the critical power due to instantaneous mechanisms, and $P_{c2} f(x)$ is the critical power for electriction.

For our particular conditions of pulse lengths and focusing, the fractional change in a from the tail to head of the track is substantially larger than the fractional change in τ. Therefore, we expect $f(x)$ to be a decreasing function of z_f casuing positive curvature in a plot of $P^{1/2}$ versus z_f^{-1} according to (1). This is consistent with the data shown in Fig. 8.

Since the first self-focus occurs at the low intensity beam focus, a is the same for all curves at $z_f = |R|$. Therefore, we would expect that x would decrease for pulses of longer duration. This means that the self-focus forms more easily (i.e., at lower powers) for a longer pulse, everything else being equal. This explains the vertical separation between the two groups of curves in Fig. 8. Similarly, one would expect that pulses of different peak power, but the same duration, would form an initial self-focus at different incident powers. In this case the critical power is less for lower peak power than for higher peak power pulses of the same duration. Take, for example, an incident pulse for which the self-focus occurs just at the peak, as compared with a pulse of the same width but much higher peak power. One would expect the self-focus to first occur at a higher power for the latter pulse, because not enough time would have elapsed for a self-focus to have occurred at the same power as for the first pulse. This accounts for the separation at the lower power end between curves of the same pulse width in Fig. 8.

The slight negative curvature seen at the high power ends of the curves in Fig. 8 is very sensitive to the "synchronization" of the pulse profile with the streak photographs. Because of the slow response of the electrostrictive mechanism, the maximum upstream excursion of the damage track would be expected to lag the pulse peak by an amount somewhat less than the response time. We did not attempt to take this into account in plotting the data. This could explain the negative curvature seen at the high power ends of several of the curves in Fig. 8. A relative shift between the oscilloscope traces and the streak photographs of the order of nanoseconds will remove this curvature. The direction of the adjustment is consistent with this explanation.

We see from (3) that the straight line plot of $P^{1/2}$ versus z_f^{-1} should have a slope of $0.369\ ka_o^2 P_c^{1/2}$. Hence we can obtain values for P_c from the slopes of the curves in Fig. 8. Values for a at the crystal entrance were obtained by measurement of the beam profile at a number of points beyond

the focusing lens. The range of critical powers obtained from the slopes in Fig. 8 is 180 kW to 5.4 MW, which is consistent at one extreme with the predictions of electrostrictive self-focusing for sapphire [10] and at the other with values of n_2 inferred from other manifestations of electronic distortion [11].

The author acknowledges the skilled technical assistance of G. R. Rickel.

5. References

[1] Budin, J.P. and Raffy, J., Appl. Phys. Letters 9, 291 (1966).

[2] Zverev, G.M., Mikhailova, T.N., Pashkov, V.A., Solov'eva, N.M., Pisma Zh, Eksp. Teor. Fiz. 5, 391, (1967); JETP Letters 5, 319 (1967).

[3] Giuliano, C.R., DuBois, D.F., Hellwarth, R.W., and Rickel, G.R., "Damage Threshold Studies in Laser Crystals," Semiannual Report No. 3, January 1971 - ARPA Order No. 1434.

[4] Winer, I.M., Appl. Optics 5, 1437 (1966).

[5] Dawes, E.L., and Marburger, J.H., Phys. Rev. 179, 862 (1969).

[6] White, D.R., Marburger, J.H., and Dawes, E.L., (to be published).

[7] Marburger, J.H., these Proceedings.

[8] Brewer, R.G., and Lee, C.H., Phys. Rev. Letters 121, 267 (1968).

[9] Polloni, R., Sacchi, C.A., and Svelto, O., Phys. Rev. Letters 23, 690 (1969); Cubeddu, R., Polloni, R., Sacchi, C.A., and Svelto, O., Phys. Rev. A 2, 1955(1970).

[10] Kerr, E.L., "Damage in Laser Glass," Glass, A., Guenther, A., Stickley, C., and Myers, J., Ed., Amer. Soc. Testing and Materials, Technical Publication 469, p 23 (1969).

[11] Wang, C.C., and Baardsen, E.L., Phys. Rev. 185, 1079 (1969).

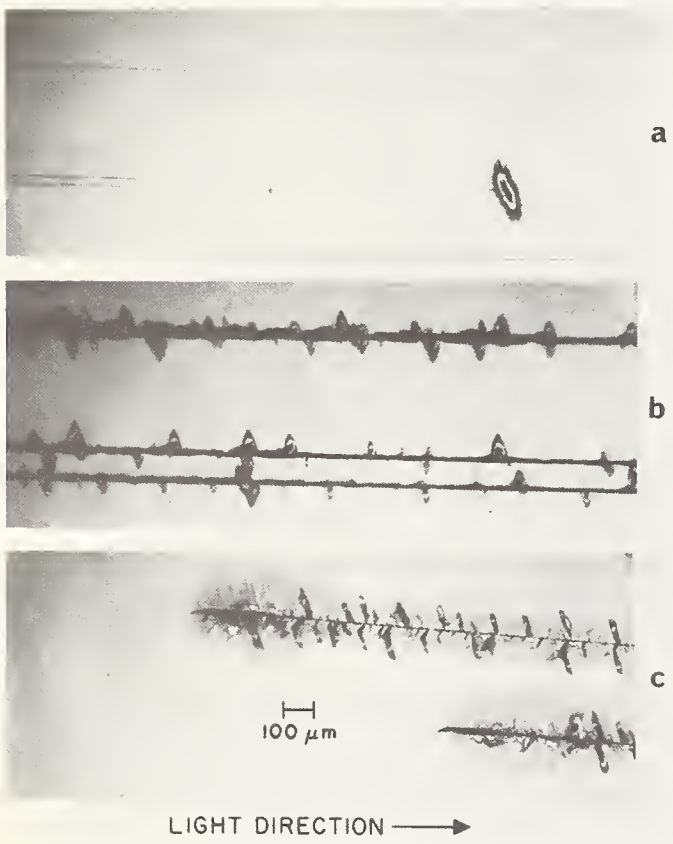

Fig. 1 Typical examples of damage tracks in sapphire caused by a temporally smooth pulse showing damage at (a) the tail, (b) the intermediate region, (c) the head.

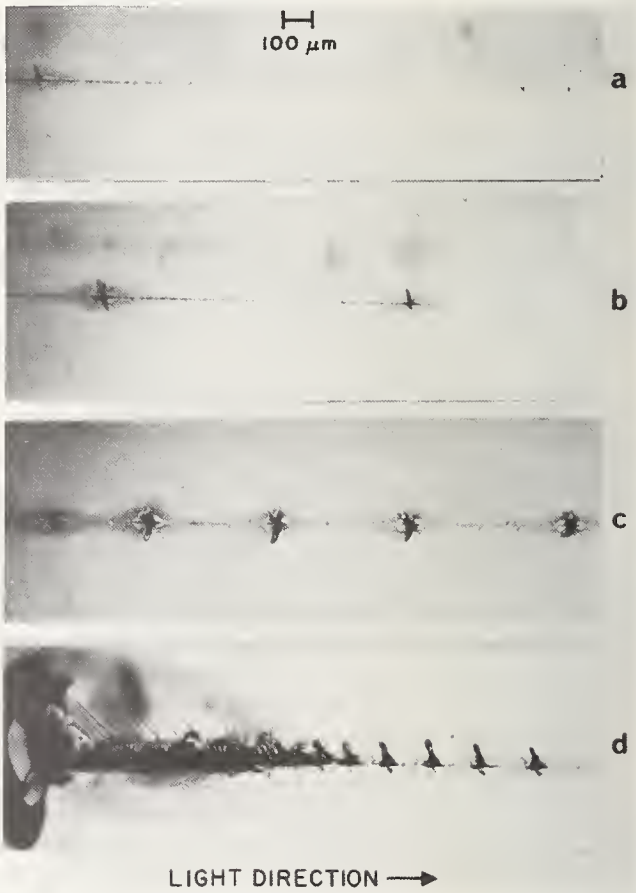

Fig. 2 Examples of damage tracks in sapphire caused by a temporally modulated pulse, (a) through (d) progressing from the tail to the head.

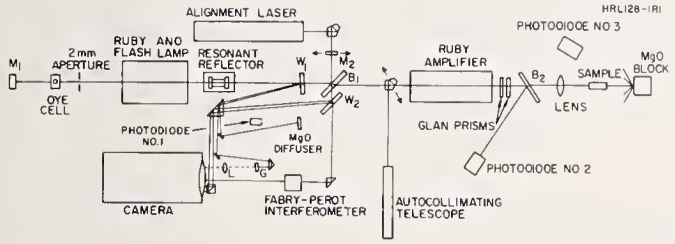

Fig. 3 Schematic representation of laser and amplifier and associated monitoring apparatus.

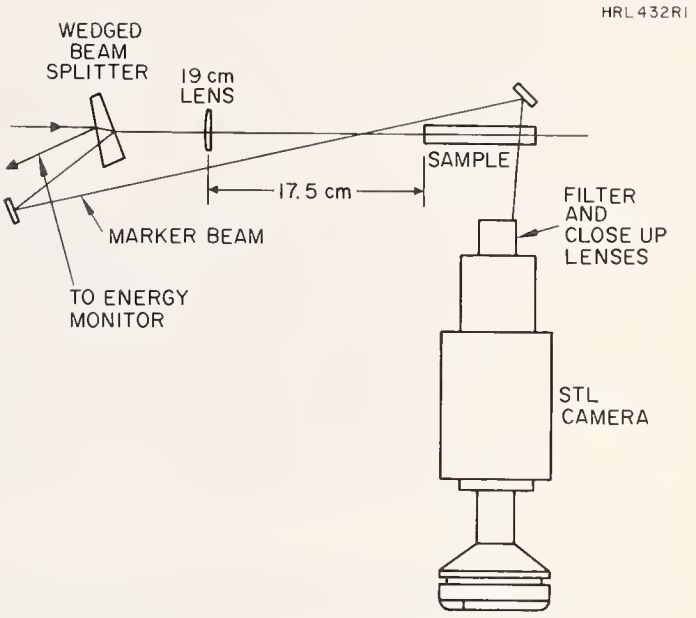

Fig. 4 Streak camera experimental setup.

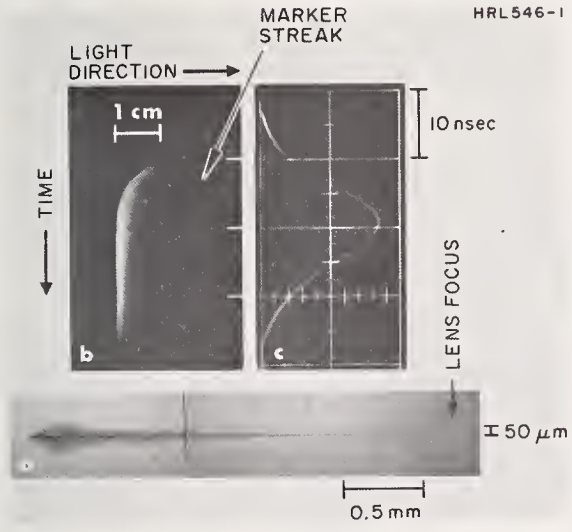

Fig. 5 Typical examples of (a) damage filament, (b) streak photograph, (c) oscilloscope trace for a temporally smooth incident pulse.

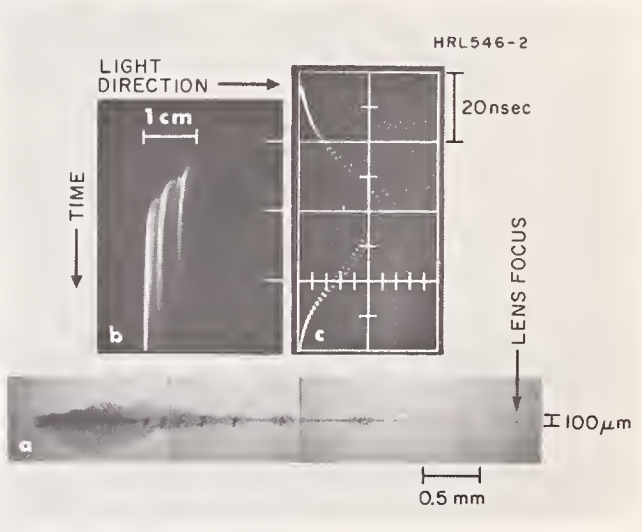

Fig. 6 Typical example of (a) damage filament, (b) streak photograph, (c) oscilloscope trace for a modulated (~ 750 MHz) incident pulse.

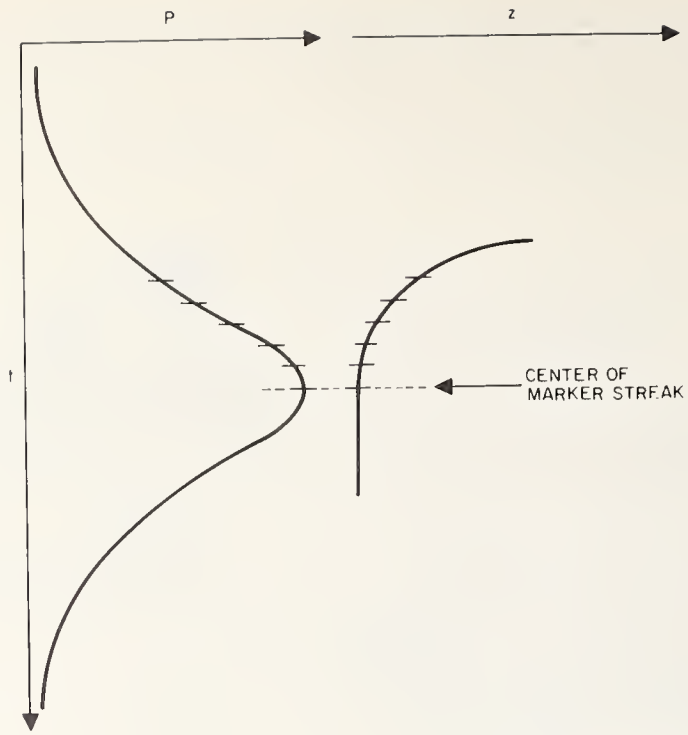

Fig. 7 Juxtaposition of oscilloscope trace and streak photograph showing method of obtaining instantaneous powers and corresponding damage location.

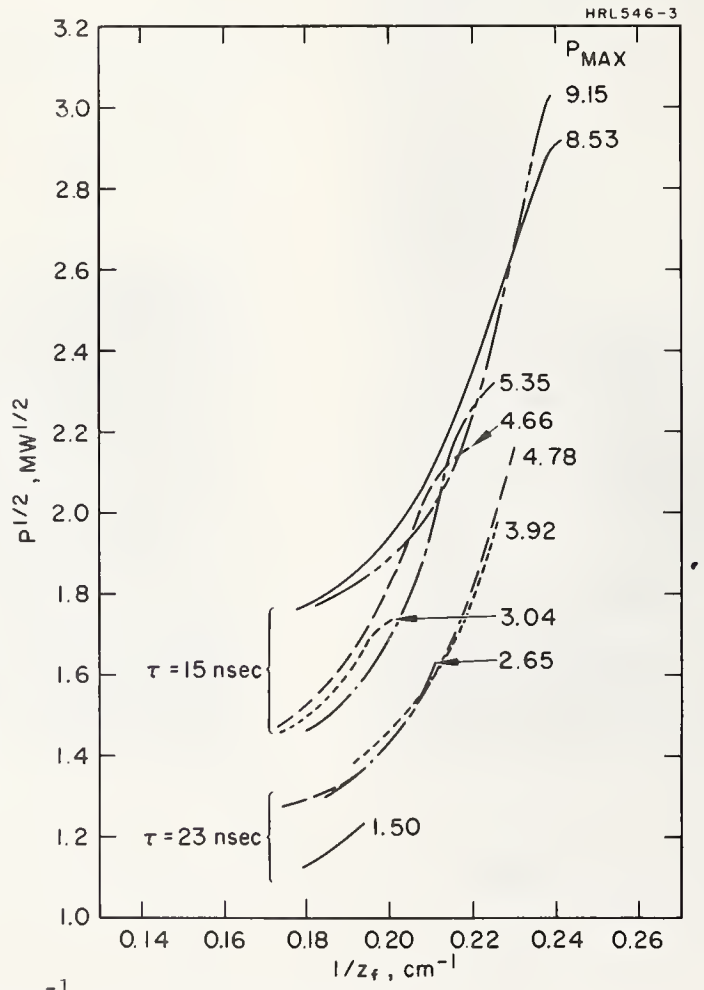

Fig. 8 Plot of $P^{\frac{1}{2}}$ versus z_f^{-1} from data taken from streak and oscilloscope photographs for different incident peak powers and pulse widths.

Theory of Self-Focusing for Fast Nonlinear Response

J. Marburger

University of Southern California
Los Angeles, California 90007

Numerical solutions of the nonlinear wave equation lead to essentially exact formulas describing the behavior of a self-focusing beam up to the first self-focus, if the nonlinear response is instantaneous. We discuss the relation of these formulas to similar ones obtained by ray tracing or quasi-optics, and the influence of terms in the vector wave equation usually ignored in numerical studies. We also give formulas for the on-axis intensity and position of the first focal point, for focussed and unfocussed gaussian beams, and we describe the effect of aberration and deviations from gaussian profile. Using these formulas, we discuss the time evolution of damage tracks in solids, and indicate how the formulas may be modified phenomenologically to account for retarded response of the nonlinear index. The possible influence on damage tracks of the self-focusing phenomena beyond the first self focus will also be discussed.

Key Words: Computer solutions, correlation with experiments, damage tracks, moving self-focus, sapphire, self-focusing theory.

1. Introduction

Theoretical analyses of self-focusing fall rather neatly into a small number of categories depending upon which aspect of the phenomenon is under study. The landmark paper of Chiao Garmire and Townes [1][1] introduces the notion of a self-trapped beam, whose optical field depends upon axial distance z (along the beam) only through a sinusoidal factor. Such a beam retains its transverse size and shape as it propagates, and its properties are governed by a nonlinear ordinary differential equation in the transverse variable r (for cylindrically symmetric beams). Unfortunately, the stable solutions of this equation depend rather sensitively on the precise form of the nonlinear term, which is fixed by the nonlinear dependence of polarization upon applied field [2]. Despite early reports of observations of self-trapping, it now appears that most (perhaps all) of the data can be understood without invoking these self-trapping solutions of the nonlinear wave equation. We shall return to this point in Section 5.

The second category of self-focusing theories began with P. L. Kelley's solution of the nonlinear partial differential equation in r and z which describes the optical field of a beam whose radial dependence is gaussian at z = 0 and evolves to a "self-focus" at z_f [3]. This self-focusing process is characterized (for gaussian incident beams) by the functional dependence $z_f^{-1} \propto P^{1/2}$, where P is the total beam power. Since the self-focus is extraordinarily intense, evidences of its existence are easily observed, and this relation has been verified repeatedly in a variety of materials [4].

Because of the difficulty of obtaining numerical solutions of the self-focusing equation, many workers developed approximate analyses which eliminate the radial coordinate [5]. These are based upon an expansion of the optical field function in powers of r near the axis, the first few (usually only the first) expansion coefficients being determined as functions of z by ordinary differential equations. Implicit in this approach is the assumption that the shape of the transverse intensity profile remains constant, and only its scale shrinks as the beam self-focuses. This constant shape approximation is easily checked by appeal to the exact numerical solutions of the self-focusing equations, and is found to be severely violated unless the beam is self-trapped [3], [6]. In particular an initially gaussian beam does not remain at all gaussian, as it would in a linear medium, but develops a sharp spike at r = 0 as it self-focuses. Nevertheless the constant shape analysis leads to important conclusions regarding qualitative features of self-focusing, offers clues to functional dependences, and even gives quantitatively correct results for the initial stages of self-focusing prior to severe beam distortion.

The self-focusing analysis described above is strictly correct only for a continuous beam of constant power incident at z = 0. We shall refer to theories which attempt to account for pulsed incident

---

[1] Figures in brackets indicate the literature references at the end of this paper.

beams as dynamical self-focusing theories. The simplest such analysis assumes that the nonlinear polarization responds "instantly" to changes in the local intensity, an "adiabatic" approximation. This means that if the solution of the time independent, or stationary, self-focusing equation is expressed as a function of the incident power, the time dependent solution may be obtained from it simply by allowing the incident power to vary with time. This approach led to the prediction of dramatic on-axis intensity pulse shaping effects [7] accompanying self-focusing, and to the prediction that the position z_f of the self focus must change as the incident power changes [8]. Both predictions have received ample verification [9].

The attractiveness of the adiabatic approximation lies in its use of the stationary results for dynamical prediction, but it is certainly incorrect for nonlinear mechanisms such as electrostriction, whose response time can exceed the duration of a typical Q-switched laser pump pulse. The "exact" solution of a set of dynamical self-focusing equations including slow nonlinear response has been attempted by Fleck and Kelley [10], but the immensity of the computing task placed severe restrictions on the range of independent variables (r, z, t) for which solutions could be obtained. This restriction can be overcome at the expense of introducing the constant shape approximation, a strategy exploited by E. Kerr [11] in connection with the electrostrictive nonlinearity. The resulting partial differential equations in z and t must still be solved numerically, but the task is far easier with two independent variables than with three. A more qualitative approach reported recently by Shen and Loy [12] employs the adiabatic approximation to obtain a rough pulse shape within the medium. This modified pulse is then inserted as a driving term in the equation for the nonlinear index change which may then be solved with relative ease (the exact approach would require simultaneous determination of the pulse shape and the index change). This approach was developed to account for the observed extensive self-phase modulation without invoking the self-trapping solutions [13].

A final category must be reserved for studies in which the radial intensity dependence plays a minor role. Here one assumes the existence of a quasi-trapped field whose surfaces of constant phase are nearly plane over a rather long distance. Certain features of a pulse propagating in such a mode are adequately represented by a wave packet comprised of colinear plane waves. With the radial coordinate thus conveniently eliminated, one may study phenomena depending upon both z and t with relative ease. These include: self-steepening [14] which arises from the alteration of phase velocity by the nonlinear index change, and self-phase modulation [15] which has the same origin. Observations of the latter phenomenon indicate that some sort of quasi-trapping takes place in some media, but it may not be as closely related to the self-trapping solutions as was once thought [12], [13].

2. Results of Stationary Self-Focusing Analysis

Starting with Maxwell's equations and the nonlinear constitutive relation $\underset{\sim}{D} = [\varepsilon_L + \varepsilon_2 \langle E^2 \rangle]\underset{\sim}{E}$, which is the simplest giving rise to self-focusing, it is not difficult to obtain the equation [3],

$$2ik\partial\mathcal{E}/\partial z + \nabla_T^2\mathcal{E} + (\varepsilon_2 k^2/2\varepsilon_L)|\mathcal{E}|^2\mathcal{E} = 0 \quad . \tag{1}$$

Here $\mathcal{E}$ is the slowly varying envelope of the linearly polarized $\underset{\sim}{E}$ field

$$\underset{\sim}{E} = \mathrm{Re}\ \hat{e}\,\mathcal{E}\exp i(kz - \omega t) \ ,$$

and ∇_T^2 is the transverse Laplacian operator. k is the wave number in the medium ignoring the nonlinear index change. The effects of other terms which must be discarded to obtain eq. (1) are negligible prior to a self-focus, but will be discussed later.

Introducing the new variables $F \equiv (\varepsilon_2 k^2 a^2/2\varepsilon_0)^{1/2}\mathcal{E}$, $z^* \equiv z/2ka^2$ and $r^* \equiv r/a$, where a is a typical transverse dimension, eq. (1) can be written in the form

$$i\,\partial F/\partial z^* + \nabla_T^{*2}F + |F|^2F = 0 \tag{2}$$

which contains no free parameters. Thus the solutions of eq. (2) are fixed uniquely by the parameters of the beam incident at $z = 0$, such as the transverse intensity profile, total power, and phase curvature.

Figure 1 shows some results of numerical solution of eq. (2) for gaussian equiphase incident beams of different powers [6]. On-axis intensity is plotted versus z^*. Three regions of incident power are clearly evident: I) $P < P_1$: no self-focusing evident, II) $P_1 < P < P_2$: very weak self-focus which appears at greater distances for larger powers, III) $P_2 < P$: strong self-focus which appears at shorter distances for higher powers. The upper and lower critical powers are given by

$$P_2 = 0.0232\ \lambda_0^2\ c\ \varepsilon_L^{1/2}/\varepsilon_2 \tag{3}$$

$$P_1 = 0.273\ P_2\ . \tag{4}$$

The lower critical power P_1 is predicted accurately by the paraxial ray-constant shape analysis [16]. P_2 is very close to the power P_c required for self-trapping with a transverse profile containing no nodes [1].

The constant shape approximation can be used to estimate the dependence of P_1 on deviations from gaussian shape of the incident beam. Writing $\mathcal{E}(r,z)$ for a cylindrically symmetric beam as

$$\mathcal{E}(r,z) = \mathcal{E}_0(z)\ g(r,z)$$

$$g(r,z) = 1 - \tfrac{1}{2}\, r^2/a^2(z) + (\beta/24)\ r^4/a^4(z)\ \ldots$$

and defining

$$f \equiv b/a(0)$$

where

$$b^2 \equiv 2 \int_0^\infty g^2(r,0)\ r\,dr\ ,$$

we have found

$$P_1(f,\beta)/P_1 = (2\beta - 3)\ f^2/3\ . \tag{5}$$

The values $(f,\beta) = (1,3)$ characterize a gaussian, $(\sqrt{2},6)$ a Lorentzian, and (1.21,5.23) the no-node self-trapped shape.

Using the solutions shown in Fig. 1 one finds the following relation between power and self-focusing length for $P > P_2$ [6]. (Here a is the 1/e radius of the incident intensity profile.)

$$[(P/P_2)^{1/2} - 0.858]^2 = 0.0202 + 0.136\ [ka^2/z_f]^2\ . \tag{6}$$

This is a hyperbola with asymptote

$$(P/P_2)^{1/2} = 0.858 + 0.369\ ka^2/z_f\ , \tag{7}$$

which may be used in place of eq. (6) for $P \gtrsim 2P_2$. For $P \gg P_2$, the slope of $P^{1/2}$ versus z_f^{-1} given by eq. (7) should be divided by f if the incident beam is not gaussian.

These equations may still be used even when the constant phase surface passing through $r = z = 0$ is curved, corresponding to a converging or diverging incident beam. One need only replace z_f^{-1} by

$$z_f^{-1} = z_f^{-1}(R) + R^{-1} \tag{8}$$

where R is the radius of curvature of the incident phase surface ($R < 0$ for converging beams) and $z_f(R)$ is the new position of the self-focus (see Fig. 2). This formula, which is identical to that for the focal length of two thin lenses in contact, has been verified numerically for a wide range of P and R values for both converging and diverging beams [17]. It plays a key role in our subsequent discussion of optical damage.

450-417 O-71—5

If the incident phase surface is not spherical, it is said to possess spherical aberration, which is conveniently measured by the deviation ν in wavelengths from a sphere when $r = a$. The phase of $\mathcal{E}$ at $z = 0$ is .

$$\phi(r) \simeq kr^2/2R + 2\pi\nu r^4/a^4 \tag{9}$$

for such a wave. Figure 3 shows how the position of the self-focus shifts for increasing positive spherical aberration for several powers [17]. For these curves, $R = -2ka^2/3\pi$.

It is important to determine to what extent all these conclusions are altered if the exact equation

$$\nabla \times \nabla \times \underset{\sim}{E} = (\omega^2/c^2)\underset{\sim}{D} \tag{10}$$

is employed in place of eq. (1). We have solved this equation numerically for a variety of initial fields and conclude from the solutions that the additional terms lead to utterly negligible corrections until very near the self-focus. In particular, the position of the self-focus itself is not altered, nor is the catastrophic increase in intensity at $r = 0$ at the self-focus. Unfortunately, it has thus far proven impossible to solve either eq. (1) or eq. (10) for E beyond the first self-focus with sufficient accuracy to tell what happens in the region $z > z_f$. Efforts to probe this region theoretically will be discussed later.

3. Dynamical Self-Focusing in the Adiabatic Approximation: Evolution of Damage Tracks in Solids

If the nonlinear polarization responds instantly to local changes in optical intensity, then above the critical power P_2 for self-focusing, a self-focus always forms at a unique point at time t for a given incident power P at $z = 0$ and time $t - z_f\varepsilon_L^{1/2}/c$ regardless of incident pulse shape. Thus the position of the self-focus at any time t may be obtained from the intersection of the pulse shape curve $P(z_f - \varepsilon_L^{-1/2}ct)$ and the curve P versus z_f given by eqs. (6) and (8) for focused gaussian incident beams [18].

This construction is shown in Fig. 4, which is drawn with parameters corresponding to Giuliano's experiments on damage in sapphire exposed to focused ruby laser light. Clearly the self-focus first appears at, or just prior to, the geometrical focal point, then splits into two foci, one of which travels down- and one up-stream. The up-stream focus reaches its minimum z_f value as the pulse maximum passes, and therefore dwells at this position for a while. This presumably allows massive damage to occur at the head of the track which scatters subsequent light in the trailing portion of the pulse. The observed damage tracks are always narrower at their down-stream ends, which is consistent with the notion that the focal spot moves more rapidly there. This picture of bulk damage has been given by several other authors, including E. Kerr [11].

This theory of the creation of damage tracks suggests that irregular temporal behavior of the incident pulse will lead to a string of heavily damaged spots along the track. Each spot occurs at the position determined by the power at a local maximum in the pulse shape. Giuliano has obtained streak photographs of the luminescence created by the passage of a focal spot in sapphire exposed to a modulated pump beam which shows a series of such damage spots being formed [19]. In this connection, it is obviously important to keep the incident pulse shape in mind when evaluating the appearance of damage tracks. What might appear to be evidence of multiple or repeated focusing could be simply an artifact of temporal spikes on the input pulse which cause <u>one</u> focus to pause occasionally as it sweeps up-stream.

By monitoring the incident pulse shape and the evolution of self-luminescence created as the focus sweeps through the crystal, Giuliano has inverted the construction shown in Fig. 4 and found curves $P^{1/2}$ versus z_f^{-1} (See paper by Guiliano, p.50, Fig. 8). The curvature of these plots can be understood by invoking the finite response time of the electrostrictive mechanism, which seems to give the largest nonlinearity in this case. At this point we simply note that the curves are rather straight, indicating that the instantaneous response approximation is at least not grossly in error, and can be trusted to give rough quantitative information.

4. Phenomenological Theory of Electrostrictive Response: Analysis of Damage Tracks in Sapphire

Electrostriction is expected to lead to an appreciable nonlinear refractive index in all dense materials. This mechanism "turns on" in a time of order a/u, where u is the longitudinal sound velocity and a the beam radius. This means, of course, that the response depends upon the input pulse duration, if

it is comparable with a/u, as well as the instantaneous power. Kerr has performed an extensive analysis of electrostrictive self-focusing, using the constant shape approximation to eliminate the radial coordinate [11]. Our approach is to start with the exact conclusions for instantaneous response, and attempt to modify them a posteriori to account for the retardation of nonlinear index.

If we have two independent sources of nonlinear response, the total critical power P_T satisfies $P_T^{-1} = P_A^{-1} + P_B^{-1}$, where $P_A(P_B)$ is the critical power for mechanism A(B) alone. This is strictly correct only for the stationary case where transient response is unimportant; but we shall adopt this form even in the transient case. P_A will be the fast critical power, arising from electronic nonlinearities [20] and perhaps libration [21], and P_B will be that due to electrostriction. Following Kerr [11], we shall write the latter as $P_B = Kf(x)$, where f is an increasing function of

$$x = a/u\tau \tag{11}$$

and τ is usually regarded as the incident pulse length. Our strategy is to replace P_2^{-1} in eq. (6) and eq. (7) with

$$P_T^{-1} = P_A^{-1} + [Kf(x)]^{-1} \tag{12}$$

where τ (and a for focused beams) will be related to the position z_f of the self-focus.

The index change responsible for a self-focus at z_f can only be induced by the portion of the pulse which has passed z_f prior to the focus formation. Focal points formed during the leading edge of the pulse occur at shorter distances for larger times, so τ is a decreasing function of z_f. Similarly, for a converging incident beam, a should also be a decreasing function of z_f: Obviously a decreases from its maximum at z = 0 to a minimum at the geometrical focal point, z = |R|. In Giuliano's experiments on sapphire, a/u varies from about 40 nsec at z = 0 to about 1 nsec at z = |R|. The effective time τ varies over a smaller range from ~ 5 to ~ 15 nsec. Thus the entire transient regime of electrostrictive response is involved during the transit of the self-focus.

If τ changes relatively less than a during the transit of the self-focus, we expect $x = a/u\tau$ to be a decreasing function of z_f, according to the argument above. Thus for the largest z_f, near |R|, the net critical power [eq. (12)] is expected to be smaller than at the regions of heavy damage near minimum z_f. A glance at eq. (7) will show that this implies that a plot of $P^{1/2}$ versus z_f^{-1} will have positive curvature. The experimental plots [19] invariably show positive curvature except for a short region near the peak power which will be shown below to be related to another feature of retarded response not included in the present discussion.

Since the self-focus first makes its appearance at the geometrical focal point, the effective beam radius at $z_f = |R|$ is always the same. Thus any change in experimental parameters which shortens τ will increase the power at which damage first appears. This can be done either by shortening the incident pulse length at constant peak power, or by increasing the peak power at constant pulse length. (In the latter case the time taken to reach any given power is decreased.) Both effects may be seen in Giuliano's data [19].

The negative curvature sometimes seen at the high power ends of the experimental plots can be removed by changing the time which is chosen on the pulse profile for peak power (on the oscilloscope trace) relative to the time at which the self-focus reaches its maximum up-stream position (on the streak photograph of self-luminescence). Because of the slow response of the electrostrictive mechanism, the maximum up-stream excursion of the focus is expected to lag the pulse peak by an amount on the order of the response time. The adjustment required to remove the negative curvature is of the order of nanoseconds, and in the right direction to be consistent with this mechanism.

The success of this phenomenological theory of electrostrictive self-focusing in explaining practically every observed qualitative feature of damage track evolution suggests that one may have some confidence in whatever quantitative information can be gleaned from it. In addition to measurements of the nonlinear index coefficients, one might also determine the phenomenological function f(x), which would allow rather detailed estimates to be made of damage thresholds in real systems. (Of course one always expects all self-focusing parameters, including f(x), to depend rather sensitively on incident transverse mode structure.)

5. Post-Focal Phenomena

In the foregoing discussion, we have invoked the motion of only a single self-focus to explain many observed features of optical damage in sapphire. We have said nothing about the rays of light which pass beyond the self-focal plane, yet it is entirely possible that these may add to damage already created by

the moving focus, or perhaps even cause damage in regions where the first self-focus did not appear at all. It is convenient to divide the discussion of post-focal phenomena into four categories.

The first category includes effects arising from the presence of a forward moving focus. According to the discussion of Section 3 a self-focus appears near the low intensity focal plane and moves forward with the velocity of the pulse. There is little direct evidence for such a self-focus, especially in the focused beam case, but if it exists, it would be an important mechanism for damage at the output crystal surface. Theoretical evidence, obtained from numerical solution of the stationary self-focusing problem, indicates that only a small amount of energy is associated with this forward travelling focus. The rays in the early leading portion of the pulse, in which the power is less than P_2, diffract very quickly away from the axis beyond the low intensity focal plane. Rays in the higher power portion may be divided into two classes: those near the axis which pass through the backward moving focus, and off-axis rays, which do not. Neither type contributes to the forward travelling focus, which is composed of rays associated with a very short interval of time during which the instantaneous power is P_2. Insufficient theoretical work has been done to say more about the effects of this focus.

The second category of post-focal phenomena is associated with the off-axis rays mentioned above which do not pass very near to the first backward moving focus. Numerical solutions of the steady state equations indicate that only the rays within the central portion of the beam containing power roughly equal to P_2 contribute to this focus. If the total power is sufficiently greater than P_2, the remaining rays may come to one or more foci beyond the first backward moving focus [8]. The trajectories of these foci may be inferred from a construction similar to that shown in Fig. 4. When the incident beam is focused, these additional foci behave just as the first focus did: additional backward moving foci appear between the first focus and the geometrical focal point. Presumably forward moving foci also appear beyond the geometrical focal point, behind the first forward moving focus, but we have not verified this numerically. Such additional foci can contribute to the damage caused by the first backward moving focus because the rays which comprise them are not necessarily scattered by the damage, which is confined to the axis. In this connection it is important to bear in mind that these additional foci can be formed by the trailing portion of the pulse as well as the leading portion. Thus, unlike the first focus which moves up-stream to a minimum z_f and may be prevented from moving back again because of scattering from axial damage, the additional foci may sweep in both directions, feeding energy into the damaged track during an appreciable portion of the pulse. If the beam is focused, most of the rays must pass very near the geometrical focal point, and one expects that damage caused there by the first focus will scatter light even from rays originally rather far off-axis. Thus the role of the secondary self-foci in causing damage beyond the geometrical focus (e.g., at the exit surface) may not be very great.

The fate of rays which have passed through the first or subsequent self-foci form the third category of post-focal phenomena. Their fate is very uncertain. These are the rays which proponents of self-trapping theories believe are trapped in filaments. If such trapping does take place beyond the self-focus, it could have two origins. Firstly, in a medium in which the nonlinear index responds "instantly", it may be that the solutions of the nonlinear wave equation show trapping behavior beyond the focus. We have demonstrated something of this sort for an index which "saturates" at relatively low intensities [6], but solutions beyond the self-focus for more realistic cases have not been obtained.† Secondly, in a medium with slower nonlinear response, such as electrostrictive, rays emerging from a backward moving focus will enter a region in which the index has not yet relaxed from the influence of the focus. That is, they enter a slowly decaying dielectric waveguide, and may be channeled, or trapped, for a while. This mechanism has been proposed by Shen and Loy [12] to account for evidences of trapping in liquids. In either case the extent to which trapped rays can propagate in a region which has experienced a self-focus depends sensitively upon the lag time between passage of the focus and appearance of damage massive enough to scatter these rays. If damage appears soon after the passage of the focus, self-trapping may not play an important role.

The fourth category of post-focal phenomena includes effects similar to the induced waveguide mechanism mentioned above, which can be understood using linear optics. Thus any spherically or axially symmetric dielectric imperfection can have a focusing effect on the beam. Such imperfections can even focus energy in the very low intensity tail into the region already damaged, or beyond. Realistic calculations of this effect have not been performed, to our knowledge, but it is accessible to experimental analysis.

6. Summary

Our intention in this discussion has been to assist the reader in organizing the complicated theoretical and experimental details which have appeared in the rather confusing self-focusing literature.

---

†The solutions reported in [8] are based upon a numerical scheme which allows power to be lost from the beam very near a focus. Thus these solutions, which do not show evidence of self-trapping behavior, may not be treating correctly the very rays which could participate in self-trapping. We have repeated the work in [8] using the reported numerical techniques and always found that the power lost at the focus was about equal to the critical power.

In summary, self-focusing does exist in solids and liquids. If it is driven by a pulsed beam, the self-focus does move, and it is responsible for observed damage tracks in solids. In sapphire, the nonlinear mechanism which determines the threshold for bulk damage is almost certainly electrostriction, but other faster mechanisms may also play a role. The damage may be enhanced by the creation of secondary foci by off-axis rays, for which there is good theoretical evidence, and possibly by self-trapping, which is probably present in sapphire because of the slow decay of the electrostrictive mechanism. Damage at the exit surface could be caused or enhanced by the first forward moving focus, and by "lensing" of rays passing through already damaged material.

I am pleased to acknowledge the assistance of C. Giuliano in bringing these ideas to focus, and in some cases to fruition. My students E. L. Dawes and Dennis R. White have also contributed much to my understanding of self-focusing. The work which led to results first reported herein was supported by the Joint Services Electronics Program through the Air Force Office of Scientific Research (AFSC), United States Air Force, under Contract F 44620-71-C-0067.

7. References

[1] R. Y. Chiao, E. Garmire, C. H. Townes, Phys. Rev. Lett. B, 479 (1964), "Self Trapping of Optical Beams".

[2] J. Marburger, L. Huff, J. D. Reichert, W. Wagner, Phys. Rev. 184, 255 (1969), "Stationary Self Trapping of Optical Beams with Lorentz Local Field Corrections", and references contained therein.

[3] P. L. Kelley, Phys. Rev. Lett. 15, 1005 (1965), "Self Focusing of Optical Beams".

[4] See, for example, C. C. Wang, Phys. Rev. Lett. 16, 344 (1966), "Length Dependent Threshold for Stimulated Raman Effect and Self Focusing of Laser Beams in Liquids".

[5] An account of this approach, and references to other work, may be found in W. G. Wagner, H. A. Haus, J. H. Marburger, Phys. Rev. 175, 256 (1968), "Self Focusing of Optical Beams in the Paraxial Ray Approximation".

[6] J. H. Marburger, E. L. Dawes, Phys. Rev. Lett. 21, 556 (1968), and Phys. Rev. 179, 862 (1969), "Computer Studies of Self Focusing".

[7] J. H. Marburger, W. G. Wagner, IEEE Journ. Quant. Elect. QE-3, 415 (1967), "Self Focusing as a Pulse Sharpening Mechanism".

[8] A. L. Dyshko, V. N. Lugovoi, A. M. Prokhorov, Zh. ETF Pis'ma 6, 655 (1967) [ZETP Letters 7, 117 (1968)], "A Possible Explanation of the Small Scale Self Focusing Filaments". Also see [18].

[9] G. McAllister, J. Marburger, L. DeSha zer, Phys. Rev. Lett. 21, 1648 (1968), "Observation of Pulse Shaping by the Self Focusing Effect". M. M. T. Loy, Y. R. Shen, Phys. Rev. Lett. 25, 1333 (1970), "Experimental Study of Small Scale Filaments of Light in Liquids".

[10] J. A. Fleck, Jr., and P. J. Kelley, Appl. Phys. Lett. 15, 313 (1969), "Temporal Aspects of the Self Focusing of Optical Beams".

[11] E. L. Kerr, "Laser Beam Self Focusing and Glass Damage Caused by Electrostrictively Driven Acoustic Waves" in Damage in Laser Glass. A. J. Glass, et al., Editors ASTM Tech. Pub. 469 (1969). Also "Track Formation in Optical Glass Caused by Electrostrictive Laser Beam Self Focusing", Ph.D. Thesis, New York University (1971).

[12] Y. R. Shen and M. M. T. Loy (to be published).

[13] R. Cubeddu, R. Polloni, C. A. Sacchi, O. Svelto, F. Zaraga, Phys. Rev. Lett. 26, 1009 (1971) and Optics Communications 3, 9, (1971), "Study of Small Scale Filaments of Light in CS_2 Under Picosecond Excitation".

[14] F. DeMartini, C. H. Townes, T. K. Gustafson, P. L. Kelley, Phys. Rev. 164, 312 (1967), "Self Steepening of Light Pulses".

[15] F. Shimizu, Phys. Rev. Lett. 19, 1097 (1967), "Frequency Broadening in Liquids by a Short Light Pulse", and references contained therein.

[16] W. G. Wagner, H. A. Haus, J. H. Marburger, Phys. Rev. 175, 256 (1968), "Self Focusing of Optical Beams in the Paraxial Ray Approximation".

[17] D. R. White, J. H. Marburger, E. L. Dawes (to be published).

[18] This construction is based upon arguments given in [7] and extended by J. P. Taran and T. K. Gustafson, IEEE Journ. Quant. Elect. QE- , (1969), "Comments on the Self Focusing of Short Light Pulses" and M. M. T. Loy and Y. R. Shen, Phys. Rev. Lett. 22, 994 (1969), "Small Scale Filaments in Liquids: Tracks of Moving Foci".

[19] C. Giuliano, J. Marburger (to be published).

[20] R. G. Brewer and C. H. Lee, Phys. Rev. Lett. 21, 267 (1968), "Self Trapping with Picosecond Light Pulses".

[21] R. Cubeddu, R. Polloni, C. A. Sacchi, O. Svelto, Phys. Rev. A2, 1955 (1970), "Self Phase Modulation and 'Rocking' of Molecules in Trapped Filaments of Light with Picosecond Pulses".

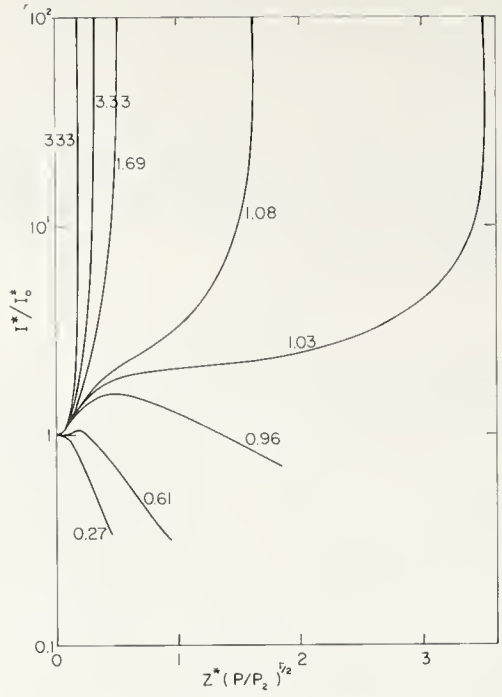

Fig. 1 Normalized on-axis intensity versus axial distance for self focusing beam whose phase surfaces were flat at z=0, and whose initial intensity distribution was gaussian. The labels are values of P/P_2 for different incident powers.

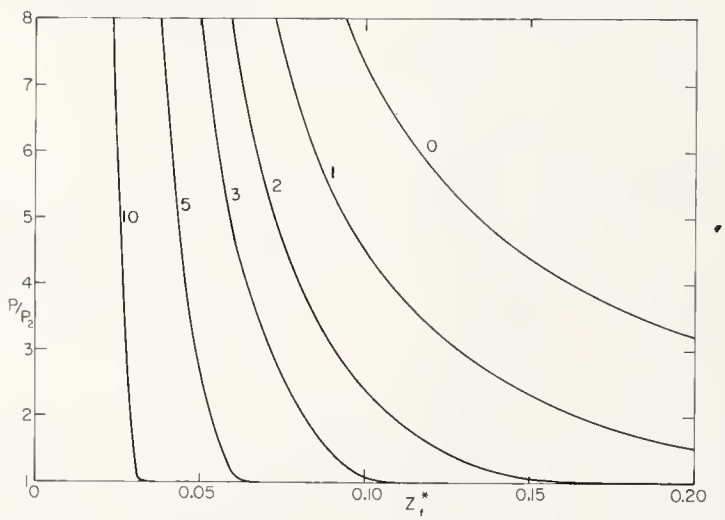

Fig. 2 Incident power, in units of P_2, versus position at which a self focus forms, for various degrees of incident phase curvature (pre focusing) at Z-0. The curves are labelled with values of $-2ka^2/\pi R$ where R is the radius of curvature of the surface of constant phase passing through r=z=0. Notice that the vertical scale begins at $P/P_2=1$.

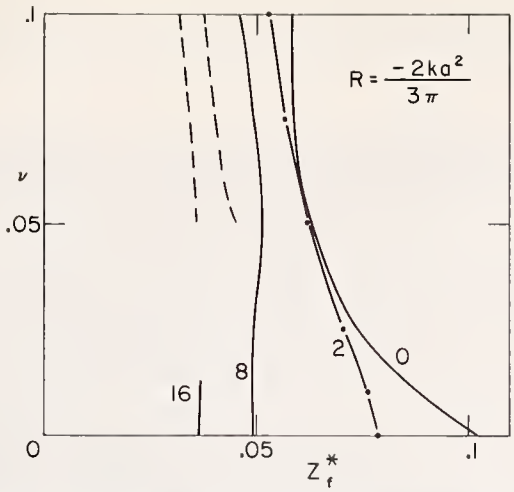

Fig. 3 Variation of the position of the self focus with increasing positive spherical aberration for several powers. The beam is prefocussed with R as shown. The solid curves are labelled with values of P/P_2. The curve for which P/P_2 is zero is the position of the low intensity focal plane. The dotted curves indicate the positions of the weak relative intensity maxima which appear prior to the focal plane when aberration is present. The positions of these maxima change very little when self focusing is included, so the dotted curves refer to P/P_2 = 0, 2, and 8.

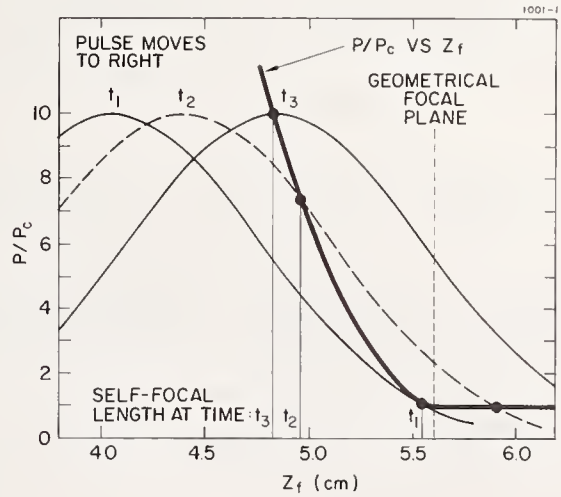

Fig. 4 Construction for the position of the self focus versus time. The self focus first appears at 5.55 cm at time t, then splits into two foci, one of which travels backwards repidly to 4.96 cm at time t_2, while the other has moved ahead to 5.92 cm. At time t_3, the backward focus has reached its minimum distance at 4.84 cm, and will reverse its motion at later times. The curve P/P_2 vs z_f has been drawn for the conditions of Giuliano's experiment [19], in which ka^2 = 220 cm, R = -5.6 cm, and the peak power can exceed P_2 by a factor of 10. The pulse width shown is unrealistically narrow (.12 n sec at 1/e point) for clarity of the figure.

COMMENTS ON PAPERS BY CONCETTO GIULIANO AND JOHN MARBURGER

A noteworthy feature of the results presented in Giuliano's paper was the fact that the observed damage tracks were most intense near the entrance face of the sample and decreased in intensity as one moved away from the entrance face towards the low intensity focus of the incident light. This morphology is exactly the opposite of that reported earlier in the symposium by Boling for damage tracks seen in glass samples. The consensus arrived at to explain this apparent discrepancy was the following. In Boling's work, the laser intensity incident on the sample was well above the threshold for damage. Under this circumstance, self-trapping plays a secondary role in the damage process. Consequently, the damage is most severe where the incident light is most intense--in this case, close to the physical focus of the incident light. In Boling's work, the incident laser beam was focused just outside the sample beyond the exit face, and therefore, the greatest intensity was present in the sample close to the exit surface and it was at this point that the damage track was most severe, growing less severe as one moved back towards the laser. On the other hand, in the work of Giuliano, the incident laser intensity was just above the threshold for damage. In this circumstance, self-trapping plays an essential role in the damage mechanism. On the basis of the theory presented by Marburger, as the laser intensity rises, the self-induced focal point of the trapped beam moves back towards the laser. The more intense the laser beam is, the closer to the entrance surface the actual focus occurs, and therefore, the damage track increases in severity back towards the entrance face away from the focal point which was located in the center of the sample. Additional evidence for this model was provided by the fact that severe damage spots were correlated in position and time with the modulation observed on the laser pulse. It is worth noting that even though self-focusing does not play an essential role in the damage mechanism when the incident intensity is well above threshold as far as bulk damage is concerned, it still seems to be an important feature of the mechanism whereby surface damage can occur at the exit face. In addition to the mechanism proposed by Marburger, the possibility was raised that a moving focal spot can occur as the result of a changing radius of curvature of the incident laser beam. This last effect, however, is much more pronounced in neodymium glass than it is in ruby and would not seem to give a full explanation of the results observed by Giuliano. These results seem to give good confirmation of the motion of the focal spot towards the laser during that portion of the pulse in which the intensity is rising, but it is, of course, not possible in these experiments to see the retrograde motion which is predicted to occur during the portion of the pulse in which the intensity decreases. There does not seem to be conclusive evidence of the observation of this retrograde motion in the literature at the present time.

C. G. Young, of the American Optical Company, reported on work on long path breakdown in air over distances in excess of 25 meters. He observed no evidence of the dynamic system lens effect described by Basov. The time-average beamspread at the focal plane of a lens on the output end of a diffraction-limited laser operating at 50 to 100 joules in 30 nsec was measured. The measured spot size (with attenuators between the laser and the lens) agreed very well with the calculated sizes, based on diffraction from the 3 cm output aperture. This would not have been the case had the total system operated as a dynamic lens.

Electrostrictive Laser Beam Focusing in Glass and Small-Scale Track Formation

Edwin L. Kerr[1]

The Perkin-Elmer Corporation, Research Dept.
50 Danbury Road
Wilton, Connecticut 06897

Electrostrictive laser beam self-focusing can form damage tracks in non-absorbing glass. The acousto-optical interaction involves a radially propagating compression wave driven by the light intensity gradient, and beam focusing caused by the compressional increase in refractive index along the beam axis.

Transient and steady-state approximate solutions of the sound and light wave equations are discussed. Calculated beam trapping thresholds are compared with experimental track formation thresholds. An expression for the parameter $\rho_o \partial n/\partial \rho$ in terms of the photoelastic constants is described.

Beam focusing is described by a newly derived "small-scale" beam tracing equation. This equation includes approximately not only Gaussian beam diffraction, but also the inhomogeneous refractive index term of the vector light wave equation. For the radial component of the electric field the equation predicts typical track diameters at the trapping power thresholds.

Key Words: Electrostriction, filaments, glass damage, laser, self-focusing, self-trapping, track formation.

1. Introduction

Electrostrictive self-focusing has been acknowledged as a cause of track formation in glass by nanosecond laser pulses for seven years [1].[2] The mechanism is an interaction between light and sound.[3]

The electrostrictive soundwave was observed by G.N. Steinberg [2]. Figure 1 shows his experimental setup and typical results. The laser pulse enters a slab-shaped sample about 7 centimeters long. Electrostriction excites a compression wave. The wave comes to an initial peak on the beam axis in the characteristic acoustic relaxation time. This time is equal to the beam waist radius a_m divided by the speed of sound v. After the initial peak, the sound propagates away from the beam axis. The wave shape is not preserved because the sound disturbance is mainly cylindrical. The sound disturbance leaves a trailing wake, that is evident in the middle trace to the right of the figure.

---

[1] Research Physicist

[2] Figures in brackets indicate the literature references at the end of this paper.

[3] Ultrasound, not hypersound. The characteristic wavelength of the electrostrictive sound wave which causes self-focusing is of the order of the beam waist radius, typically 20-200μm. Once the beam is self-focused to a high intensity, electrostriction may excite a hypersonic wave with a characteristic wavelength equal to a wavelength of light. The hypersonic wave causes stimulated Brillouin scattering, but not self-focusing.

The upper trace shows a compression peak a short time after the laser pulse, and a later rarefaction valley. The first peak represents the direct compression wave from the beam axis. The rarefaction valley is created when the compression wave impinges on the opposite face of the sample and returns as a rarefaction wave. An additional compression peak and rarefaction valley are evident in the trace after two more reflections. The time between peaks corresponds to the roundtrip time for sound in the glass sample.

These results were typical of dense flint glass and borosilicate crown glass. The result with fused silica showed much more fine structure because of the higher Q of the material.

Self-focusing is caused by an inhomogeneous refractive index distribution. The index must be greater along the beam axis than at the beam edges. Such a refractive index distribution is equivalent to a sequence of thin lenses placed along the beam axis. Figure 2 illustrates the equivalence. The lower beam guide is a focusing rod with an inhomogeneous refractive index built in. The refractive index distribution is paraboloidal in the radial direction, and uniform longitudinally. The beam trajectories for the two guides were computed from the large-scale beam tracing equation, to be described below. Each beam guide was chosen with just enough inhomogeneity to cause trapping of the beam. Trapping is defined as the amount of focusing required to balance diffraction. The beams in both of the guides are trapped, because they cannot spread to infinite radius by diffraction. However, neither one propagates with constant radius. Constant radius propagation cannot be achieved in the upper guide. In the lower guide, constant radius propagation is possible if the beam enters the medium parallel and exactly at the right radius. When the beam enters at the radius shown, focusing is strong and diffraction is weak, so the beam converges. If the beam had entered parallel at the minimum radius shown within the guide, diffraction would be strong and focusing would be weak, so the beam would diverge along the trajectory shown. There is an intermediate radius for which constant radius propagation is possible if the beam enters parallel.

If the inhomogeneity in the lower beam guide were increasing dynamically in time, the distance to the first minimum would decrease. This is often described as the "moving focus" condition.

A current controversy centers around the question "Are the tracks found in glass the result of moving foci or of formation of a trapped light filament?" The above discussion illustrates some of the theoretical difficulties concerning the formation of trapped filaments. The mere achievement of enough refractive index inhomogeneity to reach the trapping threshold is not sufficient to guarantee constant radius propagation, i.e., filament formation. Other difficulties include the small-scale radius of the tracks, the vector nature of the light wave equation, the effect of saturation of the refractive index inhomogeneity, and the possibility of trapping only a portion of the beam.

First we will discuss the electrostrictive self-focusing mechanism and the constant intensity curves in the presence of electrostrictive self-focusing. We will then make further comments on small-scale track formation.

2. Electrostrictive Self-Focusing

Electrostriction is the stress produced in a material medium by an inhomogeneous electric field. The stress tends to draw the material into the high-field region. Electrostriction is distinguished from inverse piezoelectric effect because electrostriction depends on even powers of the electric field.

There are several effects which produce self-focusing. Some of these, such as the Kerr effect, depend on molecular motion. In solids these motions are frozen out. Electrostriction therefore predominates over many other mechanisms for solid media.

2.1. The Coupled Differential Equations

All self-focusing mechanisms involve an interaction between light and matter. They are therefore described by two equations. One equation gives the dependence of the refractive index on the square of the electric field, i.e., on the intensity. The other equation gives the propagation of the laser beam through a given refractive index distribution. The latter equation is, of course, completely described by Maxwell's equations.

In the electrostrictive self-focusing mechanism, the change in refractive index is proportional to the sound wave compression. It is therefore possible to scale the sound wave equation and write down a refractive index wave equation,

$$v^2\nabla^2 n - \partial^2 n/\partial t^2 = c^{-1}\rho_o^{-1}(\rho_o \partial n/\partial \rho)^2 \nabla^2 I, \tag{1}$$

where the refractive index n is n(r,z,t), the intensity I is I(r/a), the beam radius a is a(z,t), and ρ_o is the undisturbed mass density [3].

This is essentially a sound wave equation driven by the electrostrictive forcing term on the right. Notice that in the steady state, where the time derivative term goes to zero, the spatial derivatives may also be cancelled on each side of the equation. This means that in the steady state the local change in refractive index is proportional to the light intensity, i.e., to the square of the electric field. This is exactly the same as the usual constitutive relation

$$n = n_o + \frac{1}{2} n_2 E^2. \tag{2}$$

used in many analyses. The simplicity of (2) relative to (1) explains why most of the theoretical work done to date has been for steady-state trapping.

Maxwell's equations can be reduced by suitable approximations to the large-scale beam tracing equation [4],

$$\frac{\partial^2 a}{\partial z^2} = \frac{1}{k_o^2 n_o^2 a^3} + \frac{a}{n_o}\left.\frac{\partial^2 n}{\partial r^2}\right|_{r=o}. \tag{3}$$

This equation describes the propagation of a beam with a Gaussian beam intensity distribution through a medium whose refractive index distribution varies negligibly over distances of the order of a wavelength of light. Thus, as long as the beam radius remains large relative to a wavelength of light, this equation gives a valid description. Later we will describe how this equation must be modified when the beam radius approaches a few wavelengths of light.

The above equations have been solved approximately in two different models. From these two models we can compute the trapping threshold for both the transient, transitional, and steady-state regimes of beam radius and pulse duration. In another model, we compute the power required to achieve a given intensity for various ranges of interest of beam radius and pulse duration.

a. Approximations

Both models assume that self-focusing takes place in a long interaction region of the sample. Thus the analysis applies more to internal damage in laser amplifier rods or very thick lenses than it does to thin lenses. The entering laser beam is assumed to be initially unfocused or only gently focused, so the beam radius is nearly constant throughout the interaction region. The beam intensity distribution is assumed to remain Gaussian. Under these conditions, the electrostrictive stresses are mainly two-dimensional compression. We shall assume the time constant for development of appreciable longitudinal compression is much greater than the laser pulse duration.

Inspection of (1) and (3) shows that the coupling of a with n occurs through the driving term of (1). Equation (1) is quite nonlinear because a is both space-varying and time-varying. However, the "gently focused" approximation makes the Laplacian mainly radial. If the time variation of the beam radius a is also removed, (1) becomes linear and solvable. We therefore introduce the precipitous approximation. According to the precipitous approximation, the beam trajectory remains nearly constant until it suddenly and precipitously is altered by the onset of self-focusing.

The idea that self-focusing is precipitous is borne out experimentally [5]. Figure 3 shows some experimental results obtained by G.N. Steinberg. First he placed a small round aperture downstream from the exit face of the damage sample. This aperture was large enough to transmit the gently focused laser beam if the power was too low to

cause self-focusing, because the gently focused beam diverged only at a small angle. In a second experiment, he placed a small round stop (the same diameter as the previous aperture) in the same downstream location. Behind the stop he placed a large-aperture F1 lens to collect light coming from the sample at large angles. In both of the experiments, the light transmitted through the aperture or past the stop was detected with a fast photodiode. In figure 3 we see the resulting small-angle trace and large-angle trace. They may be compared with the large-and-small-angle trace. It was recorded when both the stop and the aperture were removed, but the large collecting lens remained in place. A recording of the incident laser pulse is also shown when no sample was present.

The small angle recording shows clearly that the light is transmitted practically undisturbed during the first third of the laser. Then self-focusing occurs precipitously as shown by the very rapid fall. The cutoff is so rapid that the Techtronix 585 scope and photodiode circuit rings, producing a valley below the zero of intensity. This sudden cutoff in small angle transmission cannot be explained by the sudden formation of a plasma, because the light is merely redirected to large angles, as shown by the second trace. The sudden scattering of light at large angles occurs because the beam is suddenly self-focused to a radius of approximately a wavelength. When the small radius beam emerges from the sample, diffraction is no longer overcome by self-focusing. The beam therefore diverges with a half-angle of about half a radian. The third trace may be compared with the fourth to show that most of the light is transmitted, with very little absorption.

The precipitous approximation is also substantiated by computer calculations and a computer movie [3,5,6].

b. Method of Solution

With the above approximations, the index wave equation is linear. The driving function may be separated into a spatial factor and a temporal factor. The spatial factor is the fixed Gaussian intensity distribution. The temporal factor is the laser pulse shape. Solution is possible using the following steps. First, a Hankel transform simplifies the radial dependence. Second, a Green's function allows solution for arbitrary pulse shapes. Third, an inverse Hankel transform gives the refractive index distribution.[4] The third step can be performed along the beam axis.

2.2. Trapping Thresholds

In the first model we will calculate the power required to reach the trapping threshold.[5] The trapping criterion is selected as follows. There must be just enough refractive index inhomogeneity at the beam waist so the laser pulse, if it entered the medium as a parallel beam, would continue to propagate at constant radius. We further require that the refractive index inhomogeneity be achieved at the time of the peak of the laser pulse. Let Δn be the increase in refractive index on the beam axis. Analysis of the large-scale beam tracing equation shows the criterion is equivalent to

$$\frac{\Delta n}{n_o} = \frac{1}{2}\left(\frac{\lambda}{2\pi n_o a_m}\right)^2 . \qquad (4)$$

This criterion differs from that used by Chaio et al. [1] only by a numerical factor representing the difference between their choice of a uniform intensity beam and our choice of a Gaussian beam. In our analysis, the refractive index wave equation is linear, so it may be scaled by a coefficient that is characteristic of the medium and the laser wavelength. The coefficient K we choose has the dimensions of power and is called the trapping power coefficient.

---

[4] Inverse transformation for points off-axis is difficult analytically, but has been performed on a computer [6].

[5] As we noted previously, mere attainment of the trapping threshold power does not insure that either trapping or constant radius propagation will occur. We merely use the trapping criterion as a convenient measure of the nonlinearity.

$$K = \frac{c\lambda^2 \rho_o v^2}{8\pi n_o (\rho_o \partial n/\partial \rho)^2}. \qquad (5)$$

In the steady state the pulse duration is long compared to the acoustic relaxation time a_m/v. The trapping analysis predicts a power threshold for trapping for either long pulses or small-radius beams. On the other hand, when the pulse duration is short or the beam is large, the acoustic wave does not develop greatly until the laser pulse is over. As soon as the laser pulse begins, the electrostrictive force creates an acoustic acceleration field[6] in the medium. The acoustic velocity field therefore increases initially directly with time, and the initial acoustic displacement field increases directly as the square of time. The acoustic displacement field does not achieve its full development during a short laser pulse, so more pulse power is required to produce the required refractive index inhomogeneity at the peak of the laser pulse. In the limit of large beams or short pulses, the trapping power threshold therefore increases the the square of the ratio a_m/pv. Figure 4 shows the trapping threshold power for several pulse shapes in both the steady-state and the transient regimes. In the transient regime the threshold rises with a slope of 2 on the log-log plot, as predicted. A power threshold occurs only in the steady state. In the transient reqime the threshold is an intensity threshold for fixed pulse duration. Details of the analysis have been given elsewhere [7].

Self-focusing of picosecond laser pulse trains has recently been demonstrated [8-10], even in solids and viscous liquids [10]. While most authors have discounted the possibility of electrostrictive self-focusing for picosecond pulses, a recent analysis [11] has shown the feasibility of electrostrictive focusing for picosecond pulse trains. Indeed, if p is taken as the duration of the pulse train, and the power P is the total train energy divided by p, the threshold for trapping a train of 15 or more pulses differs from the thresholds given in figure 4 by less than 10% over the whole range plotted. This is due to the ability of the electrostrictive mechanism to average the energy in the laser pulse. Confirmation or denial of the electrostrictive explanation for picosecond pulse train trapping awaits further experimentation.

2.3. Self-Focusing to a Given Achieved Intensity

In the second model we will calculate the power required to achieve a given intensity for any beam radius and pulse duration.

Suppose it is desirable to achieve a given intensity I within the medium. If this value of intensity is low, no self-focusing will occur. The peak intensity will be achieved at the beam waist, on the beam axis, and at the peak of the laser pulse. It will be

$$I = P/\pi a_m^2 . \qquad (6)$$

Taking the logarithm of both sides produces

$$\log P = 2 \log a_m - \log \pi I.$$

Therefore, a graph showing the logarithm of power required to achieve a given low value of intensity versus the logarithm of beam radius is a straight line with a slope of 2.

Now suppose achievement of a much higher value of intensity is desired. Let the value of intensity be so high that self-focusing occurs. Self-focusing causes the beam waist radius to decrease. In the absence of self-focusing the beam waist radius was a_m. Let us designate the beam waist radius in the presence of self-focusing by a_M. Equation (6) is still approximately correct if a_M is substituted for a_m, but a_M is a function of a_m and the other parameters of beam focusing. We now introduce several approximations to calculate this function.

---

[6] The acoustic acceleration, velocity, and displacement fields are vector-point functions, to be distinguished from the "velocity of sound".

a. Approximations

All the approximations used in the previous trapping model are required. We choose the parabolic pulse as representative of typical Q-switched laser pulses.

To avoid a laborious transcendental maximization problem, we will assume the peak intensity is achieved at the peak of the laser pulse. In the transient case, where the pulse duration is short compared with the acoustic relaxation time, it seems obvious that the self-focused beam waist radius a_M reaches its minimum value some time after the peak of the laser pulse. Of course, after the peak of the laser pulse, the instantaneous pulse power falls off rapidly. Therefore the time of maximum intensity must be after the peak of the laser pulse but before the time of minimum achieved beam waist radius. According to our computations, the assumption, that the peak intensity occurs at the peak of the laser pulse, causes only a modest error, provided we do not extend the solution too far into the transient regime.

Another approximation is the assumption that the refractive index inhomogeneity develops equally everywhere along the beam axis. This assumption is quite correct if the beam is so gently focused that the beam radius is nearly constant throughout the medium. In fact, in the steady-state regime where the low-power-beam waist radius a_m is small, the laser beam converges rather sharply to a focus, and then diverges. The refractive index inhomogeneity develops more slowly (and with less strength) in regions on the beam axis far from the focus where the beam radius is larger. In the steady state the strength of the inhomogeneity varies inversely as the fourth power of the beam radius. (In the transient regime the strength initially varies even more rapidly, as the inverse sixth power of the beam radius.) We may use the approximation of uniform development of the refractive index inhomogeneity along the beam axis, provided we do not extend our calculations too far into the steady-state regime of small beam radii.

b. Method of Solution

A formula for the power required to achieve a given intensity can be obtained if the relationship between a_M and a_m is known. This relationship is provided by the large-scale beam tracing equation. First, in the absence of self-focusing, a given value of a_m corresponds uniquely to the entrance radius a_o and the entrance slope a_o'. The entrance radius and entrance slope are merely a pair of constants associated with the solution of the second order differential equation.

In the presence of self-focusing, the value of $\partial^2 n/\partial r^2\Big|_{r=o}$ is calculated by performing the differentiation under the integral sign of the inverse Hankel transform. The inverse transform can then be evaluated on the beam axis. The large-scale beam tracing equation is solved again, this time including the refractive index inhomogeneity, but using as constants the same entrance radius and slope. This process gives the required functional dependence of a_M on a_m and on the electrostrictive self-focusing parameters. After the formula is derived, the parameters may be collected into a single scaling factor,

$$I_{ET} = K/\pi(vp)^2,$$

having the dimensions of intensity. This constant gives the measure of the intensity associated with electrostrictive trapping. It may be described as the intensity (without self-focusing) of a beam having the trapping power coefficient as its power, and whose waist radius is just equal to the distance sound can travel in the pulse duration.

The function has been plotted for several decades of given achieved intensity I in figure 5. The figure is basically a log-log plot of power versus beam radius, with scaling added. When only a low value of achieved intensity is given, say 1/10th of the electrostrictive trapping intensity, the curve is simply a straight line with a slope of 2 as we said before. If the given achieved intensity is 10 times the electrostrictive trapping intensity, in the transient regime the power required is reduced. Self-focusing increases the achieved intensity by dynamically reducing the beam radius. The broken lines indicate the power required to achieve 100 and 1000 times the electrostrictive trapping intensity if no self-focusing were present. Self-focusing greatly reduces the power required to achieve these intensities. If the desired intensity is very high, the power required no longer depends very much on the desired intensity, but rather on the trapping threshold. This may be seen by comparing figure 5 with the parabolic pulse trapping threshold in figure 4.

c. Comparison with Experimental Track Formation Thresholds

We made the above analysis because we surmised that experimental track formation thresholds might follow a single given achieved intensity curve. The damage associated with track formation may be due to a variety of physical causes, most of which are dependent on the local intensity or energy density. The actual value of the threshold intensity for damage will depend on such factors as the chemical composition of the medium, the optical wavelength, and possibly the pulse duration. It is difficult to measure the value experimentally independently from self-focusing. Instead, we assumed the hypothesis was correct and chose the value of I that gave the best fit between the theoretical curves of figure 5 and the experimental track formation thresholds for each glass. This procedure gives plausible values of the damage threshold intensity. The results are shown in figures 6,7, and 8 for three common types of optical glass. Each point in the figures represents a single laser pulse passing through the sample. Open circles indicate no damage occured at that power level. Filled circles indicate the formation of a track, which was always accompanied by a bright flash of side-scattered white light, similar in appearance to an air spark. In all the experiments the wavelength was 694.3nm, and the pulse duration p was 55ns. In all cases the solid constant intensity curve chosen lies below the broken trapping threshold curve.

The worst disagreement was a factor of 2 at one point for dense flint glass. Apparently the approximations cause the constant intensity curve to rise too slowly in the right extreme of the graphs. The pronounced inflection observed for borosilicate crown glass experimentally is also shown in the best fitting constant intensity curve. In view of the many approximations, the agreement between theory and experiment is satisfactory.

2.4. The Light-Sound Coupling Constant $\rho_o \partial n/\partial \rho$

In the above analysis K depends on the light-sound coupling constant. The values we used were calculated from the Lorentz-Lorenz relation

$$\rho_o \partial n/\partial \rho = (n_o^2 + 2)(n_o^2 - 1)/6n_o.$$

This relation holds if the polarizability of molecules in the medium is constant for small density changes. The values of the light-sound coupling constant derived in this way disagree with experimental values measured under hydrostatic compression by as much as 36% for some glasses [12].

In spite of this discrepancy, the Lorentz-Lorenz formula gives good results. A.V. Shatilov *et al.* [13] have found the Lorentz-Lorenz formula gives better agreement with experimental thresholds than other formulas, such as the Drude-Newton formula. Their results agree with ours in showing that the experimental thresholds lie below the theoretical trapping threshold.

A more correct treatment would use the photoelastic constants p_{11} and p_{12} for the medium. Under hydrostatic stress, the light-sound coupling constant is related to the photoelastic constants by [12]

$$\rho_o \partial n/\partial \rho = n_o^3(p_{11} + 2p_{12})/6.$$

On the other hand, our analysis [3,5] shows that for two-dimensional compression we have

$$\rho_o \partial n/\partial \rho = n_o^3(p_{11} + p_{12})/4.$$

Futhermore, the state of strain induced by electrostriction will only be a two-dimensional compression if the beam is circularly polarized, because only then is the electrostrictive force isotropic. A linearly polarized beam produces anisotropic forces, and the whole analysis is much more complicated. A vector soundwave equation, including the effects of shearing forces, must be solved. This is the subject of further research.

3. Small-Scale Beam Tracing

When the refractive index inhomogeneity varies on a scale comparable with a wavelength of light, the large-scale beam tracing equation is no longer valid. This is because the scalar light wave equation itself is only approximately correct. A small-scale analysis is required because the tracks formed in glass are often as small as a wavelength of light in radius.

3.1. The Inhomogeneous Index Term in the Vector Light Wave Equation

Maxwell's equations in rationalized MKS units and the usual constitutive relations for a dielectric are as follows:

$$\underline{\nabla} \times \underline{E} = -\partial \underline{B}/\partial t, \qquad \underline{\nabla} \cdot \underline{D} = \rho,$$

$$\underline{\nabla} \times \underline{H} = \underline{J} + \partial \underline{D}/\partial t, \qquad \underline{\nabla} \cdot \underline{B} = o,$$

$$\underline{H} = \varepsilon_o c^2 \underline{B}, \qquad \underline{D} = n^2 \varepsilon_o \underline{E}, \qquad \underline{J} = \rho = 0.$$

Taking the curl of the first curl equation above and substituting the second curl equation, together with the constitutive relations gives the electric field wave equation

$$-\underline{\nabla} \times (\underline{\nabla} \times \underline{E}) - n^2 c^{-2} \partial^2 \underline{E}/\partial t^2 = 0.$$

We may substitute the identity

$$-\underline{\nabla} \times (\underline{\nabla} \times \underline{E}) = -\underline{\nabla} (\underline{\nabla} \cdot \underline{E}) + \nabla^2 \underline{E}.$$

We evaluate $\underline{\nabla} \cdot \underline{E}$ by expanding the constitutive relation

$$\underline{\nabla} \cdot \underline{D} = n^2 \varepsilon_o \, \underline{\nabla} \cdot \underline{E} + \varepsilon_o \, \underline{E} \cdot \underline{\nabla} \, n^2 = 0.$$

Substitution yields the vector light wave equation

$$\nabla^2 \underline{E} - n^2 c^{-2} \partial^2 \underline{E}/\partial t^2 = -\underline{\nabla} (\underline{E} \cdot \underline{\nabla} \ell n \, n^2). \tag{7}$$

In a homogeneous medium the term on the right is zero, and the equation reduces to the familiar scalar light wave equation for each component of the electric field. Even in an inhomogeneous medium, the scale of variation of refractive index is usually very large compared with a wavelength. Therefore the term on the right hand side is usually neglected, except when studying the depolarization effects of surfaces.

3.2. Depolarization Effect

The depolarization of a self-focused laser beam is evidence of the importance of the inhomogeneous index term. Suppose for example the laser beam is linearly polarized in the x direction and the intensity distribution is azimuthally symmetrical. If we neglect the anisotropy of the electrostrictive force, the gradients of refractive index during self-focusing will be radial. This means the dot product in the inhomogeneous term will be zero along the y axis, maximum along the x axis, and intermediate in value for points lying off these axes. The y component of the gradient of this dot product will be zero along the y axis (because the dot product itself is zero there), zero along the x axis (because the gradient of the dot product lies entirely in the x direction there), and nonzero for points lying off these two axes. This means that power from the x component of the electric field will be coupled into the y component only at points on the beam off the x and y axes.

This depolarization effect has been demonstrated experimentally. Figure 9 is a pair of micrographs showing the laser beam as it emerges from the sample, looking upstream through a polarizer. In the upper micrograph the polarizer was parallel with the electric field of the incident laser beam. In the lower micrograph it was perpendicular. The lower micrograph shows exactly the cross-shaped intensity distribution expected from the above discussion.

3.3. Role in Track Formation

There is a current debate over the existence of small-scale filaments. Some hold that such filaments do not exist, but are merely the traces of rapidly moving foci. One thing is certain. Small-scale tracks do exist in solid media.

The large-scale beam tracing equation does not include the effects of the inhomogeneous index term of the vector light wave equation. This omission manifests itself in an interesting way. Recall that the beam tracing equation shows the curvature of the ray path is equal to a term proportional to a^{-3} (representing diffractive spreading of a Gaussian beam), minus a term representing the focusing effect of the refractive index inhomogeneity. For steady-state electrostrictive trapping and for the various types of Kerr effect trapping the refractive index distribution is given by equation (2). When (2) is used together with a Gaussian intensity distribution, the refractive index inhomogeneity term is negative and proportional to a^{-3}. In the steady state both of the above terms are proportion to a^{-3}. The effect of self-focusing below the trapping threshold is therefore simply to decrease the strength of diffractive spreading. The solution of the beam tracing equation remains the same hyperbolic function, and only the sharpness of the focus of the hyperbola increases as the beam power approaches the trapping threshold. Precisely at the trapping threshold the two terms cancel each other. This means that curvature of the ray path is zero. A converging beam is thus predicted to come to a sharp, geometric focus with infinitely small beam radius precisely at the trapping threshold. Above the trapping threshold the large-scale beam tracing equation has no solutions valid for all points along the beam axis. The physical picture presented is unacceptable.

Recently, a new, small-scale beam tracing equation was derived [3]. The equation includes the effects of the inhomogeneous index term of the vector light wave equation to within the same approximation that the Laplacian of the electric field is included. Azimuthal symmetry of the intensity was assumed. The vector light wave equation was partially separated in cylindrical coordinates. After an eikonal was introduced according to Sommerfeld's expansion, the intensity distribution was assumed to be Gaussian. Terms were retained up to second order in $1/k_o$, where k_o is $2\pi/\lambda$, and λ is the vacuum wavelength. The result was the small-scale beam tracing equation

$$\frac{\partial^2 a}{\partial z^2} = \frac{1}{k_o^2 n_o^2 a^3} + \frac{1}{n_o}\left(a - \frac{1}{k_o^2 n_o^2 a}\right)\frac{\partial^2 n}{\partial r^2}\bigg|_{r=o},$$

where the upper sign is for the radial electric field component, and the lower sign is for the azimuthal component. The extra third term on the right is present because of the inhomogeneous index term of the vector light wave equation.

Certain equations in the derivation of this equation seemed to indicate the radial term remains nearly Gaussian, even when the beam radius becomes very small. Apparently the azimuthal component does not remain Gaussian, but is transformed into a distribution with a central minimum. This diagnosis has yet to be confirmed algebraicly. It is thought to be the most probable explanation for the failure of the small-scale beam tracing equation for the azimuthal component.

The results for the radial component are much better although some questions still require clarification. The small-scale beam tracing equation does overcome the difficulties mentioned previously for the large-scale beam tracing equation in analyzing the steady-state trapping of the radial component.

To simplify the analysis, we introduce dimensionless distances by measuring in units of the wavelength in the medium divided by 2π; thus we have

$$A = k_o n_o a, \quad Z = k_o n_o z.$$

450-417 O-71—6

We also introduce a dimensionless trapping parameter T corresponding to a Gaussian beam of instantaneous power P(t), and a medium of nonlinear coefficient n_2, so we have

$$T = 4P(t)n^2k_o^2/c.$$

T = 0 corresponds to a medium with a zero nonlinear coefficient, while T = 1 corresponds to a beam whose power is at the trapping threshold in the nonlinear medium. The dimensionless small-scale beam tracing equation then becomes

$$\frac{d^2A}{dZ^2} = \frac{1-T}{A^3} + \frac{T}{A^5}$$

for the radial electric field component. The term on the far right appears because of the inhomogeneous index term. We can now see clearly the role this term plays. As the beam radius decreases to a wavelength of light, A decreases but remains larger than one. In a medium with a weak beam or a small nonlinear coefficient, T is small. For a large beam the curvature is nearly zero. As the beam converges, A becomes smaller and the ray curvature increases. As the beam approaches the focus, the beam curvature becomes strongly positive, and the beam diverges again. The first two terms predominate when the trapping parameter T is small.

When T is 0 the beam curvature is A^{-3}. When T is 1, the beam curvature is A^{-5}. This means that at the trapping threshold the curvature of the ray is nearly zero until the beam radius becomes very small. Then the curvature suddenly becomes strongly positive. The effect is to turn the converging ray back at the last moment and prevent an axis crossing. This gives a much more acceptable physical picture, because geometric foci and infinite intensities are avoided.

The small-scale beam tracing equation has been completely integrated [3,6]. The first integral gives the high-power beam waist radius a_M as a function of a_m for various values of the trapping parameter T. This function has been plotted in Figure 10. Notice the very sharp dependence on the trapping parameter T. Above the trapping threshold the beam radius is fixed at about three quarters of a wavelength. This is typical of the center core radius for many tracks formed in solid media.

The second integral has also been performed. The equation is completely solved in terms of an elliptic integral of the third kind. When this tabulated function is plotted, it shows the same behavior described earlier, i.e., almost straight-line convergence toward the axis, with a sharp turn just before touching the axis, and straight-line propagation away from the axis.

4. Conclusions

The electrostrictive explanation for laser beam self-focusing of nanosecond pulses in solid media has been analyzed theoretically and established experimentally.

Small-scale track formation can only be analyzed correctly when the effects of the inhomogeneous index term of the vector light wave equation are included.

5. Acknowledgement

The research reported in this paper was sponsored in part by the Air Force Cambridge Research Laboratories, Air Force Systems Command, under contract F19628-69-C-0220, but the report does not necessarily reflect endorsement by the sponsor.

6. References

[1] R.Y. Chiao, et al., Self-Trapping of Optical Beams, Physical Review Letters 13,479 (1964).

[2] G.N. Steinberg, Research into the Causes of Laser Damage to Optical Components, First Quarterly Report, p. 25 (Perkin-Elmer Technical Report #7735, 1964).

[3] E.L. Kerr, Track Formation in Optical Glass Caused by Electrostrictive Laser Beam Self-Focusing (Perkin-Elmer Report #9878, 1970).

[4] P.K. Tien et al., Focusing of a Light Beam of Gaussian Field Distribution in Continuous and Periodic Lens Like Media, Proc. of the IEEE 53, p. 129 (1965).

[5] G.N. Steinberg, Filamentary Tracks Formed in Transparent Optical Glass by Laser Beam Self-Focusing. I. Experimental Investigation, and E.L. Kerr, II. Theoretical Analysis, to be published by the Physical Review.

[6] E.L. Kerr, Laser Beam Self-Focusing and Glass Damage Caused by Electrostrictively Driven Acoustic Waves, Damage in Laser Glass, p. 23 (Am. Soc. for Testing and Materials, 1969).

[7] E.L. Kerr, Transient and Steady-State Electrostrictive Laser Beam Trapping IEEE J. Quan. Elect. QE-6, 616 (1970).

[8] R.G. Brewer et al., Self-Trapping with Picosecond Light Pulses, Physical Review Letter 21, 267 (1968).

[9] R. Polloni et al., Self-Trapping with Picosecond Pulses and "Rocking" of Molecules, Phys. Rev. Letter 23, 690 (1969).

[10] R.R. Alfano et al., Observation of Self-Phase Modulation and Small-Scale Filaments in Crystals and Glasses, Phys. Rev. Letter 24, 592 (1970).

[11] E.L. Kerr, Electrostrictive Self-Trapping of Picosecond Laser Pulse Trains, (Perkin-Elmer Report No. 10633, 1971).

[12] R.M. Waxler et al., Effect of Hydrostatic Pressure on the Refractive Indices of Some Solids, Jour. of Res. the NBS 69A, 325 (1965).

[13] A.V. Shatilov et al., Non-Radiation Self-Focusing and Optical Strength of Glass, Sov. Jour. Opt. Tech. 37, 403 (1970).

7. Figures

Figures 1, 3-9 have been accepted for publication [5]. They are reproduced here by permission of the Physical Review.

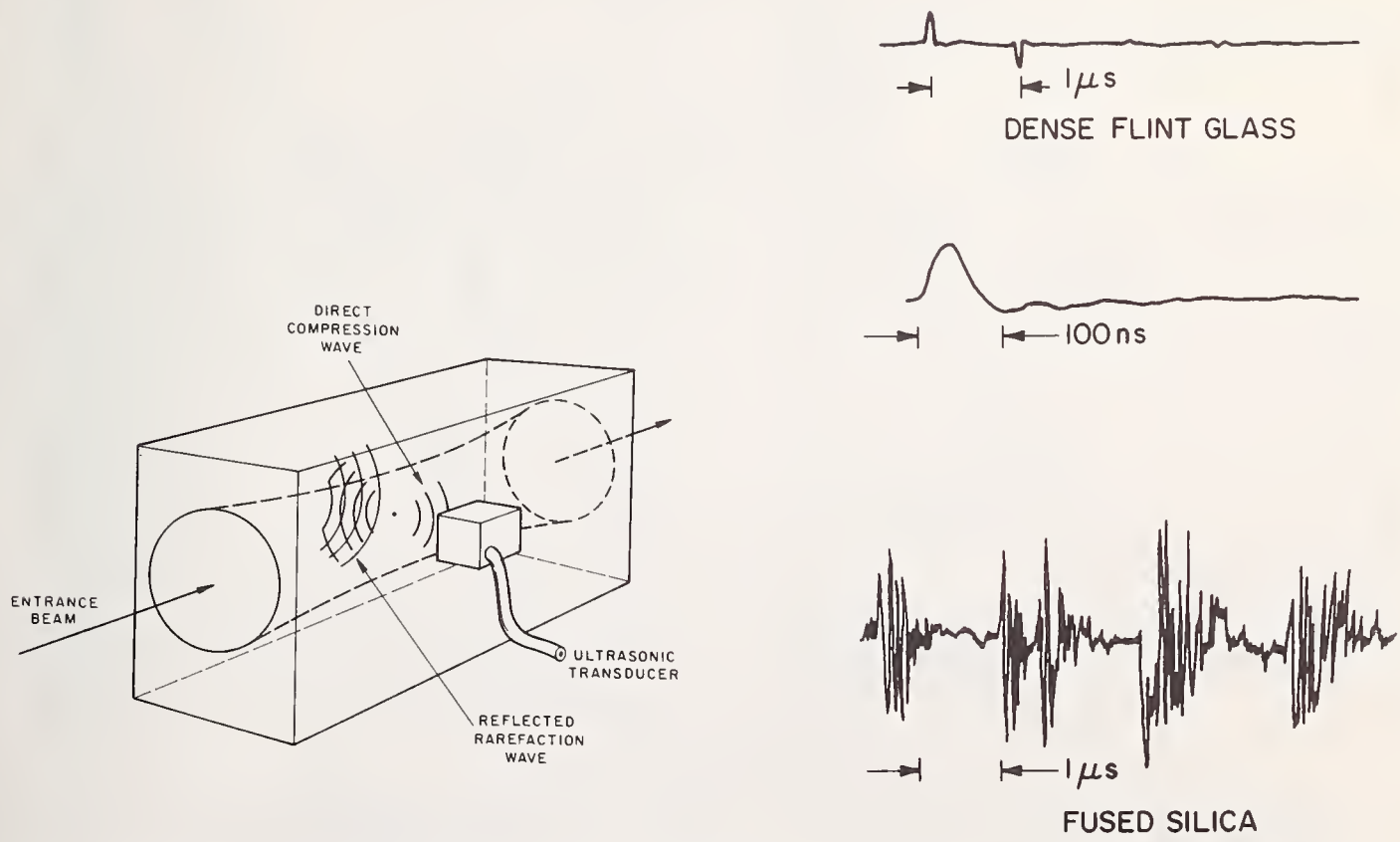

Fig. 1 Recording of sound pulses caused by electrostriction during passage of the Q-switched laser pulse.

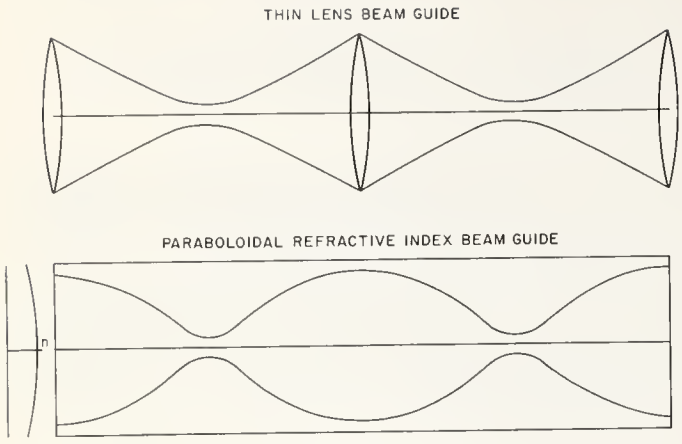

Fig. 2 Equivalent beam guides.

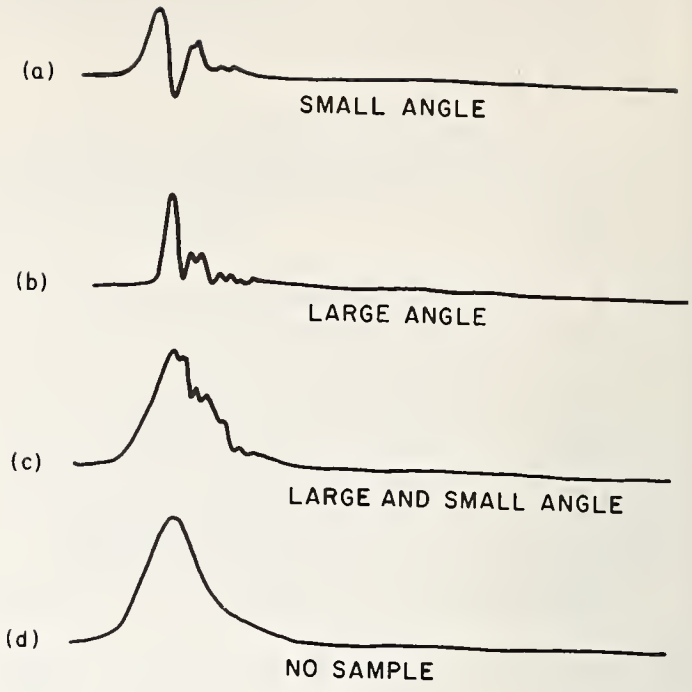

Fig. 3. Time variation of light transmitted through a glass sample during track formation.

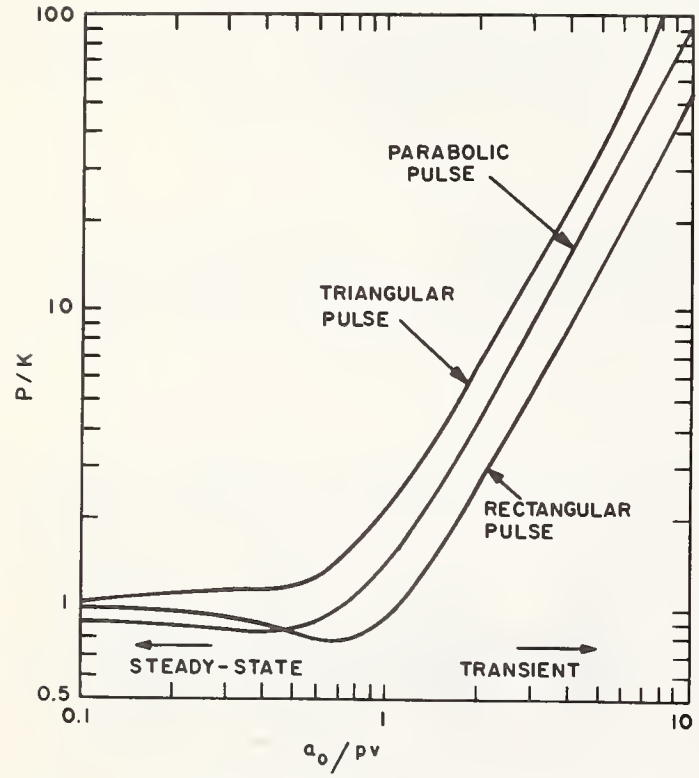

Fig. 4 Trapping threshold power as a function of beam radius and pulse duration for several pulse shapes.

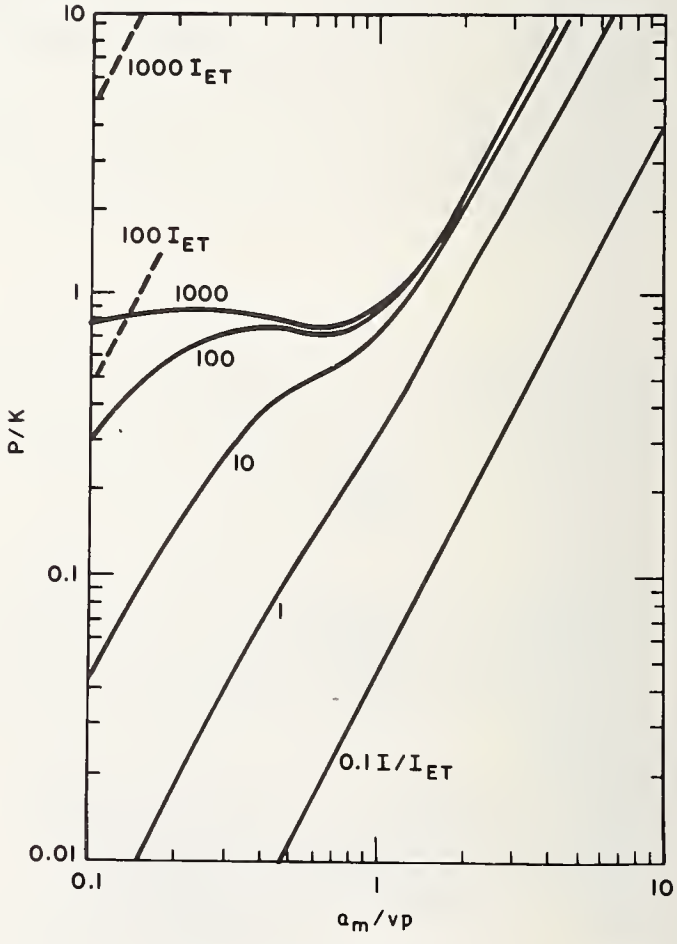

Fig. 5 Curves of constant intensity achieved during self-focusing.

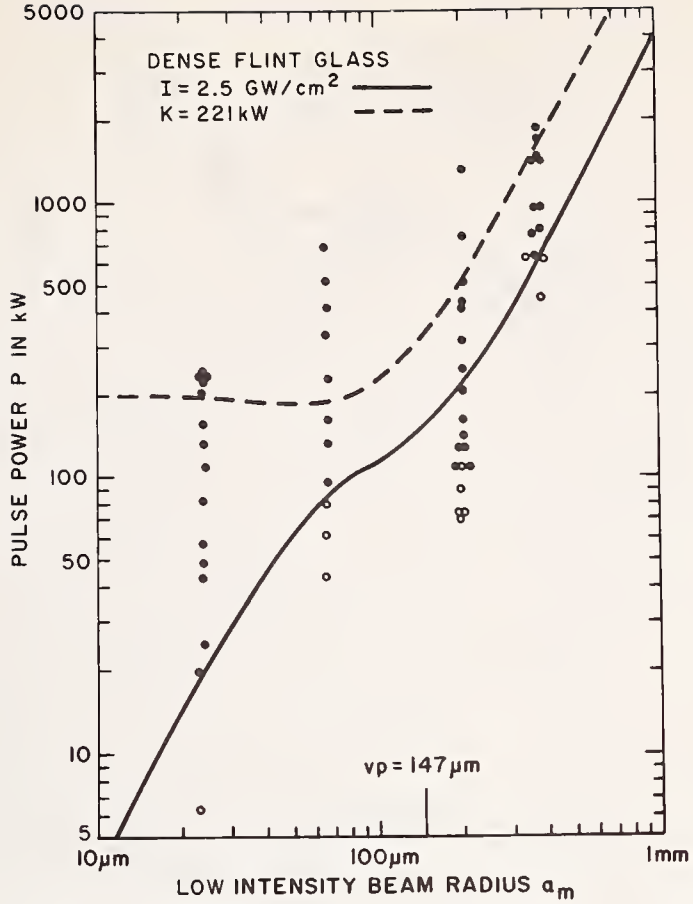

Fig. 6 Comparison of experimental track formation thresholds with a constant intensity curve for dense flint glass.

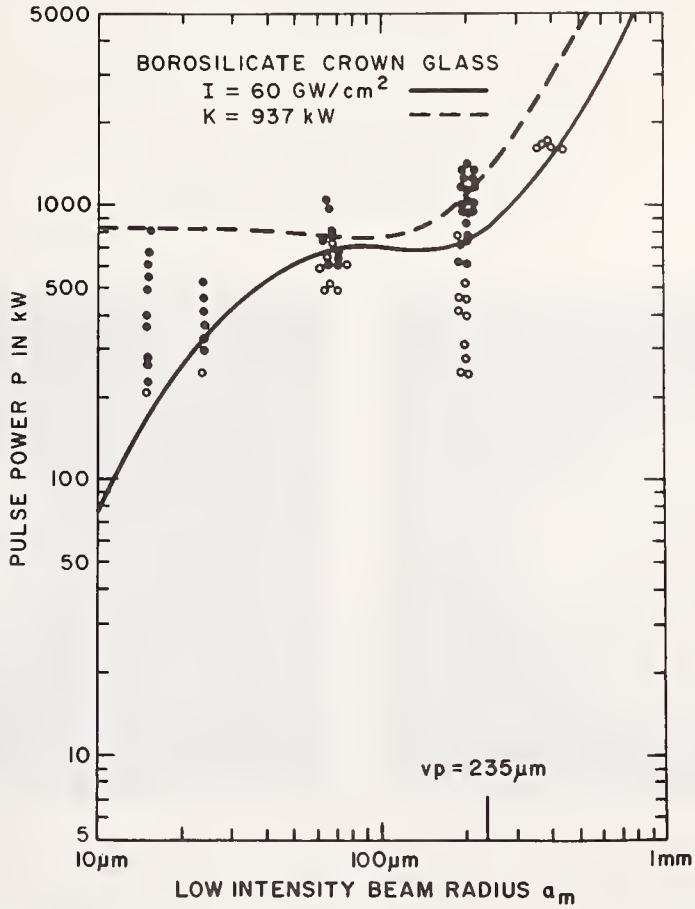

Fig. 7 Comparison of experimental track formation thresholds with a constant intensity curve for Borosilicate crown glass.

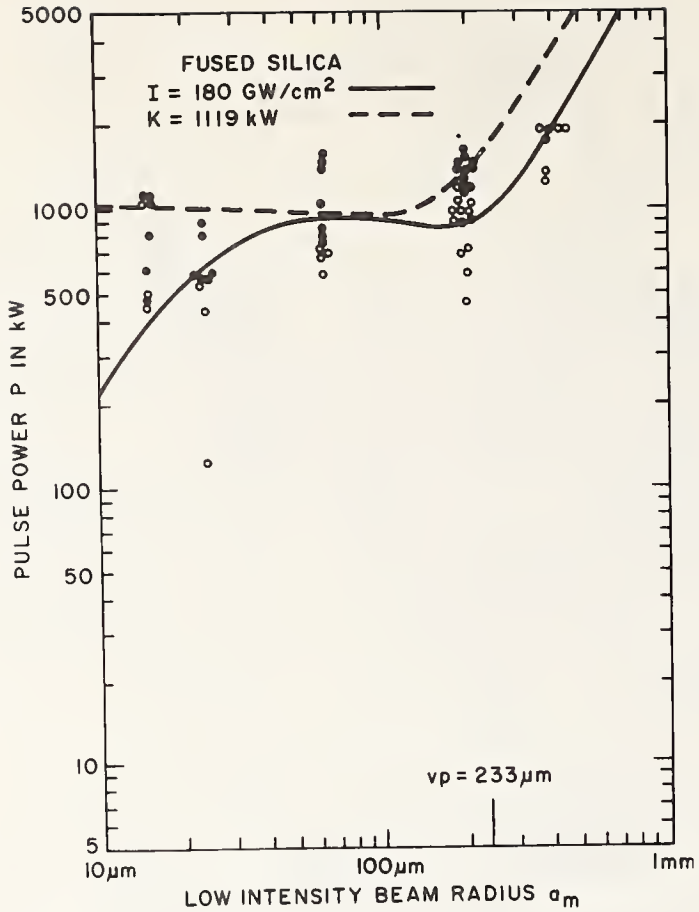

Fig. 8 Comparison of experimental track formation thresholds with a constant intensity curve for fused silica.

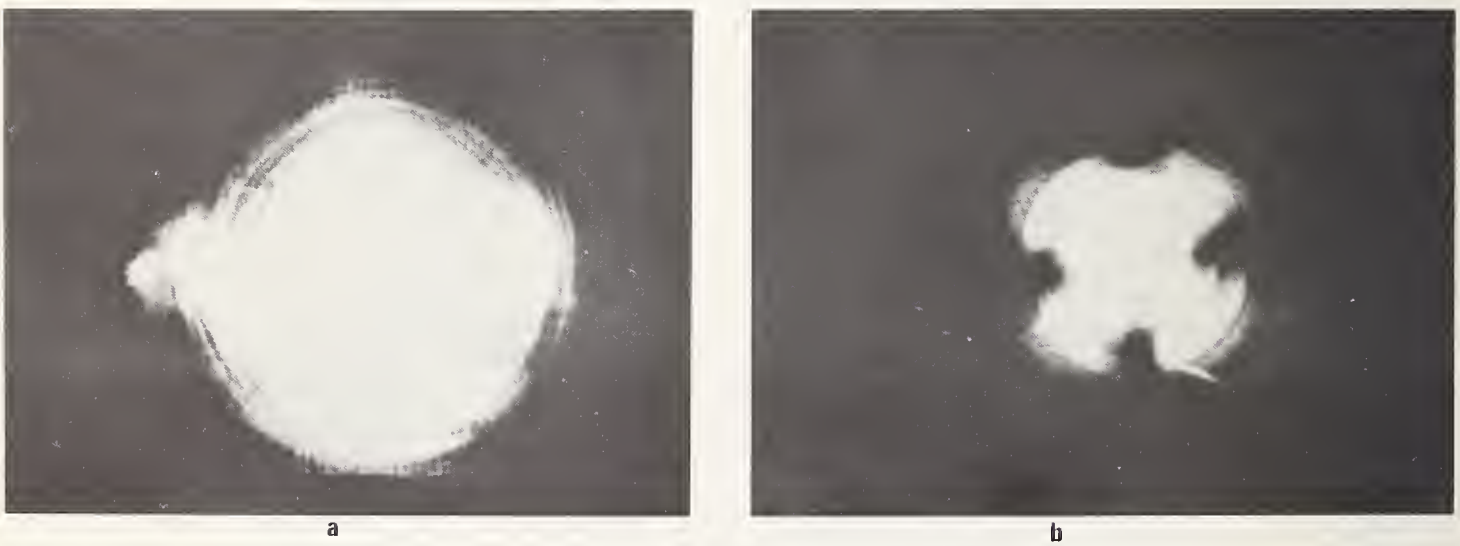

Fig. 9: Light transmitted from a small-scale track through a polarizer placed either parallel (a) or perpendicular (b) to the direction of the incident laser beam polarization.

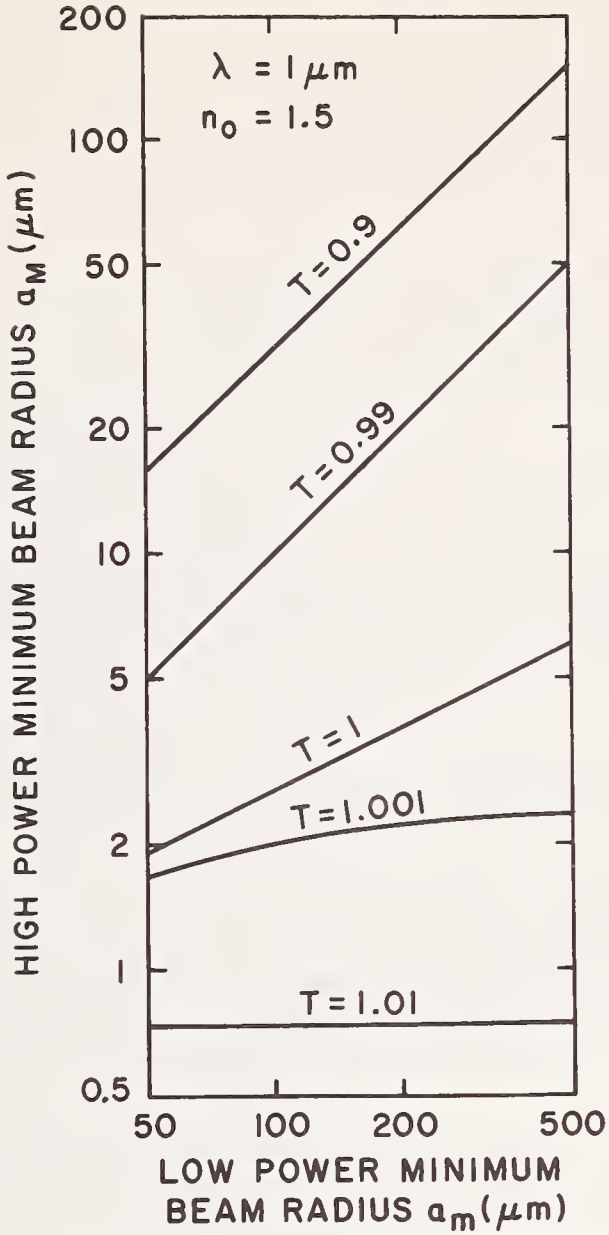

Fig. 10 High power minimum beam radius as a function of low power minimum beam radius for various values of the trapping parameter.

COMMENTS ON PAPER BY EDWIN KERR

The cruciform damage patterns shown in this paper were observed in BK-7 glass. The central spot diameter was a few micrometers. The photographs were taken through a large Fresnel lens, using the depolarized component of the light. The intensity of the depolarized light was expected to be zero at the center of the pattern, but some scattering seems to have occured, giving a non-zero central intensity. Professor Marburger reported confirmation of this cruciform pattern on the basis of computer solutions of the full wave equation he has carried out.

The Probability and Dynamics of Damaging Optical Materials with Lasers*

Michael Bass and Harrison H. Barrett

Raytheon Research Division
Waltham, Massachusetts 02154

This paper discusses the probabilistic nature of the damaging interaction between light and matter. It is shown that when one recognizes that there is some probability to induce damage at any level of optical irradiation, then the reported irreproducible damage resistance properties of many useful materials can be understood. This point of view also explains why some optical components may be safely irradiated many times before damage occurs, though no other change in the material can be detected prior to the observation of damage. Experimental data showing the probability for surface damage as a function of power density will be presented for several optically nonlinear materials as well as for glass, fused quartz, and acrylic plastic. The dependence of damage probability on optical field strength is similar to that of the dc ionization coefficients for semiconductors and gases on the applied field. This observation is discussed in the present paper, and it is suggested that a form of avalanche breakdown might be the cause of laser-induced damage.

Experiments in which an image converter streak camera was used to study the dynamics of the damage process are also described. It is shown that (1) if the laser beam is focused within the medium, then the first damage to occur is at the focus and additional damage occurs upstream (i.e., nearer the lens) at later times, and (2) new damage is formed only when the intensity of the incident light increases and never when it decreases. These observations can be explained by assuming that a fast self-focusing mechanism is essential to trigger internal breakdown and thereby cause damage.

Key Words: Avalanche breakdown, dynamics of damage process, probability for damage, self-focusing.

1. Introduction

In the year since the last Laser Damage Symposium, a great deal of progress has been made towards understanding laser-induced damage in optically linear and nonlinear materials. The following observations were obtained by careful optical and electron microscopy studies of the damaged material: 1. contrary to prior opinion, internal damage in $LiNbO_3$ and KDP occurs at the same or lower levels of irradiation than surface damage, 2. internal filamentary damage in $LiNbO_3$ is composed of two or more long, thin cracks which intersect to form one or more lines $\sim 0.4\,\mu$ in diameter, 3. internal pit damage similar to inclusion damage in laser glasses can be produced in $LiNbO_3$, 4. the damaged material was at one time molten since it shows signs of having flowed and resolidified, and 5. entrance and exit surface damage have different characteristics. These results are described in detail in Ref. 1 and will not be discussed further in this paper. However, two very practical comments are in order since they affect both the growth and use of both $LiNbO_3$ and KDP: 1. in the preparation of nonlinear crystals every effort must be made to minimize the presence of included impurities and 2. it is strongly recommended that crystals which have suffered surface damage be thoroughly examined internally before being repolished and reused.

This paper is given over to the discussion of two important concepts in the study of laser-induced damage, that of probability and that of dynamics. Last year data giving the number of pulses

* The research reported in this paper is sponsored in part by the Air Force Cambridge Research Laboratories, Office of Aerospace Research, under contract F19628-70-C-0223, but the report does not necessarily reflect endorsement by the sponsor.

required to damage $LiNbO_3$ as a function of pulse power density were presented. (2)[1] Upon re-examination of those data, it was realized that they could be more readily understood if one accepted the notion that the number of pulses required to damage a material was in fact a measure of the probability for a single pulse of that power density to induce damage. The probabilistic point of view is used to explain why particular optical devices withstand many pulses and then, with no prior warning or increase in the level of irradiation, inexplicably damage. It is similarly useful in explaining the fact that one sample of a material will withstand one number of pulses before damaging and another sample a different number of pulses even though all the pulses and both samples were identical.

Measurements of the probability for entrance surface damage to several materials have been performed and are reported herein. Surface damage was studied because there is no self-focusing and the power density can be specified. Theoretical analyses of the dependence of damage probability on power density are also reported. A consideration of avalanche breakdown due to the optical field, possibly assisted by Zener tunneling (3), suggested that the damage probability might vary as $\exp(-\text{const}/E)$ where E is the optical electric field. Plots of the logarithm of the probability versus E^{-1} are found to give excellent straight lines over several decades. Shockley's ballistic model (4) of avalanche breakdown predicts this observed field dependence. Numerical estimates of the field dependence of the damage probability for $SrTiO_3$ based on this modified theory are in order of magnitude agreement with that which is measured.

Studies of laser-induced damage remaining in or on a medium after irradiation cannot reveal the dynamics of the process which are necessary to the development of a more complete theoretical understanding. Therefore, experiments in which an image converter streak camera was used to photograph the laser-induced breakdown were performed. Evidence is presented to show that when the light is focused inside the medium the first breakdown to occur appears near the geometrical focus and other breakdowns occur upstream (i.e., nearer the lens) at later times. Internal breakdowns are initiated only during time intervals when the level of irradiation increases.

When the beam is collimated, there is no order to the starting time of the various breakdowns; an upstream breakdown may occur before or after one which is further downstream. These observations are considered to be the result of a self-focusing process which can respond to rapid changes in the light intensity (5) and which is sensitive to the beam's initial geometrical parameters.

2. Measurements of the Probability for Damage

The experimental setup is described in Ref. 2. Throughout the present series of experiments the following parameters were maintained constant:

Laser and laser wavelength: Nd:YAG with $\lambda = 1.064\ \mu$
Laser mode: TEM_{00}, linearly polarized
Pulse waveform: Nearly smooth and symmetric with $\tau = 12$ nsec (FWHM)
Pulse repetition rate: 1 pps
Focusing conditions: A 10× microscope objective was used to focus the beam to a circular spot of diameter, d, ≈ 0.003 cm. With these focusing parameters surface damage only was generally produced.
Sample temperature: Room temperature
Ambient atmosphere: Room air except for the hygroscopic samples which were maintained in a dry nitrogen atmosphere.

All the surfaces studied were polished to the best optical finish which could be obtained, not coated and carefully cleaned following procedures appropriate to the particular material. The glass and plastic samples, however, had lower quality inspection finishes but were kept clean and free of dust particles during these experiments.

The samples were irradiated at a rate of 1 pps until either the spark which coincides with the occurrence of damage was observed or the observer saw damage through the microscope. The number of pulses, N, required to damage was noted, and then the sample was moved so that undamaged material could be studied. At each power density approximately twenty-five different measurements of N were made, and the probability for damage by a single pulse taken to be

$$p_1 = \frac{\text{number of damages}}{\Sigma N} \qquad (1)$$

When no damage could be found after 500 pulses, the sample was moved and irradiated again. If this occurred five times in succession, the sequence of events was taken to indicate that $p_1 < 0.0004$. As discussed in more detail below, the sequence of N values obtained was used as a check on the constancy of the experimental parameters.

---

[1] Figures in parentheses indicate the literature references at the end of this paper.

The main experimental error in measuring the power density was incurred in determination of the focal spot diameter. As described previously (2), several different measurements agreed reasonably well with each other and so, in order to be conservative and underestimate the power density, the largest value of d was chosen. The true value of the focal spot diameter is felt to be within ±5 percent of that used, 0.003 cm. Other errors enter in measuring the pulse energy and duration so that the power density measurements herein are estimated to be accurate to ±20 percent. Note that the average, not peak, power density is computed when one divides pulse energy by τ and $(\pi/4)d^2$. Measurements of damage probability are limited at low probabilities by one's endurance in counting pulses which do no damage. At high probabilities, when damage occurs within one or two pulses, several errors of one pulse in counting the pulses required to cause damage can result in a substantial change in the value of p_1. To obtain a measure of the error in p_1, several measurements were made of a $p_1 \approx 0.01$. The standard deviation of these values from their mean was ~ 25 percent.

The data plotted in Fig. 1 shows the measured probability that one of our laser pulses damage the surface of several materials. It is clear from these data that at any power density there is always some probability that a single pulse will induce damage. Now consider the probability, p_N, that damage be produced by the Nth pulse. If p_1 is the constant probability that a single pulse produces damage, then p_N is given by the binomial distribution

$$p_N = (1 - p_1)^{N-1}(p_1) \qquad (2)$$

This is simply the composite probability that there be exactly N-1 nondamaging pulses followed by one which causes damage. If a large number of measurements of the number of pulses required to cause damage are made, the fraction of the total number of measurements in which N pulses were observed is a measure of p_N. If the measured probability distribution and that predicted by Eq. 2 using the measured value of p_1 agree, then one can conclude that the probability for damage was p_1 for each pulse. This also means pulses of light were constant throughout the experiment and that the irradiated areas of the material were all equivalent. Figure 2 shows the results obtained for fused quartz irradiated by 17.9 GW/cm^2. Under these conditions $p_1 = 0.16$ and ninety-nine measurements of N were made in order to obtain the experimental distribution.

It is evident from the analysis and data above that it is quite possible to have one sample of one material be damaged by one number of pulses and another, identical sample be damaged by another. In fact, for power densities where p_1 is small ($p_1 \lesssim 0.01$), the probability for not causing damage in N-1 pulses is large ($(1-p)^{N-1} \gtrsim 0.3$) for $N \approx 1/p_1$; therefore, $p_N \approx p_1$ for many values of N, and it is highly likely that measurements of N will yield many widely different results. Having made measurements of N at this level of irradiation, one must examine the distribution of N values in order to be certain that p_1 remained constant throughout the experiment.

Consider the data shown in Table I. The $LiNbO_3$ crystal studied in this experiment was obtained from the Union Carbide Co.* and was the only sample to show any extreme difference between the measured distribution and that calculated from p_1. Light was incident along the c axis of this sample. At 3.15 GW/cm^2, the material withstood 500 or more pulses four times in a set of twenty-five measurements. The other twenty-one times damage was achieved in the first few pulses. Since the data in Fig. 2 lends strong evidence to the notion that any laser pulse was almost identical with any other, these data suggest that this sample was not the same everywhere. If the four sets of 500 nondamaging pulses are included, then one finds $p_1 = 0.01$. Amongst the twenty-five measurements, however, there are too many low values of N and too many at values of $N > 500$ for the set of twenty-five N values to be considered a valid sample of the distribution $p_N = (0.99)^{N-1}(0.01)$. If the four measurements of no damage after 500 or more pulses are considered to represent an unusually damage-resistant material and the other twenty-one measurements are considered as representative of a more easily damaged main component of the sample, then for this component $p_1 = 0.35$. The distribution of these twenty-one values of N, although obtained from a small number of samples, is close to that predicted by $p_N = (0.65)^{N-1}(0.35)$. Therefore, we conclude that this sample of $LiNbO_3$ contains regions which are more resistant to laser-induced damage than the rest of the material. Initial measurements show that the dimensions of these regions can be ~ 1 mm. The bulk of this sample however has slightly higher damage probability at a particular power density than that shown in Fig. 1 for a light incident along the a axis of a $LiNbO_3$ sample obtained from Crystal Technology, Inc.

Table II lists two operationally interesting levels of irradiation for several materials. One is P_1, the lowest power density at which the probability for damage in a single pulse is one. The other is called P_{2500} and is a power density at which 500 pulses induced no damage in five successive trials. This sequence of events strongly suggests a very low probability for damage.

---

* Union Carbide Crystal No. TIM 348C1.

Table 1. Raw data for surface damage to $LiNbO_3$ as a function of power density*

Power Density GW/cm^2	Number of Pulses Required to Cause Damage												
> 10.4	1	1	1	1	1	1	1	1	1	1	1	1	1
8.3	1	1	1	1	1	1	1	1	1	1	1	1	1
6.4	1	6	128	2	2	1	1	1	1	2	1	1	2
3.2	4	2	2	2	2	1	2	2	2	10	4	3	2
1.15	6	6	None in 500	6	4	None in 500	None in 500	None in 500	None in 500	None in 500			

Power Density GW/cm^2	Number of Pulses Required to Cause Damage												
> 10.4	1	1	1	1	1	1	1	1	1	1	1	1	1
8.3	1	1	1	1	1	1	1	1	1	1	1	1	1
6.4	1	1	2	1	1	1	1	1	1	1	1	1	1
3.2	None in 500	5	3	None in 500	None in 500	2	None in 500	2	3	3	2	2	2

*Light was incrdent along the c axis. The crystal was prepared by Union Carbide Co.

Table 2. Two power densities of interest: P_1 = lowest power density at which damage always occurs in a single pulse: P_{2500} = A power density where the probability for damage in a single pulse is less than 0.004*

Material	P_1	P_{2500}
Fused Quartz	24.0 GW/cm^2	8.3 GW/cm^2
Plastic	16.1	11.0
Glass	14.4	6.7
KDP	14.4	2.1
$LiNbO_3$	11.1	2.0
ADP	6.4	2.0
Crystal Quartz	6.4	1.2
$Ba_2NaNb_5O_{15}$	6.4	1.2
$SrTiO_3$	6.4	0.08
$LiIO_3$	3.2	0.37

* P_1 for fused quartz is obtained by extrapolating the data plotted in Fig. 3. All other values are measured. Note that P_{2500} is not necessarily the power density at which $p_1 = 0.0004$.

The $LiNbO_3$ sample was an a axis piece obtained from Crystal Technology.

3. Avalanche Breakdown and the Probability for Damage

In avalanche breakdown in gases and semiconductors the important parameter is the ionization coefficient $\alpha(E)$, which is the average number of carriers produced by an electron (or hole) falling 1 cm in the field direction. Usually it is found experimentally (6, 7) that

$$\alpha(E) \sim \exp(-\text{const}/E) \tag{3}$$

From Fig. 3 it is seen that the damage probability also has this same functional dependence over several decades for all materials studied. Therefore, a careful review of avalanche breakdown as a possible damage mechanism is called for.

Avalanche breakdown in optical fields has been considered previously by several other workers, including Wasserman (8), Sviridenkov (9), Zverev et al. (10), Hellwarth (11), and Molchanov (12). However, since the results of their work usually showed that the calculated breakdown field was an order of magnitude larger than that which was measured, this mechanism is not generally accepted as responsible for laser-induced damage. The data presented in Fig. 3 and the discussion presented in the rest of this section show that avalanche breakdown should be considered as a possible damage mechanism.

Our review of previous work on the possibility of avalanche breakdown in an optical field begins with a discussion of the role of electron collisions. A perfectly free electron in an optical frequency electric field will simply oscillate back and forth with its velocity 90° out of phase with the driving field, and consequently there will be no average energy absorption. The coherently oscillating energy of such an electron in a field at the damage threshold is readily calculated to be only 10^{-3} - 10^{-4} eV. Therefore there is no possibility of an ionizing collision.

However, electrons in a solid are not really free. They experience collisions with phonons which tend to relax the distribution towards equilibrium. These collisions also result in a component of electron velocity in phase with the field so that there can be an average energy absorption. A phenomenological equation of motion for an electron in a solid may be written as

$$m^* \left(\frac{\partial v}{\partial t} + \frac{v}{\tau}\right) = eE\, e^{i\omega t} , \tag{4}$$

where m^* is the effective mass, v is the electron velocity, τ is some average relaxation time, e is the electronic charge and E is the amplitude of the electric field at radian frequency ω. It is easy to see that the energy $\mathcal{E}$ of the electron excited to the conduction band increases initially as:

$$\partial \mathcal{E}/\partial t = \frac{1}{2}\,\mathrm{Re}\,\langle eE \cdot v^* \rangle = \frac{\tau e^2E^2/2m^*}{1+\omega^2\tau^2} \approx \frac{e^2E^2}{2m^*\omega^2\tau} , \tag{5}$$

where the last step follows since $\omega\tau >> 1$ at optical frequencies. The electrons also lose energy, primarily by collisions with optical phonons. An equilibrium may be thus established as discussed by Wasserman (8). However, at high fields, all electrons having energy greater than some value $\mathcal{E}_c$ will, on the average, gain more energy than they lose and therefore will be accelerated to ionizing energies.

Detailed treatments based on this approach must include a calculation of the electron-optical phonon interaction and a discussion of the choice of $\mathcal{E}_c$. The problem has much in common with the dc breakdown of dielectrics, where fairly accurate calculations of the threshold are possible (13). For the optical case, this procedure was carried out by Wasserman (8) who obtained a breakdown field an order of magnitude greater than is observed.

A rather different approach has been successful for the closely related problem of avalanche multiplication breakdown in semiconductor p-n junctions. Shockley pointed out that an equation of motion such as Eq. (4) is not applicable because it gives the behavior of an average electron (4). Ionization in a dc field is produced mainly by those exceptional electrons which are accelerated to the ionizing energy $\mathcal{E}_i$ without undergoing a single collision, even though they must cover a distance of many mean free paths. The probability of a particular electron covering a distance x without a collision is $\exp(-x/\ell)$, where ℓ is the mean free path. To be accelerated to $\mathcal{E}_i$, the electron must traverse a distance $x = \mathcal{E}_i/eE$. Therefore

$$\alpha(E) \sim \exp(-\mathcal{E}_i/eE\ell) \tag{6}$$

This expression, with $\ell \sim 100$ Å, gave a good fit to Chynoweth's data (7) for avalanche breakdown in Si and Ge.

A very different approach was taken by Wolff (14) who used a Boltzmann equation and expanded the electron distribution function in Legendre polynomials retaining only the zeroth and first-order terms. He found

$$\alpha(E) \sim \exp(-\text{const}/E^2) \tag{7}$$

The basic difference between the approaches of Wolff and Shockley is that the former assumes that the distribution is only slightly distorted, while the latter assumes that it develops a large spike in the field direction.

The discrepancy was resolved by Baraff (15) and Keldysh (16) who showed that Eq. (3) is the low-field limiting form of the general solution, while Eq. (7) applies only at high fields. The crossover point is not well specified, but Shockley's result seems to work well up to E values on the order of 10^6 V/cm. In other words, the electron may make several collisions before ionization without $\alpha(E)$ showing a significant departure from the behavior (Eq. 6) which was derived on the assumption of no collisions.

Since "lucky electrons" play such an important role in dc avalanches, a similar effect might be expected in the optical case. There the lucky electron would not be one which underwent no collisions at all, since it would then simply oscillate in the field. Rather it would be one which underwent precisely the correct collisions to keep it in phase with the field. Admittedly this is an unlikely occurrence, but so is the collisionless situation postulated by Shockley. The basic point is that the electron distribution might become highly distorted developing a large spike which dominates $\alpha(E)$.

For high frequency cw fields, breakdown occurs when the rate of increase of the number of electrons, simply related to $\alpha(E)$, exceeds the rate of loss of electrons due to recombination, trapping or diffusion out of the field region (6). For pulsed fields, there is the additional requirement that the electron concentration buildup to destructive levels during the pulse period. In either case, the major problem is the calculation of $\alpha(E)$ which, to our knowledge, has not been carried out for optical fields.

In order to evaluate our data in terms of an avalanche breakdown mechanism, the ionization coefficient must be related to the probability of damage occuring within a pulse period. To do this, the distribution of avalanche sizes should be determined. This distribution, $p(n, E)$, is defined such that $p(n, E)\Delta n$ gives the number of avalanches per unit time which produce between n and $n + \Delta n$ free carriers, given a constant number of starting carriers and a fixed field E. We assume that any avalanche greater than some critical size n_c constitutes a damage event (where $n_c \sim 2^{40}$ according to Seitz (17)). Then, for a constant power optical pulse of duration T, the probability of damage in one shot is

$$p_1(E) = T \int_{n_c}^{\infty} p(n, E)\, dn \tag{8}$$

Unfortunately the relation between $p(n, E)$ and $\alpha(E)$ is complicated. The dc case has been treated by Tager (18) who found enormous variations in $p(n, E)$ depending on the relative values of $\alpha(E)$ for holes and electrons. To our knowledge no comparable analysis exists for optical fields.

However, it is possible to conceive of situations where p_1 is simply proportional to $\alpha(E)$. Recall that on the Shockely model, $\alpha(E)$ is proportional to the probability that an electron will escape from the low energy pool of electrons and reach ionizing energy $\mathcal{E}_i$. However, there may also be some additional energy gain above $\mathcal{E}_i$ before ionization actually occurs. Then both the ionizing electron and the carriers it produces may initially have energy greater than kT. Depending on the energy dependence of the momentum-loss and energy-loss relaxation times, these hot carriers may then gain energy from the field more readily than a thermal electron. If so, then once an initiating electron has escaped the thermal pool, breakdown will occur with a high probability (neglecting the avalanche formation time compared to the pulse period). In other words the statistics of breakdown will be dominated by the first stage or two of the avalanche, and $p_1(E)$ will be proportional to $\alpha(E)$. In terms of $p(n, E)$ this case is one in which low values of n are quite improbable as sketched in Fig. 4. At this time we have not performed the detailed calculation necessary to decide if this special case actually occurs under realistic conditions; however, the data in Fig. 3 suggests this as a fruitful avenue of investigation.

From the viewpoint of avalanche breakdown, let us now examine the results in Fig. 3 further. There are a number of intriguing regularities to be noted. The amorphous materials all are quite damage-resistant and show steep slopes (see Table III). If we force an interpretation in terms of Eq. (6), this could mean that amorphous materials have small values of ℓ. KDP, ADP, and crystalline quartz also show steep slopes, presumably because of their large $\mathcal{E}_i$. The other crystalline materials all have smaller slopes which, with Eq. (6), give $\ell \sim 100$ Å, in good agreement with Shockley's conclusions for Si and Ge as well as with estimates based on interactions with longitudinal optical phonons in polar dielectrics (13). In this respect $SrTiO_3$ is an interesting material to study because its electronic transport properties and band structure are well characterized and theoretical estimates of its slope may be possible.

Table 3. The measured slope of ln p_1 vs. 1/E in V/m

Material	Measured Magnitude of Slope of ln p_1 vs. 1/E	P_1
Plastic	133.0×10^8 V/m	16.1 GW/cm^2
Glass	66.5	14.4
Fused Quartz	60.5	24.0 extrapolated
ADP	31.6	6.4
KDP	28.5	14.4
Crystal Quartz	28.5	6.4
$LiNbO_3$	16.6	11.1
$Ba_2NaNb_5O_{15}$	16.7	6.4
$LiIO_3$	7.1	3.2
$SrTiO_3$	1.8	6.4

Since Wolff's work predicts that $\alpha(E)$ should vary as exp (-const/E^2), the damage probability data was tested for this dependence by making the plots shown in Fig. 5. These show that a model based on Eq. (7) is a less satisfactory description of the variation of damage probability with optical field than one using Shockley's result.

It is interesting to note that there are several other phenomena which could come into play without qualitatively altering the dependence given in Eq. (3). For example, if ionization occurs from an impurity level rather than across the gap, it will simply alter the value of $\mathcal{E}_i$. Zener tunneling, either across the gap or from impurities, also involves an exp (-const/E) factor. Finally, a Franz-Keldysh reduction of the gap, to a first approximation, will affect only the pre factor in p(E) and not the exponential.

4. Dynamic Properties of Laser-Induced Damage

Sparks can be seen both inside and on the surface of transparent media when damaging pulses of light pass through. These sparks lie along the beam axis and are bright enough to be photographed with an image converter streak camera. Fersman and Khazov (19) report that the temperature of an entrance surface spark produced by a Q-switched ruby laser on K-8 glass is initially in excess of 8000°K, certainly bright enough to be photographed and hot enough to cause damage. Since residual damage in solids is found only where and after sparks were observed, these sparks are either coincident with or the direct cause of the damage.

In this work, a TWR STL Products Model 1D image converter camera with streak plug-in units 7B or 5B was used to photograph the temporal development of the laser-induced sparks. A pulsed Q-switched Nd:YAG laser which could produce multimode pulses of energy up to 75 mJ and duration of ~ 15 nsec (FWHP) was the damage light source. The peak of the laser pulse was reached in 7-8 nsec. So that the mode pattern and pulse waveform would be nearly constant, the laser was always pulsed at 1 pps and with the same total input energy. The energy incident on the lens used to focus the light into the sample (the "damage" lens) was controlled with the polarizer attenuation described in Ref. 2. A small part of the laser output was removed with a beam splitter and frequency doubled. Several components, constituting an optical path less than 1 nsec longer than that of the 1.06 μ beam, aimed the green light parallel to the camera axis and focused in the plane containing the damage. The image of this light provides a reference on the streak photo as to the time when light entered the medium. Coupled with the pulse waveform, this streak permits one to determine which part of the pulse caused a particular spark. The experiment is diagrammed schematically in Fig. 6.

Figure 7 shows the formation of sparks in and on the entrance face of lucite acrylic plastic using two different lenses. To avoid confusion of the green light streak with streaks due to sparks, the green light was spatially offset from the line of the sparks by the indicated distances. When this offset is subtracted, these data show that the first internal spark to occur in Fig. 7a begins at the same instant that the leading edge of the 1.06 μ pulse arrives at the lens focus and that all the sparks are initiated within the 7-8 nsec required for the pulse intensity to reach its maximum. No sparks are initiated at later times. Similar results are obtained in Fig. 7b using a different focusing lens. These photos show conclusively that, when the light is focused inside the medium, the sparks are formed sequentially beginning with those nearest the focal point and ending with those nearer the lens. This result is also obtained in other transparent solids and liquids.

When the light is focused 0.123 cm inside the plastic sample, an internal spark at the focus is the only one to appear at the lowest input which always results in a breakdown. As the pulse energy is increased, more internal sparks appear until at $\sim 6\times$ this input an entrance surface spark is also produced. The delay between the arrival of light at the focus and the beginning of the first spark decreases with increasing pulse energy.

Exit surface damage can be produced by focusing through the sample and on the exit face. At the lowest input which always produces breakdown, only exit surface breakdown is observed while at higher energies internal sparks are also produced. Figure 8 shows these sparks in acrylic plastic.

Figure 9a shows breakdown produced when a 20 mJ multimode 1.06 μ pulse is focused in air. This spark begins ≈ 3 nsec after the first light arrives at the focus. The spark in Fig. 9b is formed when a plastic sample is placed 0.25 mm downstream from the focus. It begins nearly coincidentally with the arrival of the 1.06 μ light, and its growth to the right (i.e., upstream) takes place over a time interval nearly 2× that in Fig. 9a. In Figure 9c sparks are formed both within and on the entrance face with the light is carefully focused on this surface. The difference between the sparks in these photos shows that the surface breakdown which leads to damage is dependent on the presence of the material and is not due to breakdown in the ambient gas.

In order to study the fact that sparks were produced only when the laser intensity was increasing in more detail, the laser cavity was lengthened from 50 to 185 cm to produce pulses having structure as shown in Fig. 10c and total duration on the order of 100 nsec. The lengthened laser output was 29 mJ.

Figure 10a shows the relative spatial position of the green light and the line of sparks when the 3.4 cm focal length lens was used to damage plate glass. The first spark to occur, as shown in Fig. 10b, began at t_1, 14 nsec after the first light arrived at the focal point. In agreement with the results obtained with the smooth pulse above, comparison of the time coordinate for the formation of sparks in Fig. 10b with the pulse waveform in Fig. 10c shows that sparks are formed only during intervals of time when the level of irradiation increases. On the other hand, when the pulse energy or intensity is high but nearly constant, or increasing slowly, for example between t_2 and t_3, no new sparks are formed.

A qualitative model which explains these results can be constructed by requiring that self-focusing of the beam precede the initiation of an internal breakdown, that the self-focusing process is very fast, say with response time $\lesssim 10^{-10}$ sec, and that the focus moves upstream with increasing intensity. A fast self-focusing process can follow changes in the pulse intensity and give rise to the sequences of focusing conditions sketched in Fig. 11 for a smooth pulse and in Fig. 12 for a "wiggly" pulse. The beam focus can be in undamaged material only when the pulse intensity increases, implying that new breakdowns can occur only during these intervals.

The requirement that self-focusing in solids have a fast response time is satisfied in glass as the measurements of Duguay et al. (5) have demonstrated. Initial theoretical calculations of the movement of the beam focus agree with the qualitative picture given above (20). These considerations also show that the form and extent of the movement is dependent on the initial power density and geometrical parameters of the beam. In fact, no moving focal point is found for a collimated 1.06 μ, TEM_{00} mode, beam of ~ 0.6 mm diameter and ~ 700 MW/cm^2 power density. These conditions were satisfied in an experiment, and the results are shown in Fig. 12. There is no sequential ordering to the initiation of sparks which is what one would expect if there were no moving focal point. However, once again all the breakdowns are initiated during the first 8 nsecs of the pulse's duration suggesting the possibility that the light which arrives later cannot penetrate the existing sparks to produce new breakdowns.

Note that in spite of the absence of self-focusing the probability for internal damage in plastic at 700 MW/cm^2 is high, while at this level of irradiation and using the sharply focused beam geometry as in the study of surface damage, it is unlikely that one would ever see surface damage. This implies that it is easier to produce a breakdown within a material than on its surface. Viewed in terms of the avalanche mechanism, there are more chances for an avalanche to grow to breakdown when a large volume of material is irradiated. If impurity sites are important in providing the electron which starts the avalanche, then this statement is more readily understood. The sample was cut from a commercially available piece of 4' × 8' sheet plastic and so is not a material from which impurities were rigorously excluded. Thus, studies of the probability for internal damage in more controlled materials are planned to resolve this question.

Additional information about laser-induced breakdown can be inferred from the length of time during which visible radiation is emitted by the spark. The radiant energy emitted by such a hot body in general rises rapidly as the spark is formed and then falls over a much longer period of time according to the cooling law for the particular type of spark and medium. Within limits determined by its spectral sensitvity and the level of initial exposure, the streak camera can be used to measure the time interval during which a spark radiates. This provides useful information about the mechanisms available to dissipate the energy contained in the various sparks. Since the sparks in liquids can cool

by expansion as well as by radiation and conduction, the shortest lived sparks are found in water and 1, 2-dichloroethane where they typically do not exceed 70 nsec in duration. On the other hand, the same laser pulse produced internal sparks in plastic and glass having duration between 500 and 2000 nsec. Entrance surface sparks sometimes lasted as long but generally were about 300-6000 nsec in duration. Exit surface sparks did not exceed 300 nsec duration.

5. Summary

It has been demonstrated that over a wide range of optical powers there is always some probability that a particular sample be damaged by a particular pulse of light. This point of view was shown to permit one to account for many of the so-called irreproducible damage properties of optical materials. For example, it explains the fact that two identical samples of a material can withstand vastly different number of pulses of light before being damaged. The dependence of the probability to induce damage on the optical electric field strength is found to be analogous to that of the dc ionization constant of gases and semiconductors on applied field. This fact suggests the possibility that avalanche breakdown is the primary damage mechanism. Qualitative discussions of this process are presented, and good agreement with the experiments is obtained.

An image converter streak camera was used to study the dynamics of laser-induced breakdown in optical materials. When light is focused inside the medium and the probability for any breakdown is one, then the first breakdown to occur is the one nearest the focal point. Additional breakdowns occur upstream at later times, but all breakdowns are initiated during time intervals in which the light intensity increases. In the focused case no breakdowns were found to start at times when the intensity was constant or decreasing. This dynamic property can be qualitatively understood if self-focusing takes place and the resulting moving focal point is able to follow very rapid changes in the pulse intensity.

6. References

(1) Bass, M., Nd:YAG laser irradiation induced damage to $LiNbO_3$ and KDP, to be published IEEE J. of Quantum Electronics, July 1971.

(2) Bass, M., Damage in laser materials, NBS Special Publication 341, 90.

(3) Zener, C., Proc. Roy. Soc. London 145, 523 (1934) or Wang, S., Solid State Electronics, p. 373 (McGraw-Hill Book Co., New York, 1966).

(4) Shockley, W., Czech, J. Phys. B11, 81 (1961) and Sol. St. Electronics 2, 35 (1961).

(5) Duguay, M. A., Hansen, J. W., and Shapiro, S. L., IEEE J. of Quantum Electronics QE-6, 725 (1970).

(6) For a review see Von Hippel, A., Molecular Science and Molecular Engineering (Technology Press and Wiley, New York, 1959), especially Chap. 5.

(7) Chynoweth, A. G., Phys. Rev. 109, 1537 (1959) and J. Appl. Phys. 31, 1161 (1960).

(8) Wasserman, A., Appl. Phys. Letters 10, 132 (1967).

(9) Sviridenkov, E. A., Sov. Phys. Sol. St. 9, 1917 (1968).

(10) Zverev, G. M., Mikhailova, T.M., Pashkov, V. A., and Soloveva, N. M., Sov. Phys. JETP 26, 1053 (1968).

(11) Hellwarth, R. W., Damage in laser materials, NBS Special Publication 341, 67.

(12) Molchanov, A. G., Sov. Phys. Sol. St. 12, 749 (1970).

(13) For a review see O'Dwyer, J. J., Phil. Mag. Suppl. 7, 349 (1958).

(14) Wolff, P. A., Phys. Rev. 95, 1415 (1956).

(15) Baraff, G. A., Phys. Rev. 128, 2507 (1962).

(16) L. V. Keldysh, Sov. Phys. JETP 21, 1135 (1965).

(17) Seitz, F., Phys. Rev. 76, 1376 (1949).

(18) Tager, A. S., Sov. Phys. Sol. St. 6, 1919 (1965).

(19) Fersman, I. A., and Khazov, L. D., Sov. Phys. Tech. Phys. 15, 834 (1970).

(20) Holway, L., private communications.

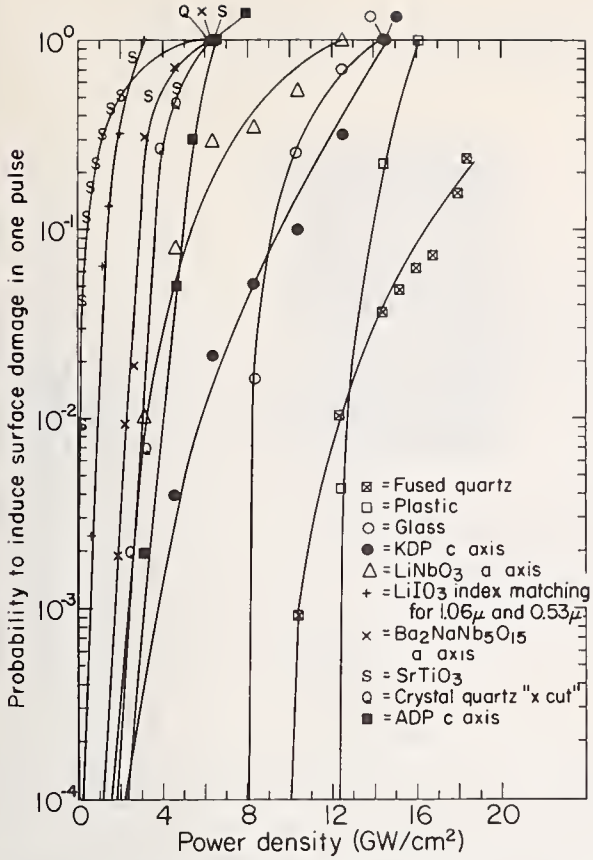

Fig. 1 Measured probability to induce surface damage in one pulse versus the pulse density. A TEM_{00} mode, 1.064μ laser beam was focused to a circular spot of diameter = 0.003 cm on the polished surface of these materials. Damage was produced on and sometimes just beneath the entrance face.

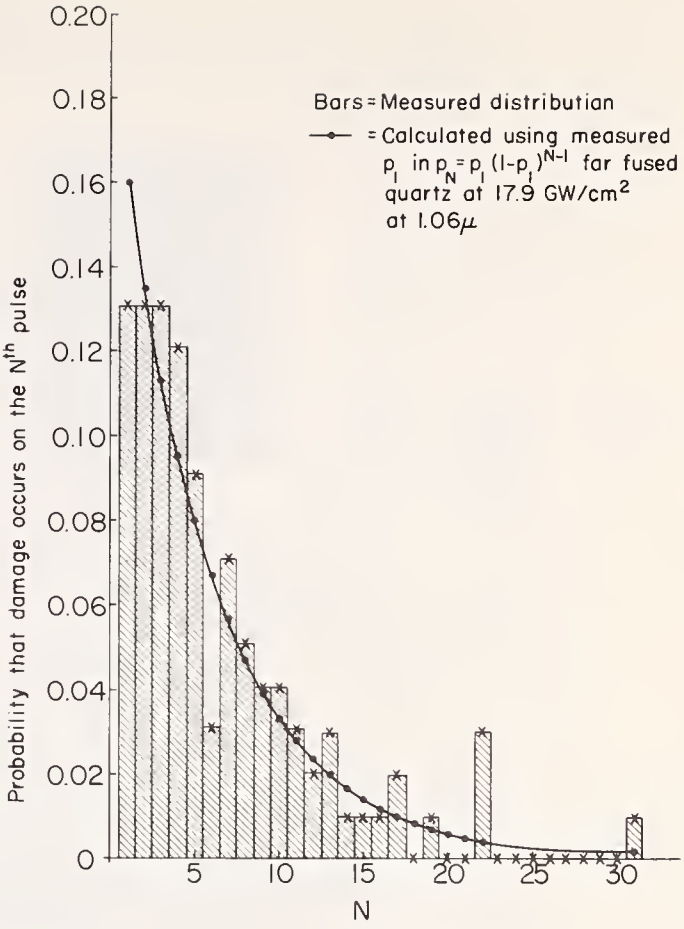

Fig. 2 Probability that damage occurs on the Nth pulse versus N for fused quartz. A 17.9 CW/cm^2 TEM_{00} mode 1.064μ beam was used.

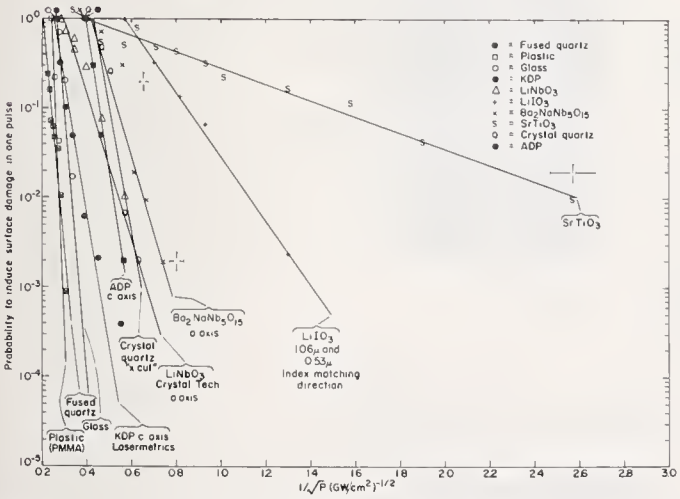

Fig. 3 Plot of the logarithm of damage probability versus the reciprocal square root of the power density. Since the abscissa is proportional to the reciprocal of the electric field, this plot serves to test for a dependence of the form p ~ exp (-const/E) as suggested by Shockley's theory of avalanche ionization.

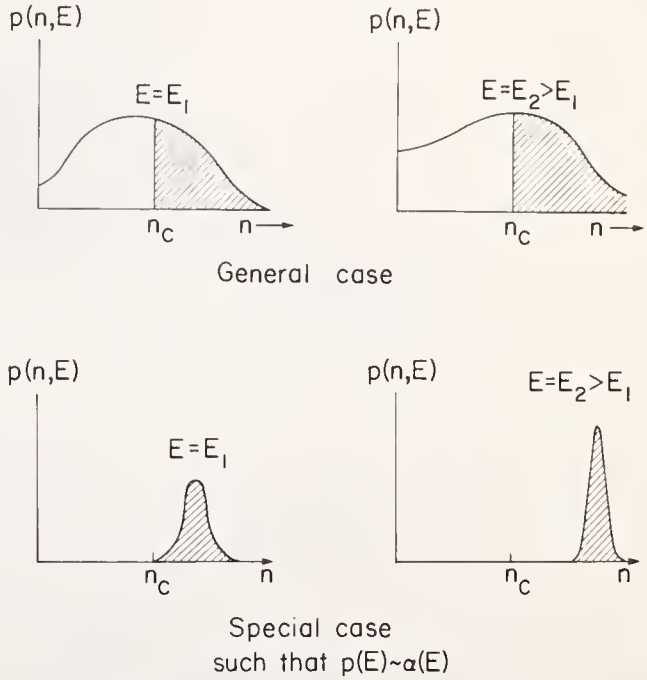

Fig. 4 Sketches of the distribution of avalanche sizes. Cross-hatched areas represent the number of damaging breakdowns per unit time. That is, they represent the integral in EQ. (8).

450-417 O-71—7

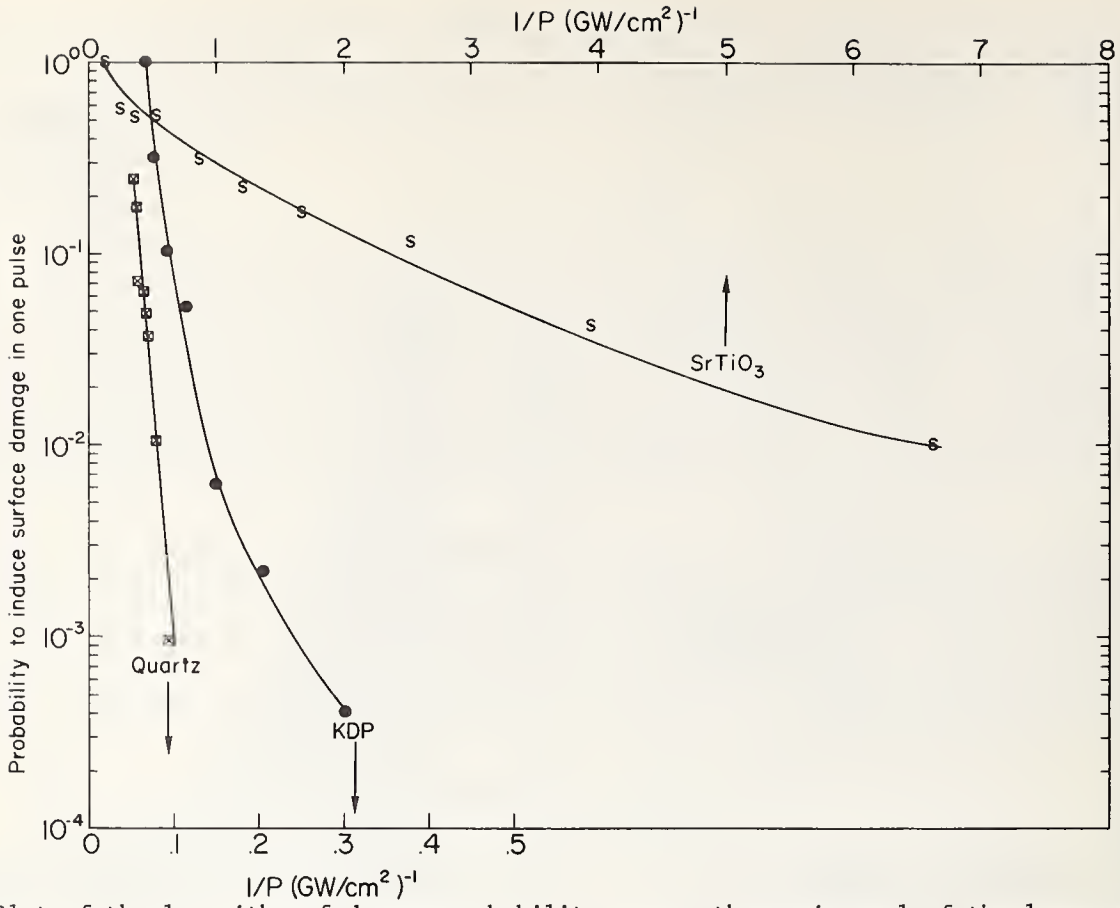

Fig. 5 Plot of the logarithm of damage probability versus the reciprocal of the laser power density. This plot serves to test for a dependence of the form $\sim \exp(-\text{const}/E^2)$ as suggested by Wolff's theory of avalanche ionization.

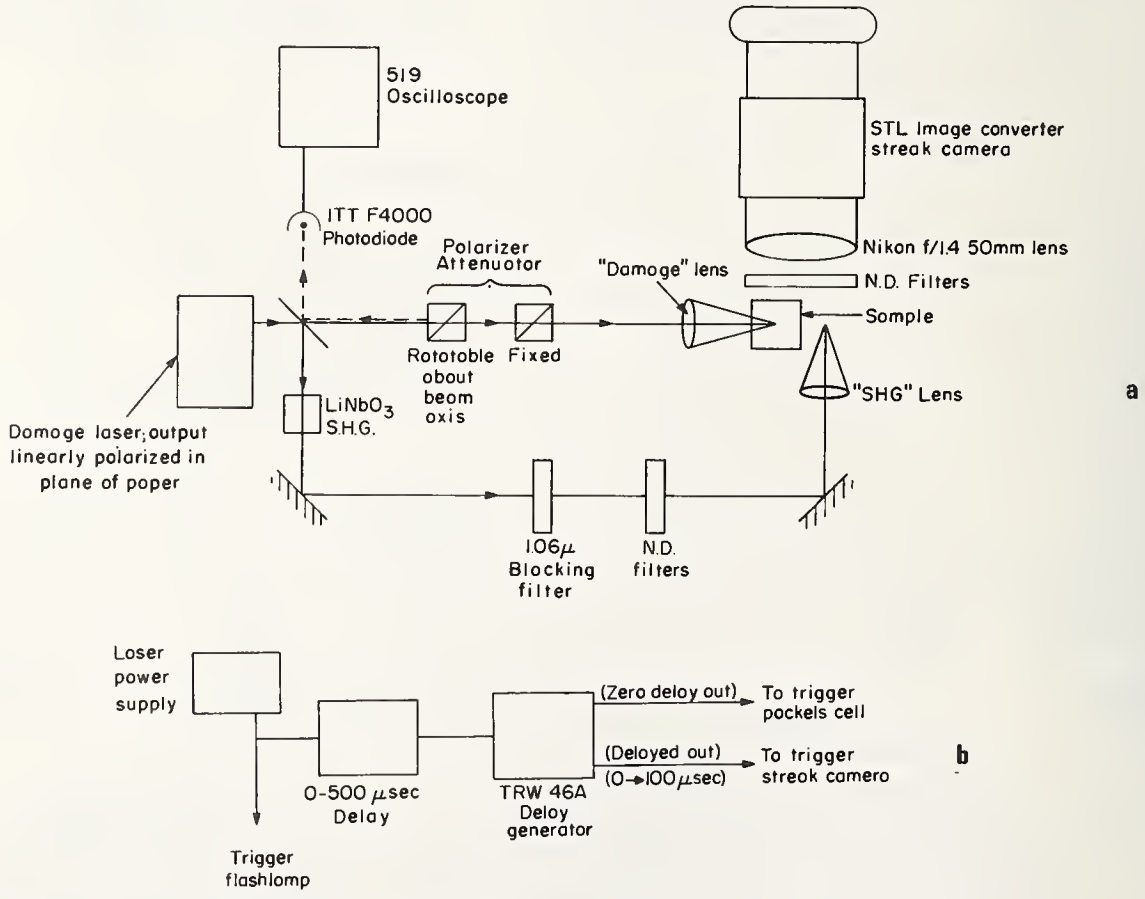

Fig. 6 Schematic diagram of streak camera experiment: (a) Optical, (b) Electrical.

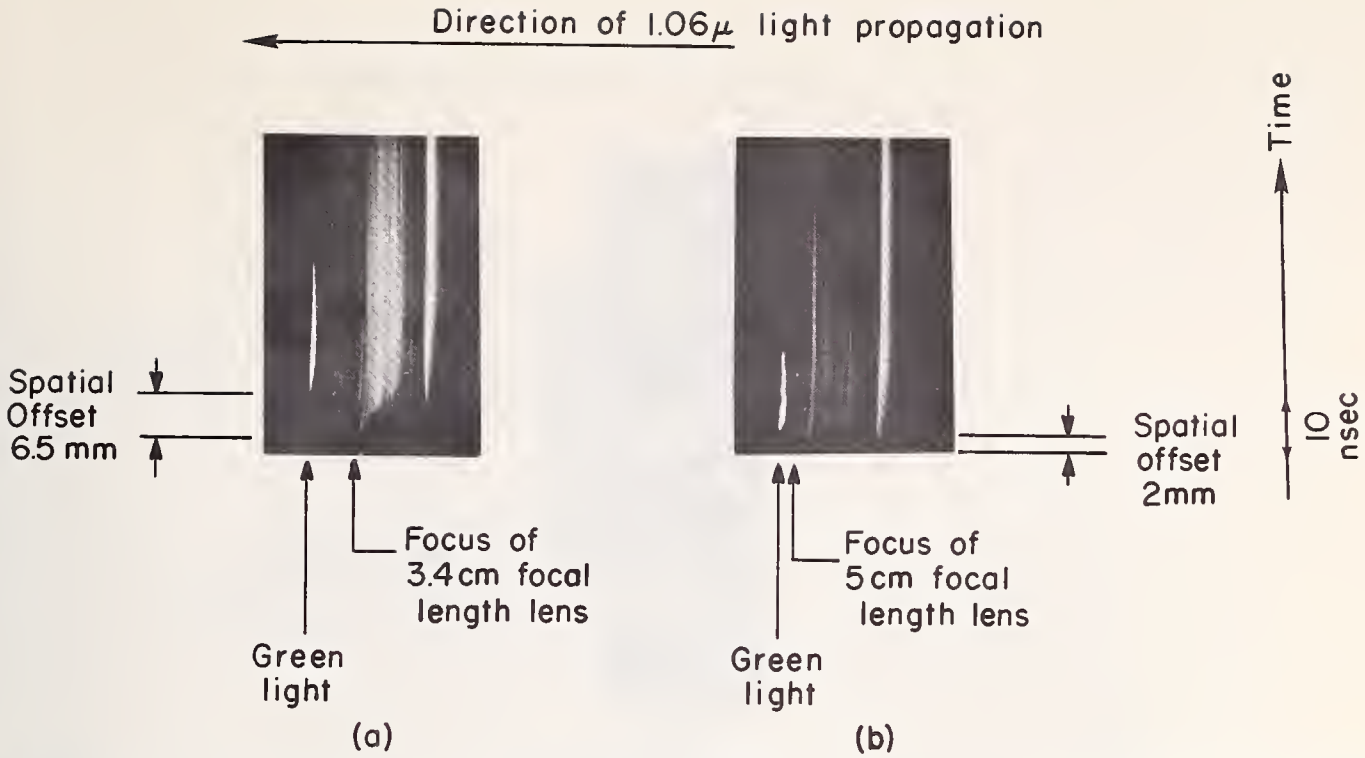

Fig. 7 Streak photographs of laser-induced sparks in lucite acrylic plastic. In (a) a 3.5 cm focal length lens was used; in (b) a 5 cm focal length lens was used. The focus was set to produce both internal and surface sparks.

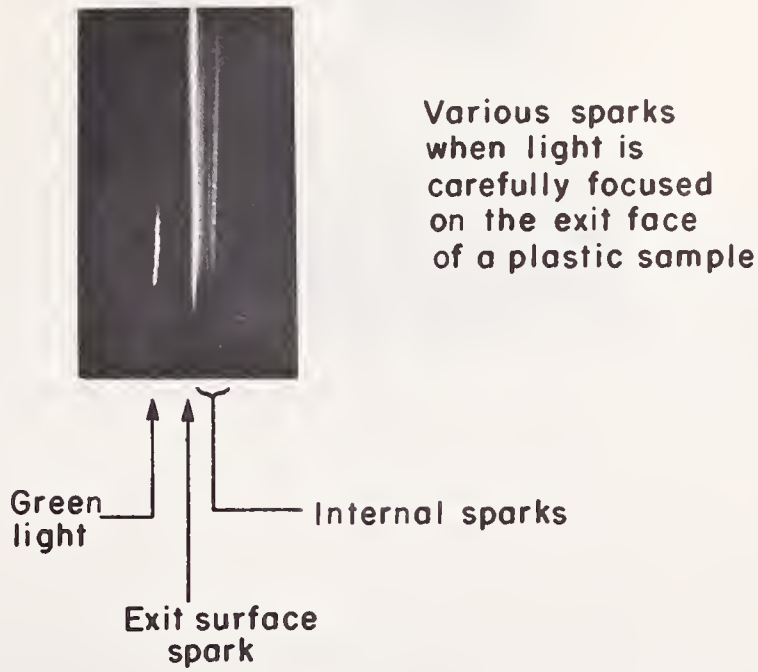

Fig. 8 Breakdown on the exit face of an acrylic plastic sample. The laser was focused through the sample and on the exit face.

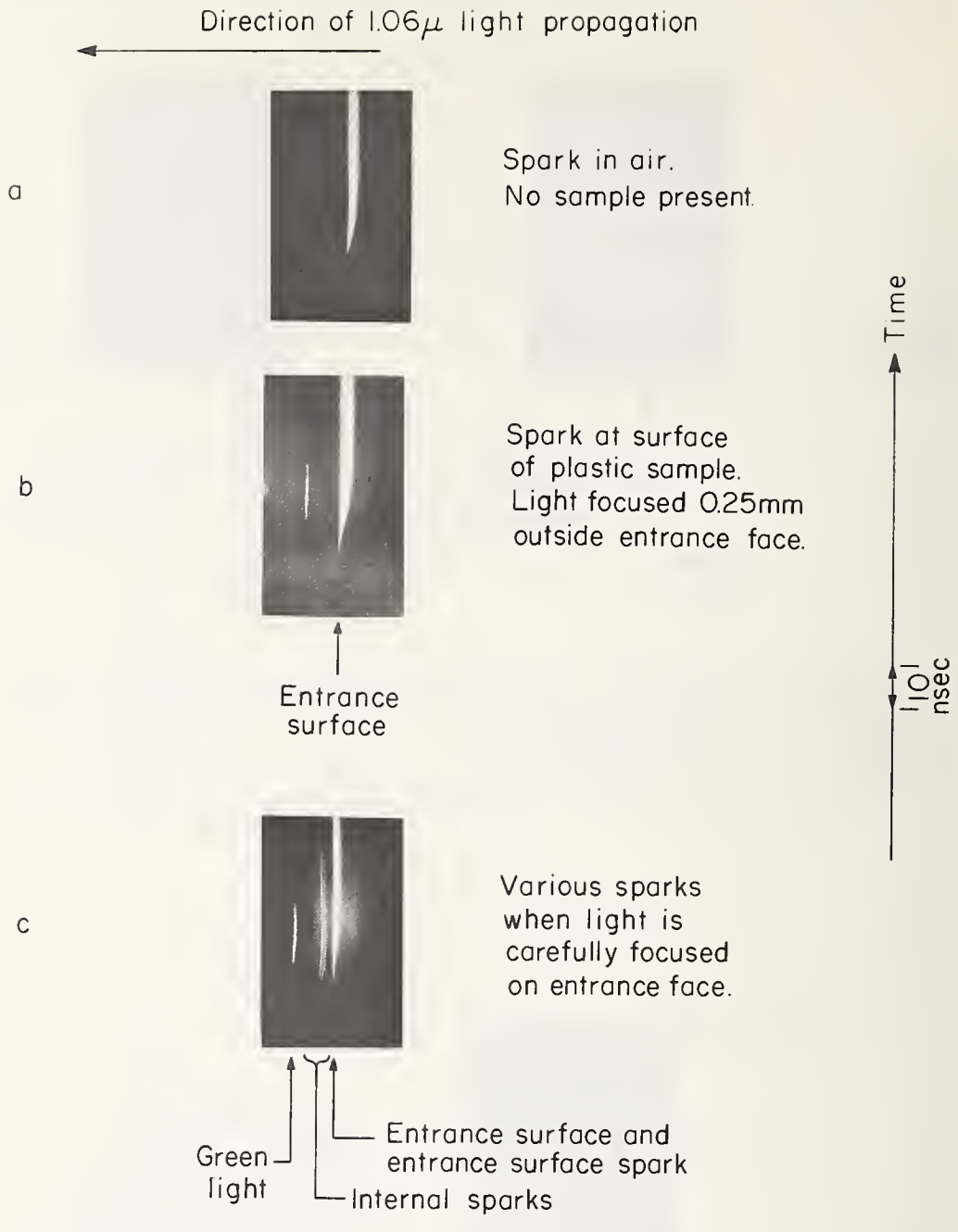

Fig. 9 Breakdown on the entrance face of an acrylic plastic sample.

a. Breakdown in air with no sample present
b. Breakdown near the surface of the sample. The focus was 0.25 mm outside the entrance face.
c. Breakdown when focused on the sample's entrance face. Note internal sparks are also produced.

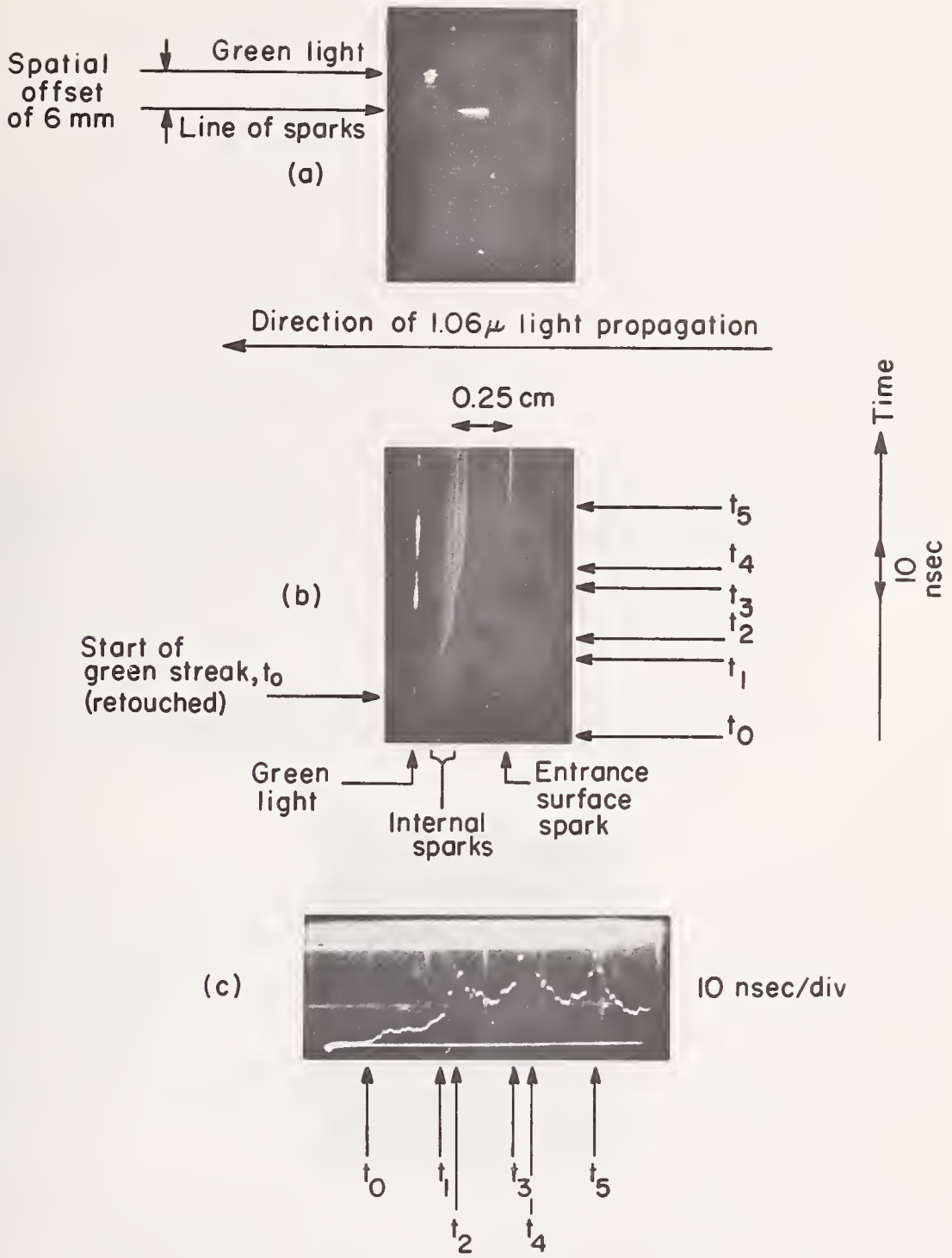

Fig. 10 Streak photographs of laser-induced sparks in plate glass.
a. Unstreaked sparks and green light
b. Streaked sparks and green light
c. Waveform of the pulse which produced the sparks in (b). Arbitrary vertical scale.

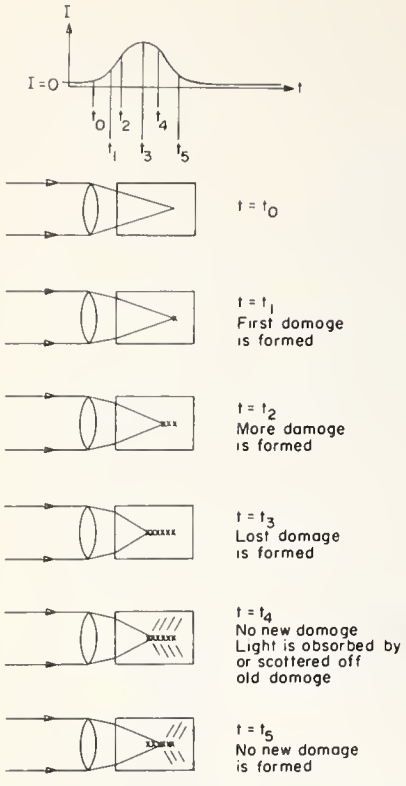

Fig. 11 Sketch of the sequence of breakdown formation assuming a fast response self-focusing process and a smooth pulse waveform.

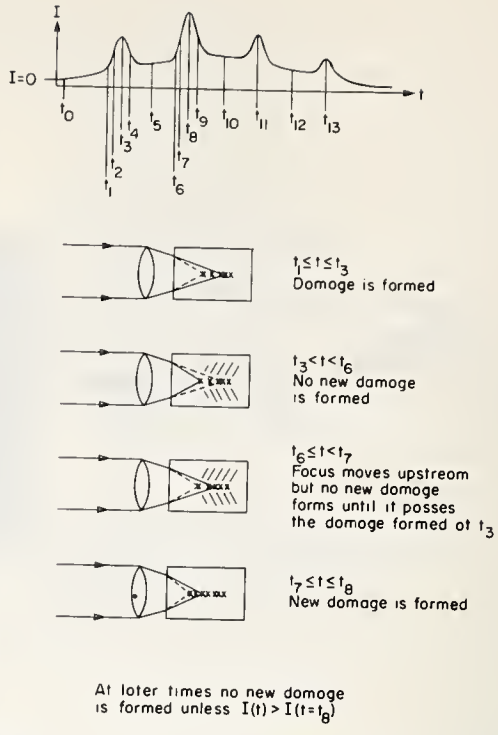

Fig. 12 Sketch of the sequence of breakdown formation assuming a fast response, self-focusing process, and a "wiggly" pulse waveform.

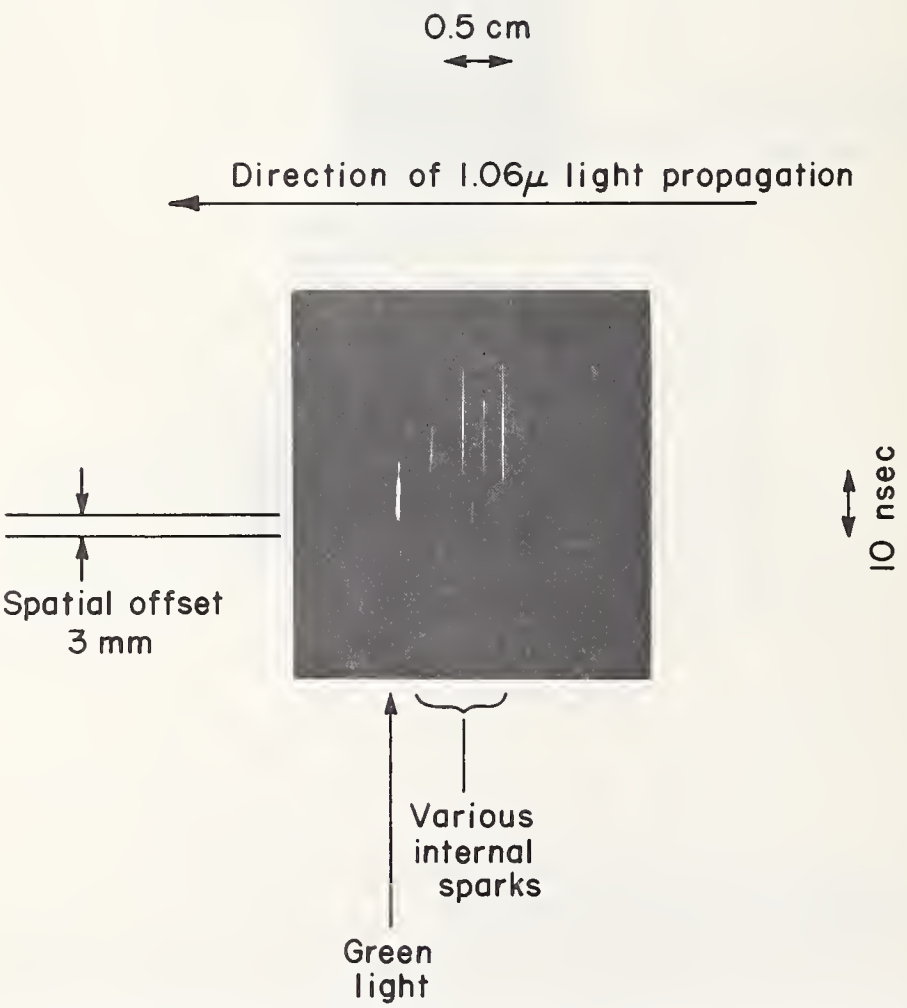

Fig. 13 Streak photo of laser-induced breakdown in a plastic sample using a collimated TEM_{00} mode laser beam. The pulse waveform was not completely smooth. Pulse power density 700 MW/cm^2.

Optically-Induced Physical Damage to $LiNbO_3$, Proustite, and $LiIO_3$ †

Wm. D. Fountain, L. M. Osterink, and G. A. Massey

Electro-Optics Organization
GTE Sylvania, Inc., Electronic Systems Group, Western Division
Mountain View, California 94040

Careful experiments have been conducted to examine physical damage generated in $LiNbO_3$, proustite, and $LiIO_3$ by 1.064 μm radiation from mode-locked and Q-switched Nd:YAG lasers. The primary emphasis has been on damage to $LiNbO_3$ from flash-pumped Q-switched lasers, but good data have also been obtained for damage in proustite in the same arrangement as well as with cw-pumped Q-switched Nd:YAG lasers. Fair data have been obtained for damage to $LiNbO_3$ from a flash-pumped mode-locked Nd:YAG laser. Further, we present semi-quantitative observations on damage in $LiNbO_3$ Q-switches used in flash-pumped and continuously-pumped Nd:YAG lasers, and on damage in "hot" $LiNbO_3$ and $LiIO_3$ used for external frequency doubling with these lasers.

The careful experiments were conducted with a diverging Gaussian beam from a Nd:YAG laser emitting 10 ns pulses at 10 Hz. In the absence of inclusions, damage in two stoichiometric $LiNbO_3$ crystals and one "hot" one always occurred at the exit face, and for power densities $\gtrsim$ 180 MW/cm^2 (Gaussian-beam average). The damage threshold for a proustite crystal was 10 MW/cm^2 (both faces damaged), and for a strained, poor-quality $LiIO_3$ crystal it was $\sim$ 465 MW/cm^2 (entrance face damaged). These $LiNbO_3$ damage threshold values are considerably higher than the 5 MW/cm^2 to 140 MW/cm^2 observed with multi-mode beams by others, and by us with coated crystals.

Key Words: Laser-induced damage, crystal damage, damage threshold, nonlinear optics, Q-switched lasers, second harmonic generation.

1. Introduction

Lithium niobate, proustite, and lithium iodate are of great interest for application in nonlinear optics, and the first of these is also of great interest for use in Pockels'-effect devices. The first limitation to their usefulness, in the absence of inclusions (ignoring the hygroscopicity of $LiIO_3$ and "optical damage" or "index damage" [1-3][1] in $LiNbO_3$ below about 170°C), generally is pitting of the surface(s) caused by intense optical radiation. We here report and discuss our observations of damage due to radiation at 1064 nm, with and without the simultaneous presence of radiation at 532 nm.

Throughout, "power density" means instantaneous peak power divided by the beam area, while "average power density" means time-averaged power divided by the beam area (for Gaussian beams, the spatial peaks are twice these spatial averages). Power and energy densities given are those at the damage site (neglecting self-focusing, which we did not observe but cannot absolutely exclude).

This paper results from research into device limitations due to materials problems, and is intended to provide a basis for the further study of damage mechanisms in these materials. We will not present a definitive explication of the general problem of damage in these crystals, but we will show that under some conditions, surface damage in $LiNbO_3$ may be attributed to momentum exchange, at the exit surface, by phonons or acoustic waves generated in the interaction of the laser beam with the crystal. We will ascribe damage in proustite to local heating caused by absorption.

---

† This work was partially supported by a Sylvania IR&D program, by NASA/ERC contract NAS12-2239, by Patrick AFB contract F08606-69-C-0054, by NADC Contract N62269-69-C-0029, and by ONR contract N00014-70-C-0224.

[1] Figures in brackets indicate the literature references at the end of this paper.

2. Experimental Arrangement

The deliberate damage measurements were performed with three different lasers in separate (but very similar) set-ups, as shown schematically in Figure 1. In each case the flash-pumped Nd:YAG laser was operated single-shot for 60 shots and then at 10 pps for 60 seconds, with an internal aperture restricting oscillation to the fundamental transverse mode. The beam angle was deliberately chosen to be small, in order to approximate the conditions ordinarily found in devices. This beam geometry was deliberately not varied, in an attempt to restrict the interactions to those which might occur in typical devices.

For the Q-switched tests, an electro-optic Q switch provided 10-ns-duration (FWHM) pulses, and the output reflector was a two-plate fused-silica etalon. This resonant reflector was not temperature-controlled, nor was the longitudinal mode structure studied; however, the design of this reflector makes it probable that no more than three longitudinal modes were oscillating at any instant [4-6].

For the mode-locked tests, the resonant reflector was replaced by a dielectric mirror and the electro-optic Q switch was replaced by a dye cell containing diluted Eastman Q-Switch Solution 9740. This set-up could be adjusted to provide a 30 ns (FWHM) fully-modulated train of pulses, with individual pulse duration less than our limit of measurement (1 ns) and pulse separation of 3 ns. These pulses could have been as short as 20 to 25 ps [7,8], but quite possibly were not [8].

3. Experimental Results

3.1 Beam Geometry

For each laser that was set up in the arrangement of Figure 1, the laser beam was sampled with a series of apertures at each of several far-field locations along the beam axis. For each such location, a Gaussian spot size (at that location) may formally be calculated from the transmission of each of the apertures. If the beam is indeed Gaussian, these calculated spot sizes (at any one location) will all agree; in fact, at each location the calculated spot sizes typically were within ± 5% of their mean, and the variations were random. The far-field beam geometry, and the location of the focal point, were obtained by projecting the spot sizes measured at the various locations.

3.2 Experimental Error

The results of the damage tests are presented in the text below and in Tables I - III. The indicated errors are error limits, rather than probable errors, and are the result of random laser amplitude fluctuations (± 10%) and of the inaccuracy of determining the focal point (± 10%). The latter of these two sources of error introduces a systematic error into the damage threshold calculations that can be large, especially for the higher damage threshold values; this is so because the beam size becomes both smaller and less accurately determined as the focal point is approached. Since this error is a systematic one, however, ratios of the damage thresholds (such as for $LiNbO_3$ with and without optically-contacted SiO_2) are relatively accurate.

Table 1. Extremal values from controlled damage measurements; 1064 nm, Gaussian beam spatial average.

Mat'l	Conditions	Max. Values (no damage, ≥ 600 shots)	Min. Values (damage, < 600 shots
$LiNbO_3$	10 ns pulses 0-10 pps	790 MW/cm^2 (Xtal #3)	180 MW/cm^2 (Xtals #1, #2, #3)
$LiNbO_3$	≤ 1 ns pulses 300 MHz (burst) 10 pps	> 320 mJ/cm^2	(could not damage)
Proustite	10 ns pulses 0-10 pps	9.2 MW/cm^2	11.0 MW/cm^2
$LiIO_3$	10 ns pulses 0-10 pps	360 MW/cm^2	460 MW/cm^2

Table 2. Approximate minimum damage thresholds; 1064 nm, Gaussian beam spatial average.

Mat'l	Conditions	Threshold	Total Error Limits	Damage
$LiNbO_3$	10 ns pulses 10 pps	th. > 170 MW/cm^2 th. $\leq$ 180 MW/cm^2	+ 10% - 30%	exit face pit (diverging beam)
$LiNbO_3$ (SiO_2 contacted)	10 ns pulses 10 pps	th. $\lesssim$ 700 MW/cm^2	+ 71% -86%	exit face pit (SiO_2 undamaged) (diverging beam)
$LiNbO_3$	< 1 ns pulses 300 MHz (burst) 10 pps	th. > 320 mJ/cm^2	+ 95% - 0%	not observed (diverging beam) (converging beam)
Proustite	10 ns pulses 10 pps	th. > 9.2 MW/cm^2 th. $\leq$ 11.0 MW/cm^2	+ 12.5% - 27%	both faces pitted (or melted) (diverging beam)
Proustite	200 ns pulses 100-5000 pps	th. $\leq$ 450 kW/cm^2	± 10%	entrance face pit (melted) (converging beam)
$LiIO_3$ (strained)	10 ns pulses 10 pps	th. > 360 MW/cm^2 th. $\leq$ 460 MW/cm^2	+ 64% - 80%	entrance face pit and fracture (diverging beam)

Table 3. Rough multimode damage thresholds; multimode beam spatial average.

Mat'l	Conditions	~ Threshold	Damage
$LiNbO_3$ (AR coated)	10 ns pulses 10 pps	30 MW/cm^2 (1064 nm)	burned/pitted faces (in absence of inclusions) (Q switch)
$LiNbO_3$ (AR coated)	200 ns pulses 2-5 KHz	10 MW/cm^2 (1064 nm)	burned/pitted faces (Q switch)
$LiNbO_3$	200 ns pulses 1-5 KHz	(*)3-10 MW/cm^2 (1064 nm)	pitted faces (but rarely entrance face) (converging beam)

(*) 100-250 mW average @ 532 nm (5-40% average power conversion)

Proustite	CW	200 - 600 W/cm^2 (1064 nm) (5W unfocused)	entrance face melted (~ 20 sec.) (diverging beam)
Proustite	CW	25 W unfocused	sliced and burned

3.3 $LiNbO_3$

The experiments on $LiNbO_3$ were performed with cubes measuring 1 cm along each edge. Damage in the two stoichiometric (#1 and #3) and one "hot" (#2; lithium-rich composition) $LiNbO_3$ crystals always occurred at the exit face, and for power densities $\gtrsim$ 180 MW/cm^2 (Gaussian beam average) or energy densities $\gtrsim$ 1.8 j/cm^2. This agrees with results obtained with glass samples at higher power densities [9]. In crystal #3, in particular, which was grown by a different company than were crystals #1 and #2, a band of high-damage-threshold material extended across the center of one face; we have not yet repolished this crystal to determine whether this was strictly a surface effect. Damage was always

accompanied by a plasma at the exit face (never at the entrance face). Damage threshold was not a function of temperature (25-165°C), polarization (two perpendicular directions) or crystal orientation (propagation along the "a" axis or "c" axis). Damage took the form of a pit, shallower than hemispherical and $\lesssim$ 100 μm in diameter; it always occurred within the first 80 shots.

These data are complemented by those of Bass [10]; however, his damage threshold (350 MW/cm^2) was obtained by focusing the laser beam on the front surface of the crystal with a microscope objective. One would expect higher thresholds with his experiments than with ours, since the mechanisms involved are likely to be different (cumulative bulk interactions are obviated).

Crystal #1 was repolished and then immersed in Dow Corning 200 dimethyl silicone fluid of 20 centistokes viscosity ($n \doteq 1.4$), contained in a fused-silica cuvette with optically flat windows. A plasma was observed at the exit face of the $LiNbO_3$ at a power density of about 60 MW/cm^2; the crystal was unharmed but had a grey deposit, which was easily wiped off, on its exit face. When the cuvette of fluid (without the $LiNbO_3$) was placed in the beam, no evidence of heating or decomposition was observed.

Another $LiNbO_3$ crystal, similar to #1 and grown by the same company, that had fused-silica flats optically contacted to its faces, was placed in the beam. A plasma was observed at the exit face of the $LiNbO_3$ (not the exit face of the SiO_2) at a power density of $\sim$ 700 MW/cm^2; the $LiNbO_3$ exhibited a pit (the SiO_2 appeared to be unharmed), and there was a very localized loss of the optical contact about the pit. Similar results were obtained with YAG plates.

Crystal #1 was then placed in the beam of the mode-locked (or partially mode-locked) laser. No damage was observed even at the focal point. The energy density at the focus due to the most intense mode-locked pulse in the train was about 320 mJ/cm^2, and was about 3.2 J/cm^2 for the whole train. A virtually identical experiment [11] with a mode-locked Nd:glass laser gave a damage threshold of about 710 mJ/cm^2 for the most intense pulse and about 8.5 J/cm^2 for the whole train; in this case, damage was observed primarily on the entrance face. In the case of surface damage in glass [12], the energy-density damage threshold decreases (and the power-density damage threshold increases) sublinearly with pulse duration. We find that the same is true for $LiNbO_3$ if the damage is caused by an individual mode-locked pulse, but we cannot exclude the possibility that the damage is caused by the cumulative effect of the train of mode-locked pulses [13], in which case both the energy and power-density damage thresholds increase.

Typical values quoted for the multi-mode damage threshold of antireflection-coated $LiNbO_3$ used in Q switches or nonlinear devices range from about 5 MW/cm^2 to about 140 MW/cm^2 [10,14,15]. We have observed Q switch damage for values of 10 to 30 MW/cm^2 (multi-mode beam average). In the absence of inclusions, this damage takes the form of irregular burned pits on the crystal surfaces. We have observed one instance in which the damage took the form of a "frosted" surface; microscopic examination indicated that this region was confined to the AR-coating, which implies that the coating is responsible for at least some of the damage in $LiNbO_3$ devices (coatings are solely responsible for damage to coated KD*P devices, we have found). The preceding paragraph applies to $LiNbO_3$ crystals from two different growers. In crystals obtained from a third grower, thousands of microscopic bubbles ("veiling") were produced throughout the bulk of the material, at lower power densities. We cannot account for the differing behavior of these samples.

In tests with two continuously-pumped, repetitively-Q-switched lasers (200 ns pulse duration, 500 to 5000 pps, 0.1 to 10 W average power at 1064 nm), uncoated "hot" $LiNbO_3$ crystals used for frequency doubling from 1064 nm to 532 nm were found to damage consistently on their surfaces at a peak power density of about 10 MW/cm^2 (Gaussian beam); this damage was induced only at the phase-matching temperature, in the presence of 532 nm light having a peak power density of about 3 MW/cm^2 (Gaussian beam). In these tests, damage occurred nearly always on the exit face of the crystal, although some entrance surface and bulk damage was observed when the beam was so sharply focused that the length of the near-field region of the beam became comparable to the one centimeter crystal length.

In contrast, we have obtained 532-nm peak powers up to 1 MW at up to 50 pps with a "hot" $LiNbO_3$ external doubler. In this case the peak green power density was about 4 MW/cm^2 (multimode average), while the infrared power density was about thrice that (10 ns pulse duration).

3.4 Proustite

The proustite experiments were conducted on a slice of proustite with a good optical polish (for this material). The low power densities required to produce a melted pit imply that the damage is largely thermal in nature and presumably attributable to absorption of the 1.064 μm radiation. This conclusion is strengthened by the observation that proustite can easily be melted with an average power density of a few hundred watts per square centimeter at 1.064 nm. An unfocused 25W Nd:YAG laser not only rapidly slices a wafer of proustite, but also actually causes it to burst into flames.

3.5 $LiIO_3$

A damage experiment was performed with a strained $LiIO_3$ boule end that had a mediocre polish applied to opposing faces. At a peak power density of about 465 MW/cm^2, a large (1 to 2 nm) pit was generated in the entrance face, together with a fracture extending 2 to 3 nm into the bulk material from the pit. The severity of the damage may well have been caused by the grown-in strains. On the other hand, the quality of the polish may not have affected the results [10].

Bulk fractures, stained with iodine, were induced in $LiIO_3$ crystals used for external frequency doubling with flash-pumped Q-switched lasers. In one case, with a 1064 nm power density of about 30 MW/cm^2 (Gaussian beam), the crystal damaged almost instantly; the 532 nm power density was probably about 15 MW/cm^2. In the other case, damage occurred after a few minutes' exposure to nominal power densities (multi-mode beam average) of 40 MW/cm^2 at 1064 nm and 2 MW/cm^2 at 532 nm; in this case the conversion efficiency was low because the laser beam divergence was large compared to the $LiIO_3$ acceptance angle. KD*P was not damaged after identical exposures to both lasers.

4. Discussion

4.1 Mechanisms

A number of mechanisms may be proposed to account for optically-induced physical damage [9,13,16, 17]. Some of these, such as beam trapping, may be considered to be initiating mechanisms because they allow conditions for damage to develop but might also exist without damage. The momentum exchange of a sound or light beam at an exit surface, the local heating produced by localized absorption of such a beam, or the dielectric stress induced by an intense optical electric field, might result directly in the damage observed and may therefore be categorized as destructive processes. The reason for our distinction between these types of processes is not only to attempt to clarify the physics of the problem but also to suggest methods for avoiding damage. Although one may not be able to prevent the formation of intense phonon beams in a given material, for example, one may still be able to avoid damage by coupling the phonons out of the crystal without momentum exchange by means of a transparent, acoustic-impedance-matching cover plate. Of course, two or more of these mechanisms may be operative, simultaneously or sequentially, in causing damage. The surfaces, and especially the exit surface, are uniquely vulnerable to damage (unless the laser beam is tightly focused) because of surface states, structural weakness, and discontinuities in dielectric constant, acoustic impedance, et cetera. Among the possible mechanisms which one may consider are: (1) local heating due to absorption, (2) thermal shock, (3) the pyroelectric effect, (4) two-photon or multi-photon absorption, (5) intense optical electric fields, (6) beam trapping, (7) optical rectification, (8) surface dielectric stress, (9) radiation pressure, (10) ionization at a surface, (11) piezoelectricity, (12) the converse piezoelectric effect, (13) electrostriction, (14) avalanche breakdown caused by acceleration of conduction-band electrons to ionizing energies, (15) phonons driven at the difference frequency between two frequency components of the laser, (16) phonons produced by energy transfer through "cold" conduction-band electrons, and (17) stimulated Raman or Brillouin scattering.

4.2 $LiNbO_3$

For $LiNbO_3$ irradiated at 1064 nm at these average power densities, we may exclude the thermal mechanisms, (1) - (3): a crystal used for frequency-doubling near (but not at) phase-matching temperature constitutes a detector sensitive to temperature changes on the order of 0.1°C, but no variation in temperature with infrared power density is observed (the crystal is operated at a temperature such that no significant amount of green light, which is slightly absorbed, is generated).

Initiating mechanisms (4) and (5) may well be operative. Mechanism (6) may be operative [18], but the beam geometry does not appear to vary with power density in $LiNbO_3$ with cover plates, exposed to levels that damage $LiNbO_3$ without cover plates. Mechanisms (7) - (11) are eliminated for surface damage by the immersion experiment (DC-200 has a refractive index of about 1.4; a dielectric strength of 420 V/mil; a dielectric constant of 2.68 from 60 Hz to 10 GHz; and a dissipation factor of about 2×10^{-5} up to 100 MHz, after which it gradually increases). Mechanism (7) is such a small effect [19] that it is unlikely to be significant; the absence of mechanisms (3) and (7) implies that mechanism (12) may also be eliminated. Mechanism (13) may be responsible for inducing mechanism (6), if the latter exists, or may cause surface damage due to the axial stress induced at the surfaces by the radial compression; in the latter case, the laser beam would have to be self-focussed to an exit-face diameter smaller than the entrance-face diameter in order to account for the lack of entrance-face damage.

Hellwarth's analysis [17] presumably obviates mechanism (14); it appears that "cold" electrons are capable of mediating damage and that the existence of "hot" electrons in significant numbers is unlikely. Similarly, Giuliano's analysis [9] eliminates mechanism (15); the driven phonons would be generated at large angles to the laser beam, and would have very long mean free paths.

Mechanisms (16) and (17), both involving phonon generation, are fully consistent with our data; mechanisms (4) and (5) may enhance the phonon-generating process, and mechanisms (6) and (13) may possibly be operative also. Hence we attribute surface damage to $LiNbO_3$, irradiated at 1064 nm under these conditions, to acoustic effects at the exit interface.

When 532-nm radiation is also present, the damage mechanism is not clear. We have observed average powers up to 6W at 540 nm (total, both directions) with an intracavity uncoated $LiNbO_3$ crystal [20]; the green peak power was 1.2 to 2.0 kW, the green peak power density was about 6 to 10 kW/cm^2 (multimode average), the green average power density was about 31 W/cm^2 (multimode average), and we did observe slow surface deterioration. Severe optical heating of the crystal was apparent at this level of green generation; this observation, combined with the external-doubling results reported above, suggests that one of the thermal mechanisms may be the primary cause of damage.

4.3 Proustite and $LiIO_3$

Mechanism (1) is undoubtedly the preponderant cause of damage by 1064-nm lasers to proustite; we can say little about the presence or absence of the other mechanisms. Bulk damage in $LiIO_3$ used for doubling 1064-nm radiation to 532 nm is presumably caused by a photochemical or thermochemical reaction, with the severity of the damage being enhanced by absorption in the iodine that is thereby liberated. We will not speculate on the cause of surface damage to $LiIO_3$ by 1064-nm radiation alone.

5. Conclusions

Damage to proustite by 1064-nm radiation occurs at an extremely low level, and may be ascribed to local heating caused by absorption. If this absorption is extrinsic, further crystal growth and purification work must be performed; if it is intrinsic, proustite will be of little or no practical utility in the near infrared.

Damage to $LiIO_3$ by 1064-nm radiation occurs at a fairly high level in comparison with most nonlinear materials (excluding KDP and KD*P [10]). The present usefulness of this material for second-harmonic generation to 532 nm is limited by bulk damage, however, which we suspect is due to a photochemical or thermochemical reaction.

Damage to $LiNbO_3$ by 1064-nm radiation occurs at a moderate level for nonlinear materials, although this level is well below that for other optical materials commonly used with lasers. We attribute this material's damage to momentum exchange, at the exit surface, by phonons or acoustic waves generated in the interaction of the laser beam with the crystal. The simultaneous presence of 532-nm radiation lowers the damage threshold.

6. Acknowledgements

We wish to thank our colleagues E. O. Ammann and J. M. Yarborough for providing much of the data on proustite, and F. O. Lopez for his able assistance in conducting some of the experiments. We gratefully acknowledge helpful discussions with S. E. Schwarz of the University of California and A. E. Siegman of Stanford University.

7. References

[1] A. Ashkin et al, "Optically-Induced Refractive Index Inhomogeneities in $LiNbO_3$ and $LiTaO_3$", Appl. Phys. Letters 9, 72-74 (1 July 1966).

[2] H. J. Levinstein et al, "Reduction of the Susceptibility to Optically Induced Index Inhomogeneities in $LiTaO_3$ and $LiNbO_3$", J. Appl. Phys. 38, 3101-3102 (July 1967).

[3] F. S. Chen, "A Laser-Induced Inhomogeneity of Refractive Indices in KTN", J. Appl. Phys. 38, 3418-3420 (July 1967).

[4] J. K. Watts, "Theory of Multiplate Resonant Reflectors", Appl. Optics 7, 1621-1623 (August 1968).

[5] H. F. Mahlein and G. Schollmeier, "Analysis and Synthesis of Periodic Optical Resonant Reflectors", Appl. Optics 8, 1197-1202 (June 1969).

[6] J. E. Geusic, "The YA1G:Nd Laser", in Solid State Maser Research (Optical), Final Report, 30 Aug. 1965, Contract DA36-039 AMC-02333(E), U.S. Army Electronics Command, Fort Monmouth, New Jersey.

[7] L. M. Osterink and J. D. Foster, "A Mode-Locked Nd:YAG Laser", J. Appl. Phys. 39, 4163-4165 (August 1968).

[8] A. R. Clobes and M. J. Brienza, "Passive Mode Locking of a Pulsed Nd:YAG Laser", Appl. Phys. Letters 14, 287-288 (1 May 1969).

[9] C. R. Giuliano, "Laser-Induced Damage to Transparent Dielectric Materials", Appl. Phys. Letters 5, 137-139 (1 Oct. 1964).

[10] M. Bass, "Laser-Induced Damage to Nonlinear Crystalline Materials", in Damage in Laser Materials (NBS Spec. Pub. 341, Dec. 1970), pp. 90-96.

[11] C. D. Lin, private communication.

[12] J. Davit, "Mechanism for Laser Surface Damage of Glasses", J. Appl. Phys. 39, 6052-6056 (Dec. 1968).

[13] ASTM Special Technical Publication 469, "Damage in Laser Glass" (American Society for Testing and Materials, Philadelphia 1969).

[14] S. E. Harris, private communication.

[15] W. A. Massey et al, "Lithium Niobate Damage Threshold Measurements Inside a Nd:YAG Q-Switched Laser Cavity", presented to the 1971 IEEE/OSA Conference on Laser Engineering and Applications (New York, 4 June 1971)

[16] H. Dupont, A. Donzel, and J. Ernest, "On Laser-Induced Breakdown and Fracture in Glasses", Appl. Phys. Letters 11, 271-272 (1 Nov. 1967).

[17] R. W. Hellwarth, "The Role of Conduction Electrons in Optical Damage", in Damage in Laser Materials (NBS Spec. Pub. 341, Dec. 1970), pp. 67-75.

[18] M. Bass, "Laser-Induced Damage to Nonlinear Crystalline Materials", presented to the IEEE International Electron Devices Meeting (Washington, 30 Oct. 1970).

[19] M. Bass, P. A. Franken, and J. F. Ward, "Optical Rectification", Phys. Rev. 138, A534-A542 (19 Apr. 1963).

[20] G. A. Massey and J. M. Yarborough, "High Average Power Operation and Nonlinear Optical Generation with the Nd:$YAlO_3$ Laser", Appl. Phys. Lett. 18, to be published (15 June 1971).

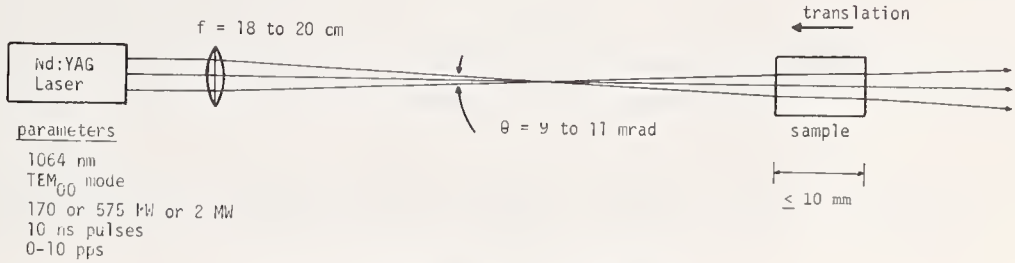

Fig. 1 Experimental Arrangement

COMMENTS ON PAPERS BY MICHAEL BASS AND WILLIAM FOUNTAIN

In the work of Bass and Barrett, the criterion for damage was taken to be the visual observation of a luminous plasma or spark. Microscopic investigation of the sample surface, both prior to and subsequent to the observation of this spark, indicated that in all cases, the appearance of a visually detectable luminous plasma preceded the appearance of any evidence of damage on the surface. As has been reported elsewhere several times, surface damage seems never to occur without the formation of a luminous plasma. As was emphasized in Bass' work, this plasma formation is intrinsically statistical in nature. It is not clear what the origin is of the first few electrons which initiate the formation of the plasma. It was pointed out that the plasma might be initiated by emission from low ionization energy impurities lodged on the surface, for which the work function of the surface is effectively lowered, or that the possibility exists of electrons being emitted into the conduction band of the solid near the surface by the mechanism of Zener tunneling in the optical field. In either case the same probabilistic nature would be shown by the damage phenomenon. Only the absolute value of the damage threshold would change. It was not possible on the basis of the investigations reported here to distinguish which mechanism was supplying the initial electrons. It was pointed out that under high vacuum conditions or in the case of extremely clean surfaces, one would still expect the same statistical description to apply--again, the only difference being that the curves would be shifted in the direction of higher threshold energies. On the subject of impurities it was pointed out that all nonlinear optical meterials which are obtained from commercial suppliers contain impurities to some degree. It was reported that potassium dihydrogen phosphate is a little more free of impurities than ammonium dihydrogen phosphate, evidence of which shows up in the variation of the ultraviolet absorption found in different samples of ADP. The same is true, for example, in lithium niobate and lithium iodate. It is therefore essential in considering the damage thresholds for these materials to take into account the possible presence of impurities or inclusions.

Catastrophic Surface Damage Produced in $Ba_2NaNb_5O_{15}$ Crystals during Intracavity Frequency Doubling[1]

Robert Webb

Holobeam, Inc.
Paramus, N. J. 07652

The original purpose of the experimental work reported herein was the production of a practical, high power, continuous green light source utilizing a frequency-doubled Nd:YAG laser in conjunction with an efficient nonlinear crystalline material, namely $Ba_2NaNb_5O_{15}$. Toward this goal, several focused intracavity geometries were studied whereby the $Ba_2NaNb_5O_{15}$ second harmonic generator was placed between the curved external end mirrors of a 1.065 micron laser; the output mirror being nearly transparent at 0.533 microns. 100% CW power conversion was consistently achieved, whereby available TEM_{oo} mode power at 1.065 microns was fully converted into green light. However, a serious problem due to catastrophic surface damage was encountered during these experiments which prevented sustained 100% conversion over periods of time greater than one minute. Since the crystals were situated within the laser cavity, the damage was always self-limiting in the sense that it completely terminated laser oscillation. Attempts to understand the reasons for this damage are outlined. The inherently nonlinear character of the damage process has been demonstrated, and it is presently conjectured that stimulated Brillouin scattering may be responsible for the observed damage effects.

Key Words: $Ba_2NaNb_5O_{15}$ CW damage threshold, laser intracavity frequency-doubling, nonlinear crystal damage, nonlinear damage, optical second harmonic generation, optical surface damage.

1. Introduction

Our earliest work in optical frequency-doubling with a CW Nd:YAG laser system involved focusing a 15 watt multimode, 1.065 micron beam of approximately 10 milliradians divergence into a 5. millimeter cube of $Ba_2NaNb_5O_{15}$ heated to its phase-matching temperature using a 2.5 cm focal length lens. In this first attempt, slightly less than 20 milliwatts of 0.533 micron power was generated. Unfortunately, the crystal was destroyed during the experiment. Figure 1 is a photograph of the resultant damage, which appears as a blackened region roughly equivalent to the size of the input beam, superimposed on the crystal fragments. No further experiments of this type were ever repeated, due to the expense involved.

From the above result, we recognized three important factors regarding optical frequency doubling; namely: (a) that only an overall 0.13% conversion efficiency had been reached, (b) that the majority of the fundamental power available within the laser cavity had not been fully utilized, and (c) that once a damage spot had been initiated external to the laser, no limitation upon its growth was easily possible within the short time interval required for complete crystal destruction due to continued absorption of the fundamental beam within the damaged region. Consideration of all these factors led us naturally toward intracavity frequency-doubling, upon which the remainder of our program was based.

---

[1] This work was sponsored by the Air Force Avionics Laboratory under Contract F33615-69-C-1841, Wright-Patterson Air Force Base, Ohio 45433

2. TEM_{oo} Mode Enhancement

Significant improvement in optical second harmonic generation was made possible by inserting the $Ba_2NaNb_5O_{15}$ crystal into the Nd:YAG cavity. An increase in 0.533 micron output to greater than 60 milliwatts was immediately produced during unfocused multimode operation. Furthermore, maximum conversion of the circulating 1.065 micron power into the second harmonic was achieved when the cavity was constrained to operate at highest power in the fundamental TEM_{oo} transverse mode, while linearly polarized with azimuth angle properly rotated for the largest nonlinear effect. Enhancement of the TEM_{oo} mode was accomplished by carefully adjusting the following parameters: (a) the spacing between the external cavity end mirrors, (b) peaking the concavity of these end mirrors as well as the end aperture faces of the Nd:YAG laser rod itself, (c) choosing the proper hole diameter and physical placement of a limiting aperture stop within the laser cavity, and (d) judiciously choosing the optimum placement of the $Ba_2NaNb_5O_{15}$ and an internal Brewster angle polarizing plate within the cavity. In addition, special attention was paid to multilayer dielectric coating of all optical surfaces to reduce the level of 1.065 micron intracavity power loss as much as possible.

One of our first optimized configurations consisted of a lengthened TEM_{oo} cavity with 150 centimeter spacing, terminated by a flat, 100% reflectance mirror at the front, and -200 cm. mirror, also of 100% reflectance, at the far end. The output mirror was 95% transmissive at 0.533 microns, behind which the $Ba_2NaNb_5O_{15}$ crystal, limiting aperture, and polarizer were situated respectively. The 0.3 cm. diameter by 5.0 cm. Nd:YAG rod, pumped by a pair of 2 kilowatt Krypton arc lamps, both water cooled, was situated initially at the approximate center of the cavity. Thirty milliwatts was generated at 0.533 microns for nearly 10 hours continuously in this geometry. Afterward, the Nd:YAG rod and pump lamp assembly was moved forward, i.e.,toward the output end as much as spatial limitations would permit. Thereupon, the 0.533 micron output was increased to 125 milliwatts, and was sustained for nearly two hours. The $Ba_2NaNb_5O_{15}$ phase matching temperature was recorded as 95.4°C. Suddenly, without prior indication, the laser oscillation ceased, and could not be restarted. Examination of the $Ba_2NaNb_5O_{15}$ crystal showed a permanent damage crater with a central blackened region having roughly the dimension of the beam previously circulating through it. Only one crater was produced, at the far side of the crystal, i.e., that side closest to the exit mirror, where the beam intensity had its highest value. From the photomicrograph shown in Figure 2, it appears that the central damage area had an approximate 0.25 millimeter cross section; and estimated power density at 1.065 microns of 0.8 megawatts/cm^2 with an additional 500 watts/cm^2 present at 0.533 microns. Together with the central blackened region is an outer cleft area, believed to be caused by the central or primary damage. This secondary damage is elongated in the direction of the $Ba_2NaNb_5O_{15}$ crystalline a-axis, and might be expected due to the anisotropic stress/strain relationship.

One interesting feature of the above experiment is that it was entirely repeatable at the same input power levels, and under identical operating conditions. Figure 3 shows a photomicrograph of a second damage spot produced in the same crystal when it was simply translated laterally to a newly exposed clear area. The newer damage was observed within less than half an hour of continuous operation. This time the secondary cleavage was incomplete insofar as the fractured region surrounding the central blackened crater did not fall away from the crystal surface.

3. Internal Cavity Focusing

Perhaps the most important series of experiments that was conducted during the program was that in which we utilized an intracavity lens system to increase the local power density in the nonlinear crystal in an attempt to increase the second harmonic generating efficiency to the point where we would reach or exceed the optimum coupling condition and attain 100% conversion of the normal 1.065 micron laser output into the second harmonic at 0.533 microns. We were indeed able to attain this goal, in the sense that the total green light output equalled the maximum 1.065 micron power output possible under identical loss conditions. However, during this series of experiments we also observed consistent serious surface damage on both aperture faces of the $Ba_2NaNb_5O_{15}$ crystals.

A schematic diagram of the intracavity focusing system is presented in Figure 4. The laser head contained a 0.3 cm. diameter by 5.0 cm. long Nd:YAG rod, again pumped by a pair of Krypton arc lamps to a level which would emit 5 to 8 watts of CW 1.065 micron power under stable TEM_{oo}, linearly polarized conditions. The lenses employed were single plano-convex elements with antireflection-coated surfaces at 1.065 microns. It was possible to insert the lens-pair combination into the laser cavity while maintaining TEM_{oo} mode operation. First the lens elements were aligned without the $Ba_2NaNb_5O_{15}$ crystal between them, and the cavity then peaked for maximum TEM_{oo} power output. Then the lenses were carefully spaced by an additional increment of length to allow for the higher index of refraction of the crystal which was next inserted between the lens pair. Figure 5 is a plot of the 1.065 micron output power obtained for several measured output mirror transmission factors. From the peak of this curve we can see that it is possible to extract a maximum of 2.1 watts of output power at 1.065 microns from this system under this set of operating conditions.

With this cavity configuration it was possible to maintain the same TEM_{oo} mode power while varying the power density within the $Ba_2NaNb_5O_{15}$ crystal and upon its surface. With 2.5 cm. focal length lenses it was possible to reach 0.85 watts of 0.533 micron output for periods of time ranging from a few seconds to five minutes. If we make corrections for surface losses at 0.533 microns, and add the power being generated in the reverse direction, we can conclude that we generated a total of 2.2 watts at 0.533 microns. However, it was generally not possible to sustain this 100% conversion for more than one minute, since in most instances catastrophic damage took place before this level had been attained, as the temperature was being peaked for maximum conversion. Since the crystal was situated within the laser cavity, the damage was always self-limiting in the sense that it terminated the laser oscillation responsible for the damage. Figures 6 and 7 are photomicrographs of the damage first encountered using this intracavity lens system. The general positions of the damage spots produced on one face of the $Ba_2NaNb_5O_{15}$ crystal coincide with those produced on the opposite side. That is, both faces received nearly identical damage, provided the lenses were accurately spaced with regard to the center of the crystal.

At first it was conjectured that the antireflection coating itself, while transparent to 1.065 micron radiation, might be sufficiently absorbing at 0.533 microns to be the cause of the damage phenomenon. The original coating material had been ThF_4. Thereupon, we had the same crystal refinished and coated with MgF_2 instead. Again, however, we discovered the same damage phenomena at the same power density levels, under the same operating conditions. Figures 8 and 9 show the photomicrographs of catastrophic surface damage produced with the newer MgF_2-coated surfaces. Power densities reached during both of these experimental runs averaged less than 3 megawatts/cm^2 at 1.065 microns, with corresponding power densities of less than 10^4 watts/cm^2 at 0.533 microns simultaneously.

4. Low-Loss Cavity

Since it was found that intracavity focusing led to a definite damage threshold of less than 3 megawatts/cm^2 in the presence of simultaneous second harmonic generation, one method of circumventing the damage problem while increasing the overall frequency-doubled output of a Nd:YAG system would be to reduce overall cavity losses, while maintaining a 1.065 micron power density somewhat below the damage threshold level. Toward this aim, we constructed a Nd:YAG system having lower loss than that used in the previous tests. Figure 10 shows a schematic diagram of the low-loss cavity geometry finally employed. Figure 11 is a plot of the TEM_{oo} power extracted from this system as a function of mirror reflectance. It should be possible to reach 0.533 micron output power levels in excess of 8 watts from this system. In practice, we were able to generate only 1 watt at 0.533 microns with this system. Although no damage was observed in this series of experiments, neither was the power density in the $Ba_2NaNb_5O_{15}$ crystal high enough to have reached the previously measured damage threshold. The chief reason for the discrepancy in 0.533 micron power produced was our inability to establish TEM_{oo} mode operation throughout the volume of the $Ba_2NaNb_5O_{15}$ crystal due to its inherent internal inhomogeneities.

5. Search for Damage Cause

In assessing our own observations, we have postulated two possible causes for the damage phenomena described above. The first possible cause would be attributable to multiple photon absorption, whereby two photons at the fundamental frequency combine under phase-matching conditions to produce a photon at the second harmonic frequency, and thereupon combine with a third photon at the original fundamental frequency to produce a third photon at the sum frequency which is quickly absorbed. Since $Ba_2NaNb_5O_{15}$ is strongly absorbing at the sum frequency, there is some credence to this argument. However, we do not as yet know what the exact mechanism for this three-photon absorption would be. Yet we can point out that we have eliminated simple absorption at 0.533 microns as the cause for the observed damage.

In a separate set of experiments we subjected an essentially identical $Ba_2NaNb_5O_{15}$ crystal to high intensity green light alone, in the absence of the 1.065 micron signal. Namely, we used the same 2.5 cm. focal length lens to concentrate up to 8 times the amount of green light at 0.5145 microns from an Argon laser source onto an equivalent spot diameter, producing no noticeable effect. Furthermore, we have operated $Ba_2NaNb_5O_{15}$ at power densities in excess of 10 megawatts/cm^2 at 1.065 microns alone, with no noticeable deterioration of any kind. Only when the $Ba_2NaNb_5O_{15}$ crystals have been properly phase matched for maximum green power generation has damage of the type mentioned above been observed.

A second cause for damage has been postulated on the basis of the stimulated Brillouin effect. Strong stimulated Brillouin scattering is produced when high intensity optical beams are focused into a crystalline lattice, such that intensification of acoustical phonons is possible under proper phase matching conditions. Whenever the acoustic nonlinearities of the material are sufficiently large, it is possible at some value of optical input signal to exceed the elastic limit of the material, producing irreparable damage. Generally, whenever such an elastic limit has been exceeded with pulsed, Q-switched lasers, an audible snapping noise, together with a flash of scattered light has been observed. Since we have never witnessed such audible signals during the onset of surface damage to $Ba_2NaNb_5O_{15}$, we are not fully convinced that stimulated Brillouin scattering alone is responsible for damage. Presently, we are attempting to determine what phase-matching conditions are being met which would suggest such

effects, even though the intensity produced on a CW basis may fall beneath the audible level. In addition, there is no reason to conclude that such acoustic effects lie within the audible range.

Returning to the conjecture that multiple photon effects may predominate, it is also noteworthy to add that we specifically searched for any possible signs of forward-scattered light at the 0.355 micron wavelength corresponding to sum frequency generation between photons at 1.065 and 0.533 microns. Using proper filtering and an S-4 photomultiplier cathode surface, we were unable to detect the presence of 0.355 micron radiation, even with a sensitivity of 10^9 beyond the level required to detect 0.533 micron radiation. This was true despite the production of surface damage during 15 to 20 consecutive runs.

Fig. 1 Damage produced during external SHG.

Fig. 2 Damage produced during intracavity frequency doubling with TEM_{00} mode laser system operated at 150 cm semi-confocal geometry.

Fig. 3 Damage produced during intracavity frequency doubling with TEM_{00} mode laser system operated at 150 cm semi-confocal geometry.

450-417 O-71—8

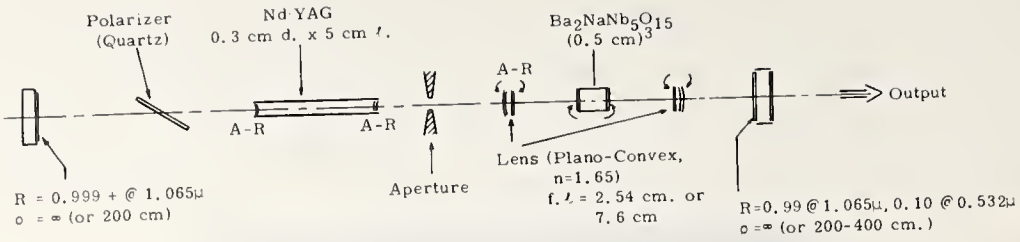

Fig. 4 Schematic diagram of laser system used to convert 100% of available TEM_{oo} mode power into SHG output.

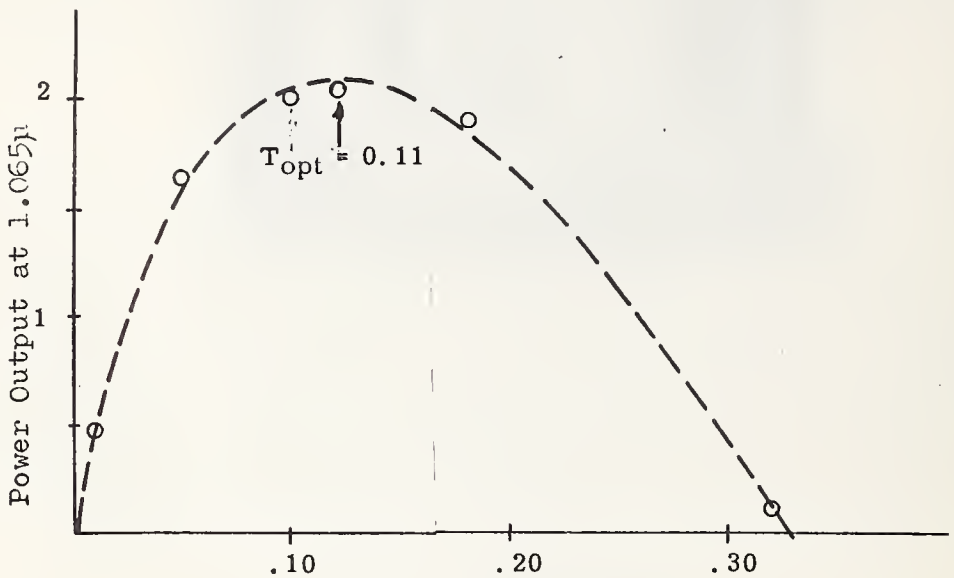

Fig. 5 T, Mirror transmission.

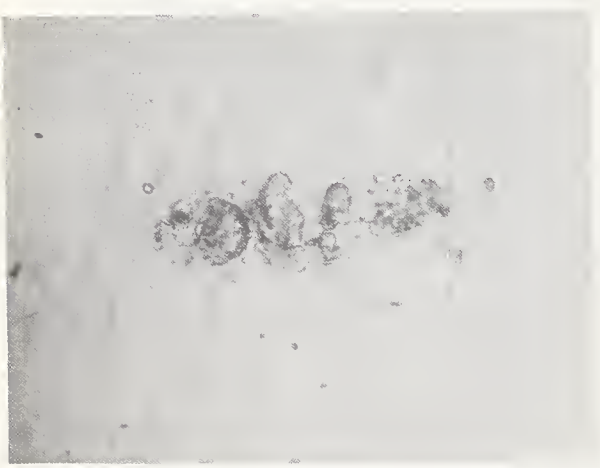

Fig. 6 Surface damage produced during focused intracavity experiment.

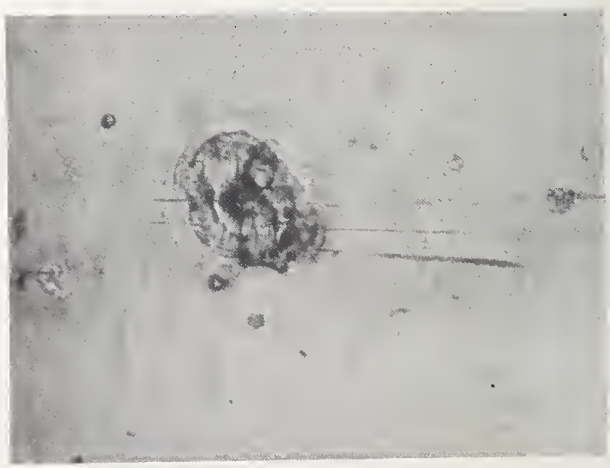

Fig. 7 Surface damage produced during focused intracavity experiment.

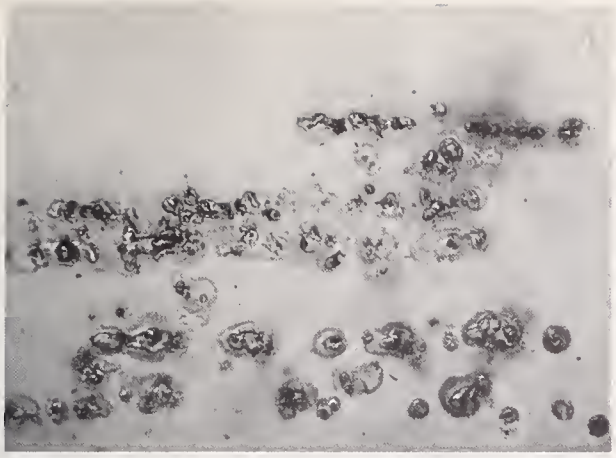

Fig. 8 Surface damage produced during repeated intracavity experiment.

Fig. 9 Surface damage produced during repeated intracavity experiment.

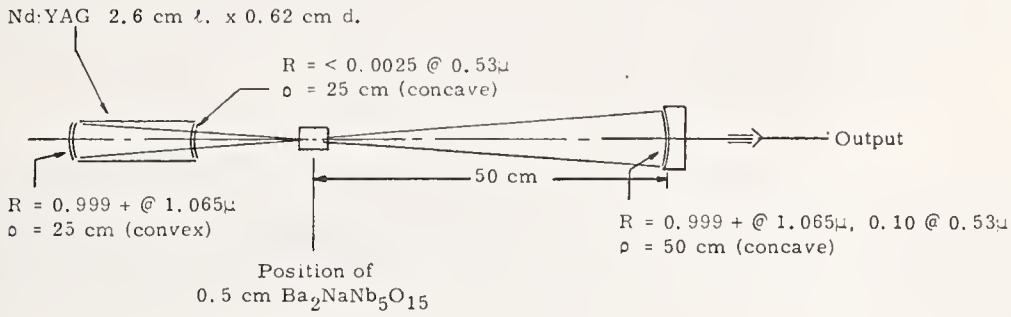

Fig. 10 Low loss cavity configuration.

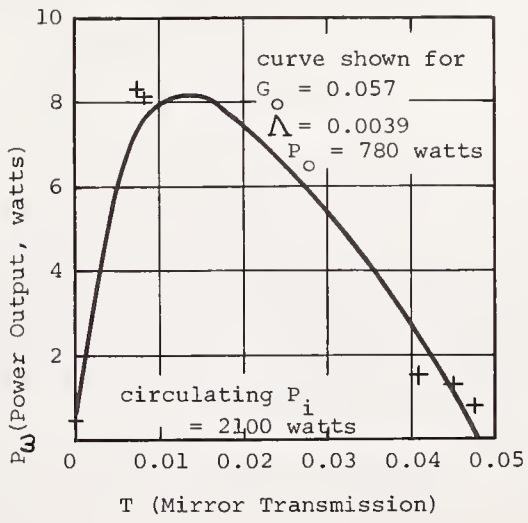

Fig. 11 P_w vs T for low loss cavity.

Investigation of Damage in Laser Glass*

Chiyoe Yamanaka, Takatomo Sasaki, Masanobu Hongyo
and Yasuaki Nagao[1]

Osaka University
Yamada-Kami, Suita
Osaka, Japan

Experiments on laser glass damage were performed to clarify the damage mechanisms and to obtain the information of the most preferable glass for a high-power laser system. For the testing method, passive and active tests were adopted. The plasma formations were always observed in internal and surface fractures. To investigate the plasma behavior, time-resolved photographic and spectroscopic methods were used. The plasma in the glass interior continued longer than that on the surface. The damage threshold on the entrance surface was larger than on the exit surface. The chemical strengthening treatment had some effect in protecting the damage growth on the surface.

The mechanism of fracture in laser glass seems to be due to the plasma formation by light which produces a shock wave to cause a cleavage in the glass.

Key Words: Breakdown plasmas, bulk, laser induced damage, passive and active testing, spectroscopy, surface, surface finish.

1. Introduction

To construct a high-power glass laser system, the characteristics of laser glass are very important, especially high durability against damage. It is reported that present laser glasses can withstand over 1000 J/cm^2 with a long pulse of about 1 ms; however, the energy passage of several tens of J/cm^2 in a short pulse of 10 ns may lead to fracture.

These results seem to show that the fundamental process of fracture can be explained by the energy balance between the laser-supplied energy and the energy lost in the glass.

Laser light can produce free electrons in glass through the multiphoton absorption process. If the energy balance between gain and loss becomes unstable, these electrons will be accelerated by the inverse bremsstrahlung and cause cascade yields of ionization. Once the plasma is produced, the shock wave due to laser-supported deflagration will be driven into the solid. This induces the cracks when the shocked stress becomes larger than the fracture threshold. In a longer duration of the laser pulse, much more energy may be necessary to heat up the plasma which is growing with time. The mechanical strength of glass has also an important role in the growth of damage in solids.

We performed the experiments on glass damage by a Q-switched laser. As for the methods of damage testing, a passive test was performed only by laser irradiation of samples, and an active test done under laser pumping conditions. In section 2, the results of the passive tests are presented. The damage threshold of platinum included and a nonincluded surface is given. The results of the active test are shown in section 3. The plasma formation was always found whenever the damage was induced. The plasma in the glass interior continued longer than that on surface. To investigate the plasma behavior, time-resolved photographic and spectroscopic methods were used. In section 4 the improvement of the damage threshold is described. The damage threshold on the surface was increased by the treatment of hydrofluoric acid. This chemical strengthening treatment seems to have some effect in preventing the damage growth on the surface.

---

* Read at the Symposium on Damage in Laser Materials by Arthur H. Guenther.

[1]Department of Electrical Engineering, Faculty of Engineering.

2. Damage by Passive Test

The method was to focus the glass laser beam onto samples by using lenses. Figure 1 shows the experimental set up. The oscillator glass rod, which was 10 mm in diameter and 150 mm in length, was pumped by a 2 kj linear flash tube. The reflectivity of the output mirror was 60%. The rotating mirror (24,000 rpm) was used in Q-switching and a calibrated beam splitter - photodiode - Tektronix 519 combination was used to measure the beam energy and pulse duration respectively. Calibration was accomplished with TRG 107 calorimeter. The average output power was about 30 MW in peak power and 25 ns in half width. The beam divergence was 2 milliradians. To regulate the power density of a focal spot, we used lenses whose focal length was 6.5 cm and 3 cm. The size of the focal spot was determined by measuring the diameter of the damage spot in aluminum foil and a copper target with a microscope. Both values fairly fit each other.

2.1. Internal Damage

a. Damage by Pt Inclusions

It was believed that micro particles of platinum existed in glass made in a platinum crucible, and that these particles served as damage sites during the passage of intense laser beams. [1,2][1] As the included particle was highly absorbent of the laser beam, a discoid fracture [3] was introduced in the glass.

To clarify the effect of inclusion, we purposely doped 10 ppm and 100 ppm platinum into barium crown glass samples which had 15 x 15 mm^2 cross section. When these samples were illuminated by a He-Ne gas laser, many scattering centers were observed. These are due to the doped platinum particles. Figure 2 shows the damage of this 100-ppm sample. The focal point of irradiation was only in a specimen near the exit surface of the laser beam. The plasma was generated at the sites where platinum particles existed. The damage threshold was 12 ± 3 J/cm^2. The same threshold was obtained with the sample of 10 ppm platinum in which the scattering centers were fewer. When we compared barium crown glass, flint glass, and sodalime glass, the damage thresholds showed no difference, but the size of fracture in flint glass was the largest. This seems due to the elastic properties of glasses.

b. Internal Damage Without Inclusions

To avoid the effect of self-trapping, we used a lens whose focal length was 3 cm. Barium crown glass samples which had no scattering centers were used. The damage threshold was up to 400 J/cm^2 and was not affected by the material of the crucibles, either platinum or clay, nor by the existence of Nd_2O_3.

Figure 2 shows the plasma light due to internal fracture. The damaged area was in a form of crushed pit of several mm in diameter.

Figure 4 shows the framing pictures of the breakdown plasma in the bulk. The plasma light in the bulk continued during 1 msec after laser irradiation. On the surface it continued at most during 50 μsec. Figure 5 shows the spectroscopic photograph of the internal breakdown. In this case, we could not find any line spectra. Figure 6 indicates the time sequence of plasma light. The half width of maximum height was about 10 μsec. The plasma in the interior glass samples continued longer than that of the surface glass.

c. Surface Damage

Figure 7 shows a picture of an exit surface fracture. The laser beam came from left to right. The focal point was in the sample near the exit.

By increasing laser power, the plasma light on the entrance surface increased slightly, whereas that on the exit surface developed remarkably. The fracture on the exit surface was more serious than that on the entrance surface and produced a network of cracks around the plasma epicenter. Figure 8 shows the fracture on both surfaces after several shots. As the plasmas tend to travel toward the direction of the incident laser beam, formation of a shock wave on the exit surface seems to be much stronger for inducing heavy fractures.

We used the barium crown glass samples with 15 x 15 mm^2 cross section and a lens of 6.5 cm focal length. Whenever the fracture was observed, plasma always formed. The damage threshold on the entrance

---

[1]Figures in brackets indicate the literature references at the end of this paper.

surface was about 28 ± 5 J/cm^2. The threshold was decreased by successive irradiation to the same site. The threshold depended upon materials and surface conditions, especially microcracks [4] and impurities on the surface.

The threshold on the entrance surface was a little larger than that on the exit surface. If we used long samples with a long focal lens, the threshold on the exit surface decreased due to self-trapping. [5]

Figure 9 shows the streak picture of the plasma light on the exit surface. The line on the left side indicates the second harmonics of glass laser light which shows the temporal sequence. Plasma light became most intense just after irradiation by the laser beam. The expansion velocity was about 5 x 10^6 cm/sec. Figure 10 shows the framing picture of the breakdown plasma on the exit surface. The exposure time was 0.5 μsec. The laser beam traveled from left to right. After 20 μsec, small pieces of hot glass burst out from the surface.

Figure 11 indicates spectroscopic photographs of surface breakdown, where (a), (b) correspond to barium crown glass and light flint glass respectively. These were exposed to ten shots. Items (c) and (d) are the spectrum of air breakdown by laser beam and the reference lines of Hg, respectively. All broad dim lines in (a), (b) were attributed to spectra of air. From this, it shows that the air is ionized by the plasma of the glass. Figure 12 is the densitometric spectrograph of the breakdown of barium crown glass. The line spectra of Ba^+ were observed intensely. Figure 13 shows the time variation of Ba^+ (4,554 Å), Ca^+ (3,968 Å) and N_2 (5,011 Å). The rise time of the emission of N_2 was slower than that of metallic ions. This shows that the deflagration wave is driven to the laser beam. The plasmas continued about 1 μsec at half width of maximum height.

3. Damage by Active Test

The effect of pumping light can be considered as one of the additional damage mechanisms in laser glass. The glass rods used as test samples, 20 mm in diameter and 300 mm in length, were made of sodalime glass and barium crown glass, containing 5 wt% and 3.5 wt% Nd_2O_3 respectively, and were excited by four linear flash tubes. (Pumping power 10 kj.) These were set as the third-stage amplifier of a laser system. The input power of the laser beam was 30 J/cm^2 in maximum. A sodalime glass rod which had many scattering centers (platinum inclusions), showed the internal fracture at 2 J/cm^2. As the input power increased, damage spots increased in number. This damage threshold was somewhat smaller than that which resulted from the passive test. In this case, the excited state absorption from the $4F_{3/2}$ level of the Neodymium ions was large enough to cause a significant conversion of laser energy to heat to induce fracture through Pt inclusions. [6] But the barium crown glass rod, which contained no scattering center, showed that the damage threshold was almost the same as the passive test. A careful treatment to eliminate PtO_2 to reduce the platinum inclusion succeeded. This barium crown glass showed very few damages at the energy of 15 J/cm^2 in the early period of operation, and after the initial fracture it could endure up to the threshold of surface damage 28 J/cm^2 without any internal damage.

We noticed sometimes that very small cracks due to inclusion in the barium crown glass rod disappeared in time. Some cracks gradually decreased in diameter and after a few days could not be observed. Other cracks immediately vanished after two or three shots. As the crack always suffers the restoring force from the surroundings if the crack is very small, these curing phenomena can be expected. These phenomena suggest that the plasma formation often can occur without permanent impairment of glass rod. It should be mentioned that the permanent damage is introduced by the displacement of ions due to shock impulse.

If the mechanical strength is strong enough to endure the shock impulse, the damage is determined by the plasma heating destroying the atomic arrangement. But the glass is usually brought into mechanical failure in the brittle region under the Q-switched operation.

As for the damage threshold, the pulse duration of the laser has remarkable influence. If G is the energy per second gain from the laser, L is that lost to surroundings, and S is the apparent specific heat, the time t to the ultimate shock formation of temperature T_s is given by

$$t = \frac{1}{G}\left(\int_{T_o}^{T_s} S dT + Lt \right)$$

where T_o is the room temperature, Ts is set at 3000°K and L is very small in the early period. In some amorphous solids [10] like glass the conduction electron has strong interaction with atoms through trapped electrons. The apparent specific heat is assumed to be proportional to the conduction electrons N which are produced by cascade ionization, as $N = N_o \exp(ct)$ and $S(N_o)$ is the order of 0.1 cal deg^{-1} g^{-1}. The avalanche of electrons is increased in factor 10^4 from the initial electrons N_o produced by multiphoton absorption during a laser pulse. A qualitative behavior of energy balance is shown in Fig. 14.

4. Improvement of Damage Threshold

When the glass was very carefully manufactured, most of the platinum inclusions could be eliminated. Even if few inclusions make fractures in laser glass, this is not practically serious. But the damage on the surface is a very important limitation [7] for operation.

There seems to be two methods to raise the damage threshold. One is treating the glass either by a hydrofluoric acid [8] or by dimethyldichlorsilane [9]. In the case of the acid etch, it is considered that small surface irregularities and cracks are smoothed over, thus making the surface stronger to damage. We used the barium crown glass which was immersed for 10 minutes in 10 % hydrofluoric acid. The damage threshold on entrance surface increased from 28 $\pm$ 5 J/cm^2 to 40 $\pm$ 5 J/cm^2.

Another is chemical strengthening treatment. This method is to diffuse larger atoms into the small alkali matrix. This method was so remarkable to increase the mechanical strength but the effect of laser damage was less effective to the present. This may be caused by the fact that the strengthen depth was almost equal to the damage depth of surfaces.

5. Conclusions

We performed the experiments of glass damage by Q-switched laser beam to investigate the damage mechanisms.

The main conclusions are as follows:

1. From the passive test, we determine the damage threshold of platinum-inclusion, platinum-free, and surface effects of barium crown glass. They were 12 $\pm$ 3 J/cm^2, 400 J/cm^2 and 28 $\pm$ 5 J/cm^2, respectively.

2. It is desirable to use the glass matrix which is mechanically strong in order to protect the growing damage.

3. Platinum included glass sample showed the difference of damage thresholds between passive and active test but platinum-free glass had the same threshold.

4. The plasma formation was always observed whenever the damage was induced. The mechanism of damage will be mainly due to the shock impulse from plasma.

5. The fracture on the exit surface was more serious than that of the entrance surface. The shock wave caused by plasma on the exit surface will be more effective in producing damage.

6. Time-resolved photographic and spectroscopic methods were adopted to investigate the plasma behavior. The plasma in the interior of the glass lasted longer than that on the surface.

7. The damage threshold on entrance surface increased from 28 $\pm$ 5 J/cm^2 to 40 $\pm$ 5 J/cm^2 by the treatment of hydrofluoric acid.

8. The chemical strengthening treatment will have small effect on the damage growth on the glass surface.

6. Acknowledgements

We thank Dr. T. Izumidani of the Technical Laboratory of HOYA Glass Company for preparing various glass samples for testing and also Mr. M. Ishiyama of Research Laboratory of the Asahi Glass Company for his cooperation.

7. References

[1] Yamanaka, C., et al, IQEC 20-3, 404 (1970).

[2] Avizonis, P.V. and Farrington, T., Appl. Phys. Letters, 7 205 (1965).

[3] Young, C.G., Proc. IEEE 57 1267 (1969).

[4] Fersman, I.A. and Khazov, L.D., Soviet Phys-Tech. Phys. 15 834 (1970).

[5] Davit, J., Damage in Laser Glass, ASTM STP 469 100 (1969).

[6] Vance, M.E., IEEE J. Quant. Elec. QE-6 249 (1970)

[7] Swain, J.E., Damage in Laser Glass, ASTM STP 469 69 (1969).

[8] Swain, J.E., J. Quant. Elec. QE-4 362 (1968).

[9] David, J., Decoux, J., Gautier, J., and Souli, M., Revue de Physique Applique 3 118 (1968).

[10] Frohlich, H., Proc. Roy. Soc. A 188, 521 (1947)

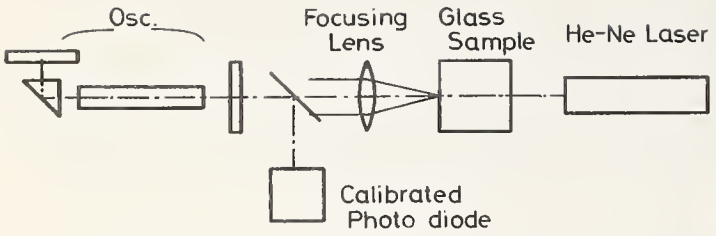

Fig. 1 Experimental arrangement of laser glass damage (passive test).

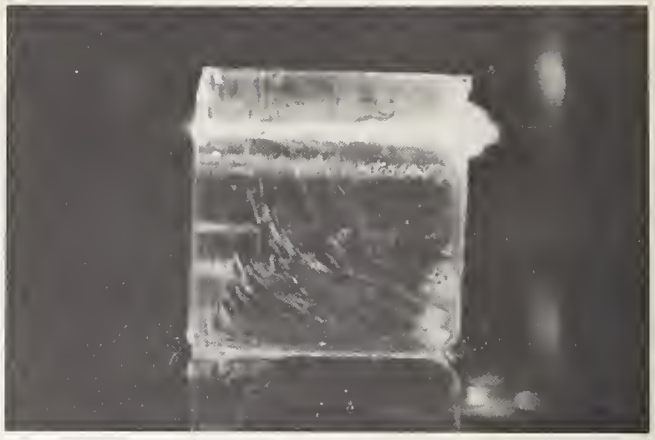

Fig. 2 Fractures in barium crown glass included platinum 100 ppm. (laser beam is from right to left).

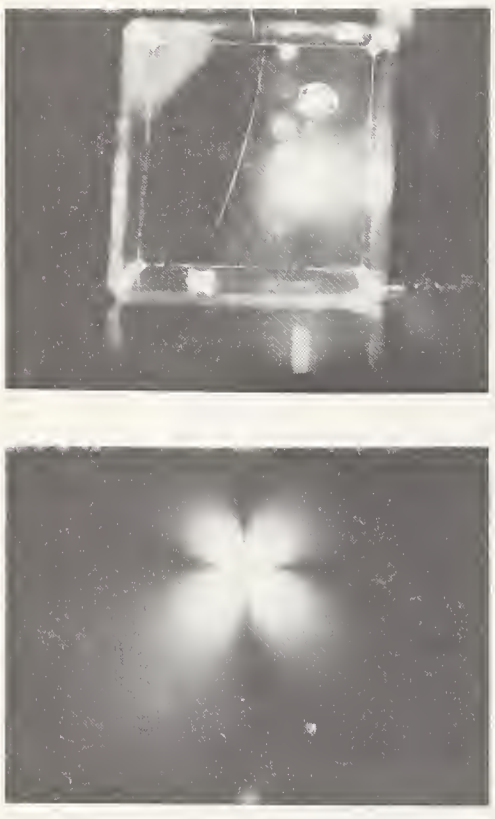

Fig. 3 (a) Internal fracture in barium crown glass. The bright spot in the middle of the sample shows plasma formation. Another spot above this spot indicates the fracture after damage. And (b) interference stress pattern.

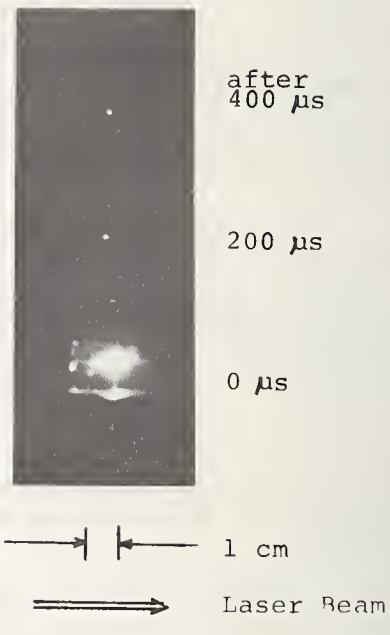

Fig. 4 Framing photograph of inner breakdown in barium crown glass.

Fig. 5 Time integral spectrum of bulk breakdown plasma.

a

b

Fig. 7 (a) Exit surface breakdown of barium crown glass without inclusions. (b) Interference stress pattern on surface.

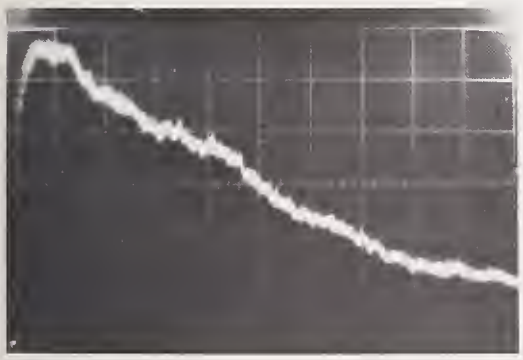

Fig. 6 Time trace of plasma light of bulk breakdown. (2 μs/div.)

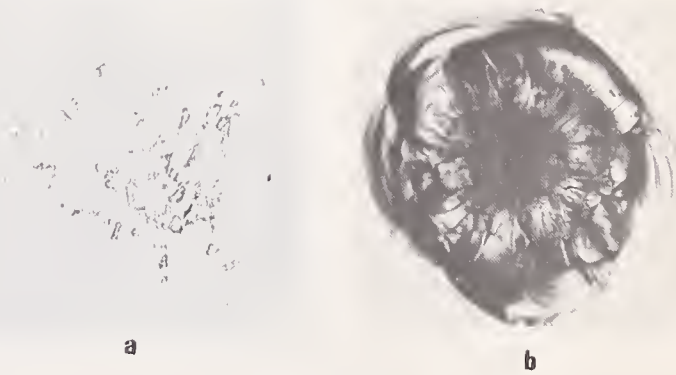

a b

Fig. 8 (a) Fracture on entrance surface and (b) exit surface (after several shots).

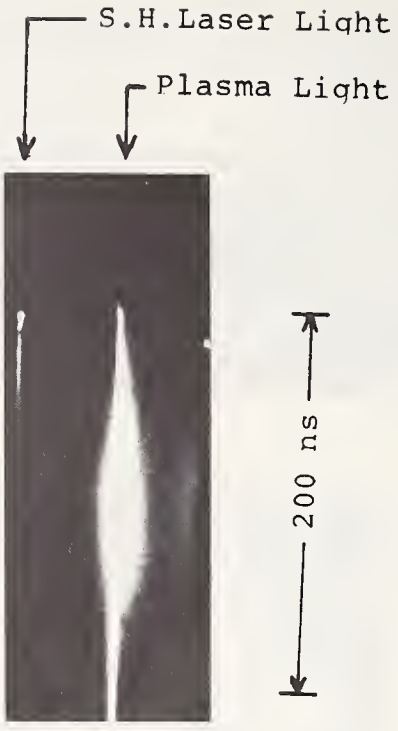

Fig. 9 Streak photograph of exit surface breakdown of barium crown glass.

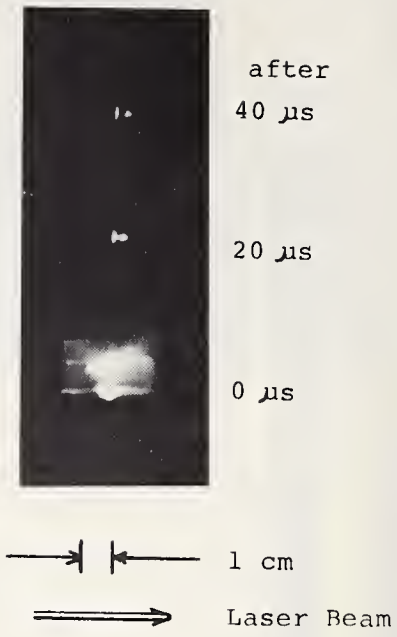

Fig. 10 Framing photograph of exit surface breakdown of barium crown glass.

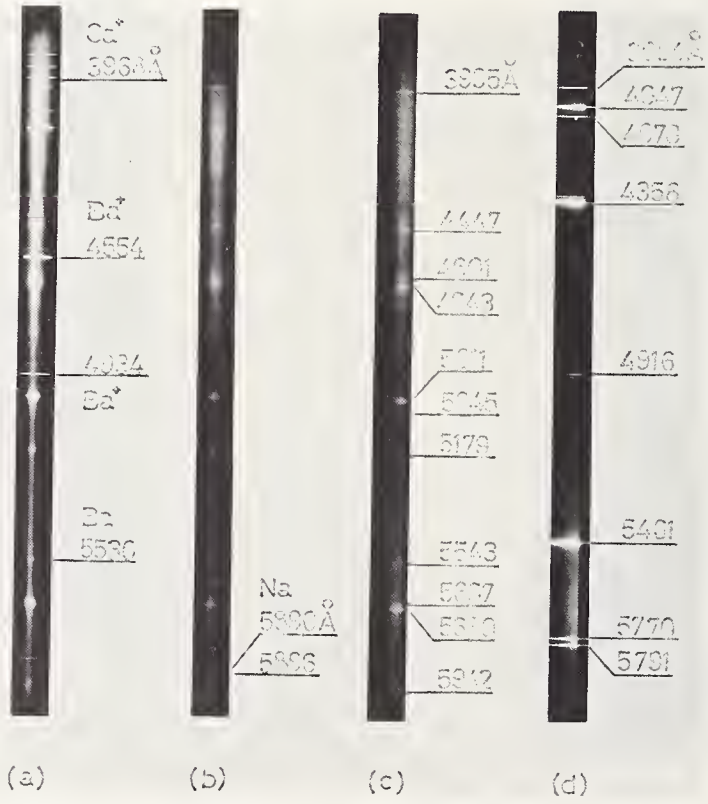

Fig. 11 The spectra of surface breakdown plasmas (a) barium crown glass, (b) light flint glass, (c) air, and (d) Hg.

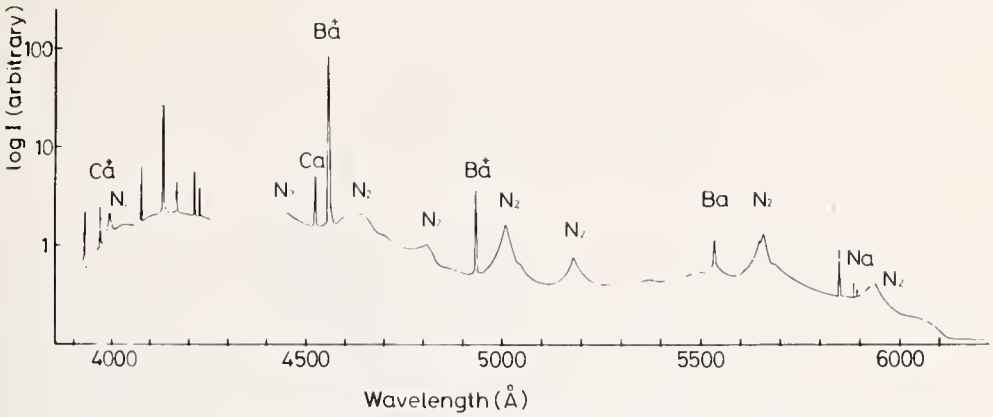

Fig. 12 Densitometric spectrograph of barium crown glass fracture.

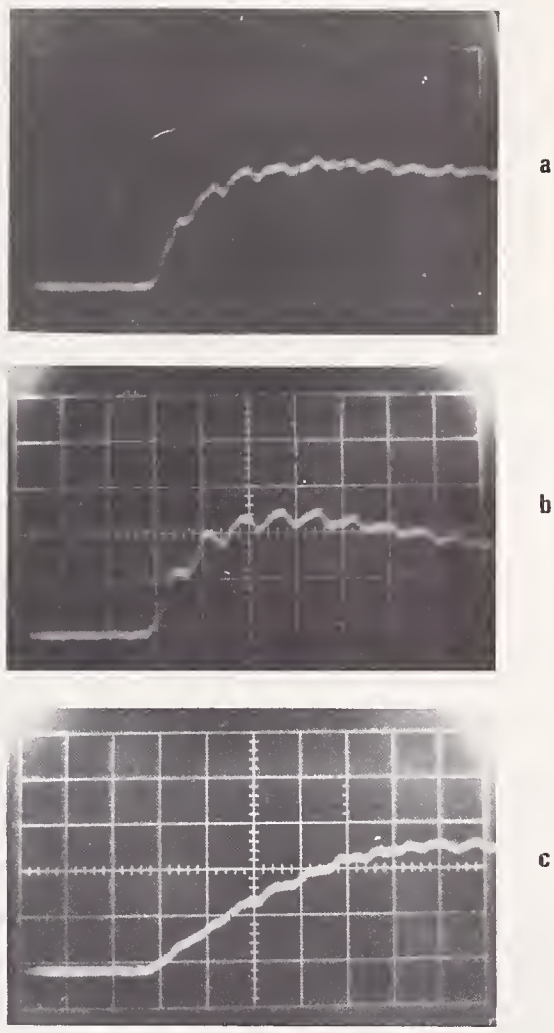

Fig. 13 Time trace of various line spectra (50 ns/div.). (a) Ba^+ (4.55 Å), (b) Ca^+ (3,968 Å), and (c) N_2 (5,011 Å).

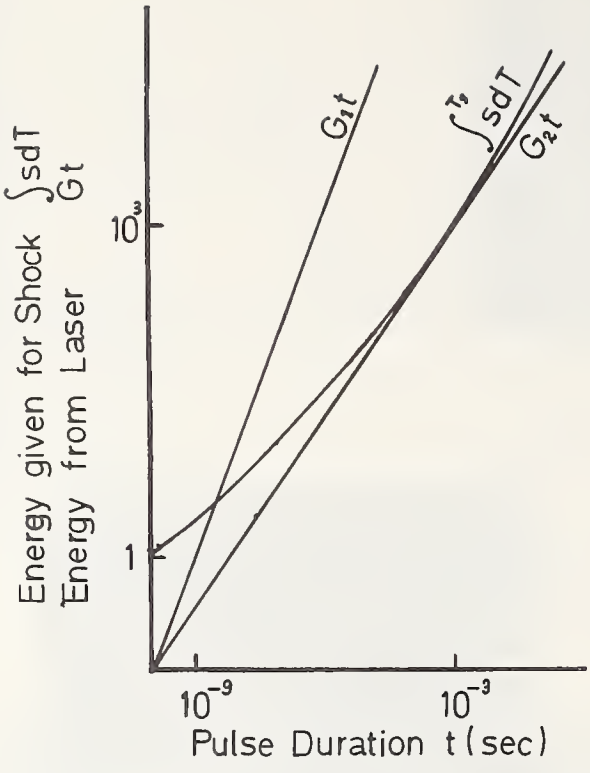

Fig. 14 Characteristics of internal damage due to various laser pulse durations.

COMMENTS ON PAPER BY YAMANAKA

It was suggested that individuals interested in the effect of surface cleanliness of optical elements on the laser-induced-damage resistance, review the paper by I. A. Fersman and L. D. Khazan, Sonet Journal of Optical Technology, 37, P. 627, (1970).

Direct Nondestructive Measurement of Self-Focusing in Laser Glass

Brian E. Newnam and L. G. DeShazer

Departments of Physics and Electrical Engineering
University of Southern California
Los Angeles, California 90007

A nondestructive technique is described which we have used to measure self-focusing in a borosilicate crown glass. It is a direct method in the sense that we observe the time evoluation of only the self-focusing of the transmitted laser pulse. The power of the input pulse is limited to prevent a self-focus from occurring within the test material, and the measurements are performed before the onset of damage or other stimulated processes. This is in contrast to other methods which measure the effects of self-focusing by damage tracks and stimulated inelastic scattering. By comparing the temporal shape of the transmitted pulse on-axis with the input pulse, we construct the nonlinear response curve of the test material which can be compared directly to the numerical solutions of the nonlinear wave equation which describes large scale self-focusing. Assuming the response of the medium is sufficiently fast, the critical power P_c and the nonlinear refractive index n_2 may then be calculated without postulating a particular physical mechanism(s) causing self-focusing. For a ten nanosecond (FWHM) pulse at 6943 Å, the preliminary results for BSC-2 glass are $P_c = 0.9$ MW and $n_2 = 2 \times 10^{-13}$ esu.

Key Words: Critical power, glass, nonlinear index, pulse sharpening, self-focusing.

1. Introduction

Many researchers have reported observations of very small diameter damage tracks in transparent dielectrics when irradiated with short duration, intense laser pulses. The input laser intensities at which damage occurs (to the bulk or at the exit surface) have been significantly lower than those expected unless the local index of refraction is assumed to be a function of the intensity. A sufficient amount of evidence has been accumulated in favor of a self-focusing phenomenon, and a nonlinear refractive index coefficient, n_2, is used to account for it. The evidence heretofore has consisted of damage tracks, induced birefringence, stimulated inelastic scattering, and frequency broadening. These important results are the effects of self-focusing on materials.

We have developed a non-destructive technique with which we have successfully measured the self-focusing process itself in a borosilicate crown glass (Corning BSC-2). It is a direct method in the sense that we observe the time evolution of only the self-focusing of the transmitted laser pulse. Furthermore, the power of the input pulse is restricted to prevent a self-focus from occurring within the test material, and the measurements are performed before the onset of damage or other stimulated inelastic processes. This measurement technique, which will be described in Section 2, was first used by McAllister [1] to accurately measure the critical power, P_c, and nonlinear index of refraction of several organic liquids. The laser source and experimental system which we assembled for the present tests will be described in Section 3. The results of our tests in BSC-2 glass are given in Section 4 and discussed in Section 5.

2. Measurement Technique

It was suggested by Marburger and Wagner [2] that a substantial sharpening of the on-axis time contour should occur during self-focusing. Subsequently, a measurement technique was developed to observe this temporal behavior [3, 4]. The time evolution of this sharpening is schematically demonstrated in Figure 1. Thus, the spatial focusing of the laser pulse can be directly measured by comparing the temporal pulse shape of the transmitted axial intensity at the exit face of the nonlinear material with that at the entrance face.

The distortion of the on-axis intensity pulse may be regarded as arising from the nonlinear response function or "characteristic curve" of the medium. From a single oscillogram of the axial

intensity versus time for the input and transmitted pulses, the characteristic curve may be constructed as shown in Figure 2. This curve is then compared to the theoretical characteristic curve obtained from numerical solutions of the self-focusing equation [5]. The solutions, of course, depend on the beam parameters of the input pulse and the length of the nonlinear material being tested. By scaling the experimental curve to fit over the theoretical curve, the critical power for self-focusing of a Gaussian equiphase beam at infinity is obtained. This critical power P_c is related to n_2 by

$$P_c = (1.22\lambda)^2 c/128\, n_2 ,$$

where

$$n = n_o + n_2 \langle |E|^2 \rangle .$$

n_o is the linear refractive index, and E is the peak electric field strength with the brackets denoting a time average over many cycles [6].

3. Experimental System

Self-focusing depends critically on the transverse intensity distribution within the focusing beam. Accordingly, most of our efforts were directed toward constructing a laser oscillator and amplifier system which produces both smooth spatial and temporal intensity profiles which are approximately Gaussian. The laser source and experimental arrangement which we use to measure self-focusing in solids is illustrated in Fig. 3. This system features a passively Q-switched ruby laser oscillator operating in a single longitudinal and transverse mode with a peak power of 1 MW in a nominal 10 nsec pulse. Single longitudinal mode control is obtained by use of a glass etalon (R = 15%) at the output end along with a cryptocyanine in methanol solution in the Q-switch cell. Transverse mode control is obtained by use of a 1.12 mm diameter polished carbide wire die aperture placed just inside the output etalon and a cavity length which sets the Fresnel number at 0.45 [7].

The amplifier was placed in the far field of the oscillator where the spatial intensity profile of the beam is smooth and nearly Gaussian. This profile is accurately determined by scanning the beam with a pinhole, which measures power versus time for each radial position. By use of these pinhole scans the alignment of the oscillator was precisely adjusted so that the temporal pulse shape was the same over nearly all of the beam. Figure 4 shows the oscillator spatial output at the amplifier.

The amplifier rod is a 1/4 x 6" ruby, 0.05% Cr doping. For a flashlamp pumping of 3 kJ, the weak signal gain was 45, and a 20 MW pulse of single mode output was obtainable. We found it necessary to focus through the amplifier with a long focal length lens in order to obtain a smooth far-field pattern from the amplifier (Fig. 5). After the amplifier the beam was recollimated. Before striking the sample, four percent of the pulse was reflected into a 35 nsec optical delay path which directed it into the same ITT F4000 photodiode as the transmitted pulse, both of which were displayed on a Tektronix 519 oscilloscope. The delayed pulse gave the temporal pulse shape and power level of the pulse entering the glass sample. The energy of the amplified pulse was monitored with a RCA 7102 photodiode and calibrated with a TRG ballistic thermopile.

Because the amplifier effect on the pulse's phase front depends on the level of flashlamp pumping, we used the same power supply voltage for each shot. To control the net power level without deflecting the beam we used a variable attenuator (aqueous solutions of $CuCl_2$) between the oscillator and amplifier. The test sample was a 40 cm long Corning BSC2 (517-645) glass rod of high optical quality. The ends were polished smooth and optical flat. This long sample permitted significant self-focusing to take place for moderate input powers so that damage to the entrance surface was avoided. An optional reducing collimator may be used to measure the dependence of self-focusing on input spot size. Without the collimator the 1/e intensity radius of the input beam was 0.5 mm.

At the sample exit surface, we placed a 94 micron dia. pinhole consisting of a section of tapered, thick-walled glass capillary tubing with a polished (tilted) entrance face. This was centered $\pm$ 0.02 mm on the axis of the transmitted pulse by monitoring the peak transmitted intensity at different transverse points on a number of shots. The light passing through the pinhole was properly attenuated before striking the photodiode in order to fit the pulse trace on the oscilloscope scale.

4. Experimental Results

An oscillogram of the axial portion of the self-focused pulse transmitted through our 40 cm long glass rod is shown together with the input pulse (delayed) in Fig. 6. The very pronounced sharpening of the transmitted pulse was measured only when the pinhole was centered on the axis at the exit fact. With the pinhole removed, the entire transmitted pulse was detected and its temporal shape was identical to that of the input. The peak input power was 5.5 MW in a 11.8 nsec (FWHM) pulse, and the 1/e radius of the input intensity profile was 0.5 mm. The peak intensity at the entrance face was 0.7 GW/cm^2; no damage to the glass occurred on this shot. Subsequent tests at higher powers caused a damage pit at only the exit surface which precluded our obtaining additional valid results. We are presently repeating the measurement to obtain a sharpened pulse properly attenuated to fit within the ordinate scale of the oscilloscope trace. The off-scale peak of the pulse presented here was an estimate. From preliminary calculations with the present data we have determined P_c to be 0.9 MW and n_2 to be 2×10^{-13} esu. This value of n_2 is comparable to that (2.7×10^{-13} esu) measured by Duguay and Hansen [8].

5. Discussion of Results

In these experiments neither stimulated inelastic scattering or filament formation in the bulk occurred since the input power was limited to prevent the self-focal point from occurring within or near the exit surface. Damage and backward stimulated Brillouin scattering would have been detectable by the photodiode. In addition, saturation of the nonlinear refractive index did not occur since the 6943 Å ruby laser wavelength is not near an absorption resonance. Linear absorption effects, which are small at this wavelength, may be taken into account [5].

Additional evidence that the observed on-axis temporal pulse sharpening is due only to self-focusing can be obtained by measuring the off-axis intensities. We did not have time to perform these measurements for glass, but we illustrate the point by using previous measurements on nitrobenzene [8]. In Figures 7 - 9 we show oscillograms of power versus time in which the pinhole was alternately placed at three positions at the output face of a cell of nitrobenzene. The transmitted pulse (leading) on-axis (Fig. 7) is seen to be very sharpened with a pulse width (FWHM) 0.5 that of the input pulse (delayed). When the pinhole was placed off-axis at 1/4 the input intensity radius a_o we observed a pronounced dip (Fig. 8). The minimum of the dip occurred just when the on-axis power was the greatest. With the pinhole at 0.5 a_o the transmitted power remained at a low level (Fig. 9). At the entrance face of the nonlinear liquid cell, however, the input intensities at $r = 0.25\ a_o$ and $0.5a_o$ were 90% and 75% that on-axis, respectively. It is evident that energy was swept from the edges of the beam into the center as the input intensity increased, and vice versa. Additionally we found that the off-axis characteristic curves prepared from these data compare very well with the corresponding curves generated from self-focusing theory.

The numerical solutions of the nonlinear wave equation which we use to obtain the theoretical characteristic curve corresponding to our measurement parameters are exact if the physical mechanism(s) which cause the self-focusing are instantaneous. If the mechanisms are sufficiently fast relative to the temporal rise time of the input pulse, the optical pulse shaping method enables one to calculate P_c and n_2 without having to postulate the particular mechanisms involved. This is a distinct advantage over previous methods. To the extent that the time response of the medium is comparable to the input pulse, the values of P_c and n_2 are approximate.

If the temporal pulsewidth is considerably faster than the material response by a particular mechanism, then any self-focusing is obviously independent of that mechanism. This is suggestive of a series of tests with a large range of input pulsewidths. With our pulse shaping technique, the dependence of n_2 on pulse width may be obtained. These values may then be compared to those predicted using the various postulated mechanisms, such as electrostriction and electronic distortion, to determine which effects are important as a function of time. In addition, varying the spot size of the input spatial intensity will provide results which can be compared directly with those predicted by the electrostriction mechanism.

6. Acknowledgements

The authors are grateful to Dr. J. H. Marburger for his continuous theoretical support, and to Mr. E. A. Maunders for the excellent optical polishing of the glass rod. Support for this

research was partially provided by the Joint Services Electronics Program through the Air Force Office of Scientific Research (AFSC), United State Air Force, under Grant AF AFOSR 69-1622 and Contract F 44620-71-C-0067. The National Aeronautics and Space Administration also provided support under Grant NGR-05-018-044.

7. References

[1] G. L. McAllister, PhD Dissertation, Direct Measurement of Self-Focusing of Laser Radiation in Organic Liquids, Univ. So. Cal., 1969.

[2] J. H. Marburger and W. G. Wagner, IEEE J. Quan. Elect. QE-3, 415 (1967).

[3] G. L. McAllister, J. H. Marburger and L. G. DeShazer, Phys. Rev. Letters 21, 1648 (1968).

[4] G. L. McAllister and L. G. DeShazer, IEEE J. Quan. Elect. QE-5, 357 (1969).

[5] E. L. Dawes and J. H. Marburger, Phys. Rev. 179, 862 (1969).

[6] R. Y. Chiao, E. Garmire and C. H. Townes, Phys. Rev. Letters 13, 479 (1964).

[7] G. L. McAllister, M. M. Mann and L. G. DeShazer, IEEE J. Quan. Elect. QE-6, 44 (1970).

[8] M. A. Duguay and J. W. Hansen, "Measurement of the Nonlinear Index n_2 of Glass using Picosecond Pulses," Damage in Laser Materials, NBS Spec. Pub. 341, 45 (December 1970).

[9] G. L. McAllister and L. G. DeShazer, to be published.

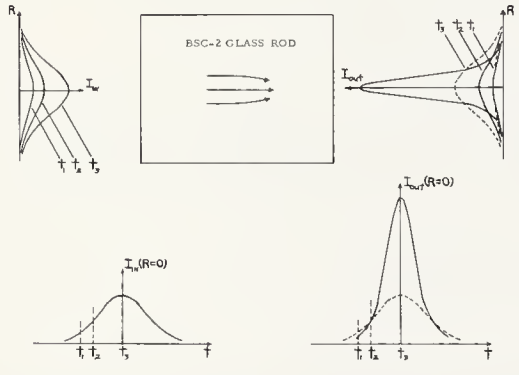

Fig. 1 Schematic diagram illustrating spatial and temporal narrowing.

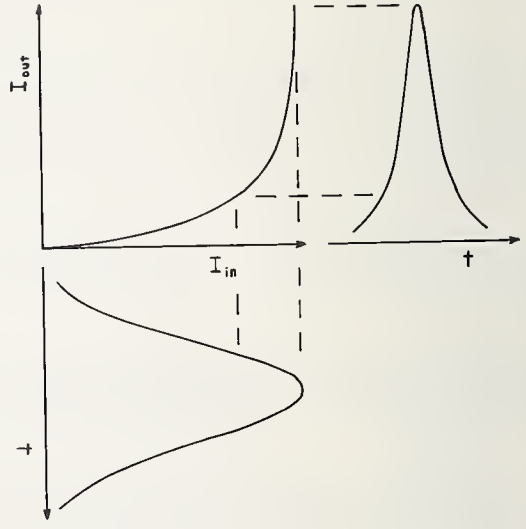

Fig. 2 Construction of the nonlinear characteristic curve from input and output axial intensity pulses

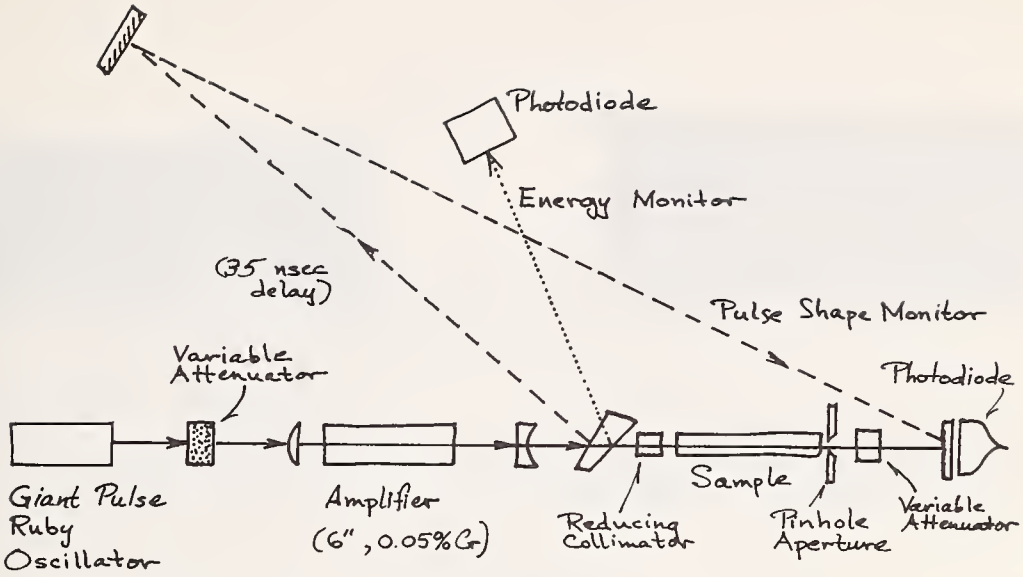

Fig. 3 Self-focusing experimental configuration.

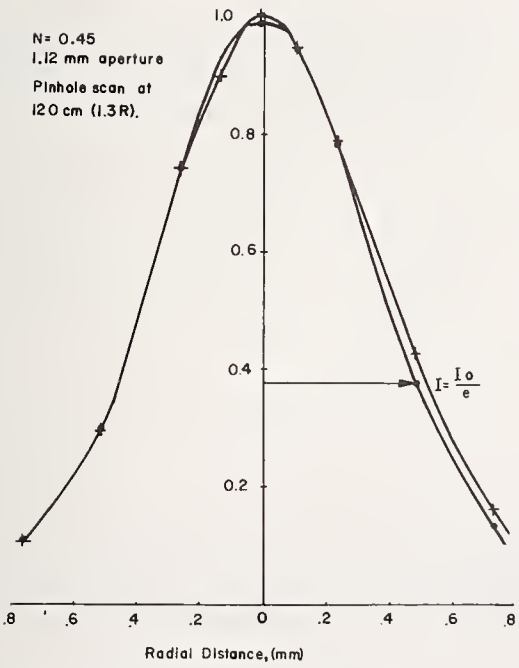

Fig. 4 Normalized oscillator intensity input to amplifier. Fresnel number N = 0.45 and amplifier is located at 1.3 Rayleigh distances from the oscillator aperture.

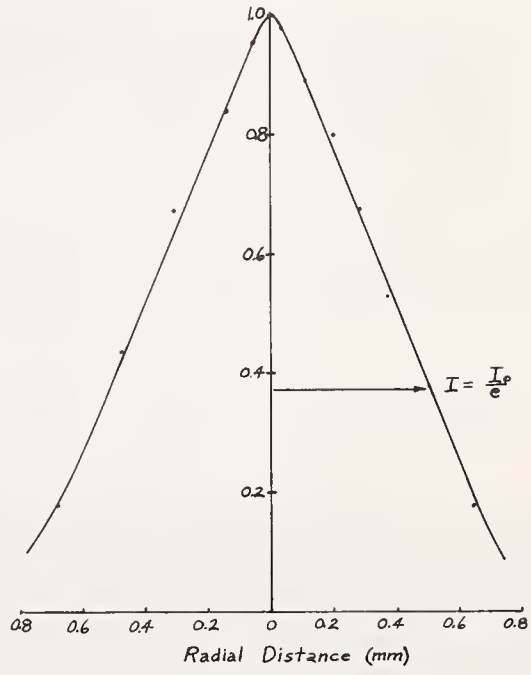

Fig. 5 Normalized amplifier intensity input to glass sample.

450-417 O-71—9

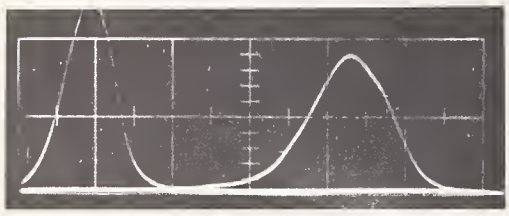

Fig. 6 Direct observation of self-focusing in BSC-2 glass. Oscilloscope trace (10 nsec/div) showing transmitted pulse at the beam center (leading pulse) and the spatially integrated reference (delayed input pulse).

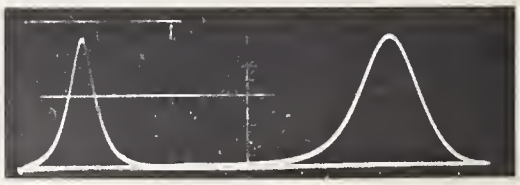

Fig. 7 Optical pulse shaping by self-focusing in nitrobenzene. Leading pulse: transmitted on-axis (r = 0). Delayed pulse: input. Scale: 10 nsec/div.

Fig. 8 Optical pulse shaping by self-focusing in nitrobenzene. Leading pulse: transmitted off-axis ($r = 0.25\ a_o$). Delayed pulse: input. Scale: 10 nsec/div.

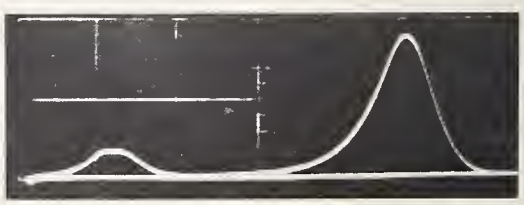

Fig. 9 Optical pulse shaping by self-focusing in nitrobenzene. Leading pulse: transmitted off-axis ($r = 0.5\ a_o$). Delayed pulse: input. Scale: 10 nsec/div.

COMMENTS ON PAPER BY BRIAN NEWNAM

The critical power P_c and n_2 values obtained for pulses of a few nanoseconds duration is a little less than that reported by Duguay at the 1970 Symposium on Damage in Laser Materials using picosecond pulses. Since additional mechanisms can contribute to the nonlinear index during the duration of the longer pulse, one would expect a higher value of n_2 to be obtained. Since several approximations were involved in obtaining the value reported in this investigation, it was not felt that the discrepancy was significant.

Ruby Laser Damage Thresholds in Evaporated Thin Films and Multilayer Coatings*

A. Francis Turner[1]

Bausch & Lomb, Inc.
Rochester, N. Y. 14602

This report describes a survey-type study of laser damage thresholds in evaporated thin films and multilayer coatings on glass substrates. Q-switched ruby lasers were employed and several common filming materials were included. In the focal plane of a 42 mm focus lens the damage thresholds ranged from 350 J/cm^2 for quarterwave films of MgF_2 or SiO_2 down to 30 J/cm^2 for quarterwave films of ZnS. Multilayer coatings generally had damage thresholds intermediate between the thresholds of their individual films.

Key Words: Bulk material damage, laser damage, multilayer coatings, quarterwave stacks, single quarterwave film, thin films, two layer coatings.

1. Introduction

The Office of Naval Research contracts referenced at the conclusion supported laser damage studies at Bausch & Lomb, Incorporated during the period 1 April 1965 - 28 February 1970. The damage thresholds for dielectric films and coatings measured during this contract work were collected and presented on January 12, 1971 to Sub-Committee II, Lasers and Laser Materials, of ASTM Committee F-1. Several numerical errors appearing in the quarterly reports on the contracts were corrected. The summary data are listed in Tables 1, 2 and 3.

2. Method

Damage thresholds were determined from a study of the damage in coated samples placed in the focal plane of a simple f = 42 mm lens. The energy in joules incident on the lens was decreased from well above to below threshold. The energy steps were selected with the help of a calibrated series of neutral density filters, the lasers always being operated under nominally constant conditions. Conversion of these energy values to energy density thresholds involved calibration of the energy density distribution in the focal plane of the lens. Calibration factors were obtained from quantitative observations of laser damage in semi-transparent aluminum films. In view of the unavoidable uncertainties in this procedure not only are the thresholds in J/cm^2 listed in the tables but also the energies incident on the lens from which these thresholds were derived. When several nominally identical samples were tested the observed minimum and maximum values only are listed. Within the accuracy limitations of the experiments (variations by a factor of 2 are not infrequent) the average of these minima and maxima may be considered to be the threshold. For any one coating there were too few samples for a meaningful statistical analysis.

The films were generally deposited on 50 x 50 x 2.3 mm glass substrates. Reasonable care was taken in cleaning them prior to deposition. The laser radiation was always incident from the air side on the coatings.

3. Equipment

All energies were measured with Lear-Siegler Model MI-2 Laser Energy Monitors. They were returned once or twice to the manufacturer for recalibration.

Two different lasers were used at different times during the contract. Their output pulse shapes were not as well defined as could be desired. Although no systematic comparison was made between them, the results from the two lasers appeared to be substantially in agreement.

---

[1] Presently at Optical Sciences Center, University of Arizona, Tucson, Arizona 85721.
*Due to illness this paper was not presented at the Third Annual Symposium on Damage in Laser Materials.

(1) Lear-Siegler LS-2 Ruby Laser with 3" x 1/4" Ruby Rod, TIR end

MH-1 Q-Switch: Multilayer dielectric coated plano output mirror: 3600 rpm

Total nominal energy per burst: 0.1 J

Typical Observed output: A series of spikes in 6 microseconds. Usually a high initial spike of 100 KW-200 KW peak was followed by spikes of much less power. Estimated spike half widths 240 nsec.

(2) Spacerays 101-6 Ruby Laser with 6" x 3/8" Ruby Rod, plano ends

Q-Switch: 25,000 rpm rotating prism
Output Mirror: Two 90° sapphire resonant reflector plates (Lear-Siegler RR-201-66)

Total nominal energy per burst: 1.5 J

Probable typical output (courtesy of the manufacturer): A series of 1 to 10 spikes in 10 microseconds. Peak powers 2 to 20 MW depending on the number of spikes. Estimated halfwidths of spikes 80-100 nsec.

4. Comments on the Entries in the Tables

4.1 Table 1 - Single QW Films

This table lists the results on quarterwave films of 13 different representative and commonly used evaporants. The thresholds cover a 10:1 range of values from about 350 J/cm^2 for SiO_2 and MgF_2 films through 200 J/cm^2 for ZrO_2 to about 30 J/cm^2 for ZnS films. (By way of comparison, aluminum films from semi-transparent to almost opaque cover the approximate range of 0.5 J/cm^2 to 5.0 J/cm^2 respectively). All the films listed were essentially absorption-free and were prepared according to good commercial practice.

The films were tested at room temperature. Not shown are the results of comparative tests of both quarter and halfwave films of MgF_2 at 77 K vs 300 K. No difference due to temperature was found.

Table 1 indicates large differences in thresholds with the chemical composition of the films. However, this may not be the primary correlation since there is also an association between higher thresholds and shorter UV wavelength absorption cut-offs of the materials.

For any given filming material the threshold decreases with increasing film thickness.

4.2 Table 2 - Two Layer Coatings

The data in Table 2 show several ways in which the damage thresholds can be affected as follows:

Firstly, an improvement can sometimes be produced by finding more optimal coating conditions, as in the Series 2 samples compared with Series 1 samples. The Series 1 samples were made in a 48" coater, all films were evaporated at a residual gas (air) pressure of 10^{-4} Torr on the glass substrates held at 125°C. The Series 2 samples were made in a 30" box coater where the pressure could be held at 10^{-5} Torr for the evaporation of the MgF_2 films. During evaporation of the ZrO_2 films oxygen was bled into the chamber to raise the pressure to 10^{-4} Torr. Furthermore, substrates were kept at 315°C throughout. The change in techniques from Series 1 to Series 2 tripled the threshold values.

The halfwave/quarterwave construction GHHLA represents an anti-reflection coating with two minima, one of which, when using ZrO_2 and MgF_2 films, can be reduced to zero by making the MgF_2 10% thinner than a quarterwave. The GHLA coatings were made primarily for a comparison of thresholds.

Secondly, as goes without saying, the selection of materials is important, if such a choice is permissible optically. For instance, in the Series 4 samples, where SiO films were substituted for the ZrO_2 films in Series 2, the thresholds decreased.

Thirdly, the film sequence can be a factor affecting the damage thresholds. In Series 3 higher thresholds were found when the MgF_2 films were outside and the ZrO_2 films inside than vice versa. Optically there may be, of course, no choice: the MgF_2/ZrO_2 beam divider coating GLHA has a maximum reflectance of about 28% per surface, whereas the ZrO_2/MgF_2 coating GHLA has a reflectance of about 8% per surface.

Table 1. Observed Damage Thresholds, Single QW Films at Focus of f = 42 mm Lens, Glass Substrate Thickness 2.3 mm, Q-Switched Ruby Lasers

Material	Joules Incident on Lens	Threshold E_t in J/cm^2	Number of Samples	Laser
ThF_4	.061	470	1	L.S.
SiO_2	.06 - .07	360 - 420	3	S.R.
SiO_2	.035	250	1	L.S.
MgF_2	.05 - .06	300 - 360	5	S.R.
MgF_2	.035 - .058	250 - 420	2	L.S.
Al_2O_3	.030 - .055	220 - 400	4	L.S.
CaF_2	.007 - .04	50 - 300	3	L.S.
ZrO_2	.022 - .026	130 - 160	4	S.R.
ZrO_2	.033 - .047	200 - 280	4	S.R.
ZrO_2	.019 - .040	115 - 240	4	S.R.
5 $NaF.3AlF_3$	.020 - .030	100 - 210	2	L.S.
TiO_2	.015 - .023	115 - 180	5	S.R.
SiO	.015 - .020	115 - 150	3	L.S.
LiF	.014	100	1	L.S.
MgO	.014	100	1	L.S.
CeO_2	.011 - .014	40 - 100	2	L.S.
ZnS	.004	30	1	L.S.
ZnS	.004	23	1	S.R.

Table 2. Observed Damage Thresholds, Spacerays 101-6 Q-Switched Ruby Laser, Two-Layer Coatings at Focus of f = 42 mm Lens

All Series L = QW MgF_2

Series 1, 2, 3 H = QW ZrO_2
Series 4 H = QW SiO

G = 2.3 mm Glass

A = Air

Coating	Joules Incident on Lens	Threshold E_t in J/cm^2	Number of Samples
Series 1			
GHHLA	.014 - .024	84 - 140	7
GHLA	.018 - .031	110 - 190	5
Series 2			
GHHLA	.054 - .054	320 - 320	2
GHLA	.045 - .049	270 - 290	2
Series 3			
GLHA	.019 - .055	110 - 330	4
GHLA	.037 - .068	220 - 410	5
Series 4			
GHHLA	.015 - .022	90 - 130	5

4.3 Table 3 - QW Stacks

The data in Table 3 illustrate several threshold features of highly reflecting quarterwave stacks as follows:

Firstly, the Series 1 and Series 2 samples in Table 3 were made with the same coating techniques as used for the Series 1 and 2 samples of Table 2, respectively. Applied to the stacks, the techniques for Series 2 again produced higher thresholds than those for Series 1.

Secondly, in comparing thresholds of stacks of any one series, there is generally a trend toward decreasing values of threshold as the number of layers, and hence the reflectance, is increased. By way of orientation, and referring to the Series 2 samples, the 6-layer $G(LH)^3A$ stack using MgF_2/ZrO_2 films has a maximum reflectance of 71%, the 15-layer $G(HL)^7HA$ stack 97.8% and the 21-layer $G(HL)^{10}HA$ stack 99.7%.

Finally, stacks using other common evaporated films will have their own characteristic thresholds which appear to be governed by the weaker of the two component films when they are tested individually in quarterwave thicknesses. Thus the Series 2 stacks have thresholds of about 250 J/cm^2, with (from Table 1) 200 J/cm^2 for single QW films of ZrO_2 and 300 J/cm^2 for single QW films of MgF_2. The Series 3 stacks have thresholds of about 120 J/cm^2, with 150 J/cm^2 for single QW films of TiO_2 and 350 J/cm^2 for single QW films of SiO_2. The Series 4 stacks have thresholds near 100 J/cm^2, much closer to the 30 J/cm^2 thresholds of single QW films of ZnS than to the 300 J/cm^2 thresholds of single QW films of MgF_2.

Table 3. Observed Damage Thresholds, Spacerays 101-6, Q-Switched Ruby Laser, Quarterwave Stacks at Focus of f = 42 mm Lens.

Series 1,2	H = QW ZrO_2	G = 2.3 mm Glass
Series 3	H = QW TiO_2	A = Air
Series 4	H = QW ZnS	
Series 1,2,4	L = QW MgF_2	
Series 3	L = QW SiO_2	

Coating	Joules Incident on Lens	Threshold E_t in J/cm^2	Number of Samples
Series 1			
$G(HL)^5HA$	.022	130	1
$G(HL)^6HA$	.029	170	1
$G(HL)^7HA$	.021 - .035	130 - 210	6
Series 2			
$G(LH)^3A$	.020 - .056	120 - 340	5
$G(HL)^7HA$	.025 - .045	150 - 270	5
$G(HL)^{10}HA$	.019 - .041	110 - 250	5
Series 3			
$G(HL)^6HA$	.015	90	1
$G(HL)^7HA$	.020 - .023	120 - 140	4
Series 4			
$G(HL)^5HA$	.027	160	1
$G(HL)^{10}HA$	.010	60	1

5. Damage Thresholds for Bulk Materials

The application of the methods above to the determination of the thresholds of bulk materials in the form of glass or crystalline plates is complicated by the diversity of damage phenomena encountered. These may, however, be classified in only two groups--surface damage and internal damage. The former occurs as an etching or "burning" of the front or rear on both surfaces of the plate. The latter, internal damage, includes fragmentation within the plate as well as ejection of chips from the incident or the emergent surface, ascribed to destructive processes arising within the bulk of the plate. It is sometimes difficult to determine surface damage when its threshold is higher than for internal damage since, if chips are ejected, they may carry away the traces of the surface damage.

In view of these circu stances only a limited number of semi-quantitative threshold determinations on uncoated plates and substrates were made. Glass, fused quartz and crystalline Al_2O_3, MgO, LiF and CaF_2 were tested with these results, using the Lear-Siegler laser equipment:

Al_2O_3 and MgO in plate form 1-2 mm thick showed surface damage at 100 J/cm^2, but it was much more difficult to cause internal damage. The reverse was true for the SiO_2 and the glass substrates. In 1.5-2.5 mm plate thicknesses these materials could be damaged internally at 250 J/cm^2 but it was more difficult to mar their surfaces. The threshold for internal damage to glass fell sharply for thicknesses below 1 mm. CaF_2 plates 1 mm thick appeared to have relatively high surface damage thresholds--possibly as high as 200 J/cm^2--but could be damaged internally at one-tenth this value.

6. Concluding Remarks

Films of different materials evaporated on glass substrates are shown to have widely different thresholds of ruby laser damage under Q-switched operation with bursts containing a few pulses of 80-240 nsec halfwidth. Thresholds are expected to be functions of pulse width so that the thresholds quoted in this report should only be applied with this in mind.

With some refinements the methods developed during this study seem to be suitable for routine threshold determinations, either on an absolute basis using the calibration techniques described, or on a comparative basis using "standard" coatings with thresholds at the extremes of the damage ranges.

This report has not inquired into the damage mechanism. During the course of the work, however, there have been numerous indications that it is a thermal effect and that the heat of sublimation, taken together with absorption in measurable or trace amounts, plays an important role in determining the level of the thresholds.

7. Acknowledgement

This work was made possible through the Office of Naval Research Contract Nos. (ARPA Order 306) NONR-4717 (00), N00014-68-C0190, N00014-68-C-0190 MOD P001, N00014-68-C-0190 MOD P002.

Investigations Toward Understanding the Physics of Laser Damage to Thin Dielectric Films

L. G. DeShazer and J. H. Parks

Departments of Physics and Electrical Engineering
University of Southern California
Los Angeles, California 90007

The initial phase of an experiment is presented which investigates the physical properties of monolayer thin-films before and after intense laser irradiation, utilizing electron microscopic techniques. The films will be irradiated with emission from three high-power pulsed lasers typical of the state-of-the-art in the uv, visible and ir spectral regions. Specific comments are made of the problems of calibration and control of laser power on both a time-resolved and time-integrated basis. The importance of transverse mode control is demonstrated. Preliminary observations of ZnS layers on cleaved NaCl crystals are presented.

Key Words: Electron microscopy, ruby oscillator, thin films, transverse mode distortion, zinc sulfide.

1. Introduction

The research program discussed in this paper is being carried on in Laboratories at USC which are primarily concerned with laser physics in the areas of solid state and ultraviolet spectroscopy. We are developing an approach to study the physics of thin film damage which is based upon the following:

i) producing damage with well defined laser sources at various wavelengths
ii) investigating the simplest structure: a monolayer dielectric film
iii) utilizing the electron microscope as an analytical tool to survey structure as well as chemical changes induced in these films by laser irradiation.

This approach is different from that of optical design in which multilayered structures of particular composition are developed to eliminate certain effects assumed to be involved in damage. We plan to investigate structural damage of the film as well as the deterioration of optical properties; and finally, attempt to correlate these processes with physical mechanisms. As the work develops, we will extend our studies to include more complex film structures.

In this paper we will present several points of interest and concern in the initial phases of the research program. The importance of controlled laser sources will be emphasized and we will discuss techniques which have been used to achieve single mode, high energy light pulses. We will also briefly consider the requirements which this program places on the ability to produce uniform, controlled films on the order of 1000 Å thick. We wish to point out the need for high film quality when attempting to evaluate and interpret damage processes, although these criteria are generally familiar to researchers in this field.

2. Characterization of Laser Sources

2.1 Requirements

Past studies on laser bulk damage have demonstrated the importance of specifying the properties of the damaging laser beam, since the morphology of the damage has been a good detector of beam inhomogeneities. This situation is aggravated for thin-film damage phenomena by the small physical dimensions of the film layers. The parameters of the beam from a high-power pulsed laser have been quite difficult to specify -- that is, to describe accurately by the electric field vector as a function of the transverse spatial coordinates (r, ϕ) and time in terms of distance z from the laser oscillator: $\vec{E}(r, \phi, z; t)$. Basically this unspecific situation originates from the pulsed nature of operation, causing the experimenter to have imperfect control over the numerous perturbations possible in the laser. Further frustration is introduced by the occurrence of damage to the laser components and,

sometimes, destruction of the measuring devices. Therefore, experimenting with high-power lasers is somewhat like handling a fire hose of optical power -- it is an important scientific tool when under control, but can create much misinformation when out of control.

In order to theoretically analyze experimental results, the field should have a smooth spatial intensity profile over the laser beam, preferably Gaussian, and in addition the temporal pulse shape must be smooth and uniform over the entire beam. Also, most experiments require that the spatial and temporal shapes and, to a lesser degree, the peak power be reproducible. Instead of just indicating that we need to know $\vec{E}(\vec{r}, t)$ to do some thin-film physics, we would now like to discuss how the Solid-State Laser Laboratory at USC determines and controls $\vec{E}(\vec{r}, t)$ for a high power ruby laser system. The procedure to be reported here is not to be construed as the only method of controlling high-power pulsed lasers, or even a method unique to our Laboratory. We felt such a presentation was necessary in order to facilitate comparison of various laser systems and to invite discussion on the more subtle features, usually unreported, of a high-power laser.

2.2 Giant-Pulse Ruby Laser

A schematic of a high-quality giant-pulse ruby laser apparatus is shown in Fig. 1. This design has been followed for two independent laser systems at USC, and has resulted in the single longitudinal and transverse mode operation. With this apparatus we have attained over twenty megawatts (peak power) in a single pulse (10 nsec FWHM) with near-Gaussian spatial and temporal profiles.

a. Longitudinal Mode Control

The laser emission must be restricted to a single longitudinal mode to obtain a smooth temporal pulse shape. In fact, observation of the power modulation of the pulse by a photodetector is a more sensitive indication of "multimoding" than by examining the frequency content of the beam by a Fabry-Perot interferometer. The methods of controlling the longitudinal modes have been well established, and involve operation near oscillation threshold in combination with a bleachable dye Q-switch and etalon reflector. For our resonator mirror separation of 50 cm the spacing between longitudinal modes is 0.01 cm^{-1} and laser action can occur simultaneously in many of these modes. During the formation period prior to Q-switching, the buildup makes several hundred transits through the bleachable dye. As shown by Sooy [1][1] this large number of transits causes most of the weaker modes to be suppressed in favor of the more intense ones which occur at the peak of the fluorescence line. Therefore in a steady-state situation there would be only one mode. This situation is most nearly approached by operation near threshold (typically, less than 5% above the threshold pumping energy) for the pulse occurs at the end of the pumping period where the change in inversion (and therefore gain) with time is at a minimum and the maximum number of transits through the dye have occurred.

The bleachable dye was a solution of cryptocyanine in methanol at a concentration of approximately 5×10^{15} molecules per cm^3. The cell length was 0.4 cm, although the length was not critical provided it was shorter than the stimulated Brillouin scattering threshold length [2]. This solution was changed daily to prevent deterioration of the dye which can occur in a few days. The liquid was contained in a cell made up of a teflon ring spacer held between a glass window (AR coated) and the back dielectric reflector (99%). An important benefit resulted from this design in addition to eliminating extra reflecting surfaces. This benefit was the substantial increase of the damage threshold of the high reflecting dielectric coating by placing it into contact with the methanol solution. No explanation for this increased damage resistance has been confirmed, although the observation had been made years before [3].

The mode selection was augmented by using an uncoated glass etalon as the output reflector [4]. The simple etalon is more stable to thermal and mechanical shocks than multi-element resonant reflectors. No special precautions were needed to match the etalon modes with the cavity modes since many cavity modes fall within the etalon's resonance width. The peak reflectivity of the etalon was 15%; this low reflectivity was found to be desirable because it prevented damage to the dielectric coatings on the ruby rod and back reflector by keeping the intensity inside the laser at a low level. For example, with an output reflectivity of 15%, the intensity inside the resonator was 36% greater than the output intensity, whereas for the identical output intensity using a 35% reflector, the internal intensity would have been 100% greater.

b. Transverse Mode Control

Unlike longitudinal mode control techniques, transverse mode control of pulsed lasers emitting high powers is generally deficient. In the past several years, many good quality lasers have been constructed and called "single-mode" giant-pulse lasers. Such a description is not entirely warranted.

---

[1] Numerals in square brackets indicate literature references at end of paper.

Theoretically, "single-mode" refers to a stationary condition, yet the duration of a giant pulse is only a few transit-times of the laser resonator. This inconsistency has been largely ignored because the experimental far-field patterns from such lasers nearly reproduced the stationary single-mode TEM_{00} pattern on a time-integrated basis [5]. Fig. 2 shows a photograph of the far-field pattern of such a "single-mode"-configured laser. The pattern appears to be the profile expected from a TEM_{00} mode, although careful scrutiny of the photographs revealed a discrepancy in that the sidelobes of the diffraction pattern were more pronounced than predicted.

Several years ago we measured the far-field pattern of a "single-mode" laser on a time-resolved basis and observed that the intensity radial profile altered significantly during the evolution of the pulse [6]. The transient behavior of the transverse mode pattern manifested itself as irregular temporal action when a small portion of the laser beam is viewed through a pinhole aperture. This irregular behavior is demonstrated in Fig. 3 for a laser having a Fresnel number[2] of 1.6. The Figure shows three oscillograms where the left-hand pulse shows the time development of the beam viewed through a 0.14-mm diameter pinhole aperture, and the right-hand pulse shows the development of the same beam viewed without a pinhole (delayed 40 nsec). The three oscillograms illustrate the differing temporal action at three different radial positions of the pinhole aperture. Thus, these fluctuations are in sharp contrast to the approximate smoothness of the temporal response when radially integrated over the laser beam. Also, the radial intensity distribution is smooth when temporally integrated. Due to the presence of this transient behavior of the transverse mode pattern, this laser can be considered "single-mode" only in the sense that it can oscillate in a single longitudinal resonance.

For background, a brief outline of our present analysis [7] is given for a pulsed laser with gain saturation. A giant-pulse laser with high gain will usually have a pulse duration of only a few resonator transit times. (A numerical comparison: with an initial numerical gain of 20, the pulse duration is about 12 nsec, while for a 50 cm long resonator, the round trip transit time is 3.3 nsec, only a factor of four different from the pulse duration.) During the development of the pulse, the population inversion of the active medium is rapidly depleted due to stimulated emission. Consequently, the gain drops from the high initial value to a very small value at the pulse termination. Pumping of the gain medium is negligible because of the short time duration of the pulse. In all present calculations, a uniform initial gain profile is assumed. Now, consideration of the transverse intensity profile of this laser shows that saturation of the gain occurs first at the radial position where the intensity is largest; thus, this portion of the profile has an amplification lower than the weaker intensity regions. Therefore the transverse profile of a pulse propagating through this gain medium is modified and usually severely distorted from any steady-state profile.

Fig. 4 shows the calculated variation of the intensity profile at the output aperture of a laser having a Fresnel number of 2.0 and gain of 20. The pulse initially has a Fox-Li (steady-state) profile which has a maximum at $r = 0.18a$, but by the time the pulse peaks at the center of the aperture the maximum has shifted to $r = 0.25a$ due to gain saturation. Only one-half transit time later (1.7 nsec later for a 50 cm cavity) the profile has distorted enough to have a maximum at $r = 0.6a$. This change of the aperture profile gives rise to temporal pulse shapes that differ greatly with radius (Fig. 5). The on-axis pulse at a distance outside a laser having Fresnel number of 2.0 is shown in the insert photograph of Fig. 5 and matches well with the calculated pulse shape. The net result is that this laser pulse contains local peak power densities of at least a factor of two greater than the spatially averaged power density. These short-duration intense regions appear to be the so-called "hot spots" suggested by many workers as responsible for some of the experimental anomalies observed when using a laser as a source [8], [9].

For resonators having large Fresnel numbers, an arbitrary transverse profile will propagate for several hundred transit times before reaching a steady-state through diffractive losses. Therefore in these resonators, perturbations in the profile due to gain saturation will not dampen out by diffraction during the giant pulse, causing the laser to emit a transverse profile differing greatly from a stable mode pattern. Also the transverse profile of such a laser will alter during the evolution of the pulse. Results of an experiment are shown in Fig. 6. Three successive laser shots were photographed with the only change in the laser configuration being the aperture radius, i. e., the Fresnel number. As the Fresnel number is changed from 90.0 to 4.0 to 1.0, the pulse gets successively

[2] Fresnel number is defined as $a^2/L\lambda$, where a = resonator aperture radius, L = round-trip distance between mirrors, and λ = laser wavelength.

smoother. Note that the irregularities become noticeable only after sizeable gain saturation occurs, which will be near the pulse peak, and these irregularities last for the duration of the pulse since any perturbations take many transits to dampen out. It is interesting to note that this type of temporal behavior has been experimentally observed since the early days of lasers [10].

For resonators with small Fresnel numbers, the change in the transverse profile is relatively slow and therefore these profiles approximate the familiar steady-state Fox-Li modes. In addition, the spatial distribution is very nearly Gaussian in the far-field in spite of the non-Gaussian character in the near-field of the aperture. The transient behavior of the transverse pattern was calculated for a Fresnel number of 0.4, which corresponds to the laser now used in our laboratory. Fig. 7 plots the intensity profile at the output aperture, Fig. 8 plots the phase profile and Fig. 9, the temporal pulse shape. Good agreement between observed and predicted transverse structure was obtained; Fig. 10 shows the intensity at the beam center (leading pulse) and the spatially integrated pulse (delayed pulse). Therefore, by making the Fresnel number small, we could achieve profiles close in appearance to the familiar Fox-Li modes.

Presently, we are searching for criteria which will delineate the existence of the transient behavior of transverse modes. One such criterion that has been proposed by us is that transient behavior will be negligible when the product of initial gain and Fresnel number is less than a certain dimensionless number. Our preliminary study indicates that this number is about 15. For our ruby oscillator, we determined the initial gain to be near 20 and therefore we operate with a Fresnel number of 0.4.

The exact transverse profiles emitted from a pulsed laser will depend on the character of the pulse buildup and hence on the method of Q-switching the laser. When switching by a bleachable dye, the pulse will initiate from a Fox-Li condition since prior to bleaching the transverse intensity profile approximates a steady-state solution. In general, other methods of Q-switching will yield different results and, in particular, we have not yet found a procedure to obtain single-mode performance by electro-optic Q-switching. Therefore, the use of a bleachable dye for Q-switching is important not only for simple longitudinal mode control but also for controlling the transverse modes.

c. Resonator Optics

(1) Laser Rod and Pumping Optics:

The oscillator laser rod is a 3/8 x 4" Czochralski ruby, 0.03% Cr doping, grown by Crystal Products Department, Union Carbide Corp. Other "select" grade rods of higher doping have been used, but the 0.03% doping level leads to superb optical quality. The radial surface is slightly roughened and the ends were flat, parallel and antireflection coated with MgF_2. The rod was held in a precision-bore pyrex glass sleeve which in turn was held in a gimbal mount fastened to the optical bench. The initial temperature of the ruby was near 7°C and the particular temperature for each run was controlled to within 0.5°C by using a thermistor-actuated temperature controller. The temperature control was necessary in order to achieve the desired reproducibility of the laser output.

The pumping optics consisted of a polished aluminum double ellipse with a linear flash tube (EG&G, FX-45C-6) at each outer focal line and the ruby at the center (common) focal line. The flash tube assembly was mechanically decoupled from the resonator optical components by a vibration isolation table. With this mechanical isolation, optical alignment could be maintained for many days.

(2) Aperture:

A circular aperture in the cavity reduces the Fresnel number which is required since a smooth spatial profile is primarily the result of regulating the transverse mode structure. Therefore the performance of the aperture is very important because scatter back into the ruby would prevent the necessary mode control. At first we used accurately-machined brass apertures, but it became quickly apparent that they scattered and damaged easily. Therefore, after some considerations, we speculated that truncation of a highly-polished hollow cone would produce an ideal aperture for high-power lasers. In thermal physics it is well known that a polished hollow cone with a small angular opening approximates a black body [11], and is called a Mendenhall wedge. Experimental results bore out the speculation and we call such an aperture a "Mendenhall aperture." Fig. 11 shows that the light intercepted by the Mendenhall aperture is reflected into a widely diverging cone in the forward direction. In contrast, the brass apertures made in our Laboratory diffused most of the intercepted light

backwards. For our laser, the aperture was an "olive hole" in polished carbide (1 mm dia.) and was located such that the surface toward the ruby was the polished cone.[3]

(3) Alignment Procedure:

The laser output depends very critically on the cavity alignment particularly for the plane mirror configuration. We have noted that various optical alignment techniques utilizing collimators or gas-laser interferometry are not sufficient to align the giant-pulse ruby oscillator. We use now a technique which we call "dynamic alignment" because the method involves operating the laser, distinct from the other passive optical techniques. We scan the far-field pattern using a small pinhole and compare the temporal pulse shapes at points placed symmetrically about beam center. If the cavity is not aligned, the pulse will not be uniform across the pattern and the comparable shapes will be different. Generally, the pulse width increases monotonically from one side to the other, and the pulse peak occurs at differing times. This deformation is especially evident near the wings of the spatial pattern. Alignment is achieved by making small adjustments to the front reflector while observing the resultant changes in the pinhole scan. These adjustments can be easily made with a differential screw mount for the front reflector. The misshapen temporal character was due to walk-off of the beam during Q-switching, and can be only properly controlled by the dynamic alignment.

3. Near Field Diffraction of Giant-Pulse Laser

If the output of the laser had an ideal Gaussian spatial profile, the beam would just diverge into the far field without undergoing any complicated profile changes. Instead, as shown in Fig. 7 for our laser, the beam profile is a Gaussian cut off near its half-power value. This truncation produces sidelobes on the far-field pattern and structure within the main lobe in the near field. The diffraction patterns of such truncated Gaussians have been calculated [12], [13] and the effect of truncation was found to be important when the aperture radius was less than twice the spot size of the Gaussian. Fig. 12 shows how the intensity at the center of the pattern varies with distance from the aperture for several cases of truncation. The on-axis intensity oscillates in the near field and then, beyond a certain distance, the intensity decreases by the inverse-square law. Fig. 13 shows two photographs of transverse patterns in the near field of our ruby laser. Photographs A and B correspond to the near-field patterns at the distances A and B labeled in Fig. 12. Thus, in the near field, diffraction causes spatial nonuniformities in the beam by nearly an order of magnitude. To avoid these nonuniformities we need to place the test samples in the far field of such a laser.

A convenient parameter to associate with aperture diffraction is the Rayleigh distance [14] which is defined as $2a^2/\lambda$. Rayleigh distance sets the scale of the axial distance from a radiating aperture, and therefore performs as the Fresnel number except that it applies to single apertures instead of resonators. Diffraction at one Rayleigh distance from the aperture locates the pattern in the transition region between the near and far fields. (Numerical example: for a 1 mm dia. aperture the Rayleigh distance is 72 cm and the distance A is 18 cm.) Fig. 14 shows the diffraction pattern of our laser at 3 Rayleigh distances with three different exposures. The central disk is nearly Gaussian and, in the overexposed pictures, the clarity of the rings appraise the fidelity of the phase front. The pictures of Fig. 14 were taken with a 12 nsec pulse having 0.5 megawatts peak power and appear remarkably like that of a gas laser.

4. Optical Isolator

We recently constructed an isolator capable of withstanding one gigawatt/cm^2 laser pulses. This isolator will prevent damage to the oscillator components by any intense backward traveling radiation. This radiation can originate from the breakdown plasmas and stimulated Brillouin scattering as well as the ever present spurious reflection. The isolator follows the usual design [15], [16] except NaCl was chosen as the Faraday material due to its high damage threshold [17]. The Verdet constant of NaCl at 6943 Å is 0.278 min Gauss^{-1}cm^{-1} [18]. A peak magnetic field of 18.6 kG is applied in a pulse to a 5.22 cm long NaCl crystal. Fig. 15 illustrates the isolator and the oscillogram shows the time varation of the solenoid current and the rotation angle (using a 6328 Å gas laser). The required condition for 45° rotation is maintained for nearly four milliseconds.

[3] Commerical tools closely resembling the Mendenhall aperture can be obtained from R. P. Gallien & Son, 220 West Fifth Street, Los Angeles, Calif. as carbide wire dies.

5. Ruby Amplifier

Recently we built and tested a laser amplifier having a weak-signal gain of 45. The amplifier rod is a 1/4 x 6" Czochralski ruby, 0.05% Cr doping, grown by Union Carbide Corp. The ends are antireflection coated and wedged one-third arc degree to prevent resonant depumping. The initial temperature of both oscillator and amplifier rods were identical before each shot. The polarization alignment of the two rubies was more critical than antipicated, and the tolerances on the adjustment are demonstrated in Fig. 16. The principal planes, the planes containing the ray and the optic axis, of both rods must be aligned to within one-quarter arc degree to achieve a reasonably smooth output profile. A further difficulty was observed which at present is not completely understood although it has been overcome. An unfocused input pulse resulted in an amplified pulse which had a profile similar to the near-field-like doughnut pattern. We found it necessary to focus through the amplifier rod with a 33-cm focal length lens in order to obtain a smooth amplified profile. The resultant pulse, when recollimated after the amplifier, has a smooth spatial profile. In this manner 20 MW laser pulses having near-TEM_{oo} profiles were consistently produced.

6. Thin Film Studies

The thin-film research program is presently in the preliminary stages of characterizing damage in monolayer films. Although these studies are just beginning it will perhaps be useful to outline the experimental procedures being developed for this purpose, and then discuss the application of these techniques to ZnS films

In the initial experiments, monolayer thin-films of several common laser-coating materials (selected from MgF_2, ZnS, $ThOF_2$, SiO_2, Al_2O_3, TiO_2) will be prepared by vacuum deposition onto cleaved NaCl substrates. NaCl crystals will be used because they provide a high damage threshold material [17] and also permit simple preparation [19] of the monolayer film for examination by transmission electron microscopy. Resistance heat and electron beam evaporation will be used to deposit these films at deposition rates which are consistent with present laser mirror coating procedures. Film thicknesses will range from one-quarter to one-half the wavelengths of lasers to be used in these experiments; and evaporation parameters will be changed to study a variety of film structural characteristics. Replication of the substrate surface properties by the film will be monitored in preparation for later experiments on substrate effects. In particular, we have observed that NaCl substrates must be carefully prepared to avoid surface discontinuities.

The transmittance and reflectance (both specular and diffuse) of the films on the NaCl substrates will be measured using available standard commercial instruments and from these measurements, the film absorption coefficients can be determined at the laser wavelengths. These films will be irradiated with emission from three sources: the nitrogen amplifier (3371 Å), the ruby laser (6943 Å) and the neodymium/yttrium aluminum garnet laser (10642 Å) which are being used in our laboratories as standard research tools. The variation of optical properties with radiation flux density and wavelength will be observed at the laser wavelengths and the spectral distribution of the transmittance will also be monitored to provide an indication of induced photochemical changes.

The optical parameters will serve primarily as useful indicators of changes in the film structure which occur during exposure to the laser sources. The physical and chemical changes will be studied in greater detail by using the techniques of transmission and scanning electron microscopy. Following laser irradiation and optical testing, we will obtain micrographs of the surface topology of the film on its substrate which can resolve structure on the order of 200 Å.

After the scanning electron microscopy, the thin film deposits will be removed from the NaCl substrates by immersion in distilled water which allows the film to float free. All the films to be studied initially are water insoluble and easily lend themselves to this technique. The laser irradiated areas will be separated from the floating film and placed on standard 200 mesh copper specimen grids. These films may then be examined using a Hitachi HU 125 electron microscope available to our research program. Micrographs obtained with transmission microscopy and also from electron diffraction patterns will permit us to observe the physical and chemical variation in the damaged and undamaged sections of the film. The correlation of data obtained in both scanning and transmission microscopy will extend the use of this analytical tool to the characterization of thin film properties on substrates which are currently being used commercially.

Several electron micrographs have been taken to examine the deposition characteristics of monolayer ZnS films and the results are presented in Figs. 17, 18 and 19. The importance of these preliminary pictures is the implication that these techniques can provide a wide range of information useful to the analysis of damage processes. The film shown in Fig. 17 indicates a uniform deposition on the scale of 1000 Å. The blackened grains result from the diffraction of electrons away from the photographic surface and yield a rough indication of the grain size, in this case approximately 100 Å. This is particularly sensitive to evaporation procedure as shown by the micrograph of a similar film in Fig. 18. In this case a slightly different configuration of the evaporation boat has produced a generally larger grain size and an obvious defect in the film surface. Finally, Fig. 19 is an electron diffraction pattern obtained from the uniform film described above. It shows the characteristic structure associated with the zincblende phase and yields a clean background on which to observe possible indications of chemical change in the material.

7. Acknowledgements

The authors are grateful to Dr. L. E. Murr for his expert comments on the electron microscopy of thin films and his assistance in obtaining Figs. 17 - 19. Mr. H. R. Owen is acknowledged for his deposition of the ZnS films on NaCl. One of the authors (LGD) expresses appreciation to his past and present students (G. L. McAllister, M. M. Mann, L. Huff, B. E. Newnam and J. W. Austin) and his technical associate Mr. E. A. Maunders for the development of the ruby laser system. In particular, Dr. G. L. McAllister is appreciated for the first clear observations of transverse mode distortion in a giant-pulse ruby laser.

Support for this research on thin-films is provided by a contract with the Air Force Cambridge Research Laboratories. The development of the giant-pulse ruby laser was supported by the Joint Services Electronics Program through the Air Force Office of Scientific Research (AFSC), United State Air Force, under Grant AF AFOSR 69-1622 and Contract F 44620-71-C-0067. Continuation of the study on the transient behavior of transverse modes in high-power pulsed lasers is being supported by Air Force Grant AFOSR-71-2066.

8. References

[1] W. R. Sooy, Appl. Phys. Letters 7, 36 (1965).

[2] R. V. Wick and A. H. Guenther, Appl. Opt. 7, 73 (1968).

[3] D. W. Gregg and S. J. Thomas, Appl. Phys. Letters 8, 316 (1966).

[4] D. Roess, Proc. IEEE 52, 196 (1964).

[5] For example see J. E. Bjorkholm and R. H. Stolen, J. Appl. Phys. 39, 4043 (1968).

[6] G. L. McAllister, PhD Dissertation, Univ. of So. Cal. (August 1969).

[7] G. L. McAllister, M. M. Mann and L. G. DeShazer, IEEE J. Quan. Elect. QE-6, 44 (1970).

[8] P. Lallemand and N. Bloembergen, Phys. Rev. Letters 15, 1010 (1965).

[9] J. E. Bjorkholm, IEEE J. Quan. Elect. QE-7, 109 (1971).

[10] E. E. Hagenlocker, R. W. Minck and W. G. Rado, Phys. Rev. 154, 226 (1967).

[11] J. M. Cork, Heat (John Wiley & Sons, New York, 1942), p. 29.

[12] A. L. Buck, Proc. IEEE 55, 450 (1967).

[13] J. P. Campbell and L. G. DeShazer, J. Opt. Soc. Am. 59, 1427 (1969).

[14] Lord Rayleigh, Phil. Mag. 11, 214 (1881). See also R. C. Hansen, ed., Microwave Scanning Antennas (Academic Press, New York, 1964), vol. 1, pp. 179-180.

[15] L. G. DeShazer and E. A. Maunders, Rev. Sci. Instr. 38, 248 (1967).

[16] C. F. Padula and C. G. Young, IEEE J. Quan. Elect. QE-3, 493 (1967).

[17] D. Olness, Appl. Phys. Letters 8, 283 (1966)

[18] S. Landau, Phys. Z. S. 9, 417 (1908).

[19] L. E. Murr and M. C. Inman, Phil. Mag. 14, 135 (1966).

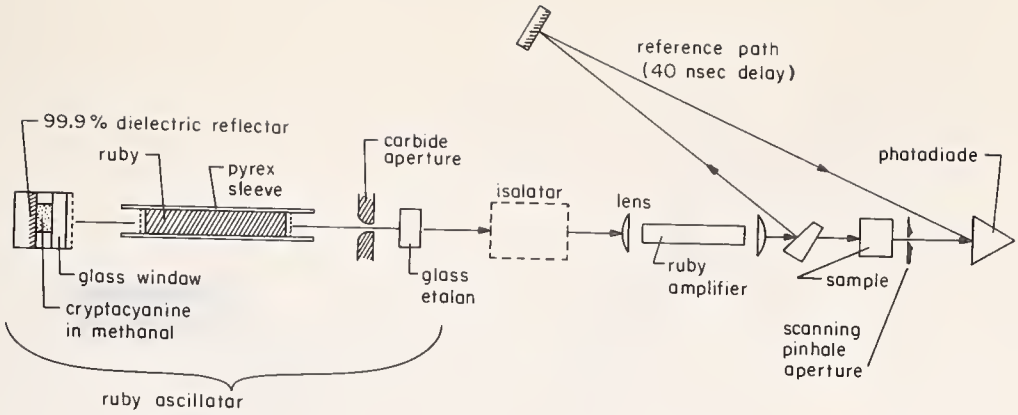

Fig. 1 Schematic of the high-power pulsed laser system

Fig. 2 Photograph of the far-field pattern of a giant pulse from a ruby laser

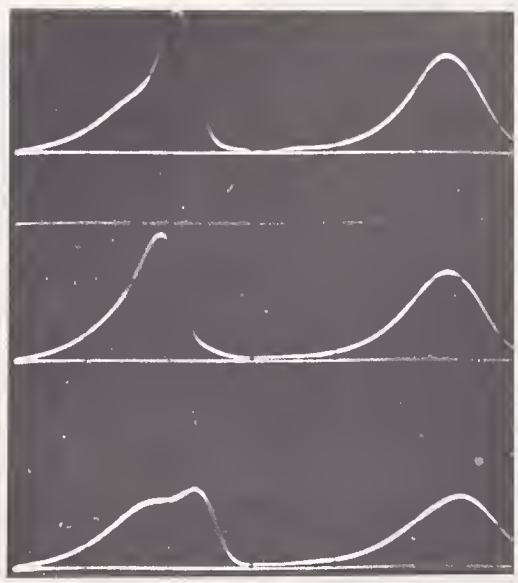

Fig. 3 Oscilloscope traces illustrating the transient behavior of the transverse mode pattern for a laser with a Fresnel number of 1.6. Leading pulse of each oscillogram shows a pulse viewed through a pinhole and the delayed pulse is the spatially integrated behavior of the same pulse.

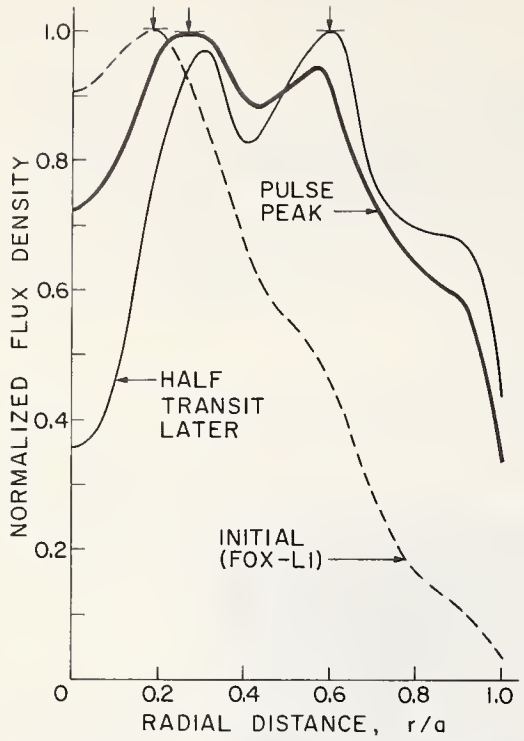

Fig. 4 Normalized intensity profiles at the output aperture of a resonator with a Fresnel number of 2.0. Profiles at the time the pulse peaks at the center of the aperture and one-half transit time later are compared with the initial profile. Ref. [7]

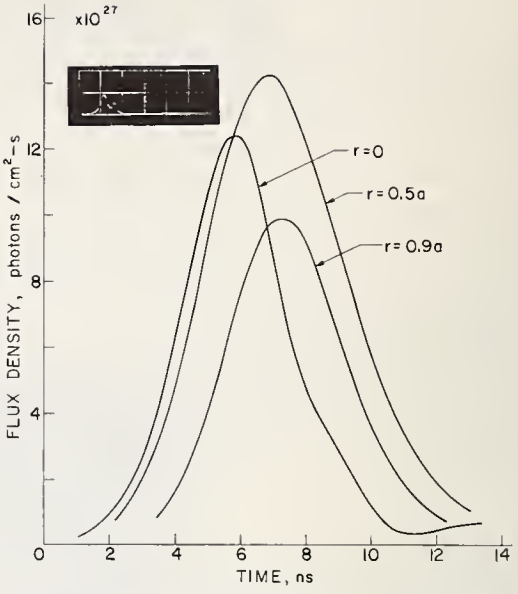

Fig. 5 Temporal pulse shapes at several radii in the output aperture plane of a resonator with a Fresnel number of 2.0.

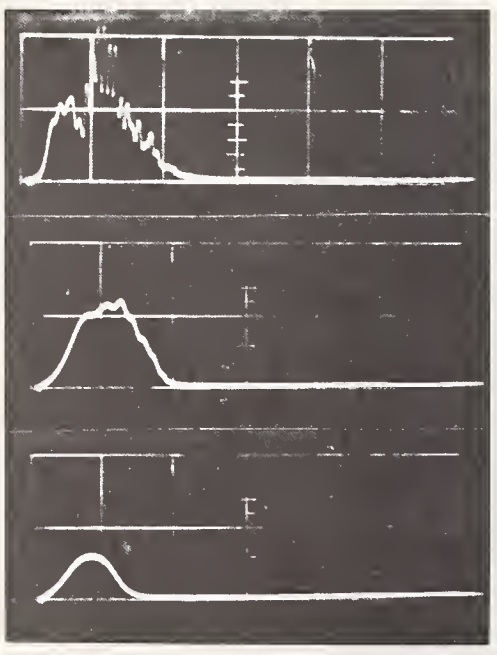

Fig. 6 Oscilloscope traces of three successive laser shots with only the aperture radius varied to give Fresnel numbers of 90.0, 4.0 and 1.0. Time scale is 20 ns/div. A small central portion of the output beam was detected through an external pinhole.

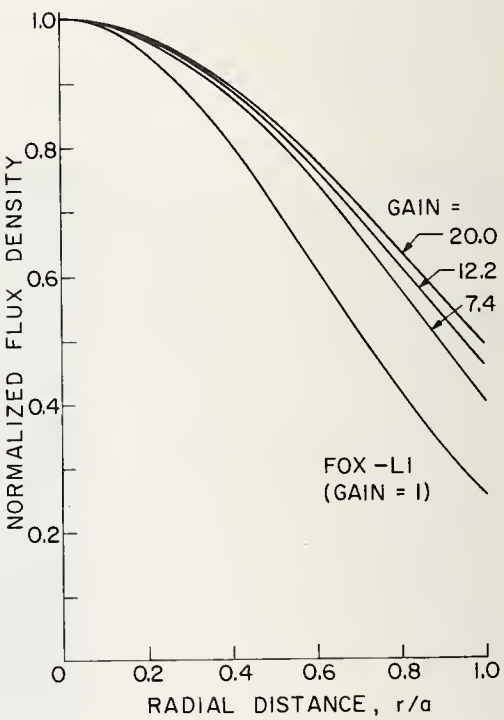

Fig. 7 Normalized intensity profiles at the output aperture of a resonator with a Fresnel number of 2.0. Profiles are at the pulse peak (in time) for numerical single-pass gains as shown

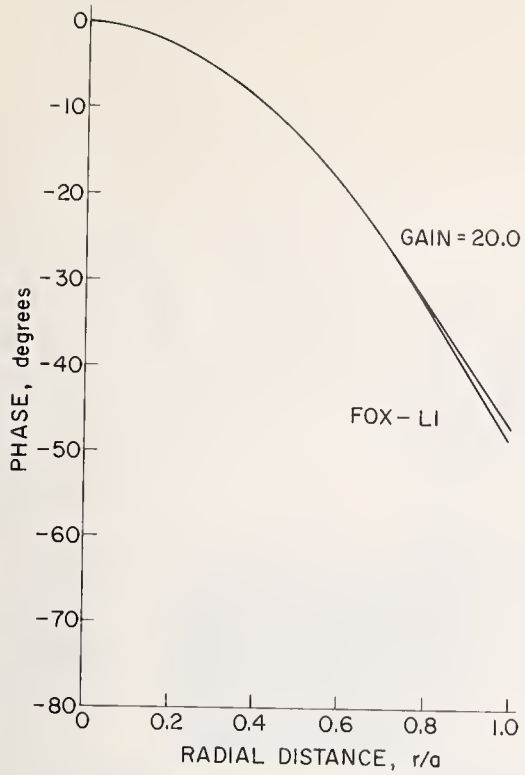

Fig. 8 Phase profiles corresponding to the intensity profiles shown in Fig. 7.

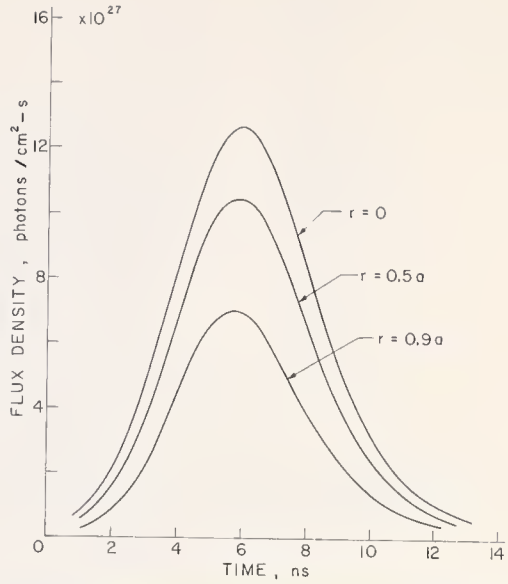

Fig. 9 Temporal pulse shapes at several radii in the output aperture plane of a resonator with Fresnel number of 0.4

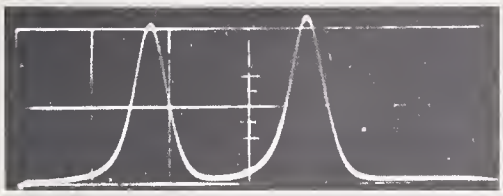

Fig. 10 Oscilloscope trace (20 ns/div) showing intensity at the beam center (leading pulse) and spatially integrated reference (delayed pulse) for gaint-puls laser with Fresnel number of 0.4.

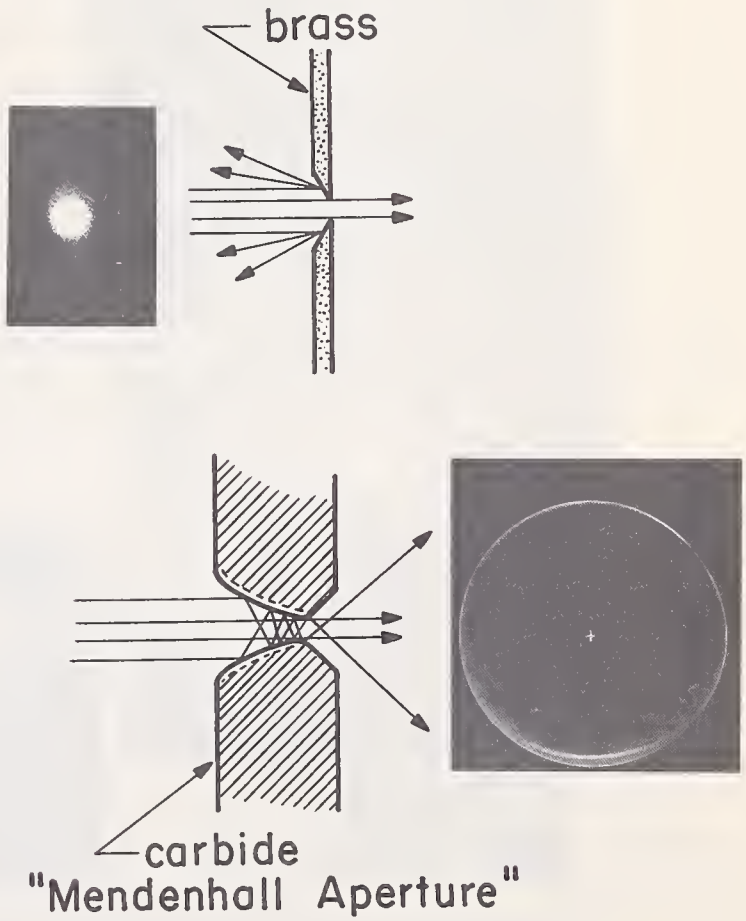

Fig. 11 Companison of apertures for high-power lasers.

450-417 O-71—10

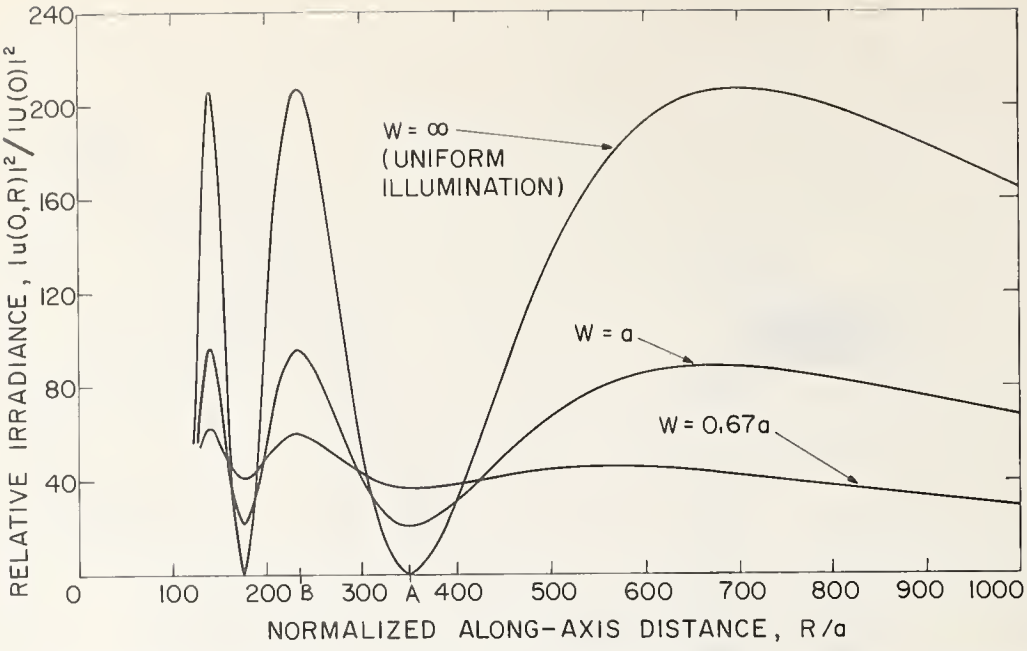

Fig. 12 On-axis intensity vs distance for various illumination spot sizes w at constant aperture radius (a = 700 wavelengths). Ref [13].

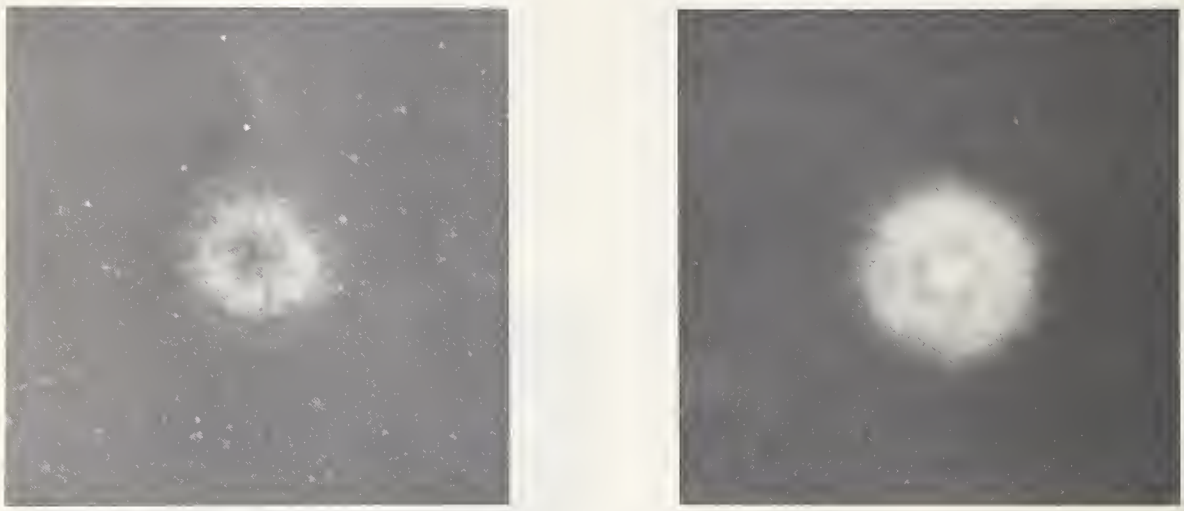

Fig. 13 a. Near-field photograph of intensity showing the ring pattern corresponding to two Fresnel zones. Photograph taken with a giant-pulse laser with a Fresnel number of 0.4.
b. Near-field photograph showing the pattern corresponding to three Fresnel zones.

Fig. 14 Photographs of the diffraction pattern of a giant-pulse ruby laser (Fresnel no. = 0.4) at 3 Rayleigh distances (far field) from laser. The three photographs were exposed under three different beam attenuations.

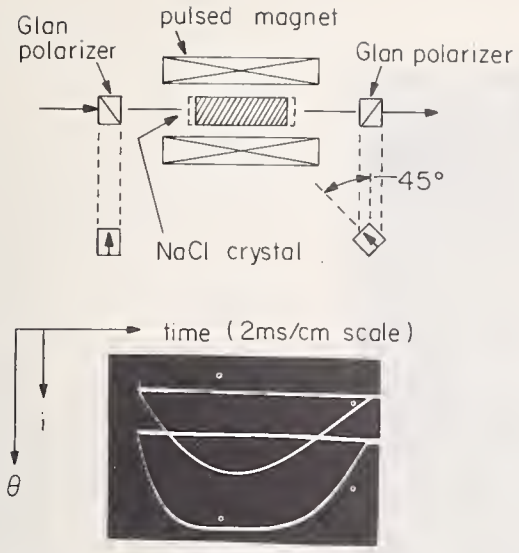

Fig. 15 Schematic of optical isolator for high-power laser. Operating characteristics are demonstrated on the oscilloscope trace: i is the current to the solenoid and θ is the rotation angle where the flat portion corresponds to a 45° rotation.

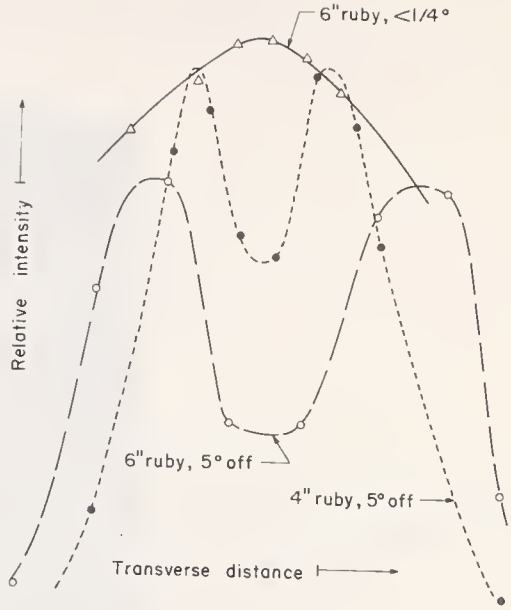

Fig. 16 Radial profiles of the output pulse from a ruby amplifier showing the effects of polarization misalignment.

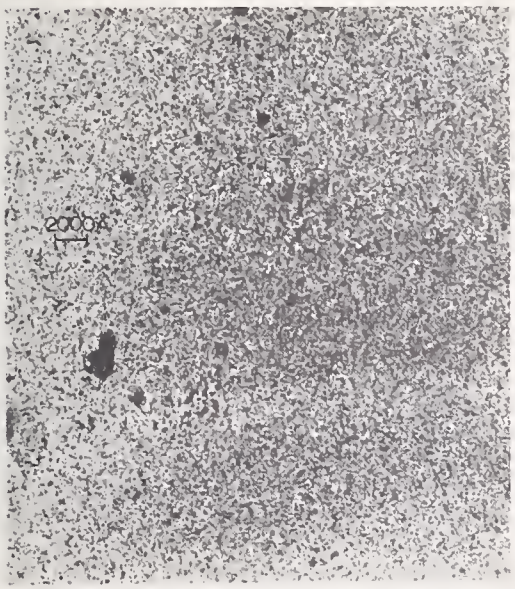

Fig. 17 Transmission electron micrograph of a quarter-wave (6943 Å) film of ZnS. Note the 2000 Å scale on the left of the photograph.

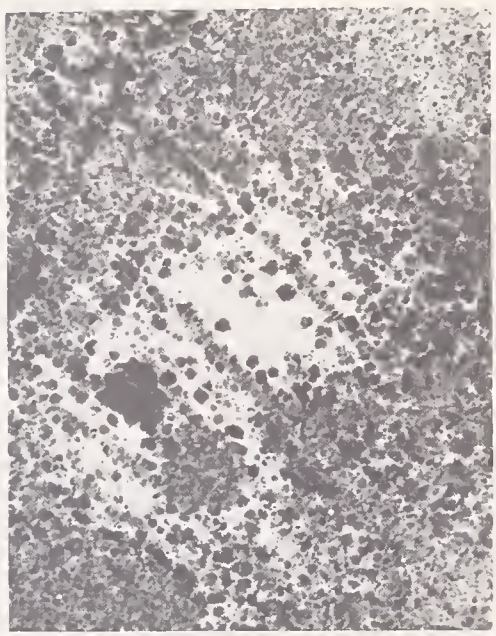

Fig. 18 Electron micrograph of a thin film of ZnS deposited by a method only slightly different from the deposition method used for Fig. 17

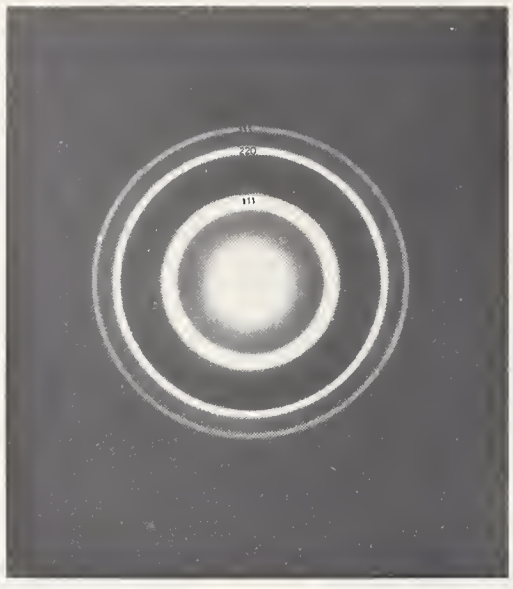

Fig. 19 Electron diffraction pattern of the film in Fig. 17 demonstrating the zincblende structure of the ZnS grains.

COMMENTS ON PAPER BY LARRY DESHAZER

In order to insure good beam quality it was necessary to align the oscillator and amplifier in this work to within less than a quarter of a degree. This high precision of alignment was achieved by using a polariscope illuminated with a helium neon laser. During the discussion it was also pointed out that unless the cylindrical axes of the oscillator and amplifier are very accurately aligned, severe distortion can result from the resultant asymmetric thermal lensing.

An Investigation of Laser Induced Damage to four Different Single Purpose Anti-Reflection Coatings on Fused Silica Substrates

R. Russel Austin
Perkin Elmer Corporation
Norwalk, Conn. 06852

and

Arthur H. Guenther
Air Force Weapons Laboratory
Kirtland Air Force Base
Albuquerque, N. Mex. 87117

The one shot laser induced damage threshold of four typical anti-reflection coatings is reported. A damage correlation is attempted on a comparison with the residual stress developed in single and multilayer systems. The coatings studied were $\lambda_o/4$ (λ_o = 1.06 μm) layers of a, MgO - MgF_2; b, MgF_2 - SiO_2 - MgF_2; c, MgF_2 - ThF_4 - MgF_2; d, MgF_2. All thin films were electron beam deposited on quartz substrates and both entering and exiting damage thresholds were determined. In terms of damage resistance for entering laser irradiation b > c > d ∿ a and for the exiting case b > d > c > a. Damage thresholds were in the range of 1 to > 2 GW/cm^2 for a 30 nsec FWHM pulse @ 1.06 μm over a ∿ 3 mm diameter area. The morphology of damage is presented through the use of Nomarski Differential Interference Contrast Micrography and Scanning Electron Microscopy (SEM).

Key Words: Anti-reflection coatings, laser damage, microscopic damage, morphology of damage, scanning microscopy, thin film stress.

1. Introduction

1.1. Film System Fabrication

Several studies [1,2][1] have been undertaken to determine the resistance of various materials in thin film form to high energy laser radiation. The most comprehensive of these studies by A.F. Turner [1] and his co-workers at Bausch-Lomb catalogues a rather complete selection of commonly used filming materials and their relative damage thresholds.

It is evident from these studies that there are certain properties of materials that are important in determining to what degree they are resistant to laser damage. The relative contribution of some of these properties are inseparable and it is therefore almost impossible to make an accurate prediction of the damage threshold solely on this basis. In any event, the whole range of damage thresholds of the common filming materials is covered by slightly more than an order of magnitude. When one considers some practical aspects of film formation, it is fairly evident particularly for multilayer reflectors which materials are recommended for use to afford the most damage resistant system.

Turner states that the damage threshold of thin film materials can almost completely be correlated in terms of their heat of sublimation, suggesting that the damage mechanism is primarily a thermal effect. The purpose of this study was to investigate certain multilayer systems in an attempt to determine whether or not any more subtle modifications of the damage thresholds might be the result of structural parameters of the film system.

In particular, a study is made on the basis of residual stress developed in single layers and systems. A seemingly simple problem is considered; that is how to provide the best anti-reflection coating for quartz optics in a high power 1.06 μm laser system. As the system is destined for field

---

[1] Figures in brackets indicate the literature references at the end of this paper.

use in less than ideal conditions, we are concerned with establishing a matrix of film system properties such as reflection efficiency, adhesion and durability in addition to the laser damage threshold so that the optimum coating for this purpose can be selected.

2. Stress Effects in Multilayer Systems

Evaporated films of dielectric materials develop internal stresses upon condensation. The mechanism of the stress formation is relatively complex and will not be discussed here. Depending primarily on the film materials, the stresses can be tensile or compressive and these stresses play an important role in determining the mechanical integrity and reliability of a film or multilayer system.

In the majority of materials which are highly stressed in film form, the internal stress will continue to increase with thicknesses until the film breaks up or disrupts in some way. The thicknesses at which this occurs is called the disruption thickness and is, like the stress itself, dependent on deposition conditions to some extent. Multilayer systems with alternating films of compressive and tensile stress can be built up to a total thickness far in excess of the disruption thickness of either component. Thus one makes use of stress relief or compensation.

In our design consideration, materials were selected which in single film form have damage thresholds relatively close to each other, but have vastly differing stress and mechanical properties, in an attempt to determine the effects of these structure properties on the laser damage threshold.

3. Choice of Materials and Designs

Turner tabulates (this proceedings) the damage thresholds and refractive indices of the commonly used film materials. Threshold values are given in Turner's data and should be treated on a comparative basis to avoid confusion with the test results from the experimental conditions described in this paper. Also shown in his paper are the general stress properties of the materials.

Using the three (3) most resistant materials; $ThOF_2$, SiO_2 and MgF_2 , three anti-reflection designs were selected. One, simply a single layer of Magnesium Fluoride, and two (2) three layer designs, using Magnesium Fluoride in combination with the Thorium Fluoride, and Magnesium Fluoride in combination with Silicon Dioxide. The other design selected was a classical two (2) layer design using Magnesium Oxide, one of the lower threshold materials, in combination with Magnesium Fluoride. The form of these designs is shown schematically in Fig. 1. In Fig. 2 the designs are tabulated along with some of their essential properties. The measured reflectivity was determined by a Cary Model 14 Spectro-reflectometer employing a semimicro specular reflectance attachment. This instrument operates at an acceptance cone angle of 23°. Figure 3 shows the theoretical spectral performance of the designs in the region of 1.06 μm.

4. Practical Aspects of Film Deposition

The fused silica substrates used for the experiment were cut from a larger piece of fused silica which was of photographic window quality. Each of the samples therefore had a wavefront deformation of less than $\lambda/10$ (at the interferometer wavelength 6328 Å) with less than one arc second wedge between the front and rear surfaces. The larger piece of fused silica has previously been checked at a surface code (scratch-dig) of better than 80:50. In any event, the surface of the test substrates were identical as nearly as possible. All substrates were prepared simultaneously and stored in a clean cabinet after cleaning. All of the coatings were performed within a span of 24 hours.

All films were deposited from an electron beam evaporator onto substrates maintained at 250°C. The pressure during deposition was held at 2×10^{-5} torr. Substrates were rotated, during deposition, in a planetary type jig; this is typical of nominal production practice. No attempt was made to control the stress of the film systems by choosing a certain set of deposition parameters. Experience shows the lower tensile stress films could be deposited if substrate temperatures were raised to higher levels, i.e. 300°C or 350°C, however, certain of the heavier optical glasses will discolor if they are heated in vacuum at high temperatures, 250°C is the safest temperature for production use consistent with an adequate degree of durability.

The choice of electron beam evaporation was made so that a common deposition method could be used for all designs. This method is almost mandatory for the Magnesium Oxide and Fused Silica materials but the Magnesium Fluoride and Thorium Fluoride materials can be readily evaporated from radiant heated or resistant heated sources.

5. Stress Measurements

Although it has been planned to use an in process stress measuring interferometer [3] to determine the film stress, lack of time prevented the setting up of the instrument and it was necessary therefore to measure the stress in the systems by observing the deflections produced when the films were evaporated on the surfaces of good optical flats. Figure 2 shows measured values of the net stress as measured for each design type.

The relative values of designs a, b, and d were in line with expectations as shown in Fig. 2 with the exception of design b. (In the case of design b the stress is so low that the tolerance of reproducibility probably lies on both sides of zero net stress).

The net stress of design c was considerably less than expected. Inspection of the film surface by the Nomarski Differential Interference Contrast Microscope showed the presence of a crazy quilt-like pattern of tiny cracks indicating that the system was close to disruption thickness, and that some stress relief had taken place as a result of this cracking. All films exhibited very few pinholes and entrapped dust particles. Those that were identifiable were randomly scattered over the total surface area.

6. Experimental

For the laser damage threshold measurements, a high brightness 1.06 μm glass laser was employed. The oscillator-amplifier system emitted in excess of 10 joules in a single 30 nsec FWHM pulse. The total beam intensity distribution is essentially flat topped with an rms intensity fluctuation of 8% over > 90% of the total energy output cone.

An experimental arrangement as shown in Fig. 4 was used for all sample irradiation. The laser system was operated at a constant pump level to insure maximum stability in experimental exposure conditions. Under this restraint the laser output and beam quality as measured by its total divergence (∿5 mr) [4] and intensity distribution was reproducible to between 2 and 3%. To vary the power density, homogeneous Schott filters were inserted before the combination 4 m and 6 m focusing lenses.

In order to afford good sampling of surface imperfections, an irradiation area 3 mm in diameter was selected. This would insure that results would be representative of large area damage thresholds with a sufficient probability of occasionally encountering pinholes, dust particles or localized high stress regions. The 2.54 cm x 2.54 cm x 0.64 cm fused silica substrates with coatings were inserted at an angle of 17° off normal to the incident laser beam to eliminate feedback into the laser. These dimensional conditions permitted nine (9) non-interfering exposures on each sample.

Since these samples were thin film coated on both surfaces, it was deemed desirable to study both entrance and exit surface thresholds; therefore, the samples were placed upstream of the focus of the incident radiation. For this geometry, the exposed area on the entrance surface was 0.087 cm^2 and 0.079 cm^2 on the exit surface. In this manner power density was approximately 10% higher at the rear surface. Thus, it was expected to first see rear surface damage and then front surface effects.

To insure limiting the beam to an approximately 3 mm diameter, a one (1) cm aperture was placed in the focusing beam at a position to define the desired exposure area. This condition resulted in the manifestation of an intensity distribution at the sample due to diffraction at this aperture. The resultant intensity distribution, [4] while quite reproducible, is shown in Fig. 5. The intensity distribution is slightly skewed to one side probably due to the action of the rotating mirror Q-switch. From this known intensity distribution a peak and average power density is calculated. To complete the experimental arrangement as shown in Fig. 6 two photodiodes were employed in the system. One recorded the incident power as a function of time and total energy in the pulse. The other served to accomplish the same measurements on the transmitted radiation to record any plasma absorption. Typical traces are shown in Fig. 7. Furthermore, all sample exposures were visually observed through a 1.06 μm blocking filter to detect the formation of any visible plasma.

Before insertion in an adjustable x-y mount for exposure each sample was cleaned by pulling a Kodak lens tissue wet with spectral grade ethyl alcohol across each face once. No detectable water droplets or surface impurities were noted upon observing the evaporation of the residual alcohol film.

7. Damage Results

Detectable laser induced damage to the anti-reflection coatings was always accompanied by the observation of a visible breakdown plasma. The damage levels given later are consistent with both plasma generation and the production of detectable surface damage. Unfortunately, there was an insufficient variety of good quality attenuation filters available to define a more specific damage threshold, or to indicate the reproducibility of that damage level. In general, two exposures were

recorded for the highest level with no damage, two exposures at lowest level of front surface damage and two exposures at lowest level of rear surface damage.

For samples a, b, and c, the rear surface damaged first and subsequently at higher power levels both front and rear surface damage was evident. For the single layer MgF_2 coating while the first detectable damage was at the rear of the sample (recall on any given exposure power density is 10% higher on rear surface than that of the front), this was followed by damage only at the front surface for slightly higher total incident power levels. Only at extreme power densities did both front and rear surface simultaneously exhibit damage on this sample. Only under this high level loading was there any detectable change in the shape of the transmitted intensity signal, as indicated in Fig. 7.

Results of these experiments are given in Fig. 8. The accuracy of the peak power flux is $\sim \pm 7\%$ and $\sim \pm 4\%$ in the average power flux. The more meaningful damage value is that of peak power flux. On this basis one can rate the relative laser resistance of the tested coatings. For exiting radiation at the rear surface b > d > c > a in order of decreasing damage threshold, while for incident radiation on the front surface of the rankings in like manner is b > c > d $\sim$ a. Thus, it is seen that the MgF_2 and SiO_2 three layer coating is the best as far as single shot damage resistance and the classic two layer MgO, MgF_2 is the worst. It is indeed unfortunate that one is limited to $\sim$ 0.5% reflectivity for coating b compared to $\sim$ 0.2% for coatings a and c.

While it is impossible to unambiguously relate the damage resistance with either net stress or reflectivity, one should note that the most damage resistant coating was that one which exhibited a net compressive stress. Furthermore, one might draw the conclusion that, had not coating c undergone stress relief, it may have damaged at a lower level. However, this is mere speculation and would require additional testing perhaps at 0.69 μm where one could probably produce an anti-reflection coating without exceeding the disruption thickness. One can state that exit damage occurs at levels less than entrance damage except in the case of single layer MgF_2.

8. Morphology of Observed Damage

Each irradiation area was carefully examined to determine presence and extent of damage. A complete survey was accomplished using a Nomarski Differential Interference Contrast Microscope, at magnifications from $\sim$ 50 X to 800 X (Figs. A through N). Each sample was photographed prior to exposure at both low and high magnification with both polarized and unpolarized light. The only observable features were those already mentioned that is, random pinholes and entrapped dust particles and the crazed appearance of sample c.

It is extremely difficult to catalog and identify the precise cause of numerous types of failure observed in the several hundred photographs obtained; however, a number of typical damage areas were selected and are presented in the following reproductions. It is important to note that there are many more types of laser induced damage to thin films as compared to laser induced damage in optical substrates or elements. The code designation is x(y,z) where x is picture identification, y is thin film system tested and z is entrance (F) or exit (R) surface. Easily identified are features indicative of stress relief by cracking, generally radial splitting of MgF_2 layers, pitting of substrate, effects due to included dust particles, layer stripping, melting and flaring of material, as well as glass fracture.

In addition to the Nomarski Differential Interference Micrograph examination, an examination was performed using a Scanning Electron Microscope. This examination revealed more detail of the relief of the damage sites than did the Nomarski examination, and because the samples were overcoated there was little confusion as to which layer the detail belonged. Sixteen micrographs are presented for discussion, the identification nomenclature for the micrographs is the same as that used in the Nomarski discussion.

Concerning the glass fracture records, in ideally brittle materials, surface free energy is the only mode of energy dissipation during fracture propagation. In amorphous solids such as glass and polymers, the energy dissipation or the fracture energy per unit crack extension, γ , is directly related to the geometry of the fracture surface, i.e., γ increases with surface roughness. Generally in glasses this surface roughness takes the form of the commonly observed rib or hackle structure. The rib structure or river line pattern is usually observed during the initiation period of crack propagation, or the reinitiation period after the crack has been arrested. The formation of these roughened surfaces is considered to be the cause of the relatively high value of fracture energy at the initiation of crack growth. The development of hackles is attributed to the formation of microcracks ahead of the main crack and in planes which are not coplanar with the main crack. These surface irregularities absorb larger energies than the relative increase in surface area would indicate and the intensity of roughness increases with increased fracture velocity and, in most cases, with an increase in temperature.

9. Some General Comments

It is unfortunate that the best film system from the point of view of damage resistance and mechanical durability (design b) is not a particularly good anti-reflection coating. This exercise does then indicate that in some circumstances trade-offs may need to be made if one particular property e.g. reflectivity, environmental durability, scatter, damage resistance, etc. is preferred. Damage here must be defined in terms of specific requirements. Is it an increase in scatter, decrease or increase in reflectivity, physical failure of film system, etc? The coatings tested do not represent all of the possible solutions to the problem by any means, simply the more common approaches, including those with potentially the highest damage thresholds.

The damage thresholds measured on the design c are surprisingly high, considering that the film system was badly cracked before irradiation with the high energy pulse. There is not doubt that the film system would be mechanically unsound, particularly in high temperature and humidity condition. Were it not for this point of weakness, the film system would be eminently suitable for the purpose considered, and well within the fabrication capabilities of the majority of commercial coating operations even those without electron beam gun capability.

It has been clearly demonstrated that damage can originate at included foreign particle sites. There is a suggested correlation, therefore, with bulk damage of optical materials due to particulate inclusion. In all probability an analysis similar to that of Bennett [5] and Hopper, Lee, and Ulman [7] should be accomplished to arrive at the most damaging particle size in relation to the thin film system employed. There is an excellent starting point in the recent work of Pearson [7] who has presented some elegant electron micrographs of the cross-sectional structure of multilayer systems. These micrographs conclusively exhibit that entrapped particles or substrate surface features are faithfully reproduced through numerous additional layers leading to irregularities in the structure of individual layers. The decrease in damage threshold attributed to dust particles strongly recommends careful cleaning of the substrate and a high degree of cleanliness in the coating chamber by a glow discharge or other low energy bombardment scheme.

The microscopic surface studies have revealed a wealth of information about the character of damage to film systems, in particular to the role of the internal stresses and stress relief mechanisms. Although the range of coatings tested was insufficient to obtain a quantitative relationship between internal stress and damage threshold, there is a wealth of evidence to indicate that it does in fact influence the damage threshold particularly on exit surfaces. On the highly stressed film samples (design C) the difference in character of the entrance and exit surface damage was very clear.

Those cases, where damage is attributable to a nucleus on the substrate or in the film system suggest there is a strong case for investigation of the influence of scatter on damage thresholds.

10. Suggestions for Further Study

This paper is a very general one which exposes a multitude of problems and effects simply as a result of tackling a seemingly straightforward design problem. The results suggest further detailed work which may well lead to a very sound definition of the laser damage problem and hopefully to prediction of the ultimate limits of damage resistance for specific coating types. Some suggestions are outlined in the following paragraphs.

10.1 Definition of Damage Threshold for one Pulse (P_1) and Threshold for an Infinite Number of Pulses (P_∞)

Bass [8] describes experiments with crystalline materials wherein the above levels are determined for $LiNbO_3$ and $Ba_2NaNb_5O_{15}$. In the case of $LiNbO_3$ these levels are separated by two orders of magnitude. These values should be determined for materials in single film form and combined in certain multilayers. It will also be interesting to determine the effects of parameters such as scatter and stress on the separation of the two values and the transition one to the other. The same experiments will also serve to determine the effects on the absolute maximum damage threshold if one uses the recommended TEM_∞ mode for the damage producing laser.

10.2 Effects of Scatter

In order to best understand this, it would be advantageous to separate two scatter effects, that of scatter from surface roughness; and that due to presence of solid particulate matter in the films.

The first experiment would be a relatively simple one to arrange. Films will faithfully replicate the surface of a substrate, and a set of substrates having a range of different scatter values can easily be made by using different grit sizes and polishing times. This experiment does have the drawback that it is only really suitable for scatter values higher than those one might expect from the internal scatter of the films so that the true surface effect could be isolated.

Internal coating scatter is kept constant by cooling all samples simultaneously. The authors intend to determine damage values as a function of bare substrate finish in the near future. It is their intention to investigate mechanical, chemical, and ion polished surfaces.

The second experiment is more difficult and may require some ingenuity in order to be able to produce internal scatter values at will. Substrates used in this experiment would ideally have the lowest possible scatter in order that film effects might predominate.

10.3 Damage Thresholds of Chemical Mixtures

It can be seen from Turner's [1] data that the majority of useful medium index materials have damage thresholds lower by a factor of 3 or 4 than the low index materials. This tends to exclude the use of classic double quarter wave design which requires a medium index film as the first film in the design. Design "a" in this study is such a design, and this was the least damage resistant sample tested.

Medium index materials can be produced artifically by mixing high index and low index materials in the vapor phase. This method has also been used [9] to produce stress free layers by mixing tensile and compressive components.

Zirconium Oxide and Silicon Dioxide are prime candidate materials and would in fact produce films with low net stress. Damage threshold versus mixing ratio of these two materials should be investigated.

Although the damage thresholds of the very high index materials, such as TiO_2, are much lower than ZrO_2, it may still be possible to form a resistant mixture with SiO_2 because of the small proportion of TiO_2 which will be required to produce the medium index. The reflectivity variable could be eliminated from these studies by using $\lambda/2$ o.t. films.

10.4 Inhomogeneous Film Systems

The evidence of damage at interfaces shown throughout this study presents a strong case for the investigation of the Periodic Inhomogeneous Multilayers discussed at the Miami meeting. This work will be undertaken during the next 9 months.

10.5 Additional Suggested Investigations

The following suggested studies should lead to a very clear understanding of the influence of various additional factors. It would be useful to determine the damage threshold for identical multilayer systems deposited on various substrates; afterall what one is interested in ultimately is the damage resistance of the total composite i.e. film system and substrate. A useful theoretical study would be to compute the electric field intensity distribution of multilayer systems under laser illumination and determine if this quantity is not the most appropriate for correlation with observed damage in multilayer systems. An obvious study is to compare the damage resistance of identical film systems deposited by the various deposition techniques employed today, e.g. sputtering, e- beam heating, thermal evaporation and perhaps chemical deposition. Finally, a study of particular use to the laser industry is related to the damage in high and medium reflectivity coatings as well as the low reflectivity coating treated here. These should then be compared to liquid immersed and optically contacted thin films as well as optical cements.

11. Acknowledgment

The authors would like to express their appreciation to the following AFWL individuals: Lt S. Patterson and Sgt P. Bledsoe, who assisted in the damage testing and Mr. J. Cooney and Sgt R. Harniman for micrographic support. The film preparation and stress value measurements were accomplished by Raymond C. Michaud and Leonard J. Rogers, of the Perkin Elmer Corporation, respectively. Comments relating to glass fracture were supplied by Dr. Charles Stein, Chief Materials Science Group, Air Force Weapons Laboratory.

12. References

[1] Turner, A.F., Interim Report to Subcommittee II of the ASTM Committee F-1, Miami, Florida, 12 Jan 71.

[2] Atwood, Steinberg, Research on Causes of Laser Damage to Optical Components, Report #2, Contract DA-28-043-AMC-0000, Army Missile Command, Huntsville, Alabama.

[3] Ennos, A.E., Applied Optics, 5, 551 (1966).

[4] Wick, R.V. and Guenther, A.H., Method of Test of Beam Divergence for Optically Pumped Lasers, ASTM, Committee F-1.

[5] Bennett, H.S., Damage in Laser Materials, p. 51, NBS Spec. Pub. 341 (1970).

[6] Hopper, R.W., Lee, C., Uhlmann, D.R., Damage in Laser Materials, p. 55, NBS Spec. Pub. No. 341 (1970).

[7] Pearson, J.M., Thin Solid Films, 6, 349-350, (1970).

[8] Bass, M., Damage in Laser Materials, p. 90, NBS Spec. Pub. No. 341 (1970).

[9] Scheuerman, R.J., J. Vac. Sci. Tech. 1, 143 (1970).

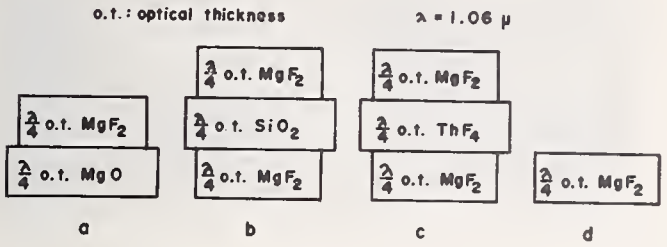

Fig. 1 Schematic representation of evaluated anti-reflection films.

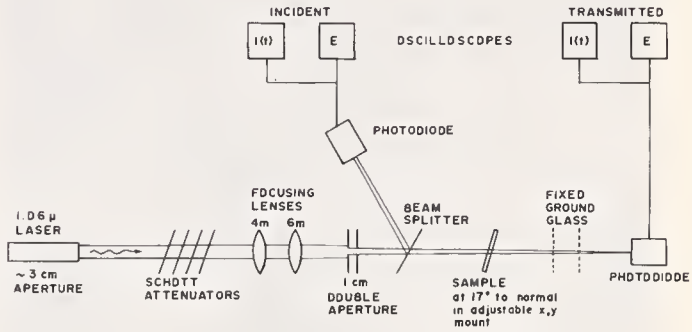

Fig. 4 Experimental arrangement for sample irradiation.

DESIGN	MATERIALS	MEASURED REFLECTIVITY 1.06 μm	DURABILITY	ANTICIPATED NET STRESS	MEASURED NET STRESS
a	MgO, MgF_2	0.30 %	Excellent	Moderate Tension	1990 Kg/cm² Tension
b	MgF_2, SiO_2	0.70 %	Excellent	Low Tension	71.5 Kg/cm² Compression
c	MgF_2, ThF_4	0 16 %	Good	Extreme Tension	1148 Kg/cm² Tension
d	MgF_2	1.98 %	Excellent	High Tension	2850 Kg/cm² Tension

Fig. 2 Important properties of tested films and net stress for various film designs from beam deflection measurements.

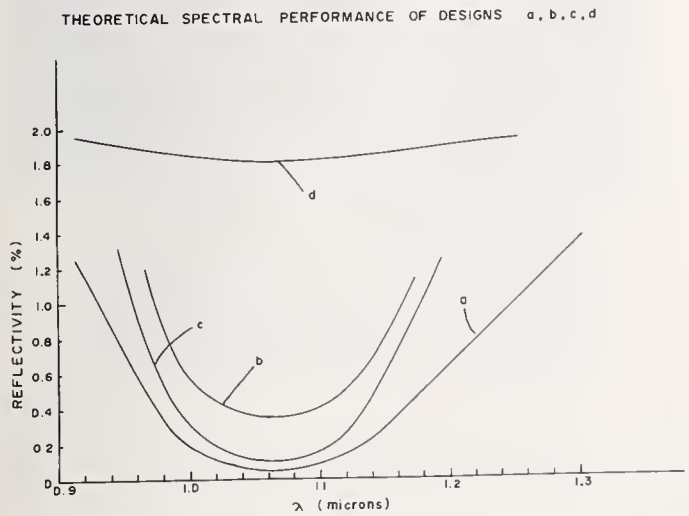

Fig. 3 Theoretical reflectivity of tested films in the region of 1.06 μm.

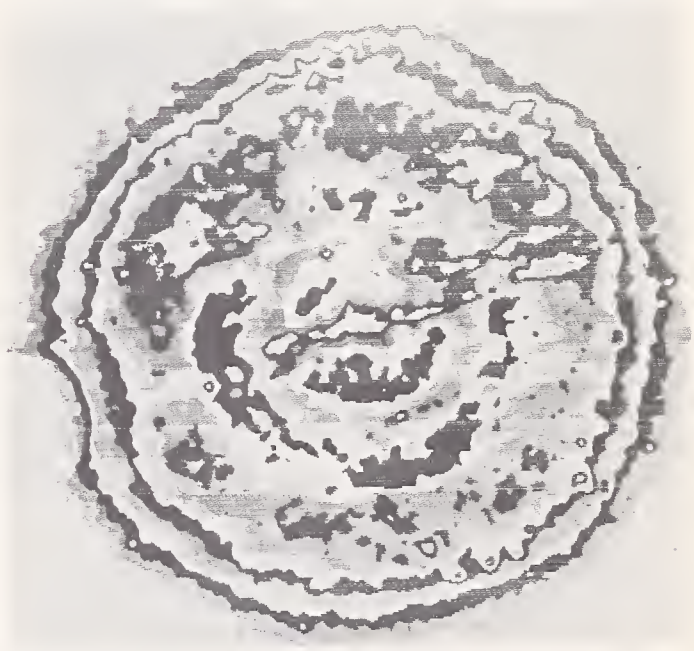

Fig. 5 Two-dimensional intensity distribution at the entrance surface of sample. Increasing intensity is indicated by white-gray-black sequence.

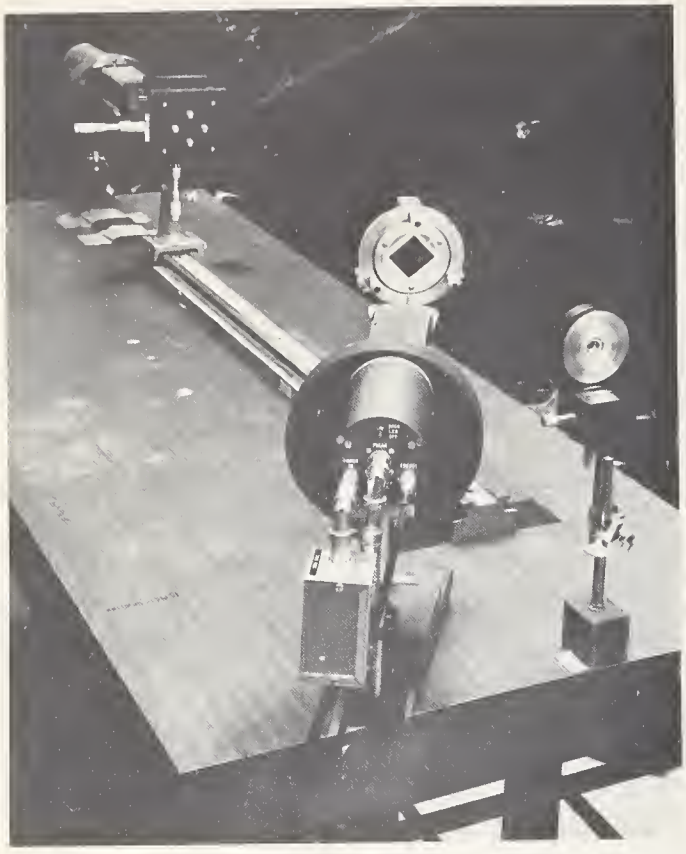

Fig. 6 Photograph of exposure area and active optical diagnostics.

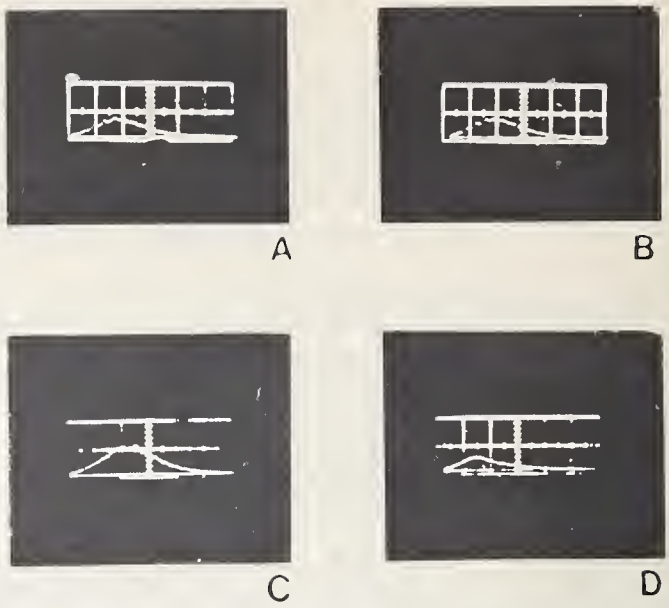

Fig. 7 Incident and transmitted photodiode oscillographs. Sweep speed 20 nsec/cm. A & B are incident and transmitted traces at low irradiation levels in which no damage was observed. C & D are similar traces at very high levels in which severe damage was manifest.

SINGLE EXPOSURE DAMAGE THRESHOLDS in GW/cm^2*

SAMPLE	DAMAGE	EXIT SURFACE				ENTRANCE SURFACE			
		HIGHEST LEVEL WITH NO DAMAGE		LOWEST DAMAGE LEVEL		HIGHEST LEVEL WITH NO DAMAGE		LOWEST DAMAGE LEVEL	
		Peak	Average	Peak	Average	Peak	Average	Peak	Average
a. $MgO - MgF_2$		1.03	0.93	1.28	1.16	1.50	1.35	1.84	1.66
b. $MgF_2 - SiO_2 - MgF_2$		2.01	1.81	1.98	1.78	2.01	1.81	2.37	2.14
c. $MgF_2 - ThF_4 - MgF_2$		1.58	1.43	1.62	1.46	1.84	1.66	2.40	2.16
d. MgF_2		1.63	1.47	1.99	1.79	1.47	1.33	1.83	1.65

Peak Power Densities ~ ±7% Average Power Densities ~ ±4%

*All experiments at 1.06 μ in 30 nsec FWHM pulse on a 0.087 cm^2 area on front surface and 0.079 cm^2 area on rear surface

Fig. 8 Experimental values of single shot damage thresholds for tested anti-reflection coatings.

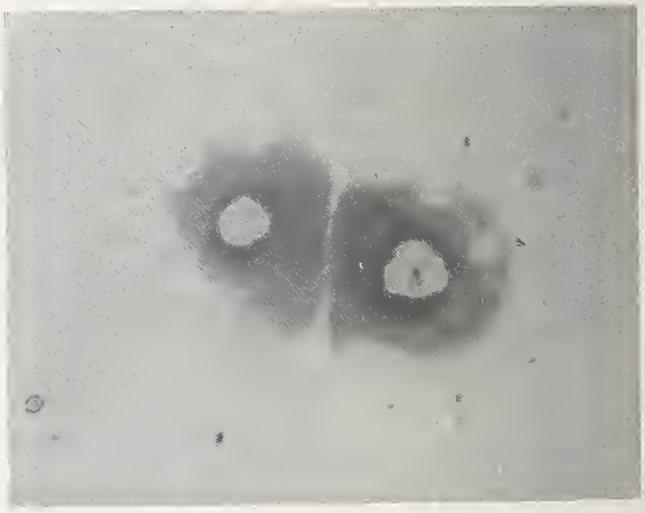

Fig. 9 A(aR)(535 X) This first picture shows a damage site clearly nucleated on dust particles. It appears as though the dust particle may be located at the film substrate interface or at the interlayer boundary. The bond appears to have been loosened without causing complete catastrophic damage of the films. This is borne out by the effect at the junction of the two sites.

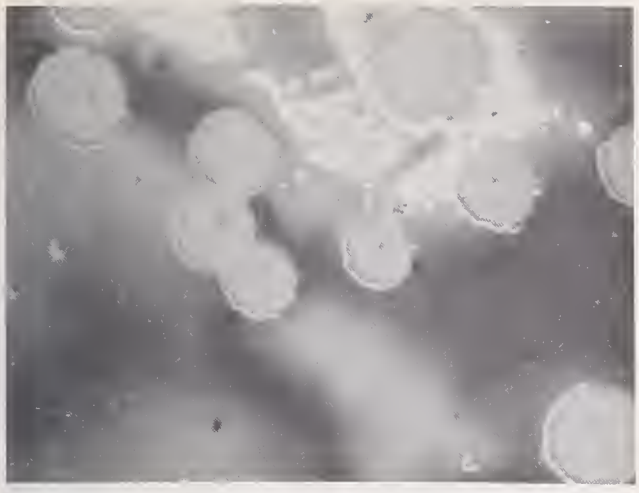

Fig. 10 B(aR)(535 X) Samples of small pit marks just at the onset of damage. Each pit appears to have a distinct point nucleus which appears to be in the substrate surface, or have been a particle at the substrate surface.

Fig. 11 C(aR)(535 X) Stress microcracks appearing in the outer MgF_2 layer close to an area of gross damage. A distinct flare effect of uncertain origin can be seen.

Fig. 12 D(aF)(535 X) Further evidence of stress microcracks in a badly damaged area on the front surface.

Fig. 13 E(bR)(60 X) An excellent example of a stepped crated damage site. Damage is gross effecting complete removal of all 3 films. A multitude of microcracks in both of the MgF_2 layers is again evident. This picture clearly isolates the microcrack problem as belinging to the MgF_2 layers. The SiO_2 film in between the two layers is completely free of these cracks.

Fig. 14 F(cR)(535 X) Complete crazy paving effect due to ultra high tensile stress in an area show no damage. It is not clearly evident from this picture whether or not one, two or all three films are cracked. As ThF_4 does not normally show a tendency to crack the cracks are most probably in one or both of the MgF_2 layers.

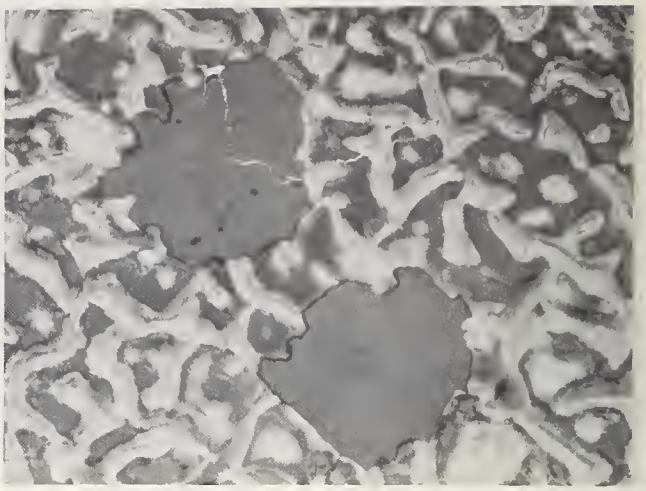

Fig. 15 G(cR)(535 X) Clean removal of two large areas. It is not clearly evident that what is visible is the substrate. It may be an intact ThF_4 film. The tensile effect in the layers is evidenced by the curling at the edges of the small areas of film.

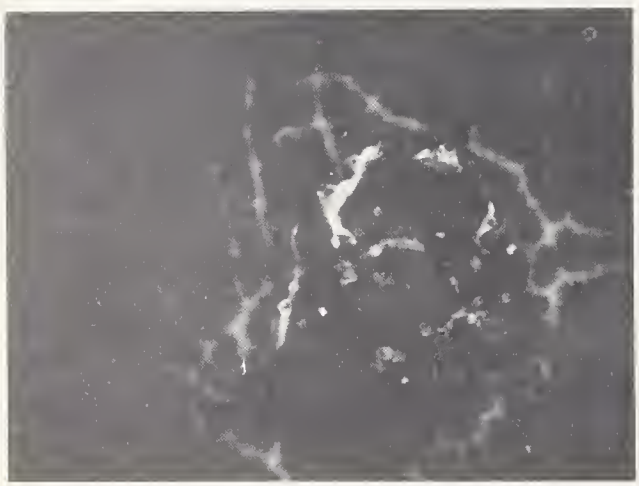

Fig 16 H(cF)(535 X) Shows a step walled crater damage site wherein the crazy paving effect is not nearly as evident as in the previous examples. None of the rear surface damage sites showed a step walled crater and this in fact was the only possible means by which it might be possible to differentiate between the front and rear surface damage i.e. simply by inspection of a micrograph.

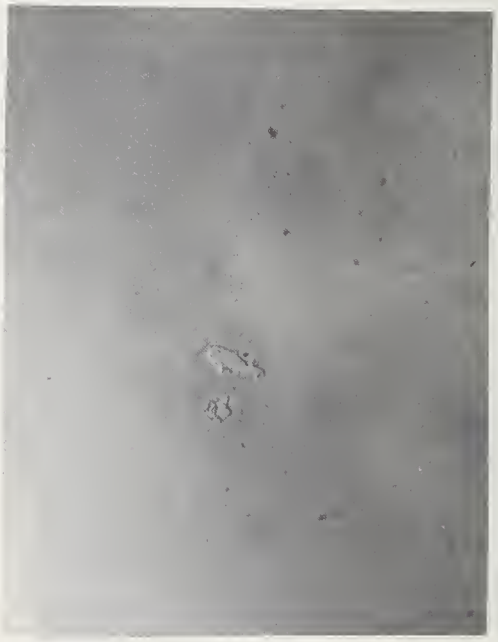

Fig. 17 I(dR)(535 X) Isolated removal of a small area of film.

Fig. 18 J(dR)(535 X) Detail of the above showing film tensile effects at the edges of the site.

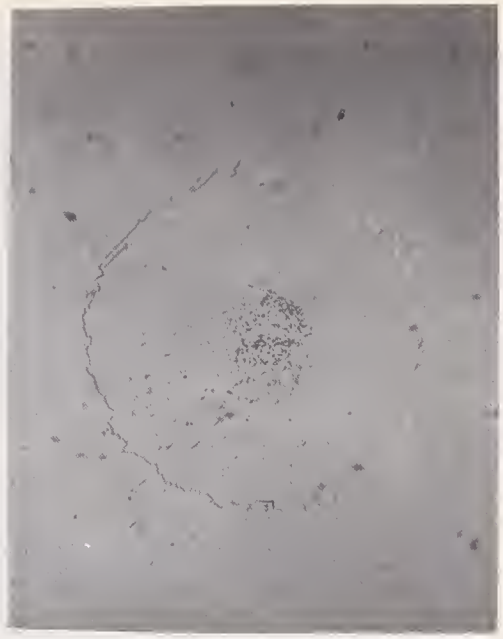

Fig. 19 K(dF)(60 X) Another example of clean removal by a front surface exposure. There is evidence of surface pitting as the substrate in the center of the site which might possibly be caused by surface contamination.

Fig. 20 L(dF)(535 X) Details of the surface pitting in the above examples.

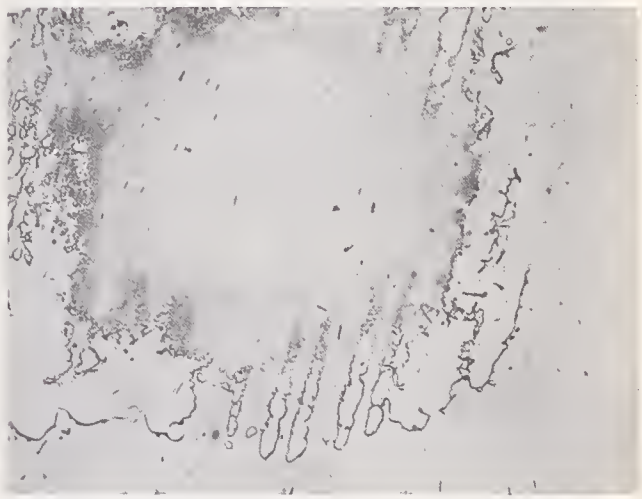

Fig. 21 M(dR)(60 X) This picture shows damage which seems to have as its origin an unclean substrate. The film removal is not as clean as in the previous examples and seems to have a strong degree of orientation. The other areas indicate that the film bond at the substrate has been loosened without effecting complete removal of the film. There is a remote possibility that this directional type of damage might be caused by interference between different modes of the incident laser irradiation.

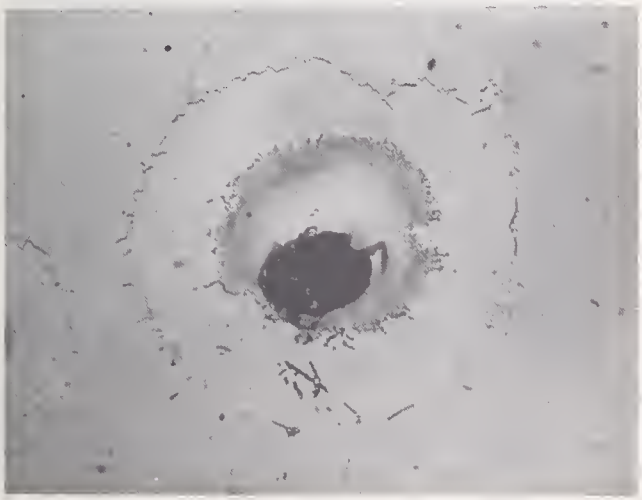

Fig. 22 N(dR)(60 X) Damage occuring in the area of a pit in the substrate. Damage seems to have occured to a certain extent in the substrate.

Fig. 23 O(bF)(1250 X) This picture shows globules of molten material in a damage area, there is some delamination but the melting process seems to be predominate, indicating the structural soundness of the stress relieved design.

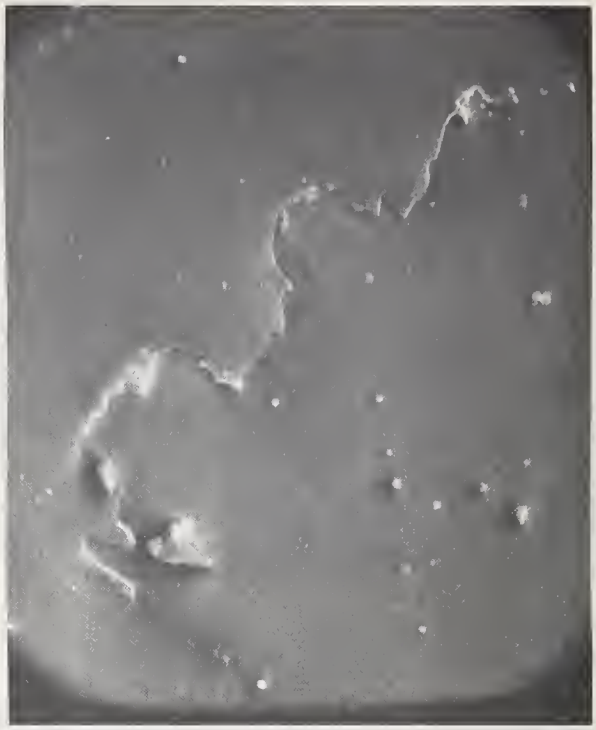

Fig. 24 P(bR)(640 X) This shows rear surface damage and extensive removal of the outer MgF_2 film before the occurrence of a significant melting. Note that the edge of the MgF_2 layer shows breakage along cracks or mechanical fault lines.

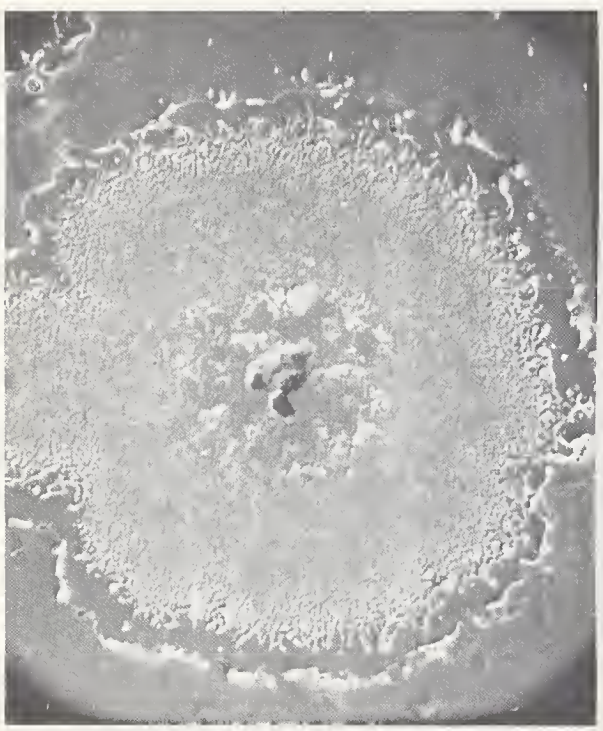

Fig. 25 Q(cF)(255 X) The following five (5) pictures shows the total area. It is difficult to determine at this magnification exactly what we are seeing except that melting, delamination, and total removal are all evident.

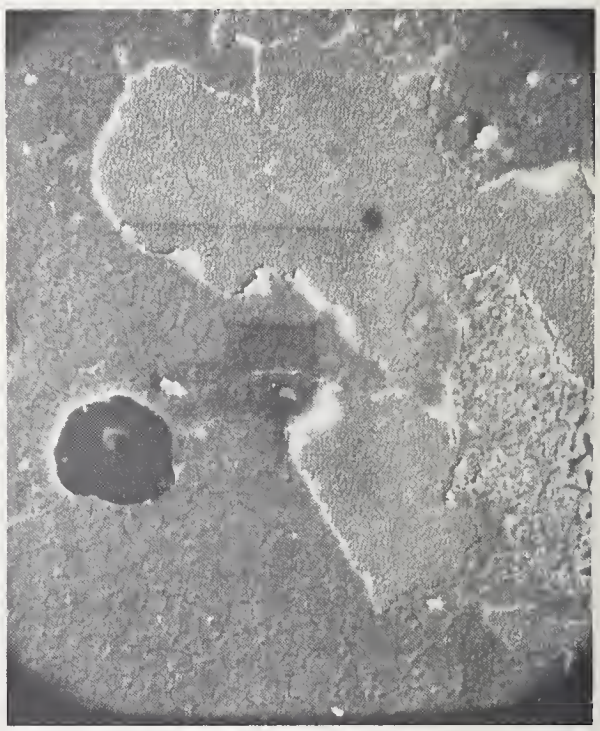

Fig. 26 R(cF)(640 X) This shows a clean removal around a particle nucleus and the removal of the upper MgF_2 layer. Note the characteristic structural difference of the ThF_4 film.

Fig. 27 S(cF)(1250 X) A striking example of the structural difference between the MgF_2 and ThF_4 layers. The edges of the MgF_2 film are slightly melted. A globule of the fused MgF_2 can be seen on the ThF_4 film.

Fig. 28 T(cF)(5700 X) This shows as area where the upper MgF_2 and center ThF_4 layers have both been fused exposing the cracked MgF_2 film on the substrate.

Fig. 29 U(cF)(5700 X) This shows some of the upper layer, fused and cracked, a cracked lower layer and the remains of the ThF_4 center film.

Fig. 30 V(cR)(1250 X) Here we see an excellent example of total stack removal, following the crack lines in the outer film. The MgF_2 layer has not even begun to fuse and the film surface shows a distinctly different character than the front surface damage films in examples Q through V.

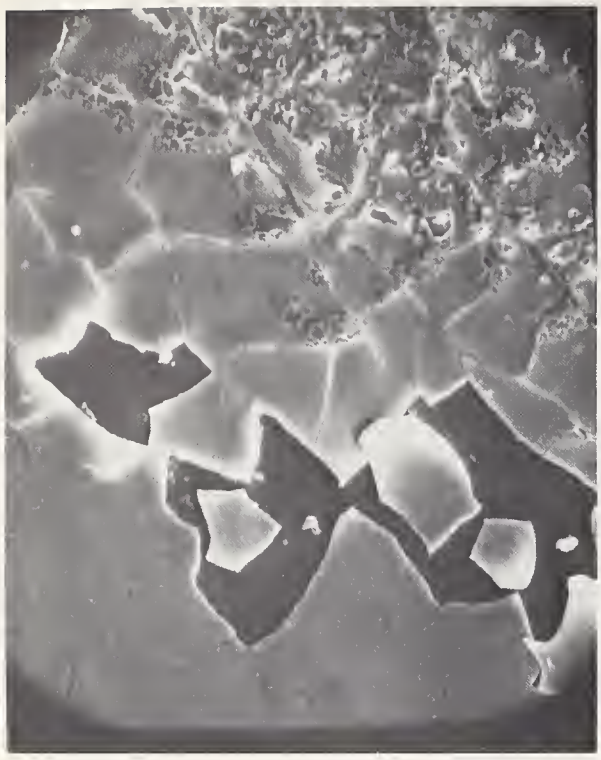

Fig. 31 W(cR)(640 X) A detail of rear surface stack removal.

Fig. 32 X(cR)(1250 X) Detail of glass fracture (Refer to text).

Fig. 33 Y(cR)(5700 X) Same as above but at higher magnification (refer to text)

Fig. 34 Z(aF)(626 X) An interesting photograph showing an exposed area of fused Magnesium Oxide film and an area of complete removal. The complete film system that remains has a jagged edge due to cracks in the MgF_2.

Fig. 35 AA(aR)(626 X) Clean removal of the film system around a nucleus. This picture shows clearly how small the nuclei actually are (were). It is possible that the nuclei were not surface dust particles but solid particles of coating material.

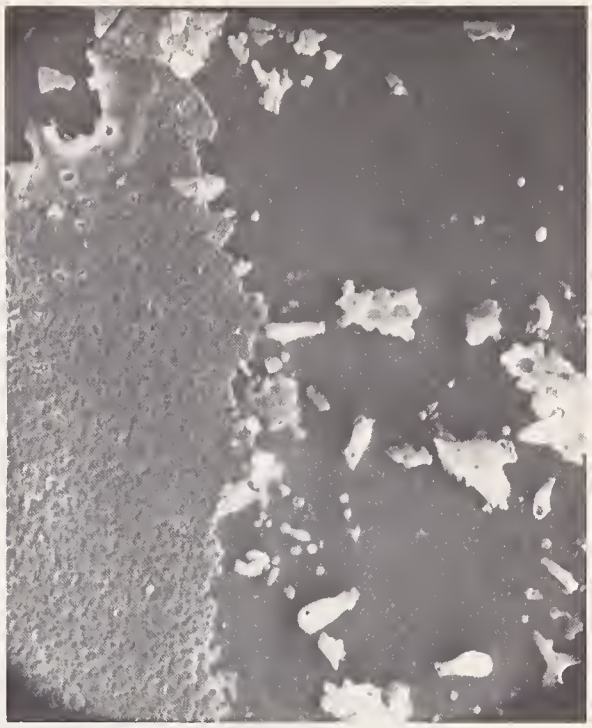

Fig. 36 BB(dR)(2110 X) Photograph of that area of the MgF_2 film where the damage had shown a strongly oriented pattern. This is one of a sequence of photographs of gradually increasing magnification. Nothing is visible in the form of the damage area that would indicate exactly why the damage had been strongly oriented.

Fig. 37 CC(dR)(5060 X) This is a high magnification photograph of a damage area where the mechanism is mainly fusion. There is however some evidence of crazy paving type cracks, due to film stress, that were not evident in the Normarski photographs. In the Nomarski photographs only short hairline micro-cracks were evident.

Fig. 38 DD(dR)(5060 X) This is an area where the damage is almost completely due to film removal at stress cracks. Note in this picture that there is some evidence of surface residue near the edges of the film.

COMMENTS ON PAPER BY R. RUSSELL AUSTIN AND ARTHUR GUENTHER

The use of rf sputtering for laying down optical coatings raises some interesting possibilities for producing coatings with higher resistance to optical damage. For example, by mixing, in the vapor phase SiO_2 and ZrO_2, one can tailor the index of refraction of the mixed coating to achieve a range of desired values. Both of these materials exhibit high damage thresholds, and the combined coating would be expected to be more damage resistant than a coating made using a naturally occuring material of the same refractive index. Work is planned in which a periodic variation of index will be used in place of the conventional multilayer dielectric coating. There are several advantages to using a continuously varying refractive index rather than a discontinuous multilayer surface. The residual stress is less since there are no discrete interfaces between layers of different materials. Additionally, there are no discontinuities in the electric field such as are found at the interfaces of media of differing dielectric constants. Since zirconium oxide is tensile and silicon dioxide compressive, one would expect a mixed coating to exhibit a certain automatic stress relief. The technique of rf sputtering is an extremely slow process and does not seem readily adaptable to the coating of large areas but does produce a coating which exhibits a lower scattering than that produced by evaporated coatings. The principal reason for this seems to be that in the process of laying down evaporative coatings, particulate matter is also deposited along with the coating material. This particulate matter is not present when rf sputtering is used.

Minimizing Susceptibility to Damage in CO_2 Laser Mirrors

H. E. Bennett

Michelson Laboratory
Naval Weapons Center
China Lake, California 93555

The absorption of mirror coatings is of major concern in cw laser operation and becomes even more crucial in pulsed operation. Very low absorption films can be made for the visible and near infrared spectral regions utilizing multilayer dielectric coatings, but at longer wavelengths the film thicknesses required and the materials available make it advantageous to use evaporated metal films instead, often with dielectric overcoatings. Although not generally realized, the infrared absorption of high reflectance metals such as silver, gold, and aluminum can easily vary by a factor of 2 and in some cases by nearly an order of magnitude depending on how the film is prepared. Dielectric overcoating layers can increase the absorption still further. Also, they will not completely stop the growth of the tarnish film which forms slowly on an unprotected silver surface. At 10.6 μ the tarnish film often will increase the absorption less than do common overcoating materials, and thus a properly prepared unovercoated silver- or gold-surfaced mirror may be the best choice at present for high power CO_2 laser applications.

Key Words: Absorption, aluminum, anomalous skin effect, evaporated films, gold, mirror damage, mirrors, reflectance, silver.

1. Introduction

Damage suffered by mirrors used in infrared laser systems occurs in part because of heating effects at the mirror surfaces. Intense local heating degrades the mirror coating and can also damage the mirror surface. A study of the problem of how to minimize damage resulting from such heating then separates into two approaches: (1) how to minimize heating of the mirrors, and (2) how to make mirror coatings which do not deteriorate under conditions of intense heating. Only the first approach will be considered in this paper.

One method of minimizing heating effects is to spread the beam on the mirror surface, so that the power incident per unit area is reduced. Once this has been done, the only ways to further reduce mirror heating are to minimize the energy absorbed by the mirror and maximize the energy carried away by cooling. Both these approaches are effective with cw lasers. However, in pulsed operation, cooling during the period the coating is being irradiated may be impossible. Heat conduction in a metal results primarily from the drift motion of the conduction electrons, while in a dielectric it is caused primarily by phonon excitation. Other mechanisms such as internal radiation and excitation of excitons may also sometimes be important, but except in the case of internal radiation, heat transfer through a solid cannot occur faster than the velocity of sound in a solid. Longitudinal sound velocities typically are between 2×10^3 and 6×10^3 m/sec, so that if a picosecond laser pulse falls on a mirror surface, the energy will only propagate to a depth of from 20 to 60 Å during the time of the pulse, no matter how hot the surface becomes. In this situation, the only way mirror heating can be minimized is to make the absorption of the mirror surface very low. Corner cube reflectors made of extremely transparent materials such as GaAs could be used, but such systems have low thermal conductivity and thus are difficult to cool if high power inputs are used for extended periods of time. The most promising approach to the problem of reducing mirror damage resulting from excessive heating appears to be to study methods for increasing the reflectance of the mirror surface. Since the reflectance plus absorbance plus transmittance (if any) equals unity, any increase in reflectance in an opaque coating guarantees a decrease in absorbance.

High reflectance, low absorbance, multilayer dielectric mirror coatings have been produced for the visible and near infrared regions of the spectrum. Some of these have extremely high reflectances, of the order of 99.9%, and thus very low absorption. Unfortunately, at longer infrared wavelengths there are relatively few transparent coating materials available, and large thicknesses are required to make quarter wave layers. Thus good multilayer dielectric mirrors are extremely difficult to design and produce. Fortunately, metals have much lower absorbances in the infrared than they do at shorter wavelengths, and metal-coated mirrors have the highest reflectance and lowest absorbance yet attained in the 10 μ region of the infrared and at longer wavelengths. The absorption of metal-coated mirrors can vary widely, however, depending on the type of metal used and the way in which the mirror is prepared. Some of the reasons for this variation and techniques for minimizing the absorption of such infrared mirrors will be discussed here.

In this paper we will first discuss the anomalous skin effect and show that the roughness of the mirror surface can affect the effective mean free path of the conduction electrons near the surface of the metal and thus cause variations in absorption of as much as 50%. We will then discuss variations in absorption which have actually been measured for different types of metal-coated mirrors, show that these variations are much larger than can be accounted for on the basis of the anomalous skin effect alone, and speculate as to their origin. Finally, we will discuss protective dielectric overcoating layers and show that in practice such layers often significantly increase the absorption of silvered mirrors at 10.6 μ over that which would be obtained even if an uncoated silvered mirror were badly tarnished.

2. Anomalous Skin Effect

Microroughness of a surface can increase its absorption in the infrared by as much as 50% through the mechanism of the anomalous skin effect. This increase occurs even though the roughness is much too small to cause diffuse scattering of light from the surface, such as occurs in the visible region of the spectrum. To understand the anomalous skin effect theory, consider an interface between a dielectric such as air and a clean metal surface. The reflectance at this interface is determined both by extrinsic parameters having to do with the roughness and shape of the surface, lattice disorder near the surface, etc. and by intrinsic parameters determined by the band structure of the material. It is not always realized that the complex optical constant $(n - jk)$, which describes the optical behavior of the metal, is a phenomenological parameter which is determined by both the intrinsic and extrinsic parameters associated with the interface. In much the same way the electrical conductivity of the metal is determined not only by its band structure but also by the number and kind of lattice dislocations, possible impurity atoms, etc. The parallel between the optical and electrical parameters associated with the metal is particularly close in the infrared, where interband transitions often are forbidden and the optical properties of the metal are determined almost entirely by free-carrier effects, which also determine its conductivity.

The reflectance at an air-metal interface is given by

$$R = \frac{(n - 1)^2 + k^2}{(n + 1)^2 + k^2} \tag{1}$$

which, when $n \gg 1$ and $k \gg 1$ as is true in the infrared for a good conductor, can be approximated by [1][1]

$$R \cong \exp[- 4n/(n^2 + k^2)] \quad . \tag{2}$$

If n and k are 10 or more, the error made in using eq. (2) instead of eq. (1) is less than 0.001 in all cases [1].

When the optical penetration depth of the incident radiation is sufficiently long relative to the mean free path of the conduction electrons so that the electrons are, to a first approximation, moving in a constant radiation field between collisions, the optical constants in regions where only quasi-free electron absorption can occur are given by [1].

$$n^2 - k^2 = 1 - \frac{4\pi\sigma_0}{\tau(\omega^2 + \tau^{-2})} + 4\pi\alpha_0 \tag{3}$$

---

[1]Figures in brackets indicate the literature references at the end of this paper.

$$nk = \frac{2\pi\sigma_0}{\omega\tau^2(\omega^2 + \tau^{-2})} \quad , \tag{4}$$

where σ_0 is the dc conductivity of the material, assumed isotropic, and τ is the "relaxation time" of the conduction electrons under the action of an exciting radiation field of circular frequency ω. The term α_0 represents the contribution to the electric susceptibility made by processes such as interband transitions, polarization of the atomic cores, etc. which occur outside of the frequency range of interest. In what follows, assume that the contribution made by α_0 can be neglected. If this assumption is not entirely justified, the contribution of α_0 to the reflectance can be computed from an expansion [1].

Neglecting α_0 and substituting eqs (3) and (4) into eq (2) we obtain

$$R = \exp\{-(2\omega/\pi\sigma_0)^{\frac{1}{2}}[(\omega^2\tau^2 + 1)^{\frac{1}{2}} - \omega\tau]^{\frac{1}{2}}\} \tag{5}$$

which is the basic equation relating the optical reflectance to the electrical conductivity. Note that if $\omega\tau << 1$, eq (5) reduces to the Hagen-Rubens relation

$$R = 1 - (2\omega/\pi\sigma_0)^{\frac{1}{2}} \quad . \tag{6}$$

However, for a good conductor such as silver or gold, the Hagen-Rubens relation is not valid in the 10.6 μ region of the infrared, and if it is used in place of the more accurate eq (5) the result is significantly in error. For example, assuming the bulk value for σ_0 and calculating τ from the Lorentz-Sommerfeld relation

$$\tau = m^*\sigma_2/Ne^2 \quad , \tag{7}$$

where m* is the carrier effective mass, N the effective number of carriers, and e the electronic charge, and assuming the free electron value for N/m*, the absorption calculated from the Hagen-Rubens relation differs from the Drude value at 10.6 μ by approximately a factor of 3 for both silver and gold. In spite of the fact that it cannot be justified theoretically, however, the Hagen-Rubens relation, by overestimating the theoretical absorption, often does fit the experimental data for good conductors rather well in the intermediate infrared. Some of the reasons for this anomaly are discussed below.

If the mean free path of the conduction electrons is much smaller than the penetration depth of the incident radiation, the infrared reflectance is given to a good approximation by eq (5). However, if these two quantities become comparable, eq (5) must be modified, and the resulting modification is often called the anomalous skin effect. Figure 1 shows that at radio frequencies the optical penetration depth or skin depth (solid curve) is much larger than the mean free path at room temperature (lower dashed curve). Only at cryogenic temperatures where the mean free path is shown by the upper dashed curve does the anomalous skin effect become important. In the infrared spectral region, however, the penetration depth is comparable to the mean free path at room temperature and hence the optical properties of metal-coated mirrors used in the infrared will be affected even at normal operating temperatures.

When the anomalous skin effect becomes important, a third parameter, p, is introduced into the theory. This parameter is related to the probability that a conduction electron striking the surface will be reflected "specularly", i.e., will maintain the same components of momentum parallel to the surface before and after reflection. How to calculate the value of p for a given surface condition is not yet entirely clear, but unless the surface is nearly atomically smooth, one would expect p to be essentially zero.

Figure 2 shows the reflectance of silver calculated from the bulk electrical parameters and plotted as a function of wavelength. The short-dashed curve merging with the solid curve shows the predictions of the Drude theory, eq (5). The solid curve, which coincides with the dashed curve except for a slight difference in the region between 10 μ and 100 μ, is calculated from the more exact theory assuming p = 1 (specular reflection of the conduction electrons). The long-dashed curve represents the theoretical value for the case p = 0 (diffuse reflection of the conduction electrons). At wavelengths shorter than one micron, interband transitions and other effects will significantly modify the calculated curves, but in the 10 micron region they should be valid. If the surface is sufficiently rough so that p = 0 rather than p = 1, the infrared absorption in silver should change from 0.0047 to 0.0071, an increase of 0.0024 or about 50%.

In the case of gold, the absorption should increase from 0.0062 to 0.0090, again about 50%. Figure 3 shows the infrared reflectance of gold. The solid line is calculated assuming the bulk conductivity, one free electron per atom, and p = 1. The dashed line shows a similar calculation except that

p = 0. No optical data went into these calculations. The squares are the experimental reflectance values for a gold film deposited in ultrahigh vacuum on a supersmooth quartz substrate. This surface had an rms roughness of about 8 Å, so it was approximately 3 times as smooth as a conventional optical flat. Although at wavelengths shorter than 3 μ the measured reflectance of the gold film falls below the calculated curve, largely because interband transitions are not included in the calculations, at longer wavelengths the agreement between the measured reflectances and the calculated curve for p = 1 is excellent. Similar results have been obtained for silver [1].

If the roughness of the substrate surface is larger, the measured reflectance would be expected to fall to the value indicated by the dashed curve. This prediction has been verified for silver [1]. In the case of aluminum, the calculations are clouded by the possibility that mechanisms other than free carrier effects may play a role even at infrared wavelengths as long as 10.6 μ. However, if we disregard this possibility and calculate the reflectance at 10.6 μ assuming first p = 1 and then p = 0, we find that the difference in reflectance between these two cases is much less than for either silver or gold. This prediction has also been verified experimentally. Thus, surface microroughness is not too important for aluminum, but is very important if one is trying to produce silver or gold mirrors having the highest reflectance (and thus the lowest absorption) in the infrared.

3. Influence of Evaporation Conditions

Although surface microroughness does influence the absorption of infrared energy via the anomalous skin effect, it cannot account for the large variations in absorption of infrared mirrors found experimentally. Recently Dr. Kelsall of Lincoln Laboratory measured the reflectances at 10.6 μ of over 50 mirrors obtained commercially or produced at Lincoln Laboratory [2]. His results are summarized in table 1 along with our measurements on silver, gold, and aluminum mirrors prepared in our laboratory

Table 1. Optical properties of infrared mirrors at 10.6 μ

	Silver	Gold	Aluminum	Enhanced metal	All dielectric
			(a) Reflectance		
Kelsall R_{max}	0.9888	0.9915	0.9840	0.9933	0.9907
Kelsall R_{min}	0.9589	0.9705	0.9710	0.9789	0.9579
Kelsall R_{av}	0.9705	0.9846	0.9787	0.9881	0.9783
Bennett R	0.9953	0.9940	0.9875		
			(b) Absorption		
Kelsall A_{min}	0.0112	0.0085	0.0160	0.0067	0.0093
Kelsall A_{max}	0.0411	0.0295	0.0290	0.0211	0.0421
Kelsall A_{av}	0.0295	0.0154	0.0213	0.0119	0.0217
Bennett A	0.0047	0.0060	0.0125		

using special evaporation techniques. In obtaining the absorption values given in the lower part of the table, we have assumed that the energy not reflected is absorbed. Notice first that the absorption of the best gold- and silver-coated mirrors is lower than that observed for either enhanced metal or all-dielectric coatings at 10.6 μ, and is in excellent agreement with the theoretical values for these metals calculated from the anomalous skin effect theory assuming p = 1. However, the variation in absorption for either material is enormous, nearly an order of magnitude in the case of silver and a factor of 5 for gold. By contrast, in the case of aluminum this variation is only a little over a factor of 2. These variations are much too large to be accounted for by the anomalous skin effect alone. They do illustrate one reason why aluminum has been a preferred material to use for infrared mirror coatings. Although the absorption of aluminum coatings is over twice as large as that of the best silver and gold coatings, at least it is reasonably reproducible.

Since both silver and gold are significantly superior to other coating materials both theoretically and experimentally, it becomes doubly important to understand the origins of the large variability in absorption found in coatings made from these materials. Purity of material may well play a role, but there are significant differences in the infrared absorption of samples of apparently the same purity. For example, in figure 4 the dashed curve shows the reflectance of aluminum films deposited under

standard vacuum conditions ($\sim 10^{-5}$ Torr) and then aged. The experimental points are measured reflectances of freshly deposited aluminum films prepared under ultrahigh vacuum conditions ($\sim 10^{-9}$ Torr). Both films were made from aluminum having a purity of 99.999% or better and were evaporated from tungsten spiral heaters with similar rates of deposition on similar supersmooth substrates. At 10.6 μ the reflectance of the aged standard vacuum films differs from that of films deposited in ultrahigh vacuum by 0.0064. Since the absorption of the latter films is about 0.0125 at 10.6 μ, the films deposited under standard vacuum conditions have over 50% more absorption than do those prepared in a better vacuum. One may argue that since aluminum is highly reactive, the residual gas bombardment of the substrate during deposition produces significant oxidation of the aluminum film as it is being deposited. There may be some truth in this observation, since much of the residual gas is composed of water vapor, which does react with aluminum, and the arrival rate of residual gas atoms at the substrate surface at 10^{-5} Torr is approximately the same as the arrival rate of aluminum atoms at normal deposition rates. However, similar effects have been observed for gold and silver films which do not react strongly with water vapor, so that a more complete explanation of the influence of residual gas pressure on film characteristics seems desirable.

Figure 5 shows another example of the difference in absorption which may result from differences in sample preparation. In this case the material is OFHC (oxygen-free, high conductivity) copper. Two samples were cut from the same ingot; one was mechanically polished to an excellent figure and the other was electropolished. In spite of the fact that the bulk material in both samples was of identical purity, the reflectances are markedly different, causing the absorption at 10 μ to differ by nearly a factor of two.

What can be the cause of such discrepancies in the infrared absorption of metals? Thin dielectric corrosion films may be ruled out since naturally occurring oxide films at room temperature for materials such as aluminum are self-limiting and do not exceed 30 to 40 Å in thickness. Films of this thickness can be shown analytically to introduce a completely negligible change in absorption in the infrared, at least if the mechanism which determines the change in absorption is the conventional thin film interference phenomenon. Corrosion films larger than a few monolayers do not generally form on gold. The tarnish layer on silver is transparent at 10.6 μ, and has relatively little effect, as will be discussed in the next section. However, all three metals show a pronounced variation in infrared absorption. Why?

The answer to this question may lie in the area of metal physics. The same types of phenomena which cause the bulk conductivity of a metal to vary--dislocations, impurity scattering, etc.--should also produce changes in the infrared absorption of metals. As was pointed out in the discussion of the anomalous skin effect, the infrared absorption is closely connected theoretically with its conductivity, and mechanisms which affect the latter should also affect the former. There is one major difference, however. Whereas changes in electrical conductivity, particularly at low frequencies, are determined almost entirely by changes in dislocation density and impurity concentration deep inside the material, changes in optical absorption will be determined entirely by changes within a few hundred angstroms of the surface. Physical metallurgists have concentrated their efforts on understanding how dislocations behave inside a metal. Relatively little work has been done on the physical metallurgy of the surface, but enough is known to be sure that it is not the same as that in the bulk of the material. I feel sure that this area, surface physics of metals, offers a challenging new field for investigation by the physicist and physical metallurgist, and that Optics offers a powerful tool for this investigation. Furthermore, from such an investigation may emerge a better understanding of the effect of different procedures of surface preparation on the infrared properties of metals. In any event, it seems clear from what has been done so far that how a mirror coating is prepared and not simply what material is used in making the coating is of primary importance if coatings with very low infrared absorption are to be obtained.

4. Dielectric Overcoated Metal Mirrors

In theory, and occasionally even in practice, the infrared reflectance of a metal-coated mirror may be increased and the absorption reduced by overcoating the metal with a multilayer dielectric film. However, although it is simple to design a multilayer dielectric overcoating film which will enhance the reflectance of a metal such as silver or gold, it is difficult to achieve this enhancement in practice. Dr. Kelsall did not report, nor have we yet seen, any "enhanced" metal mirrors which have as high reflectance at 10.6 μ as the best uncoated silver or gold mirrors. One should not conclude from these data that improvements cannot be made by utilizing the overcoating technique, but at present the use of dielectric overcoatings seems more likely to increase than to reduce the amount of absorption in mirrors at the CO_2 laser wavelength. There is another reason for a dielectric overcoat, however. Both silver and gold are quite soft when first evaporated and silver tarnishes readily when exposed to the atmosphere. By overcoating the metal film with a dielectric, one may produce a hard coating and also inhibit tarnish formation on silver. The questions to be answered are the following: (1) how well does a dielectric overcoating protect the surface, (2) how well does it prevent silver from tarnishing, and (3) do the advantages offered by the dielectric offset the penalty paid in terms of increased absorption.

Since gold does not generally tarnish even when exposed to the atmosphere, we have concentrated on studying the effects of dielectric overcoatings on silver. One of the first questions to answer is how much does the tarnish change the reflectance and absorbance in the infrared. The silver sulfide tarnish films absorb strongly in the visible region of the spectrum, but, since Ag_2S is a semiconductor with an absorption edge at about 1.4 μ, it is nearly transparent in the infrared [3]. Thus, silver sulfide tarnish would be expected to have relatively little effect on mirror performance at wavelengths longer than 1.4 μ.

Figure 6 shows the reflectance of three unprotected silvered mirrors in the ultraviolet, visible, and near infrared as reported by Bennett, Stanford, and Ashley [3]. The solid line represents freshly deposited silver, the long-dashed line silver with a 39 Å tarnish film on it, and the short-dashed line silver with a 109 Å thick tarnish film on it. The tarnish film significantly reduces the reflectance in the visible, but has very little effect in the 2 μ wavelength region. The thickest silver sulfide film required 19 months to form on the silvered mirror, which was stored in our laboratory in a loosely covered dish.

The rate of formation of silver sulfide on silver is highly variable, depending on the concentration of H_2S in the air, the humidity, air circulation, and the condition of the silver surface [4]. At 100% humidity, in air containing 10% H_2S, a film as thick as that which required 19 months to grow in the example cited would form in only an hour's time. On the other hand, by flushing a mirror enclosure with dry nitrogen, tarnish formation can be almost completely inhibited. Encapsulating the silver in a dielectric will also inhibit tarnish formation, although since silver ions are highly mobile, the diffusion rate through the dielectric and the tendency to form pinholes should be as low as possible. Studies of encapsulating materials carried out in connection with microelectronics fabrication suggest that two of the best dielectrics to use are quartz and aluminum oxide.

Figure 7 shows the results obtained when unprotected silver and silver protected by a 1500 Å thick film of SiO_2 were exposed to a flowing gas containing 10% H_2S and 100% humidity. In an hour an Ag_2S film about 100 Å thick would be expected to form under these conditions on unprotected silver. The solid lines indicate the reflectance measured for unprotected silver at wavelengths of 1 μ and 7 μ, and the dashed lines the reflectance measured for protected silver. The reflectance of the unprotected silver decreased significantly at 1 μ but relatively little at 7 μ. The protected film maintained nearly its initial reflectance longer than did the unprotected film. As exposure continued, however, the protective film broke up and the specular reflectance dropped much more rapidly than for the unprotected film both at 1 μ and at 7 μ. Part of this drop may have been caused by the greatly increased scattering of light from the mechanically disturbed protected surface. Possibly the formation of Ag_2S may also have been more rapid on the shattered protected surface than on the bare silver. Whatever the reason was for the observed drop in reflectance of the protected sample, it is clear that once the protective film was breached, the mirror having a protective dielectric overcoat deteriorated much more rapidly upon further exposure to H_2S than did the silvered mirror which was unprotected.

Figure 8 shows the reflectance of freshly deposited silvered mirrors with and without a dielectric SiO_2 protective overcoat as a function of wavelength from 1 - 20 μ. The short-dashed line shows the reflectance of an unprotected silvered mirror. The long-dashed line shows the measured reflectance of a second mirror deposited in the same evaporation as the unprotected mirror and overcoated with a 1500 Å thick SiO_2 film. The solid line shows the calculated reflectance which would be predicted if a 1500 Å thick SiO film were deposited on the silver mirror. The predicted reflectance would be essentially the same if optical constants for SiO_2 instead of SiO had been used [5,6], except that the dip in reflectance near 10 μ would occur at a slightly shorter wavelength and thus would be in poorer agreement with experiment.

There are several interesting features shown in figure 8. First, the quartz dielectric overcoating layer does not increase the infrared reflectance above that for uncoated silver at any wavelength. Because of strong absorption, the 3 μ and 10 μ regions are the least favorable regions in which to use a quartz-overcoated silvered mirror. Second, the actual performance obtained with an overcoating film may be significantly worse than that expected from the calculations. In this case the increase in absorption at 10 μ caused by the overcoating film is over 3 times as large as would be expected from theory. At longer wavelengths no significant decrease in reflectance should be observed according to theory. However, in practice, the observed reflectance of the overcoated sample is lower than that of the unprotected sample even at 20 μ, the long-wavelength limit of the measurements. The reason for this result is not well understood but the result itself is very common. A third point is that it is very difficult to eliminate the absorption at 3 and 10 μ caused by absorption in the quartz. Figure 9 shows the only dielectric multilayer coated silver mirror we have yet seen in which the infrared reflectance was actually enhanced over an extended region by the multilayer overcoat. However, in spite of the low absorption which this coating had over most of the spectrum, in the 3 μ and 10 μ regions the absorption is considerably more than that of uncoated silver, presumably because either quartz or silicon monoxide was used as the low index dielectric layer.

What alternate materials can be considered as low index dielectric films in the infrared? One is aluminum oxide, which can be deposited readily using an electron gun and which has been found to be probably the best encapsulating material available for microcircuit applications. In spite of its

toughness and freedom from pinholes, not even a thick (3200 Å) film of Al_2O_3 prevented degradation of a silvered mirror surface exposed to 10% wet H_2S for an extended period. At a wavelength of 4 μ, to give a representative example, the reflectance started to drop after 4 hours' exposure, and after 30 hours the absorption at this wavelength had increased by a factor of 3. Even before H_2S exposure, this thick Al_2O_3-coated silver had an absorption at 4 μ a factor of 2 larger than uncoated silver, and the absorption increased with increasing wavelength. Thus, one would not want to coat a silver surface with a thick, tarnish-inhibiting layer of Al_2O_3 unless the mirror was to be exposed to very severe tarnishing conditions, in which case even the Al_2O_3 will not completely prevent tarnishing. Also aluminum oxide has a Reststrahlen resonance in the vicinity of the 10.6 μ CO_2 laser line, making it similar to SiO_2 in this respect.

Another coating material, magnesium fluoride, is essentially transparent in the 10.6 μ wavelength region, and freshly deposited thin coatings of MgF_2 do not increase the absorption of silver mirrors in this region. With time, however, the absorption of some MgF_2-overcoated silvered mirrors has been observed to increase while that of an uncoated silvered mirror deposited at the same time remained constant. The reason for this behavior is not yet understood, but it is clear that even nominally nonabsorbing overcoating materials may introduce additional absorption in the infrared when used as a protective overcoating on metal mirrors.

5. Conclusions

The damage threshold of mirrors used in infrared laser systems is strongly dependent on the absorption in the mirror coatings. In the intermediate infrared spectral region, metals offer the greatest promise for minimizing absorption; evaporated metal films of silver or gold have the lowest absorption yet observed at 10.6 μ. The absorption of the best of these films is in good agreement with theoretical values calculated from the electrical parameters of the metal. However, the absorption of silver and gold films prepared in different ways may vary by as much as a factor of 5 for gold and by nearly an order of magnitude for silver. Some of this variation would be expected to be caused by surface microroughness via the anomalous skin effect, but the magnitude of the observed variation is too large to be completely accounted for in this way. Dislocations and lattice disorder near the metal surface may also be factors, but much more work needs to be done in this area before these effects are clearly understood. Finally, protective dielectric overcoating films designed to encapsulate the surface and prevent tarnish formation in the case of silver do not completely prevent corrosion even if applied in rather thick layers. They also tend to increase the absorption of the coating, particularly in the 10.6 μ region. Since the silver sulfide tarnish does not strongly affect absorption in this region, even in rather thick layers, an uncoated, properly prepared, silver mirror may be the best choice at present for many high power infrared laser applications.

6. References

[1] Bennett, H. E., Bennett, J. M., Ashley, E. J., and Motyka, R. J., Verification of the anomalous-skin-effect theory for silver in the infrared, Phys. Rev. 165, 755 (1968).

[2] Kelsall, D., Absolute specular reflectance measurements of highly reflecting optical coatings at 10.6 μ, Appl. Opt. 9, 85 (1970).

[3] Bennett, Jean M., Stanford, J. L., and Ashley, E. J., Optical constants of silver sulfide tarnish films, J. Opt. Soc. Am. 60, 224 (1970).

[4] Bennett, H. E., Peck, R. L., Burge, D. K., and Bennett, J. M., Formation and growth of tarnish on evaporated silver films, J. Appl. Phys. 40, 3351 (1969); Burge, D. K., Bennett, J. M., Peck, R. L., and Bennett, H. E., Growth of surface films on silver, Surface Sci. 16, 303, (1969).

[5] Spitzer, W. G. and Kleinman, D. A., Infrared lattice bands of quartz, Phys. Rev. 121, 1324 (1961).

[6] Hass, G. and Salzberg, C. D., Optical properties of silicon monoxide in the wavelength region from 0.24 to 14.0 microns, J. Opt. Soc. Am. 44, 181 (1954).

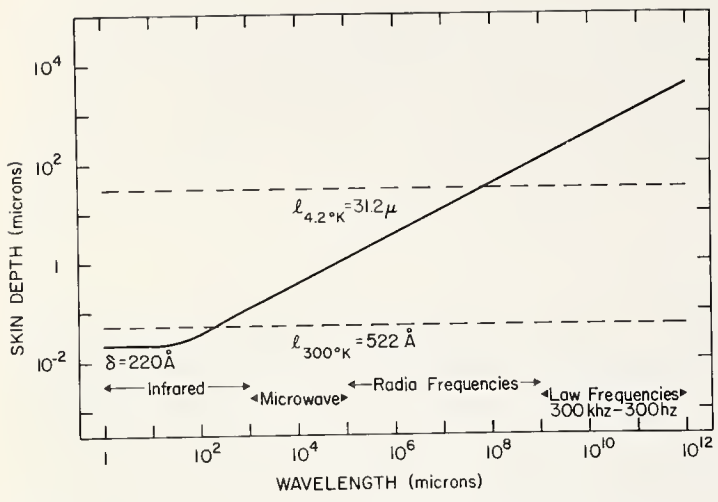

Fig. 1 Plot of the optical penetration depth or skin depth versus wavelength for silver (solid curve), and the mean free path of the conduction electrons at two different temperatures (dashed curves).

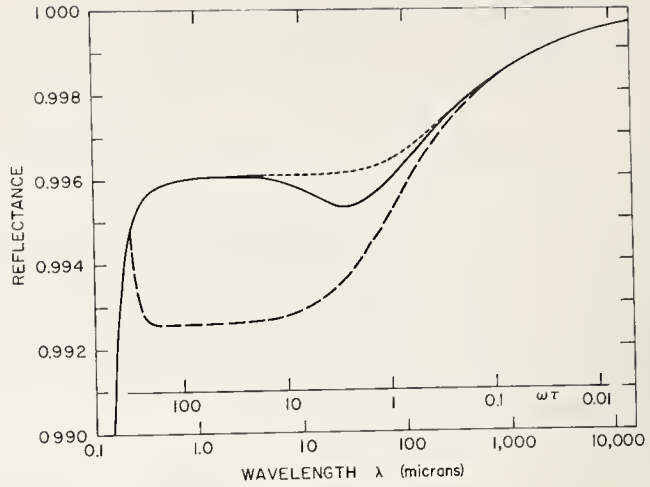

Fig. 2 Reflectance of silver calculated from the anomalous skin effect modification of the Drude theory assuming bulk dc conductivity, 1 free electron per atom, and p = 1 (solid curve) or p = 0 (long-dashed curve). The simple Drude theory is given by the short-dashed curve and connecting solid curve. Since absorption caused by interband transitions and other effects has not been included, these curves cannot be directly compared with measured values for wavelengths shorter than about 1μ.

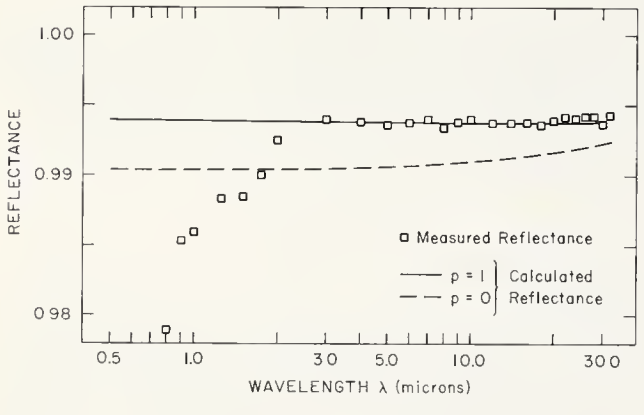

Fig. 3 Calculated and measured infrared reflectance of gold in the wavelength range 0.8 - 32μ. The squares are measured points for gold evaporated in ultrahigh vacuum. The curves were calculated from the anomalous skin effect modification of the Drude theory assuming bulk dc conductivity, 1 free electron per atom, and p = 1 (solid curve) or p = 0 (long-dashed curve).

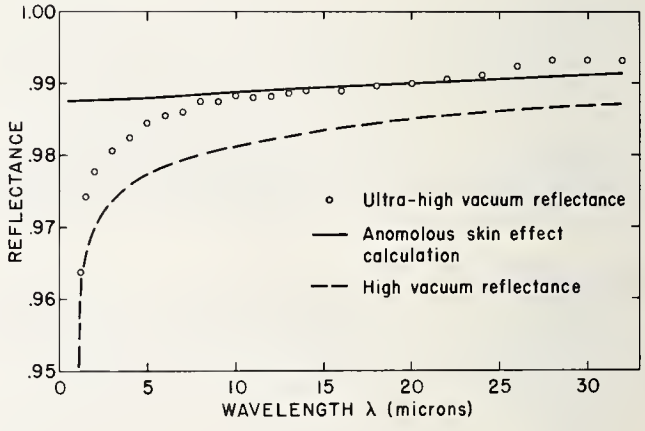

Fig. 4 Calculated and measured infrared reflectance of aluminum in the wavelength range 1.2 - 32μ. The circles are measured points for a film evaporated in ultrahigh vacuum, and the dashed curve represents the average reflectance of aluminum films evaporated in standard vacuum and then aged. The solid curve was calculated from the anomalous skin effect modification of the Drude theory assuming bulk dc conductivity, 2.6 free electrons per atom, and p = 1.

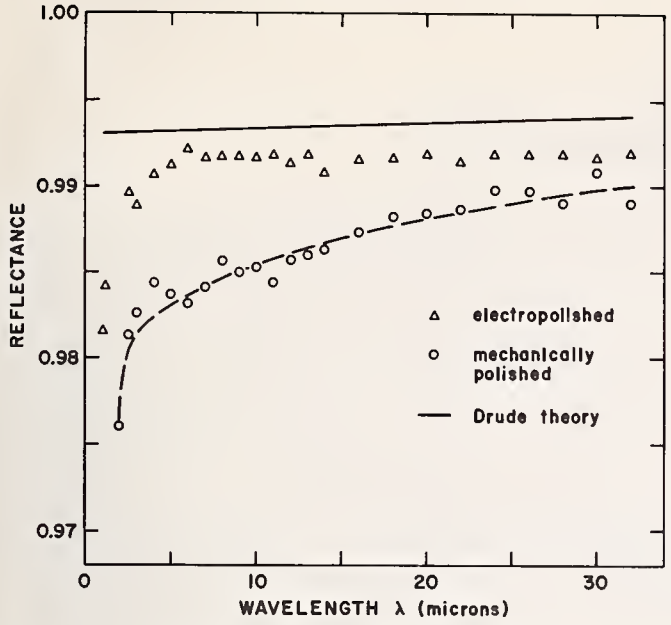

Fig. 5 Calculated and measured infrared reflectance of copper in the wavelength range 1 - 32 μ. Circles and triangles are measured points for mechanically polished and electropolished samples, respectively. The solid curve was calculated from the anomalous skin effect modification of the Drude theory assuming bulk dc conductivity, 2 free electrons per atom, and p = 1.

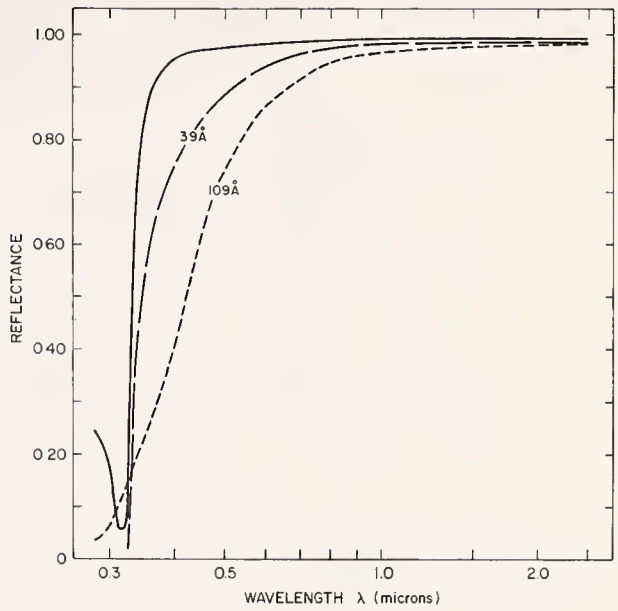

Fig. 6 Reflectance of fresh silver (solid curve) and silver covered with two thicknesses of silver sulfide tarnish films: 39 Å (long-dashed curve), 109 Å (short-dashed curve).

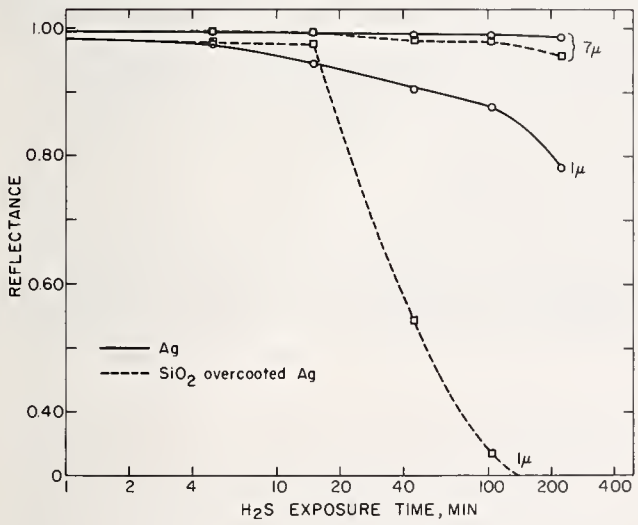

Fig. 7 Change in reflectance with time for unprotected silver (solid curves) and silver covered with a 1500Å thick film of SiO_2 (dashed curves). Measurements were taken at wavelengths of 1 μ and 7 μ.

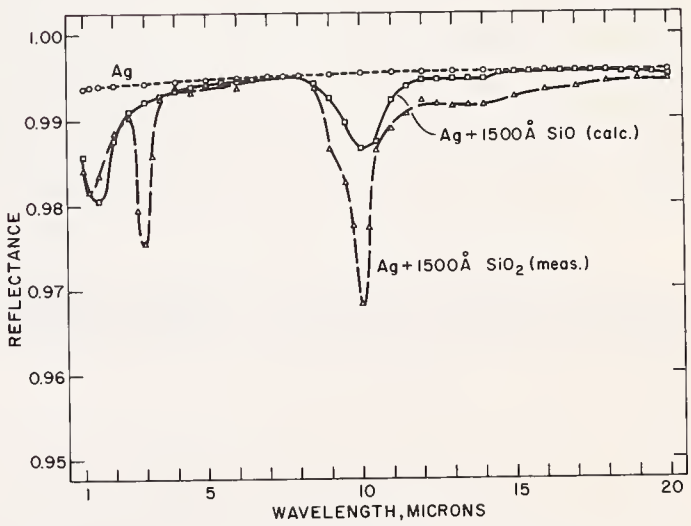

Fig. 8 Measured reflectance of fresh silver (short-dashed curve) and silver covered with a 1500Å thick film of SiO_2 (long-dashed curve). The solid curve is the calculated reflectance of silver covered with a 1500Å thick film of SiO.

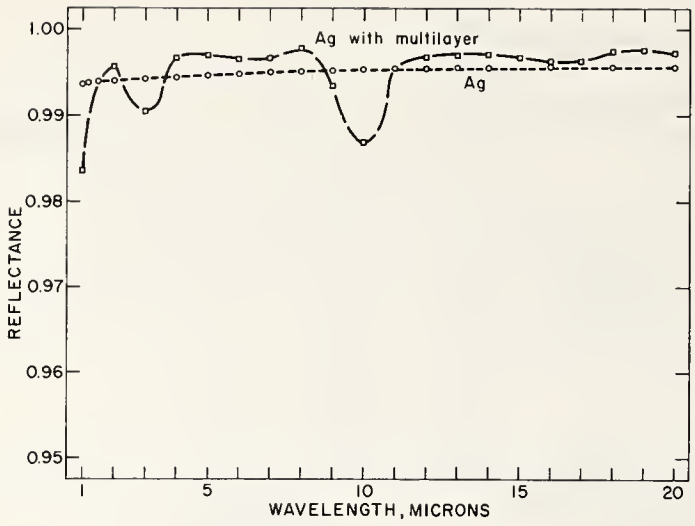

Fig. 9 Measured reflectance of fresh silver (short-dashed curve) and silver covered with a multilayer dielectric coating

COMMENT ON PAPER BY HERBERT BENNETT

Dr. Bennett, in collaboration with co-workers at the National Bureau of Standards, in Gaithersburg, reported on the explosive vapor release accompanying surface damage in glass. Samples of NG-1 Schott filter glass, with a neutral density of 4, were exposed to the output of the NRL test laser. The major constituents of the glass sample are lead, silica and potassium. Electron microscopy of the damaged surface indicated that both melting and fracture had taken place. Electron microprobe analysis showed a decrease in the potassium content of the surface in the areas of laser damage. The content of lead and silica was essentially the same in both damaged and undamaged areas of the surface. These results are consistent with the suggestion that the volatilization of the glass constituents plays a role in the damage process. The potassium is the most volatile component of the glass. It is not clear, however, at what point in the damage process the volatilization occurs.

Several comments were made to the effect that both melting and fracture are generally seen in areas of surface damage. It would seem that in areas of intense heating, melting will occur, while in areas of less intense heating, fracture can still occur due to thermal stresses.

Appendix

Participants[1]

W. B. Alexander, Schott Optical Glass, Duryea, PA 18642
R. R. Austin, Perkin-Elmer Corp., Wilton, CT 06897

E. D. Baird, Lawrence Radiation Laboratory, Livermore, CA 94550
M. Bass, Raytheon Research Div., Waltham, MA 02154
H. S. Bennett, National Bureau of Standards, Washington, DC 20234
E. S. Bliss, A.F. Cambridge Research Lab., Bedford, MA 01730
N. L. Boling, Owens-Illinois, Toledo, OH 43607
H. S. Boyne, National Bureau of Standards, Boulder, CO 80302
S. W. Bradstreet, Consultant, Dayton, OH 45409

A. Carlson, Gould Labs., Cleveland, OH 44167
W. J. Coleman, Battelle N.W., Richland, WA 99352

J. Davit, C. GE Marcoussis, 91 Marcoussis, France
D. J. Dentz, Airtron, Morris Plains, NJ 07950
L. G. DeShazer, University of Southern California, Los Angeles, CA 90007

D. F. Edwards, Colorado State University, Fort Collins, CO 80521

A. Feldman, National Bureau of Standards, Washington, DC 20234
W. D. Fountain, GTE Sylvania, Mountain View, CA 94040
W. M. Franklin, Kent State University, Kent, OH 44242
D. L. Franzen, National Bureau of Standards, Boulder, CO 80302
A. D. French, General Electric Co., Syracuse, NY 13201

R. R. Getty, Michigan State University, East Lansing, MI 48823
C. R. Giuliano, Hughes Research Labs., Malibu, CA 90265
A. J. Glass, Wayne State University, Detroit, MI 48202
P. M. Gruzensky, National Bureau of Standards, Boulder, CO 80302
A. H. Guenther, U.S.A.F. Weapons Lab., Kirtland A.F.B., NM 87117

F. T. Harris, Spacerays, Andover, MA 01810
B. E. Henderson, Michigan State University, East Lansing, MI 48823

P. M. Johnson, Lawrence Raidation Lab., Livermore, CA 94559

E. L. Kerr, Perkin-Elmer, Wilton, CT 06877

---

[1]Approximately 115 others, who did not formally register, attended selected sessions.

H. A. Lee, Owens-Illinois, Toledo, OH 43607

J. R. Lenhoff, A.F. Cambridge Research Lab., Bedford, MA 01730

G. E. Leroi, Michigan State University, East Lansing, MI 48823

R. J. Mahler, National Bureau of Standards, Boulder, CO 80302

L. D. Malmstrom, Monsanto Company, St. Louis, MO 63166

J. Marburger, University of Southern California, Los Angeles, CA 90007

J. D. Myers, Owens-Illinois, Toledo, OH 43607

N. Neuroth, Schott Optical Co., Schott Optical Co., 65 Mainz, Hassenbergsh. 10, West Germany

B. E. Newnam, University of Southern California, Los Angeles, CA 90007

J. C. Ososkie, Philco Ford, Newport Beach, CA 92663

J. H. Parks, University of Southern California, Los Angeles, CA 90007

R. J. Phelan, National Bureau of Standards, Boulder, CO 80302

P. M. Rushworth, Martin-Marietta, Orlando, FL 32808

C. Y. She, Colorado State University, Fort Collins, CO 80521

C. M. Stickley, ARPA, Arlington, VA 22209

R. Watt, LASL, Los Alamos, NM 87544

R. Webb, Holobeam, Inc., Paramus, NJ 07652

E. J. Woodbury, Hughes Aircraft Company, Culver City, CA 90230

R. F. Woodcock, American Optical Corp., Southbridge, MA 01550

C. G. Young, American Optical Corp., Southbridge, MA 01550

FORM NBS-114A (1-71)

U.S. DEPT. OF COMM. BIBLIOGRAPHIC DATA SHEET	1. PUBLICATION OR REPORT NO. NBS-SP 356	2. Gov't Accession No.	3. Recipient's Accession No.

4. TITLE AND SUBTITLE

Damage in Laser Materials

5. Publication Date: November, 1971

6. Performing Organization Code

7. AUTHOR(S) Various: Edited by Alexander J. Glass, Wayne State University and Arthur H. Guenther, Kirtland AFB, N.M.

8. Performing Organization

9. PERFORMING ORGANIZATION NAME AND ADDRESS

NATIONAL BUREAU OF STANDARDS
DEPARTMENT OF COMMERCE
WASHINGTON, D.C. 20234

10. Project/Task/Work Unit No. 2710585/2710900

11. Contract/Grant No.

12. Sponsoring Organization Name and Address

American Society for Testing and Materials and by the National Bureau of Standards (Div. 271) Boulder Laboratories, Boulder, Colorado

13. Type of Report & Period Covered Final

14. Sponsoring Agency Code

15. SUPPLEMENTARY NOTES

16. ABSTRACT (A 200-word or less factual summary of most significant information. If document includes a significant bibliography or literature survey, mention it here.)

The third ASTM Symposium on Damage in Laser Materials was held at the National Bureau of Standards in Boulder, Colorado, on May 19-20 of this year. They symposium is held as part of the activity of Subcommittee II on Lasers and Laser Materials, of the ASTM. Subcommittee II is charged with the responsibility of formulating standards for laser materials, components, and devices. The chairman of Subcommittee II is John D. Myers, of Owens-Illinois, Inc. Co-chairmen for the damage symposia are Dr. Arthur H. Guenther, of the Air Force Weapons Laboratory, and Professor Alexander J. Glass, Chairman of the Department of Electrical Engineering at Wayne State University.

Approximately 50 attendees at the symposium heard 17 papers on topics relating to laser-induced damage in glass, crystalline materials, nonlinear optical materials, thin film dielectric coatings, and mirrors. Particular attention was given to the processes of plasma formation at dielectric surfaces, and to the role played by self-focusing in bulk damage in solids. The principle recommendations for future investigations are summarized below.

The proceedings of these Symposia represent the major source of information in the field of damage in laser materials. The Symposia themselves, along with the periodic meetings of Subcommittee II, provide a unique forum for the exchange of information regarding laser materials specifications among the manufacturers and users of laser devices, components and systems. The Symposium also serves as a mechanism of information gathering, to enable the Subcommittee to write informed and realistic specifications.

17. KEY WORDS (Alphabetical order, separated by semicolons)

Laser damage; laser materials; self-focusing.

18. AVAILABILITY STATEMENT

[X] UNLIMITED.

[ ] FOR OFFICIAL DISTRIBUTION. DO NOT RELEASE TO NTIS.

19. SECURITY CLASS (THIS REPORT): X UNCLASSIFIED

21. NO. OF PAGES: 176

20. SECURITY CLASS (THIS PAGE): UNCLASSIFIED

22. Price

U.S. GOVERNMENT PRINTING OFFICE : 1971 O—450-417

NBS TECHNICAL PUBLICATIONS

PERIODICALS

JOURNAL OF RESEARCH reports National Bureau of Standards research and development in physics, mathematics, chemistry, and engineering. Comprehensive scientific papers give complete details of the work, including laboratory data, experimental procedures, and theoretical and mathematical analyses. Illustrated with photographs, drawings, and charts.

Published in three sections, available separately:

• Physics and Chemistry

Papers of interest primarily to scientists working in these fields. This section covers a broad range of physical and chemical research, with major emphasis on standards of physical measurement, fundamental constants, and properties of matter. Issued six times a year. Annual subscription: Domestic, $9.50; $2.25 additional for foreign mailing.

• Mathematical Sciences

Studies and compilations designed mainly for the mathematician and theoretical physicist. Topics in mathematical statistics, theory of experiment design, numerical analysis, theoretical physics and chemisty, logical design and programming of computers and computer systems. Short numerical tables. Issued quarterly. Annual subscription: Domestic, $5.00; $1.25 additional for foreign mailing.

• Engineering and Instrumentation

Reporting results of interest chiefly to the engineer and the applied scientist. This section includes many of the new developments in instrumentation resulting from the Bureau's work in physical measurement, data processing, and development of test methods. It will also cover some of the work in acoustics, applied mechanics, building research, and cryogenic engineering. Issued quarterly. Annual subscription: Domestic, $5.00; $1.25 additional for foreign mailing.

TECHNICAL NEWS BULLETIN

The best single source of information concerning the Bureau's research, developmental, cooperative, and publication activities, this monthly publication is designed for the industry-oriented individual whose daily work involves intimate contact with science and technology—*for engineers, chemists, physicists, research managers, product-development managers, and company executives.* Annual subscription: Domestic, $3.00; $1.00 additional for foreign mailing.

NONPERIODICALS

Applied Mathematics Series. Mathematical tables, manuals, and studies.

Building Science Series. Research results, test methods, and performance criteria of building materials, components, systems, and structures.

Handbooks. Recommended codes of engineering and industrial practice (including safety codes) developed in cooperation with interested industries, professional organizations, and regulatory bodies.

Special Publications. Proceedings of NBS conferences, bibliographies, annual reports, wall charts, pamphlets, etc.

Monographs. Major contributions to the technical literature on various subjects related to the Bureau's scientific and technical activities.

National Standard Reference Data Series. NSRDS provides quantitative data on the physical and chemical properties of materials, compiled from the world's literature and critically evaluated.

Product Standards. Provide requirements for sizes, types, quality, and methods for testing various industrial products. These standards are developed cooperatively with interested Government and industry groups and provide the basis for common understanding of product characteristics for both buyers and sellers. Their use is voluntary.

Technical Notes. This series consists of communications and reports (covering both other agency and NBS-sponsored work) of limited or transitory interest.

Federal Information Processing Standards Publications. This series is the official publication within the Federal Government for information on standards adopted and promulgated under the Public Law 89–306, and Bureau of the Budget Circular A–86 entitled, Standardization of Data Elements and Codes in Data Systems.

Consumer Information Series. Practical information, based on NBS research and experience, covering areas of interest to the consumer. Easily understandable language and illustrations provide useful background knowledge for shopping in today's technological marketplace.

NBS Special Publication 305, Supplement 1, Publications of the NBS, 1968-1969. When ordering, include Catalog No. C13.10:305. Price $4.50; $1.25 additional for foreign mailing.

Order NBS publications from:

Superintendent of Documents
Government Printing Office
Washington, D.C. 20402

UNITED STATES
GOVERNMENT PRINTING OFFICE
PUBLIC DOCUMENTS DEPARTMENT
WASHINGTON, D.C. 20402

OFFICIAL BUSINESS

PENALTY FOR PRIVATE USE, $300

POSTAGE AND FEES PAID
U.S. GOVERNMENT PRINTING OFFICE

U.S.MAIL